REGULATION OF ENDOCYTOSIS AND POSTENDOCYTIC TRAFFIC IN POLARIZED EPITHELIAL CELLS

by

Som-Ming Leung

BS in Computational Biology, Carnegie Mellon University, 1995

Submitted to the Graduate Faculty of

School of Medicine in partial fulfillment

of the requirements for the degree of

Doctor of Philosophy

University of Pittsburgh

2002

UNIVERSITY OF PITTSBURGH

SCHOOL OF MEDICINE

This dissertation was presented

by

Som-Ming Leung

It was defended on

January 28, 2002

and approved by

Dr. Rebecca Hughey

Dr. John Johnson

Dr. Sandra Murray

Dr. Ora Weisz

Dissertation Director: Dr. Gerard Apodaca

REGULATION OF ENDOCYTOSIS AND POSTENDOCYTIC TRAFFIC IN POLARIZED EPITHELIAL CELLS

Som-Ming Leung

University of Pittsburgh, 2002

The endocytotic and postendocytic trafficking pathways in polarized epithelial cells was examined. First, sorting of fluid and membrane internalized from the apical plasma membrane was analyzed. Internalized fluid and membrane were initially delivered to apical early endosomes (AEE). Fluid remained in the AEE while membrane was rapidly sorted and delivered to the $Rab11^{+}$ apical recycling endosome (ARE). The delivery of membrane markers to the ARE was microtubule-dependent. Transferrin, a marker of basolateral recycling pathway, had access to the AEE but not the ARE. Next, the role of Rac1 and RhoA in endocytosis and postendocytic was determined. Both Rac1 and RhoA were involved in regulation of endocytosis from both plasma membrane domains. Furthermore, Rac1 was implicated in regulation of apically targeted traffic from both the endocytic and secretory pathways. Expression of dominant active Rac1 (Rac1V12) caused the formation of a central aggregate of membranes composed in part of the ARE. Markers targeted for the apical plasma membrane were trapped within this aggregate. RhoA was involved in the regulation of traffic from basolateral early endosomes (BEE). Expression of dominant active RhoA (RhoAV14) trapped ligands internalized from the basolateral plasma membrane in BEE that were also associated with filamentous actin (F-actin). A subset of BEE from control cells were also f-actin positive. Colocalization of BEE with proteins involved in actin polymerization based propulsion (ABPB) and myosin motor-based propulsion was determined. Proteins involved in ABPB were not associated with BEE but MIc, a type I myosin, did colocalize with a subset of BEE. This suggests that BEE are transported along associated f-actin to the level of stress fibers carried by MIc. Finally, the role of SNAP-23 in basolateral recycling of transferrin was determined. SNAP-23 was localized to the endosomes throughout the cell and to the basolateral plasma membrane. Treatment of permeabilized MDCK cells with botulinum neurotoxin E or addition of exogenous SNAP-23 or anti-SNAP-23 antibodies all inhibited transferrin recycling. This suggests that SNAP-23 is important for basolateral recycling in polarized epithelial cells.

TABLE OF CONTENTS

LIST OF FIGURES

INTRODUCTION

I. OVERVIEW OF THE ENDOCYTIC PATHWAY

Endocytosis plays an important role in several cellular processes including antigen presentation, maintenance of cell polarity and regulation of channel and receptor density on the cell surface (Mukherjee et al., 1997). Mechanistically, endocytosis allows the cell to internalize extracellular material through the formation of membrane bound vesicles. Examples of endocytosis include phagocytosis, pinocytosis, clathrin-dependent endocytosis and clathrin-independent endocytosis (Mukherjee et al., 1997). Once internalized, endocytosed material is delivered to endosomes, sorted, and transported to several intracellular destinations.

A. Endocytic Pathway in Nonpolarized Cells

In nonpolarized cells such as fibroblasts, endocytosed fluid and membrane is delivered to early sorting endosomes. This compartment has a tubulovesicular morphology and its physical properties are involved in sorting. The majority of fluid phase markers remain within the vesicular portion of the endosome while most of the membrane markers are found in the membrane rich tubular sections (Griffiths et al., 1989; Gruenberg et al., 1989; Marsh et al., 1986). The tubular sections are thought to pinch off and are either directly recycled or delivered to the pericentriolar recycling endosome (Dunn et al., 1989). From this compartment membrane is returned, i.e. recycled back to the plasma membrane. Fluid remains within the vesicular portion of the sorting endosome and then matures into or is transported to late endosomes (the exact mechanism of this process is not fully understood) and eventually delivered to lysosomes to be degraded. Finally, there is an

alternative recycling pathway from early and late endosomes via the trans-Golgi network (TGN). Therefore in nonpolarized cells, endocytosed markers are trafficked along one of two basic pathways, those involved in recycling or in degradation.

B. Endocytic Pathway in Polarized Epithelial Cells

Polarized epithelial cells are more complex than nonpolarized cells because of their asymmetry. Polarized cells have distinct apical and basolateral plasma membrane domains that are separated by tight junctions (Simons and Fuller, 1985) and endocytosis can occur at both plasma membrane domains. Internalized macromolecules have several possible fates; they can be recycled back to their original plasma membrane domain, they can be degraded, or they can be transcytosed to the opposite plasma membrane domain. Traffic back to the plasma membrane can occur through endosomes or back through the TGN. This results in at least six different postendocytic pathways in polarized epithelial cells.

C. Postendocytic Fate of Fluid in Polarized Epithelial Cells

Initial attempts to analyze the endosomal pathways in epithelial cells used fluid phase markers internalized from opposite poles of the cell. Short internalization times, $\leq$ 10 min, labeled two separate populations of early endosomes (Bomsel et al., 1989; Parton et al., 1989). The peripheral basolateral early sorting endosomes (BEE) underlie the entire basolateral plasma membrane up to the tight junctions. The apical early sorting endosomes (AEE) are found throughout the cytoplasm between the level of the tight junctions and the Golgi apparatus. No mixing of these fluid phase markers was observed during this short internalization period. In fact, the BEE and the AEE are biochemically distinct structures. *In vitro* endosome-endosome fusion assays revealed that homotypic BEE-BEE and AEE-AEE fusion was possible but AEE and BEE do not fuse (Bomsel et al., 1990). Longer internalization periods, however, did result in colocalization of basolaterally and apically internalized fluid phase markers in common supranuclear structures (Bomsel et al., 1989; Parton et al., 1989). These compartments were analyzed by electron microscopy and found to be positive for

mannose-6-phosphate receptor, a marker of late endosomes (Parton et al., 1989). In addition to being transported along the degratory pathway, fluid phase markers internalized from either apical or basolateral plasma membrane domains could also transcytose and recycle. The ratio of delivery between these three postendocytic fates differed depending on which plasma membrane domain is used for internalization. After delivery to the BEE, 73% of the fluid phase marker was degraded while 13% was recycled and 14% transcytosed (Bomsel et al., 1989); but of the fluid phase markers delivered to the AEE 45% was recycled, 45% was transcytosed and only 10% was delivered to late endosomes for degradation (Bomsel et al., 1989). This suggests that the AEE and BEE are distinct spatially, biochemically and functionally.

D. Postendocytic Fate of Membrane in Polarized Epithelial Cells

Studies using membrane bound markers reveal an even more complex picture. There is significant mixing of membrane bound markers internalized from both poles of the cell in endosomes found above the nucleus near the apical pole of the cell. Several studies have examined these endosomes and they have been variously described as the common recycling endosome (CE), the apical recycling endosome (ARE) and the subapical compartment (SAC) (Apodaca et al., 1994; Barroso and Sztul, 1994; Hughson and Hopkins, 1990; Knight et al., 1995; Odorizzi et al., 1996). The relationship of these compartments to one another and within different cell types is unclear.

Hughson and Hopkins first observed that apically and basolaterally internalized cargo was capable of mixing using Caco-2 cells (a polarized intestinal epithelial cell line) (Hughson and Hopkins, 1990). This study showed that the transferrin receptor (Tf-R), a marker of the basolateral recycling pathway in many cells, was found in a series of apical endosomes that colocalized with apically internalized concanavalin A or fluid phase HRP (Hughson and Hopkins, 1990). This compartment also was shown to contain EGF and ∝-2 macroglobulin, markers of the degratory pathway (Knight et al., 1995). Therefore this apical endosome was termed the CE, as it received cargo from either plasma membrane domain.

Other studies used Madin Darby canine kidney (MDCK) cells to examine the basolateral to apical transcytotic pathway (Apodaca et al., 1994; Barroso and Sztul, 1994). The polymeric immunoglobin receptor (pIgR) transports IgA and IgM from fluid surrounding the basolateral plasma membrane and secretes the IgA/IgM from the apical cell surface. After delivery to the basolateral plasma membrane from the TGN, pIgR binds IgA and the pIgR-IgA complex is endocytosed and transported to BEEs. This complex is then delivered to apical endosomes that are accessible to apical membrane markers internalized for $\leq$ 10 min (Apodaca et al., 1994). These endosomes were termed the ARE. From this compartment the receptor-ligand complex is then delivered to the apical plasma membrane where it is proteolytically cleaved and released into the apical medium (Apodaca et al., 1994). A small fraction remains uncleaved and can be subsequently reinternalized and then eventually recycled to the apical plasma membrane.

E. Relationship between ARE of polarized epithelial cells and RE of nonpolarized cells

Analysis of the ARE suggests that it is related to recycling endosomes (RE) found in nonpolarized cells. Both compartments are composed of tubular structures, localized around the centrioles, and delivery to these compartments requires intact microtubules. In addition, van IJzendoorn and Hoekstra demonstrated that endocytosed IgA, Tf-R and sphingolipids could be accumulated in the ARE or RE of polarized or nonpolarized HepG2 cells, respectively (van IJzendoorn et al., 1997). The small GTPase rab11 is localized to the ARE and RE (see chapter 1, — the function the rab GTPases will be discussed below) (Green et al., 1997; Ren et al., 1998; Ullrich et al., 1996). Although similar in many respects, the ARE differs from the RE. Recent studies have demonstrated that the ARE, unlike the RE, may in fact be composed of at least two functionally different endosomal compartments. Rab11 and rab25 have both been shown to colocalize with transcytosing and recyling IgA but the two rabs do not completely colocalize with each other (Casanova et al., 1999). This suggests the possibility of two biochemically distinct compartments. In addition, we have demonstrated that apically recycling IgA is initially delivered in to AEE and is

then rapidly sorted (within 10 min) to small punctate rab11-positive apical endosomes characteristic of the ARE. This compartment was inaccessible to basolaterally recycling Tf that in nonpolarized cells is transported through the RE. Therefore, we redefined the ARE as rab11 positive IgA^{+}/Tf^{-} compartment that can be labeled kinetically with IgA internalized apically for 10 min, and termed the rab11-negative IgA^{+}/Tf^{+} compartment as the CE (see chapter 1).

II. PROCESS OF VESICLE TRANSPORT

Traffic through the endocytic pathway includes a series of compartments. For example, basal to apical transcytosis of IgA starts with internalization at the basolateral plasma membrane and delivery to BEE, then to the CE, then the ARE and finally the apical plasma membrane. Transport between compartments of the endocytic and secretory pathways is primarily mediated by carrier vesicles or tubules (Kirchhausen, 2000). The process of vesicle transport can be delineated into three steps - formation of the vesicle, transport of the vesicle to its target membrane and fusion of the vesicle with the target membrane.

A. Formation of the Vesicle

The best understood processes of vesicle formation use coat proteins such as COPI, COPII or clathrin (for review see Kirchhausen, 2000). COPI and COPII vesicles are involved in transport along the secretory pathway, although some evidence suggests that some COPI proteins may be involved in the formation of multivesicular bodies (i.e., late endosomes) within the endocytic pathway. Clathrin-coated vesicles are formed at the plasma membrane, the TGN and early endosomes.

The process of vesicle formation can be delineated into four steps - initiation, propagation, vesicle budding and uncoating (Kirchhausen, 2000). These steps will be discussed below in the context of clathrin coat formation since it is most relevant to the endocytic pathway (for COPI and COPII please see Kirchhausen, 2000). Initiation starts with the activation and binding of a small

GTPase at the starting membrane. For clathrin bud formation at the TGN, the GTPase is ARF1 (Seaman et al., 1996; Stamnes and Rothman, 1993),and ARF6 has been implicated in clathrin-mediated endocytosis at the apical pole of polarized MDCK cells (Altschuler et al., 1999). The GTPases involved in clathrin coat formation at other locations is not known. Following GTPase activation, adaptor protein (AP) complexes are recruited to the membrane and are important for cargo incorporation into the forming vesicle. AP1 is involved in TGN vesicle formation and AP2 is part clathrin vesicles at the plasma membrane. Furthermore, AP complexes binding to the membrane requires phosphotidylinositol 4,5-bisphosphate (PIP_2). Addition of a PIP_2 binding peptide inhibits transferrin endocytosis and mutations of AP-2 that block PIP_2 binding also affect endocytosis (Jarousse and Kelly, 2001). Clathrin then binds the AP complexes starting coat assembly. During the propagation step, cargo recruitment and coat formation continue and as the coat assembles, it also drives membrane invagination. Once a deeply invaginated pit is formed the vesicle buds from the membrane. This budding event involves the GTPase dynamin although the exact function of dynamin has not been fully resolved. Localization of dynamin to the neck of the invaginated pit requires PIP_2 (Achiriloaie et al., 1999; Lee et al., 1999; Vallis et al., 1999). Finally, the budded vesicle uncoats, which is driven by the Hsc70 ATPase (Newmyer and Schmid, 2001; Schlossman et al., 1984). In addition to Hsc70 ATPase, synaptojanin (a phosphoinositide 5'-phosphatase) may also play a role in coat release. Addition of anti-synaptojanin antibodies inihibits uncoating *in vivo* and clathrin coated vesicles accumulat in synaptojanin knockout mice (Cremona et al., 1999; Gad et al., 2000).

Although the formation of COPI, COPII and clathrin vesicles are the best understood, there are several types of clathrin-independent endocytosis including pinocytosis, phagocytosis and caveolae (see Nichols and Lippincott-Schwartz, 2001). Some of these processes are known to involve coat proteins (such as caveolin) but not all. Vesicle formation can also occur using other process. The tubuluovesicular structure of early endosomes sorts membrane from fluid, and scission

of the tubular portion form carriers to the RE. Finally, in some instances entire organelles are used as transport vesicles. Early endosomes have been shown to undergo homotypic fusion and late endosomes fuse with pre-existing lysosomes.

B. Transport of the Vesicle to its Target Membrane

1. Microtubule based Transport

Next, the newly formed vesicle must be transported to the target membrane. Although simple diffusion of the vesicle through the cytoplasm may account for some transport, many transport steps utilize the cytoskeleton. Microtubules are important in vesicle transport. Microtubule based motility requires two motor proteins, kinesin (generally involved in plus-end movement) and dynein (involved in minus end movement). Several transport steps in polarized epithelial cells require intact microtubules. Treatment with nocadozole, a microtubule disrupting agent, blocks transport from EE to LE (Gruenberg et al., 1989). In polarized epithelial cells, delivery of Tf to the CE from the BEE is also impaired while basolateral Tf recycling is not impaired (Apodaca et al., 1994; McGraw et al., 1993). This is presumably because Tf can also recycle back to the plasma membrane directly from the BEE without intact microtubules. Apical recycling, however, is inhibited 20-30% by nocadozole treatment (Breitfeld et al., 1990b). We have now demonstrated that this is primarily due to a block in AEE to ARE transport (see chapter 1). Finally, microtubules are also required for basal to apical transcytosis (Breitfeld et al., 1990b; Hunziker et al., 1990; Matter et al., 1990). Much of this may be due to impaired BEE to CE transport but the requirements for intact microtubules for CE to ARE transport is not known.

2. Actin Based Transport

In addition to microtubules, the actin cytoskeleton has also shown to be required for vesicle transport. Treatment of Hep-2 cells with cytochalasin D (CD), an actin filament disrupting agent, inhibits late endosome fusion with lysosomes (Durrbach et al., 1996). CD-treatment of MDCK cells does not significantly inhibit either basolateral or apical recycling but latrunculin A, an actin

monomer binder, does slow Tf recycling in Caco-2 cells. The reason for this discrepancy may be due the difference in the effects of the toxins on the actin cytoskeleton. CD creates a number of short disorganized actin filaments while latrunculin A leads to the depolymerization of all actin in the cell. Therefore it is possible that CD-treated MDCK cells retain enough filamentous actin (F-actin) to allow recycling to continue unabated.

In CD-treated MDCK cells, basal to apical IgA transcytosis is significantly inhibited (Maples et al., 1997). As such, basal to apical IgA transcytosis is dependent on both actin and microtubule based transport. Order of addition experiments demonstrated that the actin dependent transport step precedes the microtubule dependent transport (as noted above) and treatment with both CD and nocadozole inhibits transcytosis by >95% (Maples et al., 1997). Some IgA-labeled basolateral vesicles localized below the level of the stress fibers are associated with F-actin (Leung et al., 1999). One possible function of the associated actin is to facilitate vesicle transport through the cortical actin and from there it is carried further into the cell via microtubules (examined in chapter 4). Therefore, transport is likely to require a coordinated transfer between the actin cytoskeleton and microtubules. A similar phenomenon is seen in melanosome transport in melanocytes. Melanosomes are first transported out to the periphery of dendridic extensions using microtubules and once at the periphery the melanosome then utilizes the actin cytoskeleton for short distance travel to be anchored out at the periphery (Wu et al., 1998).

a. Actin Polymerization Based Propulsion

Two actin dependent transport models are actin polymerization based propulsion (APBP) and myosin motor based propulsion. APBP was first discovered as a motility mechanism for two unrelated bacterial pathogens (*Listeria monocytogenes* and *Shigella flexneri*) (Frischknecht and Way, 2001; Steele-Mortimer et al., 2000). Phagocytosed *Listeria* escapes in the host cytoplasm and then usurps cellular machinery to polymerize actin into dense crosslinked network forming an actin tail. Actin polymerization at the front of the tail propels the bacterium forward through the cytoplasm.

It is thought that the cellular machinery is normally used by the cell in lamellipodia movement is co-opted by the bacterium for APBP (Rohatgi et al., 1999; Welch et al., 1997). Several cellular proteins are utilized for this mechanism including: the Arp2/3 complex, N-WASP, cofilin, profilin and capping protein (discussed in detail in chapter 4). Recently, evidence has emerged that vesicles may utilize this as a method of transport. In mast cells, pinosomes are propeled from the plasma membrane by short lived actin tails (Merrifield et al., 1999) while increases in PIP_2 induced actin tail formation on vesicles in Swiss 3T3 fibroblasts (Rozelle et al., 2000). Finally, vesicle preparations from HeLa cells or *Xenopus* oocytes could form tails in an *in vitro* system (Taunton et al., 2000). These data suggests that cells may be using APBP as a mechanism for vesicle and organelle propulsion.

b. Myosin Based Propulsion

Myosin motors have also been implicated as a mechanism of F-actin dependent transport. Several classes of unconventional myosins (I, V, VI, VII and II or conventional myosin) are implicated in endocytic trafficking (Tuxworth and Titus, 2000). As mentioned above, melanosomes in melanocytes utilize the actin cytoskeleton for short movements and to anchor the melanosomes in the periphery of the dendritic processes. Myosin Va is required to capture the melansomes at the periphery. Wu et al. demonstrated that melanosomes in melanocytes from myosin Va null mice were incapable of both peripheral anchoring and short-ranged movements (Wu et al., 1998). Similarly, two yeast class V myosin have been implicated in organelle transport and anchoring at the bud tip (Bertrand et al., 1998; Pruyne et al., 1998).

Class VI myosins are unique in that they move towards the pointed end of actin filaments. It is has been hypothesized that myosin VI may play a role in vesicle transport through the cortical actin which is oriented pointed end inwards. Recently, Buss et al. demonstrated that myosin VI can

be localized to apical clathrin coated vesicles in polarized Caco-2 cells (Buss et al., 2001). In addition, expression of the myosin VI tail domain inhibited transferrin uptake in fibroblasts . This suggests that myosin VI may play a role in clathrin-dependent endocytosis.

In yeast, class I myosins have been implicated in endocytosis. Deletion of either myosin I isoform in yeast results in a defect in the rate of receptor-mediated endocytosis and deletion of both increases its severity (Geli and Riezman, 1996). In the fungus *Aspergillus nidulans*, expression of a constitutively active myosin I results in stimulation of endocytosis (Yamashita and May, 1998). A myosin I deletion mutant, however, has no effect on endocytosis but does exhibit a defect in secretion and polarized growth of *Aspergillus nidulans* (McGoldrick et al., 1995). In metazoans, a myosin I subclass exists of which the founding member is brush border myosin I. This subset has been implicated in both apical delivery from the Golgi and in late endosome transport to the lysosome. Brush border myosin I and dynein were localized to Golgi-derived apically targeted vesicles from intestinal crypt cells (Fath and Burgess, 1993). This suggests another two step mechanism of transport where initial transport from the Golgi utilizes microtubules and the actin-rich cortex myosin I transport the vesicle to the membrane. Secondly, another class I myosin, myosin Iα, is localized to the plasma membrane, endosomes and lysosomes (Raposo et al., 1999). Overexpression of the myosin Iα tail domain inhibits transport of fluid phase markers to lysosomes (Raposo et al., 1999; Ruppert et al., 1995).

Shaker-1 mice express a deficient myosin VII mutant. In the retinal pigment epithelial (RPE) cells of these mice, melanosomes do not reach the outer periphery (Liu et al., 1998). This suggests that myosin VII may play a role in either transport or localization of the melanosomes to that region of the cell. Similarly, opsin distribution in the photoreceptors of these mice is altered (Liu et al., 1999). Finally, these mice exhibit a deficiency in an undefined aminoglycosides endocytic pathway in the hair cells of the ear (see chapter 4) (Richardson et al., 1997).

Non-muscle myosin II has been implicated in vesicle budding from the TGN. Myosin II was found on TGN derived vesicles. In addition, recruitment onto these vesicles was GTP-dependent and brefeldin A sensitive which suggests a role for the small GTPase Arf1 (Ikonen et al., 1997; Musch et al., 1997). Depletion of myosin II inhibited vesicle formation of vesicular stomatitis virus G protein vesicles and re-addition of myosin II restored normal budding (Musch et al., 1997). Simon et al., however, have suggested that the antibody used in those studies recognizes β-COP and coatomer is required for vesicle budding but myosin is not needed (Simon et al., 1998). Finally, there is evidence that suggests the myosin II may play role in vesicle transport. Vesicles isolated from clam oocytes have associated myosin II and in an *in vitro* assay myosin II propelled these vesicles along F-actin (DePina and Langford, 1999).

3. Other Roles for the Cytoskeleton in Endocytosis

In addition to the role that the cytoskeleton plays in vesicle transport, it has also been implicated in other facets of endocytic trafficking including intracellular organelle localization and endocytosis. As mentioned above, actin plays a role in anchoring melanosomes at the tips of melanocyte dendrites (Wu et al., 1998). Microtubules have been implicated in the organization of both the Golgi complex and the ARE. Treatment with nocadozole disperses the Golgi and the ARE. Secondly, the actin cytoskeleton has been implicated in endocytosis but its exact function has not been elucidated. Several models of the role of actin in endocytosis have been proposed including acting as a molecular fence, acting as scaffold for budding, acting as part of the vesicle scission event and as a part of the propulsion machinery for the nascent vesicle (reviewed in Apodaca, 2001; Qualmann et al., 2000).

C. Vesicle Fusion with the Target Membrane

The final process in vesicle transport is docking and fusion with the target membrane. Early studies demonstrated that the cytoplasmic N-ethylmaleimide-sensitive fusion protein (NSF) was required for vesicle fusion to occur (Block et al., 1988). *In vitro* assays of intercisternal Golgi

transport resulted in the accumulation of vesicles at the target membrane in the absence of NSF. In addition to NSF, another group of cytoplasmic proteins, soluble NSF atttachment proteins (SNAPs), was required for vesicle fusion (Clary et al., 1990; Whiteheart and Kubalek, 1995). Both of the components could be replaced by yeast homologs suggesting that they are part of a general fusion mechanism. In 1993, Sollner et al. isolated SNAP receptors (SNAREs) from bovine brain as part of a 20S fusion complex (Sollner et al., 1993). One component (VAMP 2) of this fusion complex had previously been shown to localize to synaptic vesicles while a second (syntaxin) was localized to the plasma membrane (Sollner et al., 1993). The third component (SNAP-25 – no relation to SNAP) was not precisely localized at the time (Sollner et al., 1993). These observations suggested SNAREs were a family of proteins that where compartmentally distributed with one set associated with vesicles (v-SNAREs) and the other set associated with target membranes (t-SNAREs). These observations lead to the formation of the SNARE hypothesis that postulates both that SNARE assembly mediates membrane fusion and that specificity of vesicle fusion was determined by specific v-SNARE and t-SNARE pairings (Sollner et al., 1993).

1. SNARE Classification

The SNARE family of proteins was initially identified in neuronal tissue (Sollner et al., 1993) and yeast cells (Novick et al., 1980). These proteins share a weakly homologous sequence called a SNARE motif that mediates the association of SNAREs. Initially, SNAREs were classified into t-SNAREs and v-SNAREs based on structural relationship to the initial SNAREs found in neuronal tissue (Sollner et al., 1993). SNAREs related to VAMP were classified as v-SNAREs while t-SNAREs were composed of syntaxin and SNAP-25 related SNAREs. The association of the SNAREs has been best studied using the three neuronal SNAREs, VAMP 2, syntaxin 1a and SNAP-25. The three neuronal SNAREs assemble into a highly stable ternary complex called the core complex that is resistant to heat (Yang et al., 1999), treatmet with SDS (Hayashi et al., 1994) and proteolytic cleavage by botulinum and tetanus neurotoxins (Hayashi et al., 1994). This core complex assembly is mediated by the association of the four SNARE motifs of the neuronal SNAREs

(one from VAMP 2, one from syntaxin 1a and two from SNAP-25). The crystal structure of the core complex has been solved (Fasshauer et al., 1998; Sutton et al., 1998). The complex is composed of four helices twisted together in a coiled-coil structure. The majority of the interactions are hydrophobic but in the center of the helical bundle is an ionic layer that is composed of an arginine residue (from VAMP 2) and three glutamine residues (from syntaxin 1a and SNAP-25) (Fasshauer et al., 1998). This analysis has resulted in a new method of SNARE classification based on the predicted central residue in the SNARE motif, R-SNAREs and Q-SNAREs (Fasshauer et al., 1998), respectively.

2. SNARE - Minimal Fusion Machinery

It was initially hypothesized that SNAREs would mediate membrane attachment of vesicles while NSF, an ATPase, would drive the fusion event. More recent studies have shown that the role of NSF is to dissociate the SNARE core complex (Mayer et al., 1996) and it is now suggested that the SNARE proteins themselves that drives membrane fusion (Chen et al., 1999; Chen et al., 2001; Nickel et al., 1999; Weber et al., 1998). Treatment of neurons with botulinum and tetanus neurotoxins resulted in the inhibition of synaptic vesicle exocytosis (Jahn and Niemann, 1994). The cause of this inhibition was proteolytic cleavage within the SNARE motif of VAMP, syntaxin or SNAP-25 by these neurotoxins. This cleavage prevented the formation of a stable core complex thereby linking core complex formation with vesicle exocytosis. Additional evidence supporting the requirement of core complex formation comes from studies using mutants of yeast SNAREs (Jahn and Sudhof, 1999; Ungermann et al., 1998b). Mutations affecting the core complex formation resulted in loss of fusion. Furthermore, analysis of the crystal structure of the SNARE core complex revealed that it resembled the helical bundles found in viral fusion proteins (which are required for viral envelope fusion with cell membranes) (Jahn and Sudhof, 1999; Weber et al., 1998). This led to the proposal that SNARE core complex formation drives membrane fusion.

Weber et al. recently demonstrated that SNARE proteins reconstituted in liposomes were capable of catalyzing liposome fusion (Weber et al., 1998). This liposome fusion required the proper SNARE pairing and was inhibited by the addition of exogenous SNAREs or pretreatment with Botulinum toxin D. Hence, the formation of the highly stable core complex may provide the energy to drive vesicle fusion. However, these liposomes do not reflect the composition of physiological cell membranes. Many other treatments of liposomes can induce fusion including addition of clathrin, annexin and phospholipases C and D. In addition, a recent study of homotypic vacuole fusion in yeast required two sequential interactions (Ungermann et al., 1998b). The first interaction is an initial tethering by a Rab protein (discussed below) and then the second interaction is the formation of a SNARE complex. Subsequently, the SNARE complexes can be dissociated and prevented from reassembling with the addition of blocking antibodies. This disruption of the SNAREs did not affect the mixing of the vacuole contents (Ungermann et al., 1998b). Therefore, SNAREs may not be the minimal machinery required for fusion of physiological membranes.

3. SNARE - Role in Vesicle Targeting

One of the most intriguing aspects of the early SNARE hypothesis was the postulation that specific t-SNARE and v-SNARE interactions determined vesicle targeting. However, there were some flaws in this hypothesis. First, all the SNARE proteins in yeast have been identified from the complete genome and although there are several syntaxin homologs, there are only two SNAP-25 homologs (Neiman, 1998; Pelham, 1999; Rossi et al., 1997). In addition, both of these are found at the plasma membrane. The recent reclassification of Q- and R- SNAREs, however suggests an alternative possibility. Fukuda et al. demonstrated that the two Q- SNARE helixes contributed by SNAP-25-related SNAREs can be replaced by two individual Q-SNAREs in an *in vitro* fusion assay (Fukuda et al., 2000). What then is the function of the connected helixes in SNAP-25? One possibility is to facilitate faster fusion since the two chains are linked and accelerate fusion by constraining the formation of the fusion complex (Fukuda et al., 2000).

A second problem with the SNARE based targeting is that several studies have demonstrated that SNARE core complex formation is very nonspecific. Yang et al. have shown that *in vitro* complex formation can occur in the 21 Q- and R-SNARE helix combinations formed using five VAMP family members, three SNAP-25 members and three syntaxin family members (Yang et al., 1999). In addition, 16 of these combinations were resistant to both SDS and heat denaturation (Yang et al., 1999). Similarly, Fasshauer et al. also showed that several combinations of SNAP-25, three members of the syntaxin family and two members of the VAMP family could also form SDS- and heat-resistant complexes (Fasshauer et al., 1999). These combinations also were protease-resistant, dissasembled with NSF and SNAP and by circular dichroism spectroscopy showed major conformational changes during complex formation (Fasshauer et al., 1999). Those studies, however, did not examine whether those complexes are fusion competent.

Recent studies, however, suggest that SNARE proteins are capable of determining fusion specificity. Scales et al. examined the fusion specificity of SNAREs using cracked PC12 cells following dense core vesicle fusion with the plasma membrane (Scales et al., 2000). Addition of the cognate syntaxin or VAMP had a greater level of fusion inhibition when compared to the addition of noncogate SNAREs. Furthermore, rescue of dense core vesicle fusion after BotNT E treatment was also more effective with SNAP-25 compared other SNAP-25 related proteins (Scales et al., 2000). Secondly, McNew et al. demonstrated that only the proper combination of Q- and R-SNAREs could facilitate fusion in a liposome fusion assay (McNew et al., 2000), and the localization of the SNAREs on the fusing liposomes has to be correct for fusion to occur. Three Q-SNAREs helixes must be on one liposome and one R-SNARE on the other in order for fusion to occur (Parlati et al., 2000). One problem with this study is that promiscuous fusion occurred between the plasma membrane Q-SNAREs Sso1/Sec9c and two noncognate R-SNAREs (Nyv1 and Sec22) (McNew et al., 2000). However, Nyv1 is located on yeast vacuoles and may represent an alternative fusion pathway similar to lysosome secretion found in higher cell types (McNew et al., 2000). Sec22 is

localized to the Golgi and therefore not likely to interact with SNAREs found at the plasma membrane (McNew et al., 2000). These studies suggest that SNAREs do play a role in vesicle targeting, perhaps as a final checkpoint before fusion occurs.

4. SNAREs in Polarized Epithelial Cells

Although the localization and function of various SNAREs have been studied in many types of cells (for example - yeast, neurons, various nonpolarized cells), only a small subset of SNAREs has be examined in polarized epithelial cells. This distinction is important since the localization of specific SNAREs can differ in polarized cells compared to nonpolarized cells (or even from cell type to cell type).

Ikonen et al. analyzed the function of SNAREs in polarized delivery from the biosynthetic pathway using SLO-permeabilized polarized MDCK cells. These experiments led to the conclusion that TGN to basolateral traffic is SNARE dependent while TGN to apical transport is SNARE independent (Ikonen et al., 1995). Recent studies, however, suggest that this is not the case. Analysis of the localization of syntaxin 2, 3 and 4 demonstrated a polarized distribution (Low et al., 1996). Syntaxin 2 is found on both plasma membrane domains of MDCK cells while syntaxin 3 is primaily apical and syntaxin 4 is basolateral. Furthermore, overexpression of syntaxin 3 inhibited both TGN to apical transport and apical recycling. Interestingly, overexpression of syntaxin 3 had no effect on basal to apical transcytosis (Low et al., 1996).

SNAP-23, a SNAP-25 homolog, is endogenously expressed in polarized MDCK cells. It localizes to both the apical and basolateral plasma membrane as well as small vesicles through out the cytoplasm. Treament of SLO permeablized MDCK cells with BoTNE inhibited both basolateral recycling of transferrin, basolateral to apical transcytosis of IgA and biosynthetic traffic from the TGN to both the apical and basolateral plasma membranes (see chapter 5 and Apodaca et al., 1996).

Recently, Steegmaier et al. have examined the trafficking of VAMP8 and VAMP3 in polarized MDCK cells (Steegmaier et al., 2000). VAMP8 was found to localize to the apical plasma membrane of nephric tubules and polarized MDCK cell although there was also a reasonable level of nonspecific intracellular staining. Furthermore, analysis of the cycling of VAMP8 between both the apical and basolateral plasma membrane domains and intracellular compartments revealed that VAMP8 primarily cycles between the apical plasma membrane and endosomes. In contrast, VAMP3 was found to cycle through both the apical and basolateral plasma membranes (Steegmaier et al., 2000).

III. RAB FAMILY OF SMALL GTPASES

A. Rab - GTPase cycle

A second group of proteins that has been implicated in vesicle docking and fusion is the Rab family of small GTPases. The Rab family of small GTPases is the largest branch of the Ras superfamily of small G proteins (which also includes the Rho family - discussed below). There are 11 Rabs in yeast and analysis of the human genome predicts over 60 potential human Rab proteins (Martinez and Goud, 1998; Takai et al., 2001; Zerial and McBride, 2001). Rabs are synthesized in the cytosol but are attached to membranes by the addition of two C-terminal geranylgeranyl groups. Like all small GTPases, Rabs function in a cyclical fashion alternating between a GTP-bound active state and an inactive GDP-bound state. In addition, they also cycle between the cytosol and membranes (Martinez and Goud, 1998; Takai et al., 2001). The cycling of Rabs is controlled by at least three different types of regulators: guanine nucleotide exchange factors (GEFs), GTPase-activating proteins (GAPs) and GDP dissociation inhibitors (GDIs). At the donor membrane, rab GTPase is activated by a GEF converting it from an inactive GDP-bound form to an active GTP-bound form. Rab is then incorporated into forming vesicles and is capable of binding effector molecules (the current understanding of many Rabs and Rab effectors will be discussed below). The vesicle is then delivered to and fuses with the target membrane. Rab then interacts with a GAP that increases the intrinsic GTPase activity of Rab converting it back to an inactive GDP-bound

form. Rab-GDP is removed from the target membrane through the interaction of GDI. Finally, through an unknown mechanism (a putative GDI displacement factor (GDF)) Rab dissociates from GDI and is reinserted into the donor membrane. Between 10-50% of Rab is found in cytosol associated with GDI. The remaining pool of each Rab is localized to specific organelles or vesicles (see Figure I-1).

B. Rab as a Tether

Although recent evidence suggests that SNAREs may be capable of mediating vesicle targeting, there is significant evidence that Rabs also play an important role. One primary function of Rabs is to control the tethering of the vesicle to its target membrane. Rab5 and its effector, early endosome antigen-1 (EEA1), have been shown to play a role homotypic early endosome fusion (Bucci et al., 1992; Chistoforidis et al., 1999; Gorvel et al., 1991b). EEA1 contains two separate Rab5 binding sites and a FYVE finger domain, a phosphatidylinositol 3,4,5-trisphosphate (PIP_3) binding site (Simonsen et al., 1998). Rab5 recruits EEA1 to early endosomes. EEA1 can then span the gap between early endosomes acting as a tether by interacting with Rab5 on both membranes (Zerial and McBride, 2001). PIP_3 may stabilize EEA1 interaction with one membrane and intriguingly, phosphotidylinositol 3-kinases have been shown to be Rab5 effectors. Rab5 may bind the kinase to create a microdomain coupling PIP_3 production with EEA1 function. Furthermore, EEA1 is part of a larger complex that includes Rabex-5 (the Rab5 GEF), Rabaptin-5 (a Rab5 effector) and NSF (McBride et al., 1999). This complex interacts with syntaxin 13 via EEA1. This provides a mechanism by which Rab5 can coordinate early endosome docking and fusion in a temporal and spatial manner. A similar system has been found in yeast. Vps 21p, a yeast Rab protein, is involved in Golgi to endosome transport in budding yeast. Vps21p in its active state interacts with Vac1p, a yeast EEA1 homolog (Peterson et al., 1999; Tall et al., 1999). Vac1p can also interact with PIP_3, Vps45p (a protein regulates SNARE interaction) and Pep12p (a yeast SNARE) (Peterson et al., 1999; Tall et al., 1999).

Rab	Localization	Function
Rab1	ER-Golgi intermediate compartment	ER-Golgi transport
Rab2	ER-Golgi intermediate compartment	
Rab3	Secretory vesicles	Regulated secretion
Rab4	Early and recycling endosomes	Sorting/Recycling to the plasma membrane
Rab5	Clathrin coated vesicles and early endosomes AEE and BEE (epithelial cells)	Cargo Sequestration at plasma membrane Clathrin coated vesicle and early endosome Fusion
Rab6	Golgi	Retrograde Golgi-ER transport Intra Golgi transport
Rab7	Late endosomes	
Rab8	TGN	TGN-plasma membrane transport (basolateral membrane in epithelial cells
Rab9	Late endosomes	Transport form late endosomes to the TGN
Rab11	Golgi and recycling endosomes ARE (epithelial cells)	Export from the Golgi via endosomes Recycling to plasma membrane Apical and basolateral (?) recycling in epithelial cells
Rab13	Tight junctions (epithelial cells)	Tight junction formation
Rab15	Early and recycling endosomes	Inhibitor of endocytic internalization
Rab17	ARE and CE(?) (epithelial cell specific rab)	
Rab18	Kidney dense apical tubules and basolateral domain of intestine (epithelial cell specific rab)	
Rab20	Kidney dense apical tubules (epithelial cell specific rab)	
Rab21	Apical plasma membrane of epithelial cells	
Rab22	Endsomes and plasma membrane	
Rab24	ER, Golgi and late endosomes	
Rab25	ARE and CE(?) (epithelial cell specific rab)	
Rab33	Golgi	Intra-Golgi transport

Figure I-1 - Localization and Function of Rab GTPases
Adapted from (Rodman and Wandinger-Ness 2000; Zerial and McBride 2001)

C. Rab - Role in Budding

In addition to its role in vesicle docking and fusion, Rabs have also been implicated in both vesicle budding and transport. Several lines of evidence suggest that Rabs are required for vesicle budding. Expression of dominant negative Rab1 blocked budding from the endoplasmic reticulum (Nuoffer et al., 1994) and similarly, dominant negative Rab9 blocked budding from late endosomes (Riederer et al., 1994). In yeast two Rabs, Ypt31 and Ypt32, have been implicated in transport vesicle formation from the Golgi (Benli et al., 1996). Finally, Rab5 complexed with Rab GDI is required in receptor sequestration into clathrin coated pits (McLauchlan et al., 1998).

D. Rab - Transport to Target Membrane

The role of Rabs in vesicle movement is primarily linked to the cytoskeleton. Rabkinesin-6, a kinesin-like protein, is an effector of Rab6, which is associated with tubular structures that move along microtubules (Echard et al., 1998; Hill et al., 2000). Rab6 may recruit Rabkinesin-6 to these structures or modulate its function to regulate transport of these structures. Rab11B and its effector, Rabphilin-11, colocalize along microtubules (Mammoto et al., 1999; Simon et al., 1995). Rab11 may also play a role in transport along the actin cytoskeleton. In nonpolarized cells, transferrin recycling requires the interaction of Rab11 and the actin cytoskeleton. In addition, myosin Vb is the downstream target of Rab11A (Hammer III and Wu, 2002). The yeast Rab, Sec4p, interacts with its GEF, Sec2p, to regulate polarized transport of post-Golgi vesicles along the actin cytoskeleton (Zerial and McBride, 2001). Finally, Rab5 and its effectors have been shown to bind actin (Rodman and Wandinger-Ness, 2000). Expression of active Rab5 stimulated cell migration and induces lamellipodia formation as a leading edge (Spaargaren and Bos, 1999). Rab5 is also linked to movement of early endosomes along microtubules (Hammer III and Wu, 2002; Nielsen et al., 1999). This movement is dependent on active Rab5, PI-3 kinase activity and minus-end directed kinesin. In addition, Rab5 stimulation of endosome movement along microtubules can be separated from Rab5 regulated docking and fusion. This suggests that Rabs act as scaffolding for multiple effectors throughout the vesicle transport process.

E. Rab in Polarized Epithelial Cells

In mammalian cells, twelve Rabs are localized along the endocytic pathway and four of these are epithelial cell specific: Rab17, Rab18, Rab20 and Rab25 (Rodman and Wandinger-Ness, 2000). In polarized epithelial cells, several of the endocytic pathways are similar to nonpolarized cells but they have a specialized series of endocytic compartments that include the CE and ARE. In polarized MDCK cells, Rab11 is localized to ARE but not the CE (see chapter 1) and has been implicated in apical transport from the ARE. Expression of the GTP-binding deficient mutant of Rab11 in polarized MDCK cells inhibited both pIgR transcytosis and apical recycling but not basolateral recycling of transferrin. A GTPase-deficient form of Rab11 only inhibited pIgR transcytosis. In gastric parietal cells, Rab11 regulates H^+/K^+ ATPase apical recycling (Goldenring et al., 1994). Of the four epithelial specific rabs, little is known about Rab18 and Rab20 but recent studies have implicated both Rab17 and Rab25 in trafficking through the ARE and CE (Casanova et al., 1999; Hunziker and Peters, 1998; Zacchi et al., 1998). Overexpression of wild-type Rab17 inhibited transcytosis but expression of two Rab17 mutants stimulated both transcytosis and apical recycling. Finally, expression of wild-type or the active mutant of Rab25 inhibited transcytosis and apical recycling but had no effect on basolateral recycling of transferrin. The exact localization of Rab17 and Rab25 in relation to the ARE and common endosome has not been examined.

IV. RHO FAMILY OF SMALL GTPASES

The Rho protein family, similar to the Rab family (discussed above), is also part of the Ras superfamily of small GTPases. There are at least 15 known members of this family (RhoA,B,C / Rac1,2,3 / Cdc42,G25K / RhoG / Tc10 / TTF(RhoH) / Chp / Rnd1,2,3(RhoE) / RhoD) although most research is concentrated on RhoA, Rac1 and Cdc42 (Ellis and Mellor, 2000). Similar to Rab, Rho small GTPases function as molecular switches that cycle between and active GTP-bound state and an inactive-GDP bound state with Rho-specific GEFs, GAPs and GDIs regulating the cycling

of Rho GTPases. Unlike Rab GDI however, Rho GDI appears to be capable of weakly associating with Rho GTPases bound to GTP (Takai et al., 2001). This suggests that Rho GDI may be able lock Rho proteins in both the inactive and active states.

Initially, the Rho family of GTPases was shown to link extracellular signals to the machinery for actin cytoskeleton rearrangement. Treatment of quiescent fibroblasts with lysophosphatidic acid (LPA) induces the formation of stress fibers and focal adhesions through RhoA (Ridley and Hall, 1992a). This can be blocked by microinjection of C3 transferase, which inactivates RhoA-related proteins. Furthermore microinjection of a dominant active form of RhoA also induces stress fiber formation. Other growth factors have been shown to link Rac and Cdc42 to changes in the actin cytoskeleton. Platelet derived growth factor (PDGF) and insulin have been shown to induce lamellipodia formation through Rac1, and bradykinin has been shown to induce filopodia through Cdc42 (Kozma et al., 1995; Ridley et al., 1992a). In addition, there is signalling between Rho family members. Active Cdc42 can activate Rac1 and active Rac1 can activate RhoA. In addition to their role in cytoskeleton regulation, the Rho family of proteins has also been implicated in several other cellular functions including transcriptional activation, growth control, development and membrane traffic (Van Aelst and D'Souza-Schorey, 1997). The following will examine the role of Rho GTPases in membrane traffic (for review of other Rho functions see Van Aelst and D'Souza-Schorey, 1997).

A. Rho and Endocytic Internalization

1. Pinocytosis

The process of pinocytosis has been linked to the formation of membrane ruffles. Expression of dominant active mutants of Rac1 stimulates pinocytosis in Swiss 3T3 fibroblasts and presumably this effect is due to Rac1 stimulation of membrane ruffles. Recent studies using immature dendritic cells suggest that Rac1 may have a more direct role in pinocytosis (Ridley et al., 1992a). Microinjection of dominant negative Rac1 inhibited pinosome formation, but surprisingly had no

effect on membrane ruffling (West et al., 2000). This suggests a direct role for Rac1 in pinocytosis. Furthermore, Dharmawardhane et al. have shown that pinocytic vesicles are coated with PAK1, a Rac1/Cdc42 effector, and active mutants of PAK1 also stimulate pinocytosis (Dharmawardhane, 1997).

2. Caveolae

Another endocytic mechanism linked to the Rho GTPases is internalization mediated by caveolae. Caveolae are specialized omega shaped invaginations of the plasma membrane coated by the protein caveolin. They are composed of glycosphingolipid and cholestrol enriched microdomains and linked to the actin cytoskeleton. Recent studies have shown that filamin, an F-actin crosslinker, interacts directly with caveolin-1. Treatment of cells with Rho-stimulating *Escherichia coli* cytotoxic necrotizing factor 1 induces stress fiber formation and moreover, caveolin-1 positive structures are aligned along the stress fibers (Stahlhut and van Deurs, 2000). Recent studies have demonstrated that both Rac1 and RhoA can be found on caveolae and this localization is increased upon activation of both proteins (Ellis and Mellor, 2000). In addition, GST-RhoA fusion proteins could specifically precipitate caveolin-1 from cell lysates while GST-caveolin-1 could precipitate RhoA. GST-caveolin could also pull down bacterially expressed RhoA (Gingras et al., 1998). Finally, Senda et al. demonstrated that activation of Rho by *Bordetella bronchiseptica* dermonecrotizing toxin also induces the formation of caveolae. These data suggest that Rho is involved in the formation of caveolae (Senda et al., 1997).

3. Phagocytosis

Several lines of evidence have linked the Rho family to phagocytosis. In Fc receptor (FcR) mediated phagocytosis, membrane protrusions extend around the particle engulfing it. RhoA, Cdc42 and Rac1 all accumulate at the forming phagosome during FcR mediated phagocytosis (Chimini and Chavrier, 2000). Treatment with toxin B from *Clostridium difficile*, an inhibitor of all Rho family members, blocks FcR mediated phagocytosis (Chimini and Chavrier, 2000). Expression of

dominant negative Rac1 or Cdc42 inhibits particle uptake and decreases F-actin at particle attachment sites (Chimini and Chavrier, 2000). Examination of RhoA using C3 transferase has yielded contradictory results, therefore it is unclear whether RhoA plays a role in FcR mediated phagocytosis (Chimini and Chavrier, 2000). In contrast, complement receptor (CR) mediated phagocytosis does involve RhoA (Chimini and Chavrier, 2000). CR mediated phagocytosis does not involve the extension of pseudopodia but rather the particle is drawn into actin lined invaginations of the plasma membrane (Chimini and Chavrier, 2000). Treatment of the cells with C3 transferase inhibits particle uptake but expression of dominant negative Rac1 or Cdc42 has no effect (Chimini and Chavrier, 2000).

4. Clathrin-Mediated Endocytosis

Clathrin-mediated endocytosis also involves the Rho family members. Expression of dominant active RhoA or Rac1 inhibits transferrin receptor internalization in nonpolarized cells and expression of dominant active RhoA also inhibits muscarinic acetylcholine endocytosis (Ridley, 2001). In polarized epithelial cells a more complex system has emerged. Expression of dominant active RhoA stimulated both apical and basolateral endocytosis of IgA while dominant negative RhoA inhibited uptake (see chapter 3). In contrast, dominant active Rac1 was inhibitory and dominant negative Rac1 increased IgA endocytosis (see chapter 2). Expression of dominant active Cdc42 inhibited both basolateral and apical IgA endocytosis but dominant negative Cdc42 only inhibited apical IgA endocytosis (Rojas et al., 2001).

B. Rho GTPases and Postendocytic Traffic

In addition to a role in endocytic internalization, the Rho family of small GTPases is also involved in postendocytic trafficking. Expression of dominant active RhoA in polarized MDCK cells altered traffic of basolaterally internalized markers but had no effect on apical recycling. In addition, basolaterally internalized IgA was trapped in basolateral early endosomes (see chapter 3). In contrast, dominant active Rac1 had no effect on basolateral traffic but did inhibit apically targeted

traffic. Basal to apical trancytosis of IgA, apical recycling of IgA and newly syntheiszed GP-135 were all trapped in central aggregate that corresponds in part to the ARE (see chapter 2). Expression of dominant active Cdc42 inhibited postendocytic traffic from both the apical and basolateral plasma membranes and dominant negative Cdc42 inihbited basal to apical transcytosis (Rojas et al., 2001).

Two members of the Rho family have been shown to localize to endocytic vesicles, RhoD and RhoB (Ridley, 2001; Van Aelst and D'Souza-Schorey, 1997). RhoD has been localized to early endosomes. Cells expressing dominant active RhoD exhibited decreased endosome motility but had little effect on the kinetics of transferrin endocytosis or recylcing. RhoD also altered endosome organization in the cell. RhoB has also been localized to endocytic vesicles. Examination by electron microscopy shows that RhoB is associated with multivesicular bodies. Furthermore, trafficking of the EGF receptor to lysosomes is regulated by RhoB.

Finally, the Rho family is co-opted by bacterial pathogens for both internalization and motility. The invasion of certain bacteria, such as *Salmonella* and *Shigella*, morphologically resembles FcR mediated phagocytosis Adherence of the bacteria to epithelial cells induces membrane protrusions that lead to entry into the cell. *Salmonella* injects a bacterial protein, SopE, that acts as a GEF for Cdc42 (Steele-Mortimer et al., 2000). *Shigella* introduces a complex of proteins that induce signal cascades resulting in activation of Src kinase and Rho family GTPases. Furthermore, *Shigella* uses APBP for motility in the cell cytoplasm through the binding and activation of N-WASP similar to Cdc42 (Steele-Mortimer et al., 2000). Recent experiments using *Xenopus* egg extracts have shown endogenous vesicles can use APBP for motility and this action is Cdc42-dependent (Taunton et al., 2000).

V. GOALS OF DISSERTATION RESEARCH

This dissertation examines several mechanisms involved in regulation of the endocytic pathway. An initial goal was to determine the organization of endosomes and define sorting of fluid and membrane at the apical pole of polarized epithelial cells. Comparison of the early endocytic pathway in nonpolarized cells and the basolateral early endocytic pathway of polarized epithelial cells revealed similarities. In both cases, fluid and membrane were both internalized and rapidly delivered to EE. Fluid remained within the EE while membrane is removed and delivered by microtubule dependent transport to a recycling compartment. I hypothesized that sorting of fluid and membrane at the apical pole of polarized epithelial cells is also similar to the mechanism in nonpolarized cells. Apically internalized fluid and membrane were rapidly sorted from each other in the AEE and membrane delivered via a microtubule dependent transport mechanism to the ARE. Furthermore, identification of biochemical markers for the compartments involved in endocytic sorting allowed for a more complete analysis of endosome organization along the apical endocytic pathway of polarized epithelial cells. The AEE was EEA1-positive (and presumably rab5-positive) and the ARE was rab11-positive. Finally, the relationship of these compartments with the basolateral recycling pathway was analyzed. Basolaterally recycling transferrin had access to the AEE but not the ARE. This led to the redefining of the ARE as a rab11-positive compartment that can be labelled kinetically only by apically internalized IgA.

The second goal was to examine the role of the Rho family of small GTPases in the regulation of endocytic and postendocytic traffic in polarized epithelial cells. The actin cytoskeleton has been shown to play a significant role in endosome movement. Extracellular signals are coupled to alterations in the actin cytoskeleton via the Rho family of small GTPases. Furthermore, more recent studies have demonstrated that the Rho family GTPases control a variety of cellular events including transcription, development and membrane trafficking. I hypothesized that RhoA and Rac1 are both involved in regulating endocytosis and postendocytic traffic. Expression of dominant active or

dominant negative mutants of Rho family GTPases in MDCK cells should alter trafficking. Expression of dominant active Rac1 (Rac1V12) and dominant negative Rac1 (Rac1N17) also altered endocytosis. Rac1V12 expression inhibited both apical and basolateral endocytosis while Rac1N17 stimulated them both. Expression of Rac1V12 also apically targeted traffic from both the biosynthetic and postendocytic pathways. This transport was blocked in a central aggregate composed of both the ARE and CE that formed when Rac1V12 is expressed. Similarly, dominant active RhoA (RhoAV14) stimulated both apical and basolateral endocytosis while dominant negative RhoA (RhoAN19) inhibited endocytosis. Futhermore, expression of RhoAV14 altered basolateral trafficking pathways in MDCK cells. This was due in part to trapping of markers within BEE possibly due to an increase of associated F-actin.

The third goal was to further analyze the function of the F-actin associated with BEE. One likely purpose for the associated F-actin is to provide a mechanism for endosome motility. Two models of actin-based transport have been proposed. APBP was first shown a mechanism for bacterial motility. Further studies have demonstrated that mammalian cells may use it for endosome movement. Alternatively, myosin motors have been linked to several transport mechanisms that use the actin cytoskeleton. To examine whether either of these models is involved in BEE motility, the distribution of proteins involved in either APBP or myosin based propulsion was analyzed. Proteins involved in APBP were not localized to BEE but instead where distributed to the corners (where three or more cells meet) of the lateral membrane. Analysis of MDCK cells by Western blot demonstrated that brush border myosin I (BBMI) and myosin Ic (MIc) are both endogenously expressed. MIc was localized to BEE but BBMI was not found there. This suggests that MIc may be involved in BEE transport.

The final goal was to examine the role of SNAP-23 in transferrin recycling. SNAREs have been shown to play a role in many fusion events. It has been previously suggested that a SNAP-25 like protein is involved in postendocytic trafficking in MDCK cells. Treatment of permeabilized

MDCK cells with BoNT/E, that specifically cleaves SNAP-25, inihibits both basolateral recycling and basl to apical transcytosis. SNAP-25 is not expressed in MDCK cells but recently, SNAP-23, a SNAP-25 homolog, has been found. Analysis of MDCK cells showed that SNAP-23 is expressed and sensitive to BoNT/E cleavage and SNAP-23 was shown to be required for basolateral transferrin recycling.

CHAPTER 1

Sorting of Membrane and Fluid at the Apical Pole of Polarized MDCK Cells*

ABSTRACT

When fluid-phase markers are internalized from opposite poles of polarized Madin-Darby canine kidney (MDCK) cells, they accumulate in distinct apical and basolateral early endosomes before meeting in late endosomes. Recent evidence suggests that significant mixing of apically and basolaterally internalized membrane proteins occurs in specialized apical endosomal compartments including the common recycling endosome (CE) or apical recycling endosome (ARE). The relationship between these latter compartments and the fluid-labeled apical early endosome is presently unknown. We report that when the apical recycling marker, membrane-bound IgA (a ligand for the polymeric immunoglobulin receptor; pIgR), and fluid-phase dextran are cointernalized from the apical pole of the MDCK cells they enter a shared apical early endosome (≤ 2.5 min at 37˚ C) and are then rapidly segregated from one another. The dextran remains in the large supranuclear EEA1-positive early endosomes while recycling pIgR-bound IgA is delivered to a Rab11-positive subapical recycling compartment. This latter step requires an intact microtubule cytoskeleton. Receptor-bound transferrin, a marker of the basolateral recycling pathway, has limited access to the fluid-rich apical early endosome but is excluded from the subapical elements of the Rab11-positive recycling compartment. We propose that the term ARE be used to describe the subapical Rab11-positive compartment and that the ARE is distinct from both the transferrin-rich CE and the fluid-rich apical early endosome.

* Reprinted from *Molecular Biology of the Cell*, (2000, volume 11, pg. 2131-2150), with permission by the American Society for Cell Biology

INTRODUCTION

Endocytosis is involved in multiple cellular functions including: recovery of exocytosed membrane, down-regulation of growth-factor receptors, modulation of channel/receptor recycling in response to extracellular signals, degradation of internalized particles, antigen presentation, and maintenance of cell surface polarity (reviewed in Mukherjee et al., 1997). Because inefficient sorting would disrupt normal cellular polarity and function, trafficking of proteins in the endocytic pathways is constantly modulated during development and in response to changes in the cell's extracellular milieu. Upon internalization, membrane and fluid are delivered to peripherally localized early endosomes. The small GTPase Rab5 and the Rab5 effector EEA1 are localized to these compartments (Gorvel et al., 1991a; Gorvel et al., 1991b; Stenmark et al., 1996). It is within the tubulovesicular elements of the early endosome that fluid (as well as ligands dissociated from their receptors) is segregated from membranous cargo that will recycle back to the cell surface. While dissociated ligands and fluid are delivered in a microtubule dependent process to late endosomes and then lysosomes, recycling receptors and bulk membrane can be delivered to a pericentriolar recycling endosome (reviewed in Mukherjee et al., 1997). The recycling endosome is comprised of 50-60 nm tubular elements and is involved in the delivery of recycling receptors to the cell surface. Rab11 has been localized to the recycling endosome and *trans*-Golgi network of non-polarized cells and transport between recycling endosomes and the plasma membrane is thought to require the Rab11 GTPase (Green et al., 1997; Ren et al., 1998; Ullrich et al., 1996).

Polarized epithelial cells have added complexity because they are capable of endocytosing macromolecules from either of their apical or basolateral plasma membrane domains (Bomsel et al., 1989). When fluid-phase markers are internalized for short periods of time from opposite poles of filter-grown Madin-Darby canine kidney (MDCK)[1] cells they label two spatially distinct populations of early endosomes: the peripheral basolateral early endosomes (BEE) that underlie the basolateral cell surface (up to the level of the tight junctions), and the corresponding apical

early endosomes (AEE) that lies between the apical plasma membrane and the Golgi complex (Bomsel et al., 1989; Parton et al., 1989). No mixing of fluid-phase markers is observed after incubation of ≤ 10 min at 37˚ C; however, mixing of internalized fluid-phase markers is observed in a shared supranuclear late endosomal compartment after ≥15 min at 37˚ C (Bomsel et al., 1989; Parton et al., 1989). The meeting of these markers is prevented in cells treated with the microtubule depolymerizing agent nocodazole.

Fluid-phase labeled AEE and BEE of MDCK cells are biochemically distinct. AEE and BEE, labeled with fluid-phase markers for 10 min at 37˚ C, do not fuse in a cell-free assay that reconstitutes endosome-endosome fusion, while homotypic BEE-BEE and AEE-AEE fusion is observed in this system (Bomsel et al., 1990). These observations led to the conclusion that no mixing of contents occurs between fluid-labeled AEE and BEE and that mixing only occurs in late endosomes. However, in both Caco-2 and MDCK cells, basolateral recycling transferrin (Tf) and its receptor have access to apical endosomal compartments that label with apically internalized membrane markers (Hughson and Hopkins, 1990; Knight et al., 1995; Odorizzi et al., 1996). In Caco-2 cells, this Tf-rich compartment is termed the common recycling endosome (CE)(Knight et al., 1995). A similar compartment is thought to exist in MDCK cells (Odorizzi et al., 1996). Moreover, the transcytotic movement of basolaterally internalized IgA, a ligand for the polymeric immunoglobulin receptor (pIgR), requires sequential traffic between BEE and an apical endosomal compartment termed the apical recycling endosome (ARE) (Apodaca et al., 1994; Barroso and Sztul, 1994).

Operationally, the ARE was originally defined as the endosomal compartment labeled with a 10-min pulse of an apically internalized membrane marker (Apodaca et al., 1994). The ARE is comprised of tubulovesicular elements that are found both above the nucleus in a supranuclear distribution and under the apical plasma membrane in a subapical distribution. The relationship between the supranuclear and subapical elements of the ARE is unclear. We suggested that the

ARE, as originally defined, might in fact represent several distinct compartments (Apodaca et al., 1994). It is known that the subapical elements of the ARE receive membrane, but little fluid. They are organized about the centrosome and are dispersed upon treatment with nocodazole, indicating that microtubules may be required for their organization. Tf is found in the supranuclear IgA-labeled elements of the ARE, but only limited colocalization of IgA and Tf is observed in the subapical elements of the ARE (Apodaca et al., 1994). Although the exact relationship of the CE and supranuclear and subapical elements of the ARE remains to be clarified, it is likely that the CE overlaps to some extent with the supranuclear elements of the ARE.

A confluence of recent data suggest that sorting of basolaterally internalized cargo may occur in multiple compartments (Brown et al., 2000; Gibson et al., 1998; Sheff et al., 1999). Initially, basolaterally internalized IgA, Tf, and fluid markers are delivered to BEEs (Apodaca et al., 1994; Brown et al., 2000). As these endosomes move toward the apical pole of the cell, the membrane markers are sorted away from fluid, and the IgA and Tf are directed to the supranuclear CE that also receives apically internalized membrane markers (Brown et al., 2000). Some Tf recycling may occur directly from the BEE (Sheff et al., 1999). It is within the tubular evaginations of the CE that Tf is packaged in 60-nm vesicles and recycled back to the basolateral cell surface (Odorizzi et al., 1996). The transcytosing IgA, sorted from Tf, is then delivered to the subapical elements of the ARE (Brown et al., 2000). Exit of IgA from the subapical elements of the ARE may be via C-shaped vesicles (Gibson et al., 1998). The similar pericentriolar, subapical distribution of Rab11 and Rab25 in MDCK cells suggests that these two GTPases may be markers of the subapical elements of the ARE (Casanova et al., 1999). Similarly, Rab 17 has been shown to label a series of subapical tubules and to colocalize with transcytosing IgA. As such, it too may be a marker of the subapical elements of the ARE (Hunziker and Peters, 1998; Zacchi et al., 1998).

While these observations define the sites of sorting along the basolateral pathway, there is relatively little known about the sites of sorting at the apical pole of the MDCK cell. The goal of this analysis was to answer the following questions: Is membrane and fluid segregated at the apical pole of MDCK cells? If so, in which compartment does this sorting occur? Are there markers associated with these compartments? What is the role, if any, of microtubules in the sorting process? Finally, what is the relationship of the fluid-phase labeled AEE and the supranuclear or subapical elements of the ARE or the Tf-rich CE?

RESULTS

Sorting of Apically Internalized Membrane and Fluid Markers Is Rapid at 37˚ C

To characterize potential sites for sorting we determined the kinetics of membrane and fluid segregation at the apical pole of MDCK cells. As a membrane marker we used apically internalized IgA, a ligand for the pIgR. Although the pIgR is cleaved at the apical pole of the MDCK cell, a significant fraction of the receptor escapes cleavage and can be internalized from the apical cell surface (Breitfeld et al., 1989b). pIgR-IgA complexes internalized from the apical pole of the cell are rapidly and efficiently recycled back to the apical pole of the cell (Apodaca et al., 1994; Breitfeld et al., 1989b) and as such are markers of the apical recycling pathway. Less than 3% of IgA internalized from the apical surface of the cell is transcytosed and released at the basolateral pole of the cell (Apodaca et al., 1994; Breitfeld et al., 1989b). As described previously, we used FITC-dextran as a marker of fluid-phase uptake (Apodaca et al., 1994).

In our first set of experiments we cointernalized IgA and FITC-dextran from the apical pole of the cell for a short pulse (2.5 min at 37˚ C) and determined if these markers colocalized or whether they were sorted from one another (Figure 1-1A-F). Colocalization was assessed by simultaneously acquiring dual-color fluorescent images of fixed and stained cells with a scanning

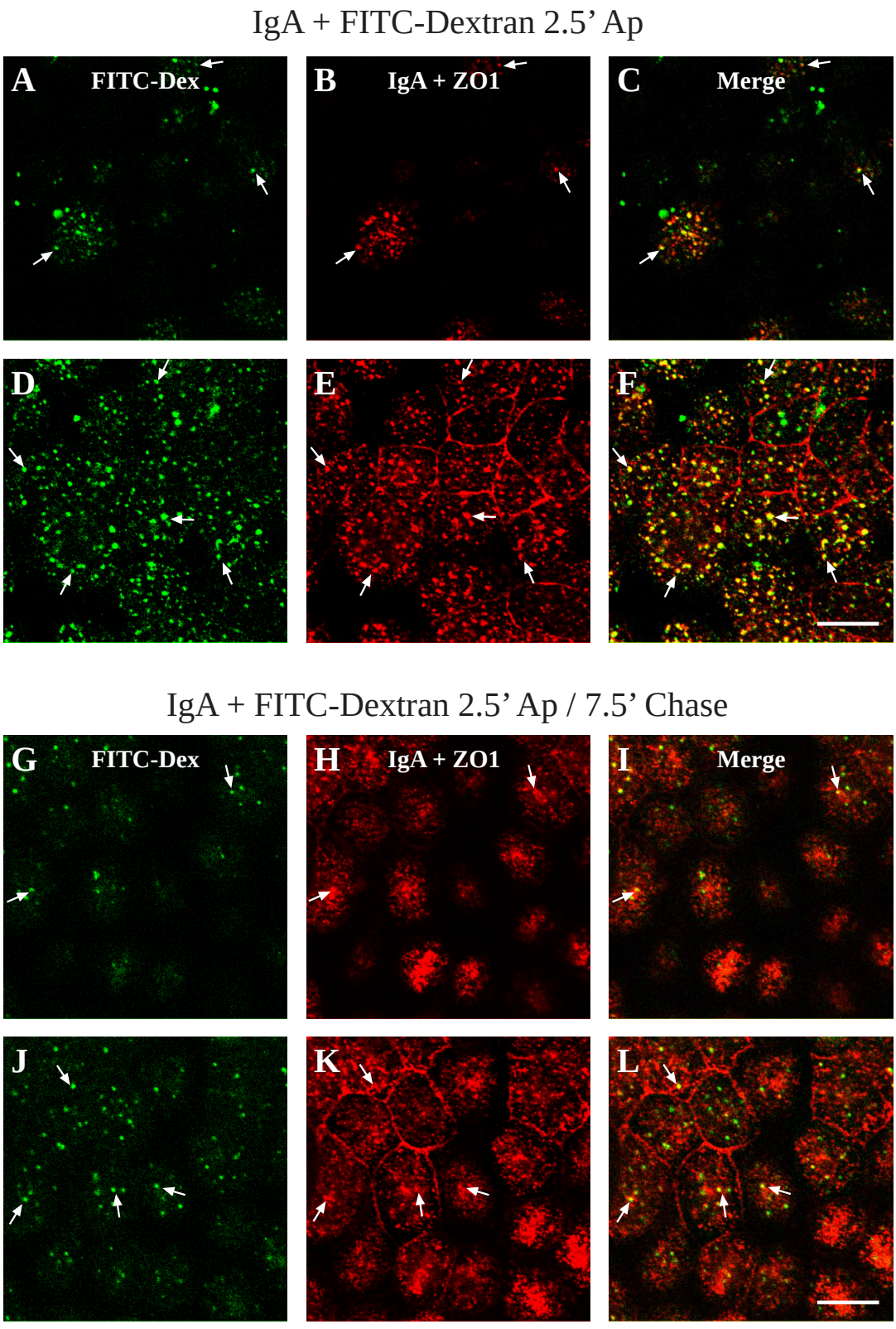

Figure 1-1. Distribution of IgA and FITC-dextran co-internalized from the apical pole of the cell

for 2.5 min at 37˚C (**A-F**) or a 2.5 min pulse followed by a 7.5 min chase at 37˚ C (**G-L**). Following IgA and FITC-dextran internalization, the cells were rapidly cooled, cell surface IgA was removed by trypsin treatment, and the cells were fixed with paraformaldehyde-lysine-periodate fixative. The fixed cells were incubated with IgA and ZO1 specific primary antibodies, and then reacted with CY5-labeled secondary antibodies. The CY5 signal is shown in the center panels, the FITC signal is shown in the left panels, and merged images of the CY5 and FITC signals are shown in the right panels. ZO1 appears as a thin red line at the periphery of each cell. Single optical sections, obtained with a confocal microscope, are shown from the apex of the cell (**A-C** and **G-I**) or at the level of the tight junctions (**D-F** and **J-L**). Note that the cells in the lower right corner of panels **A-L** are shorter than the cells in the upper left hand corner of these panels. Representative regions of colocalization are marked with arrows. Bar = 10μm

laser confocal microscope and digitally merging the images. Regions of colocalization appear yellow in the micrographs. The cells were also stained with an antibody that recognizes the tight-junction associated protein ZO1, as this structure serves as a convenient landmark to identify the border between the apical and basolateral plasma membrane domains. In this figure ZO1 appears as a thin red line that surrounds each cell. Shown are two optical sections (nominally 1.5 μm apart) taken from the apical pole of the cell (Figure 1-1A-F). Sections directly above the nucleus and from the lateral or basal pole of the cell are not shown as the majority of labeled structures were within 2-3 μm of the apical plasma membrane. When FITC-dextran and IgA were co-internalized for 2.5 min at 37˚ C a significant degree of colocalization of the two markers was observed in all focal planes. The labeled compartments had a vesicular appearance, were relatively large, and were concentrated in a supranuclear focal plane coincident with the brightest ZO1 staining (Figure 1-1D-F). There were few labeled structures in the apical-most sections (i.e those closest to the apical plasma membrane; Figure 1-1A-C). Although some IgA-labeled structures were found above the nucleus, little of the FITC-dextran was found in this position (data not shown). No staining of either marker was observed at the basal pole of the cell.

Sorting of the two markers became apparent when the 2.5 min pulse was followed by a 7.5 min chase in the absence of added marker. While a fraction of the IgA remained colocalized with the FITC-dextran in the larger vesicular endosomes (for example, see arrows in Figure 1-1 I & L), a larger fraction of IgA was associated with numerous fine punctae that did not colocalize with the FITC-dextran (Figure 1-1 I & L). Some of the IgA-labeled endosomes were in close proximity to the nucleus (data not shown). Unlike the shorter internalization protocol, IgA internalized using the pulse-chase protocol was localized to abundant small punctate structures that accumulated at the apical pole of the cell in a subapical distribution (Figure 1-1H). FITC-dextran labeled structures were less concentrated in these apical sections (Figure 1-1G). Sorting of the IgA and FITC-dextran

markers was also apparent when IgA and FITC-dextran were cointernalized for 5-10 min at 37˚ C. Again, IgA was found in small punctate structures that accumulated under the apical plasma membrane, most of which did not colocalize with FITC-dextran (data not shown).

Whereas IgA moved from supranuclear endosomes to a subapical endosomal compartment, we observed little difference in the distribution of the fluid-phase marker after a 2.5 min pulse ± a chase. In fact, if a 7.5 min pulse of Texas Red-dextran was followed by a 2.5 min pulse of FITC-dextran (in the continued presence of Texas Red-dextran), almost all of the labeled endosomal structures colocalized (data not shown). These results confirm that the distribution of the fluid-phase marker remains largely unchanged after a 10-min internalization period.

Sorting of Membrane and Fluid Markers Is Observed in Flotation Gradients and in Density-Shift Assays

To confirm that sorting had occurred under the conditions described above we analyzed the distribution of [^{125}I]IgA- and HRP-labeled endosomes in flotation gradients (Bomsel et al., 1990; Gruenberg et al., 1989). HRP is a classical marker of the fluid phase. [^{125}I]IgA and HRP were cointernalized for 2.5 min at 37˚ C from the apical pole of the MDCK cells and the cells were either rapidly chilled or incubated in marker-free medium for 7.5 min at 37˚ C. The cells were homogenized and the post nuclear supernatant from a low speed centrifugation was adjusted to 40.2% sucrose and overlaid with 35%, 25%, and 8.5% (w/w) sucrose. The samples were centrifuged and fractions were collected from each gradient. In these gradients, plasma membrane and Golgi are found at the interface between the 40.2% and 35% sucrose layers, while fluid-labeled early endosomes are found at the interface of the 35% and 25% sucrose layers. Late endosomes float to the interface between the 25%/8.5% sucrose layers (Gruenberg et al., 1989).

Following the 2.5 min chase at 37˚ C the majority of [^{125}I]IgA and HRP activity was found at the 35%/25% interface as expected for proteins residing in early endosomes (Figure 1-2A).

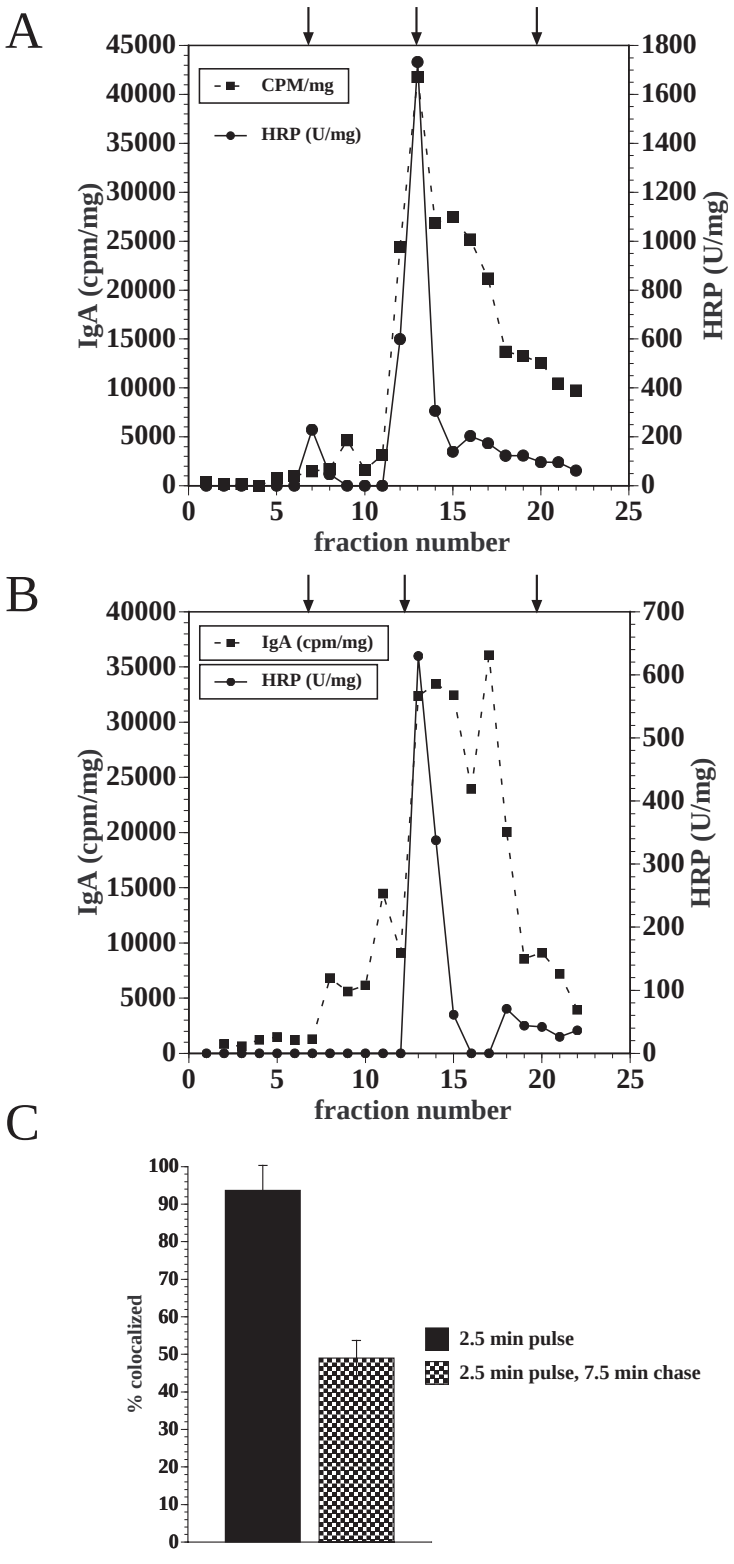

Figure 1-2. Colocalization of fluid and membrane markers assessed by sucrose flotation gradients and by density shift assays. (**A** & **B**) Sucrose flotation gradients. [^{125}I]IgA and 5 mg/ml

of HRP were co-internalized for 2.5 min at 37˚ C from the apical pole of the MDCK cells and the cells were either rapidly chilled (**A**) or chased in marker-free medium for 7.5 min at 37˚ C (**B**). The cells were homogenized, a postnuclear supernatant was generated, and the postnuclear supernatant (adjusted to 40.2% sucrose) was overlaid with 35%, 25%, and 8.5% (w/w) sucrose solutions. The samples were centrifuged and 0.45 ml fractions were collected from the top of the gradient. Samples of each fraction were assayed for protein content, associated [^{125}I]IgA cpm, and HRP activity. The interfaces between the 40.2% / 35% sucrose layers, the 35% / 25% sucrose layers, and the 25% / 8.5% sucrose layers are indicated, from right to left, by arrows atop the panels. Data from a representative experiment are shown. (**C**) Density shift assay. [^{125}I]IgA and 5 mg/ml of HRP were cointernalized for 2.5 min at 37˚ C from the apical pole of the MDCK cells and the cells were either rapidly chilled or chased in marker-free medium for 7.5 min at 37˚ C. Cell surface [^{125}I]IgA was removed by trypsin treatment at 4˚ C. A DAB reaction was performed, cells were lysed in detergent and the lysates centrifuged. Details of the quantitation are given in the Materials and Methods. Results are mean ± S.D. ($n \geq 3$).

While the HRP displayed a sharp peak, the [^{125}I]IgA peak trailed towards the denser fractions, suggesting that some sorting may have already occurred under these conditions. When the 2.5 min pulse was followed by a 7.5 min chase, segregation of the [^{125}I]IgA and HRP became more apparent (Figure 1-2B). While the HRP remained in a sharp peak at the 35%/25% interface, the peak of [^{125}I]IgA activity shifted toward the denser fractions. These observations are consistent with the morphological analysis presented above and provide evidence that fluid-phase markers remained in the AEE while pIgR-bound IgA was sorted and delivered to a physically distinct compartment.

Sorting of fluid and membrane markers was also confirmed by use of a modified density-shift assay (Apodaca et al., 1994). Based on the morphological data presented above one would predict that under short internalization conditions there would be maximal colocalization of the IgA and HRP. If the IgA was sorted away from the fluid marker during a subsequent chase, it is expected that there would be less colocalization of the two markers. [^{125}I]IgA and HRP were cointernalized for 2.5 min at 37˚ C and then either placed on ice or chased for an additional 7.5 min at 37˚ C. Following the pulse-chase protocol, cell surface [^{125}I]IgA was removed by trypsin treatment, and the cells were reacted with DAB reagent. In the presence of H_2O_2, the HRP catalyzes a reaction that crosslinks the contents of the HRP associated vesicles into a detergent insoluble complex that can be recovered by centrifugation. After a 2.5 min pulse approximately 95% of the [^{125}I]IgA was found in HRP-labeled endosomes (Figure 1-2C). In contrast, following the 7.5 min chase the amount of [^{125}I]IgA found in the HRP-labeled endosomes had decreased by 50%. These results are consistent with the morphological evidence presented above that fluid and membrane are delivered to a common AEE and then rapidly sorted from one another.

In summary, the above morphological, flotation gradient, and density shift data indicate that membrane and fluid markers are internalized into a shared endosomal compartment from which pIgR-IgA complexes are sorted. By convention we define this sorting compartment as the apical

early endosome (AEE). While the distribution of cell-associated FITC-dextran remained unchanged, pIgR-IgA was delivered to small vesicles which accumulated subapically. In this manuscript we define this downstream subapical compartment as the ARE.

EEA1 Is Localized to the AEE while the Pericentriolar ARE is Rab11 Positive

The next series of experiments focused on establishing the biochemical identity of the compartments in which recycling IgA was observed. It has previously been observed that Rab5 is associated with the early endosomes of MDCK cells (Bucci et al., 1994). We have used an antibody that specifically recognizes the early endosomal antigen EEA1. EEA1 is an effector of Rab5 function and is localized to Rab5-positive compartments (Simonsen et al., 1998). To label the AEE, IgA was internalized from the apical pole of the cell for 2.5 min at 37˚ C and the samples were then costained for IgA and EEA1. EEA1 was localized to large vesicular structures that were occasionally found at the base of the cell and along the lateral margins of the cell. The majority of EEA1 positive structures were found in the apical cytoplasm of the cell in a supranuclear position (Figure 1-3E), but were not abundant in the most subapical sections (Figure 1-3B). Many of the EEA1 positive structures overlapped with apically internalized IgA (Figure 1-3C& F). However, there were IgA-positive punctae that did not colocalize with the EEA1. The identity of these compartments is unknown but some of them could represent IgA in transit to the ARE or CE.

We confirmed, but do not show that AEE labeled with FITC-dextran (internalized from the apical pole of the cell for 10-min at 37˚ C) show extensive colocalization with EEA1. When a 2.5 min pulse of IgA was chased into the ARE (by incubating 7.5 min in the absence of ligand) there was little colocalization of the subapical IgA containing endosomes and EEA1 (Figure 1-3I). In the supranuclear sections there were larger IgA-labeled vesicular structures that colocalized with EEA1 and smaller ones that did not (Figure 1-3L). The above observations show that a subset of the IgA-labeled AEE colocalize with EEA1, but the subapical IgA-labeled ARE elements do not colocalize with EEA1.

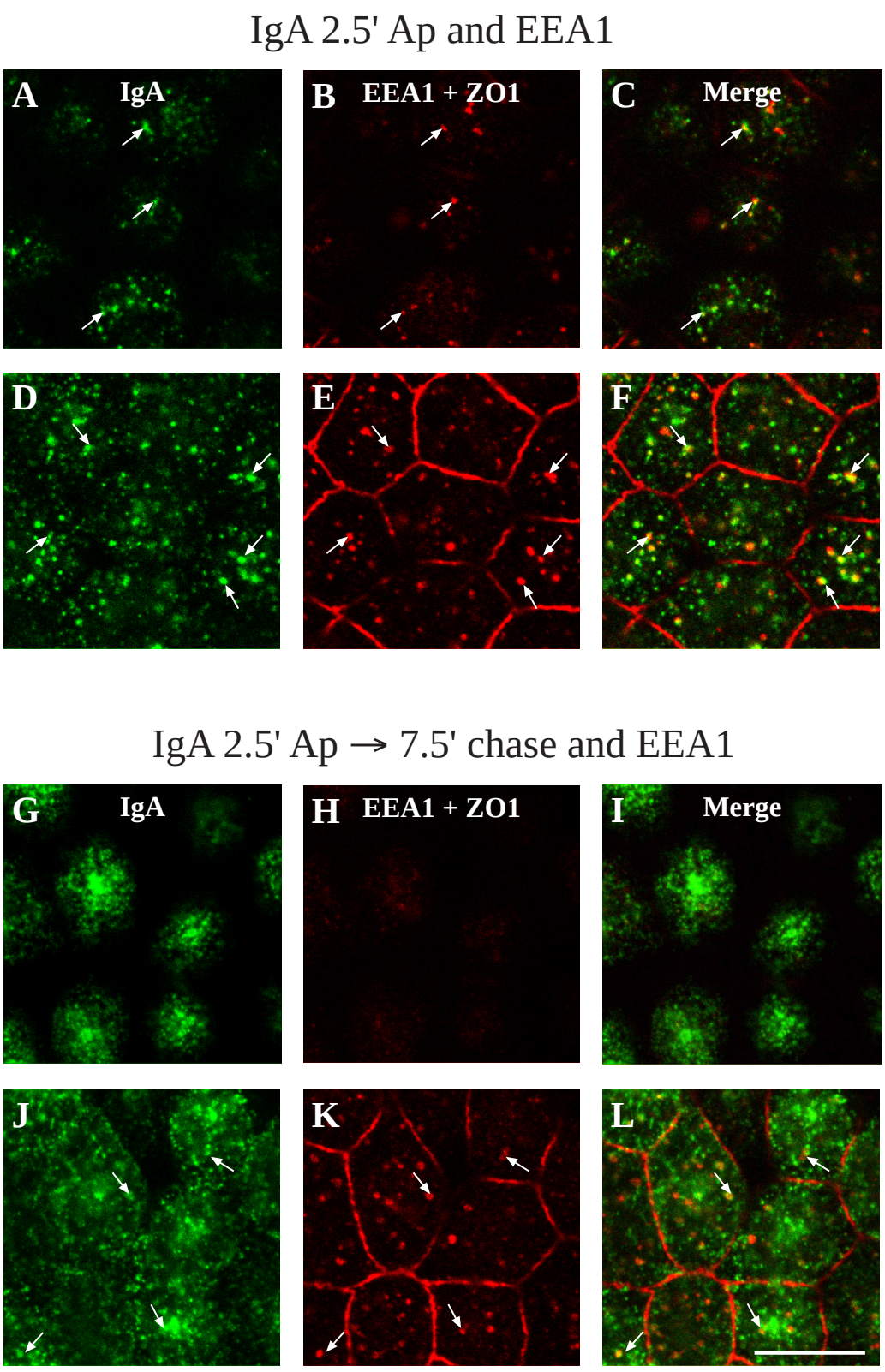

Figure 1-3. Distribution of EEA1 and apically internalized IgA in polarized MDCK cells. IgA

was internalized for 2.5 min at 37˚ C from the apical pole of the MDCK cells and the cells were either rapidly chilled (**A-F**) or chased in marker-free medium for 7.5 min at 37˚ C (**G-L**). Following IgA internalization, the cells were rapidly cooled, cell surface IgA was removed by trypsin treatment, and the cells were fixed using a pH-shift protocol. The fixed cells were incubated with primary antibodies directed against IgA, ZO1, or EEA1 and then reacted with either FITC- or CY5-labeled secondary antibodies. The FITC signal is shown in the left panels, the CY5 signal is shown in the center panels, and merged images of the FITC and CY5 signals are shown in the right panels. ZO1 appears as a thin red line at the periphery of each cell. Single optical sections, obtained with a confocal microscope, are shown from the apex of the cell (**A-C** and **G-I**) or at the level of the tight junctions (**D-F** and **J-L**). Representative regions of colocalization are marked with arrows. Bar = 10μm

Recent evidence indicates that Rab11 may be a marker of recycling compartments including the ARE (Casanova et al., 1999; Green et al., 1997; Ren et al., 1998; Ullrich et al., 1996). To determine if Rab11 was associated with the AEE or ARE we colocalized Rab11 with either IgA internalized for 2.5 min at 37˚ C, FITC-Dextran internalized for 10 min at 37˚ C, EEA1, or IgA internalized for 10 min at 37˚ C. As described above, AEE labeled with a 2.5 min pulse of IgA were found in a supranuclear distribution (Figure 1-4D) and were largely excluded from the apical most sections (Figure 1-4A). In contrast, Rab11 was associated with fine punctate elements that accumulated under the apical plasma membrane in a centralized distribution (Figure 1-4B) and at the apical margins of the cell (Figure 1-4E). Rab11 was not found in sections directly above the nucleus or at the basolateral pole of the cell (data not shown; see also Figure 1-8G). The distribution of Rab11 we report is similar to that described previously (Brown et al., 2000; Casanova et al., 1999). There was little colocalization of the AEE (labeled with a 2.5 min pulse of IgA) and the Rab11-positive compartment (Figure 1-4C & F). Moreover, there was little colocalization of Rab11 and FITC-Dextran internalized from the apical pole of the cell for 10 min at 37˚ C (data not shown), or of Rab11 and the EEA1 (Figure 1-4G-L). However, a small amount of the total Rab11 signal was associated with an occasional EEA1 positive endosome (Figure 1-4L).

Whereas there was little colocalization of Rab11 and IgA internalized for 2.5 min at 37˚ C, there was extensive colocalization of Rab11 and IgA, internalized for 10 min at 37˚ C (conditions under which large amounts of the IgA are present in the ARE). Both IgA and Rab11 were observed in the fine centralized array of subapical vesicles (Figure 1-5A-C). The extensive colocalization extended to deeper sections as well (Figure 1-5D-F). Similar results were observed when the distribution of Rab11 was compared to that of IgA pulsed for 2.5 min at 37˚ C and chased for 7.5 min at 37˚ C (data not shown). To confirm that Rab11 and recycling IgA were indeed colocalized we examined the distribution of IgA conjugated to HRP (internalized for 10 min at 37˚ C) and Rab11 by electron microscopy. The electron-dense reaction product produced by the IgA-HRP was

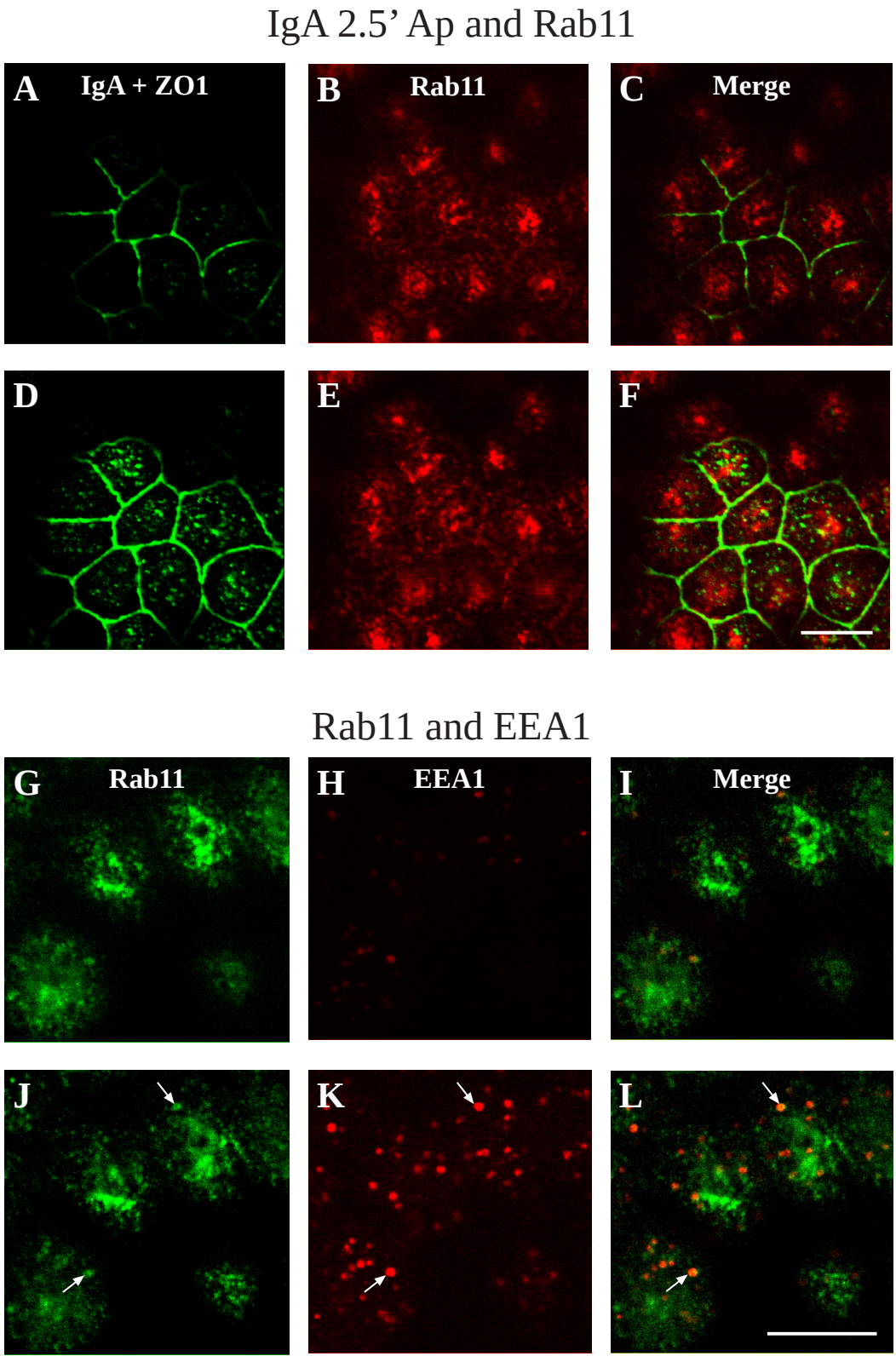

Figure 1-4. Distribution of IgA-labeled AEE, Rab11, and EEA1 in polarized MDCK cells. In (**A-**

F) IgA was internalized for 2.5 min at 37˚ C from the apical pole of MDCK cells. The cells were then rapidly chilled, cell surface IgA was removed by trypsin treatment, and the cells were fixed using a pH-shift protocol. In (**G-L**) the cells were immediately fixed. (**A-L**) The fixed cells were incubated with primary antibodies directed against IgA, Rab11, ZO1, or EEA1 and then reacted with either FITC- or CY5-labeled secondary antibodies. The FITC signal is shown in the left panels, the CY5 signal is shown in the center panels, and merged images of the FITC and CY5 signals are shown in the right panels. In (**A-F**) ZO1 appears as a thin green line at the periphery of each cell. Single optical sections, obtained with a confocal microscope, are shown from the apex of the cell (**A-C** and **G-I**) or at or near the level of the tight junctions (**D-F** and **J-L**). Representative regions of colocalization are marked with arrows. Bar = 10μm

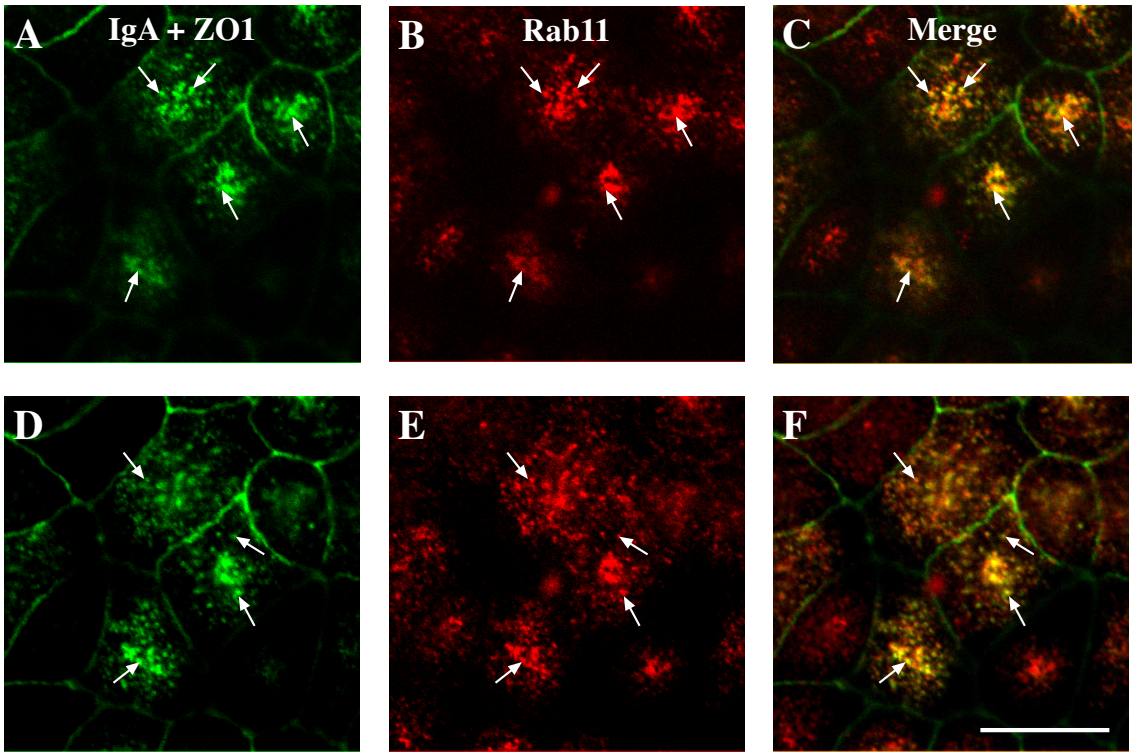

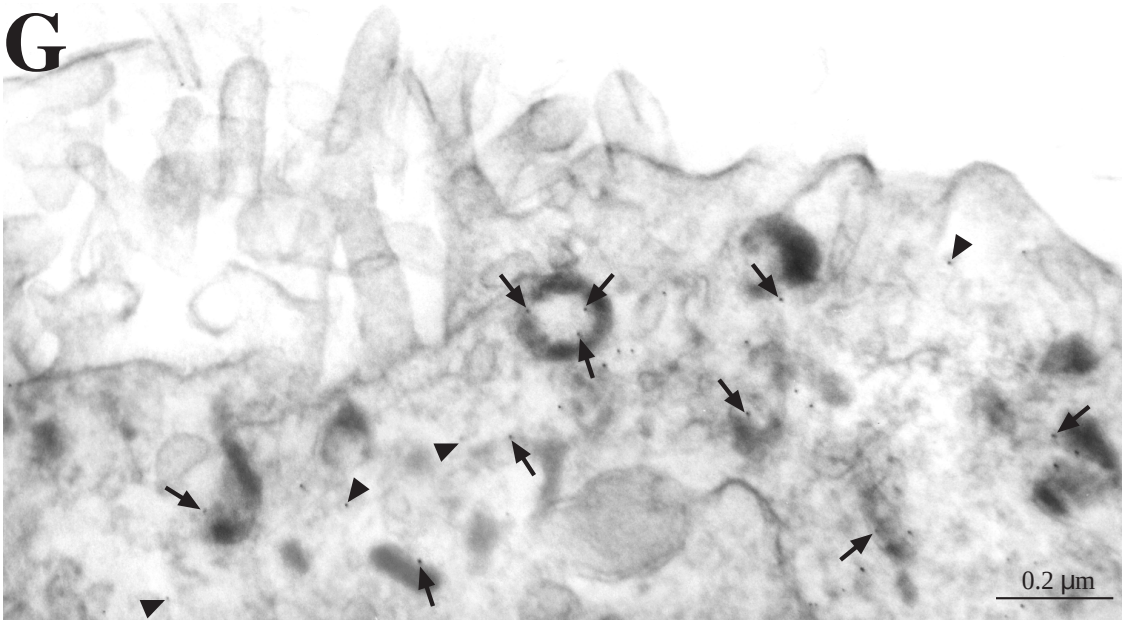

Figure 1-5. Distribution of IgA and Rab11 in polarized MDCK cells. (**A-F**) IgA was internalized from the apical pole of MDCK cells for 10 min at 37˚ C. The cells were then rapidly chilled, cell

surface IgA was removed by trypsin treatment, and the cells were fixed using a pH-shift protocol. The fixed cells were incubated with primary antibodies directed against IgA, Rab11, or ZO1 and then reacted with either FITC- or CY5-labeled secondary antibodies. The FITC signal is shown in the left panels, the CY5 signal is shown in the center panels, and merged images of the FITC and CY5 signals are shown in the right panels. ZO1 appears as a thin green line at the periphery of each cell. Single optical sections, approximately 1 μm apart, are shown from the apical region of the cell. Representative regions of colocalization are marked with arrows (bar = 10μm). (**G**) IgA-HRP was internalized from the apical pole of the cell for 10 min at 37˚ C, the cells were fixed using a pH-shift protocol, and a DAB reaction was performed. The cells were permeabilized with digitonin and then reacted with anti-Rab11 antibodies, followed by Protein A coupled to 5 nm colloidal gold particles. The cells were then processed for electron microscopy as described in the Materials and Methods. A semithick section (~ 250 nm) is shown. Legend: arrows, examples of structures in which IgA-HRP and rab-11 colocalize; arrowheads, examples of areas where Rab11 is found in the absence of IgA-HRP. Bar = 0.2μm

observed in short tubules, vesicles, and signet-ring elements that accumulated directly under the apical pole of the cell (Figure 1-5G). The morphology and distribution of these elements is similar to our previous characterization of ARE elements (Apodaca et al., 1994). Many of these IgA-HRP-labeled endosomes colocalized with Rab11 (identified using 5 nm gold; small arrows in Figures 1-5G). However, there were some Rab11-positive elements that were unlabeled with IgA-HRP (arrowheads in Figure 1-5G). The nature of these endosomes is unknown. Non-specific gold labeling of mitochondria or the nuclear membrane was not observed, nor was gold label associated with structures at the basolateral pole of the cell. Finally, no gold labeling was observed if the primary anti-Rab11 antibody was omitted in the staining protocol. The above observations indicate that the Rab11 compartment is distinct from the AEE, and is a reasonable marker of the recycling endosome through which IgA passes *en route* to the apical plasma membrane.

Entry into the Rab11 Compartment Requires an Intact Microtubule Cytoskeleton

We observed previously that the distribution of the ARE is altered in cells treated with the microtubule depolymerizing agent nocodazole (Apodaca et al., 1994). To determine if disruption of the microtubule cytoskeleton altered traffic from the AEE to the ARE we performed the following experiments. IgA and FITC-dextran were internalized from the apical pole of nocodazole- or mock-treated cells for 10 min at 37˚ C. In mock-treated cells IgA was found in the subapical elements of the ARE as well as in larger supranuclear vesicles. As described above the IgA present in the supranuclear vesicles colocalized with FITC-dextran (Figure 1-6D-F). In contrast, in cells treated with nocodazole there was extensive colocalization of the FITC-dextran and IgA in large vesicular structures that appeared randomly distributed in the apical cytoplasm (Figure 1-6I & L). We noticed that more FITC-dextran accumulates in cells treated with nocodazole. We believe this may reflect the slower exit of markers from the AEE – in part the result of inhibition of fluid transport along the degradative pathway. There were some IgA-positive vesicles that were not dextran positive. These could be IgA containing vesicles that were sorted from the dextran positive AEE and were in the process of recycling. To quantify these observations we measured the extent of HRP and ^{125}I[IgA]

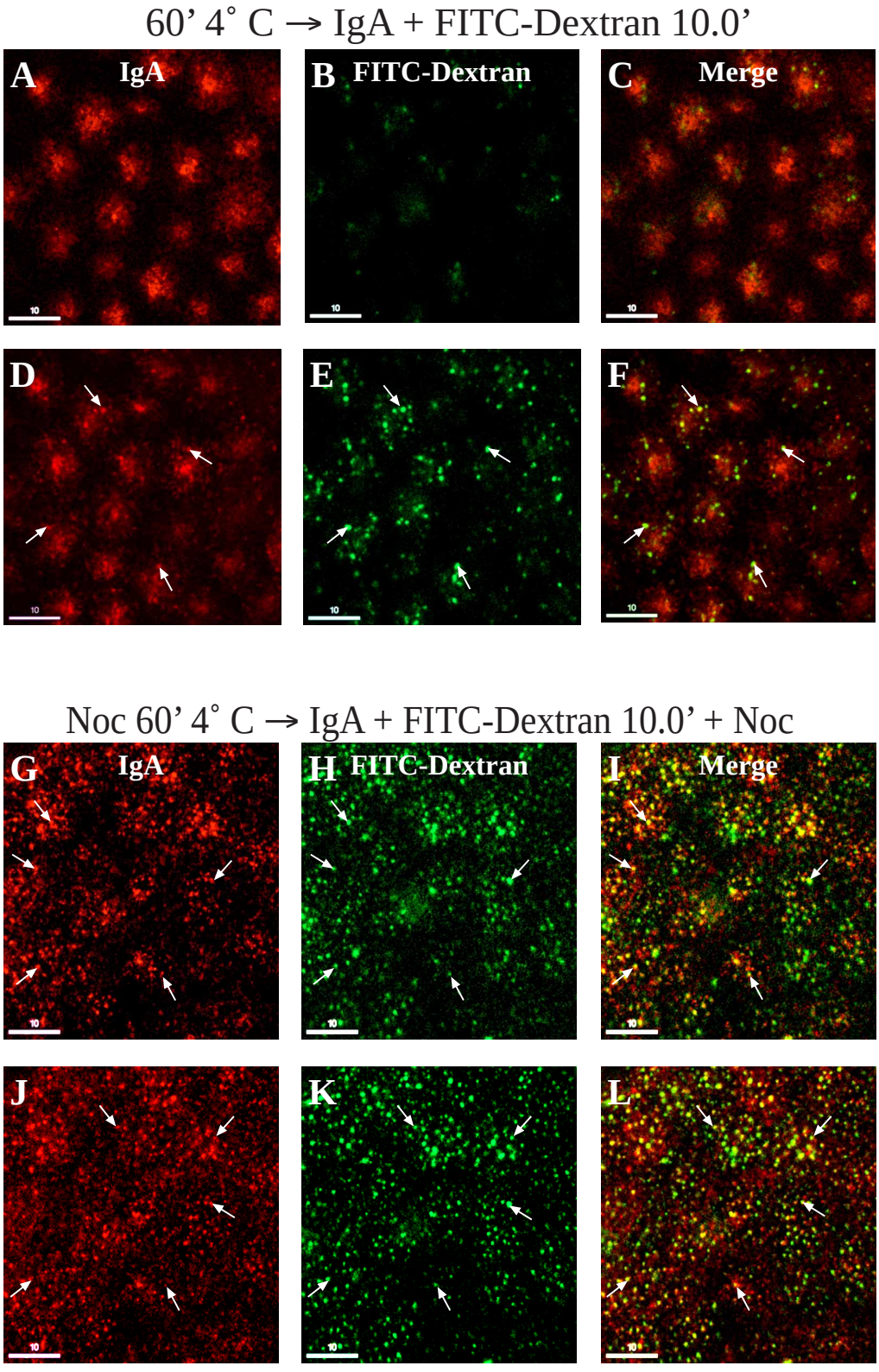

Figure 1-6. Distribution of IgA and FITC-dextran in control and nocodazole-treated cells. In (**A-F**) cells were incubated for 60 min at 4˚ C and then IgA and FITC dextran were co-internalized

for 10 min at 37˚ C from the apical pole of MDCK cells. In (**G-L**) cells were nocodazole-treated for 60 min at 4˚ C and then IgA and FITC dextran were co-internalized (in the continued presence of nocodazole) from the apical pole of the cell for 10 min at 37˚ C. (**A-L**) The cells were then rapidly chilled, cell surface IgA was removed by trypsin treatment, and the cells were fixed using a periodate-lysine-paraformaldehyde fixative. The fixed cells were incubated with primary antibodies directed against IgA and then reacted with CY5-labeled secondary antibodies. The CY5 signal is shown in the left panels, the FITC signal is shown in the center panels, and merged images of the CY5 and FITC signals are shown in the right panels. Single optical sections, obtained with a confocal microscope, are shown from the apex of the cell (**A-C** and **G-I**) or 1-2 μm below the level of the previous section (**D-F** and **J-L**). Representative regions of colocalization are marked with arrows. Bar = 10μm

colocalization in mock or nocodazole-treated cells using the density-shift assay described above. Following cointernalization (for 10 min at 37˚ C) we observed that 47.4±7.2% of the IgA colocalized with HRP in mock treated cells, while in nocodazole pretreated cells we observed that 88.2±7.1% of IgA colocalized with the HRP maker.

The above results indicate that either nocodazole treatment prevented efficient exit of IgA from the AEE, or that it caused the ARE elements to collapse into the AEE. To distinguish between these two possibilities, IgA was internalized for 10 min at 37˚ C from the apical pole of nocodazole-treated cells and the distribution of IgA and Rab11 was examined by confocal microscopy. We observed that there was little colocalization of IgA and Rab11 indicating that the Rab11 positive ARE elements had not collapsed into the AEE, and instead remained distinct (Figure 1-7C & F). If, however, IgA was internalized first and then cells were treated with nocodazole, there was significant colocalization of the Rab11 and IgA (Figure 1-7I & L). The results are consistent with the AEE being distinct from the ARE, and confirm that delivery of IgA from the AEE to the ARE requires microtubules.

The Rab11-Positive Compartment is Distinct From the Tf -Rich CE

We next examined the relationship of the Tf-rich CE and the EEA1-positive AEE or Rab11-positive ARE. Initially, we determined whether Tf and Rab11 colocalized. In fact, Tf was largely excluded from the apical most sections of the cell (Figure 1-8B), the sections where maximal staining of Rab11 was observed (Figure 1-8A). Even in supranuclear sections, little colocalization was observed between Rab11 and the large supranuclear Tf-rich endosomal elements (the rare regions of colocalization are noted in Figure 1-8F). While Tf-labeled endosomes were found in abundance just above the nucleus (Figure 1-8H), little Rab11 was found in this region of the cell (Figure 1-8H).

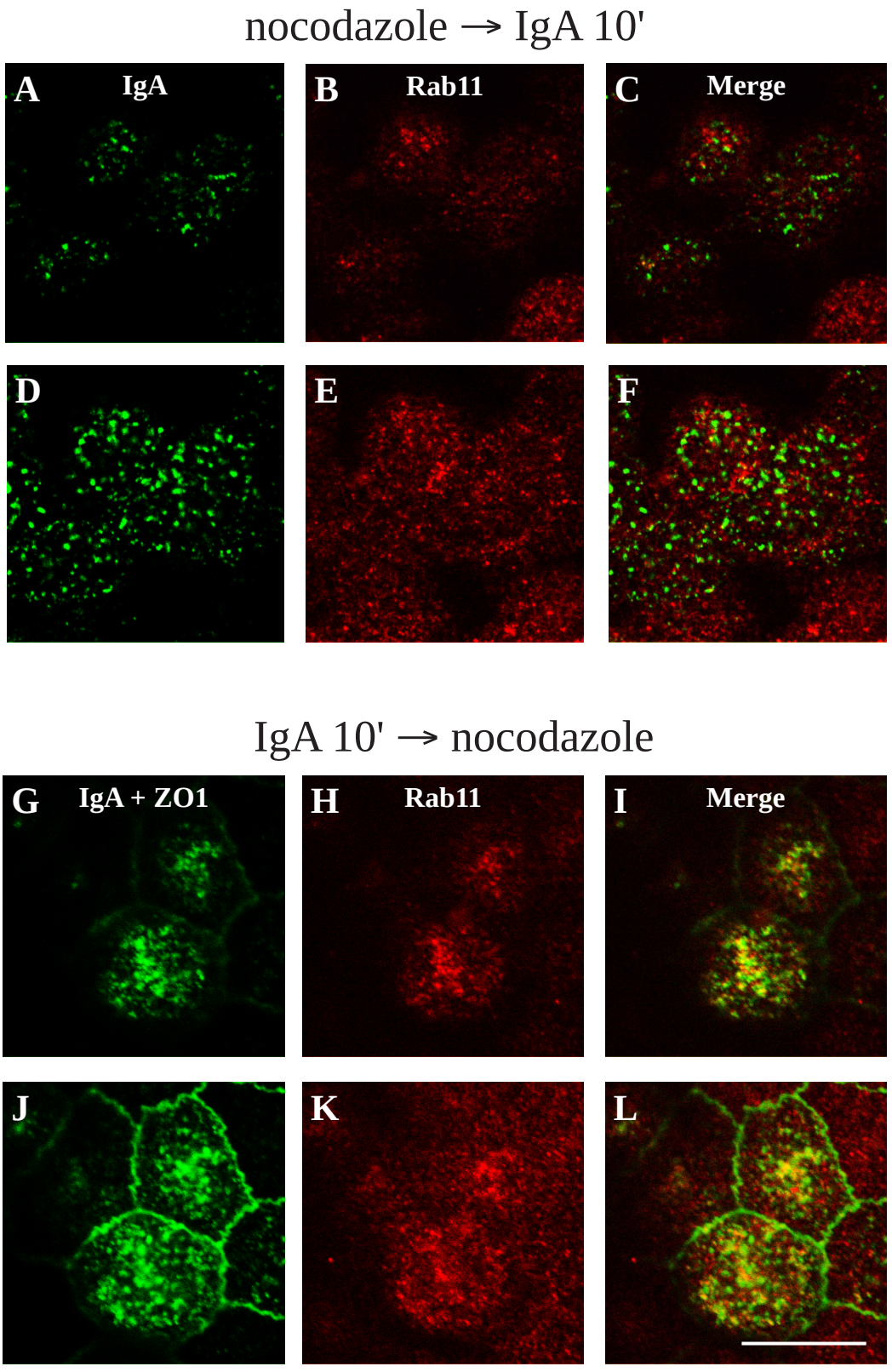

Figure 1-7. Distribution of Rab11 and IgA in nocodazole-treated cells. In (**A-F**) cells were

nocodazole-treated for 60 min at 4˚ C and then 10 min at 37˚ C. Subsequently, IgA and FITC dextran were co-internalized from the apical pole of MDCK cells for 10 min at 37˚ C in the continued presence of nocodazole. In (**G-L**) IgA was internalized from the apical pole of the cells for 10 min at 37˚ C. The cells were then rapidly chilled, nocodazole-treated for 60 min at 4˚ C, and then warmed up for 10 min at 37˚ C in the continued presence of nocodazole. (**A-L**) The cells were then rapidly chilled, cell surface IgA was removed by trypsin treatment, and the cells were fixed using a pH-shift protocol. The fixed cells were incubated with primary antibodies directed against IgA, Rab11, or ZO1 and then reacted with FITC or CY5-labeled secondary antibodies. The FITC signal is shown in the left panels, the CY5 signal is shown in the center panels, and merged images of the FITC and CY5 signals are shown in the right panels. In (**G-L**) ZO1 appears as a thin green line that surrounds each cell. Single optical sections, obtained with a confocal microscope, are shown from the apex of the cell (**A-C** and **G-I**) or at or near the level of the tight junctions (**D-F** and **J-L**). Representative regions of colocalization are marked with arrows. Bar = 10μm

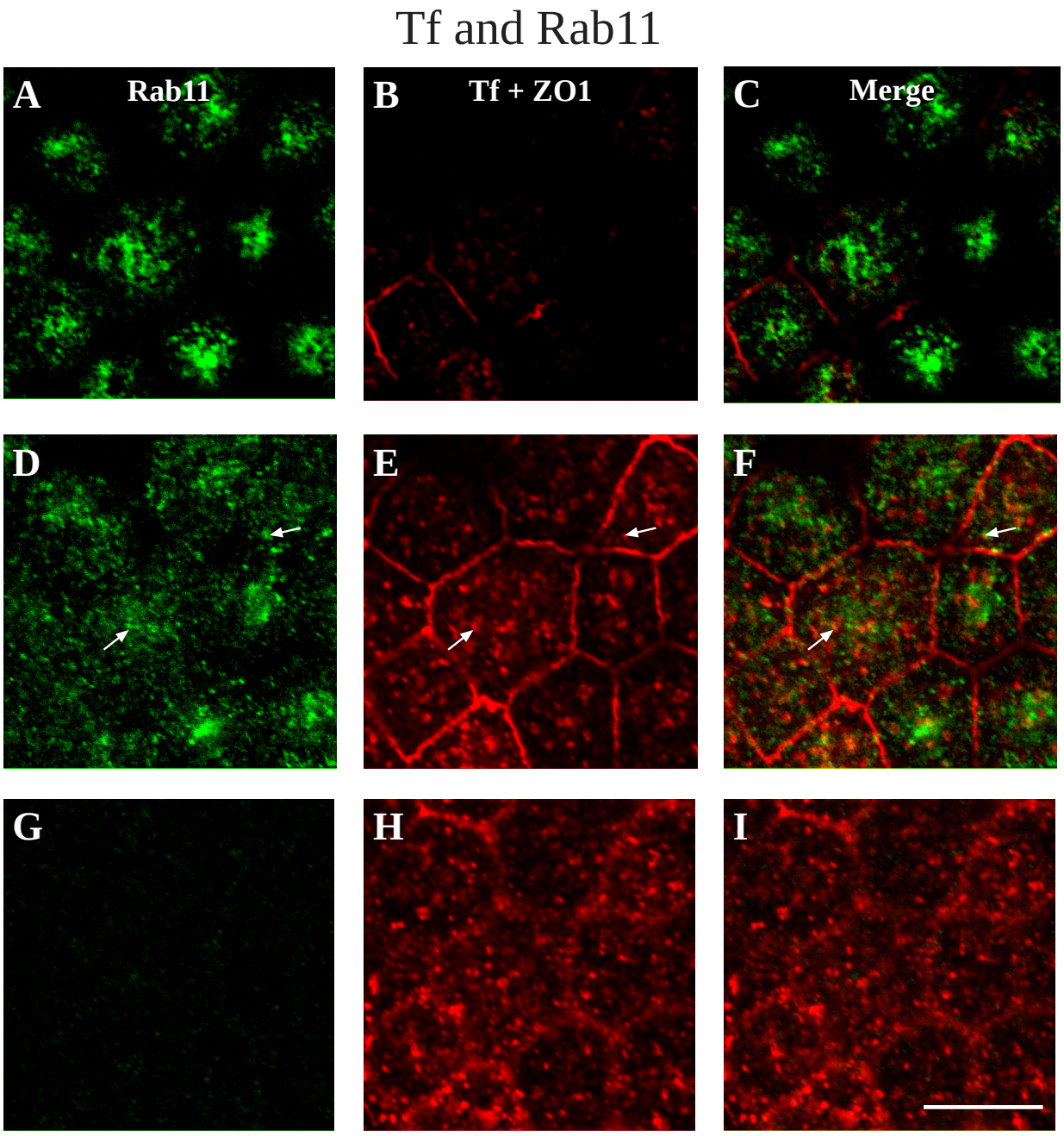

Figure 1-8. Distribution of Tf and Rab11 in polarized MDCK cells. (**A-I**) Tf was internalized from the basolateral pole of the cell for 30 min at 37˚ C. The cells were fixed and then incubated with primary antibodies directed against Rab11, ZO1, or Tf and then reacted with either CY5- or FITC-labeled secondary antibodies. The FITC signal is shown in the left panels, the CY5 signal is shown in the center panels, and merged images of the FITC and CY5 signals are shown in the right panels. ZO1 appears as a thin red line at the periphery of each cell. Single optical sections, obtained with a confocal microscope, are shown from the apex of the cell (**A-C**), at or near the level of the tight junctions (**D-F**), or directly above the nucleus (**G-I**). Representative regions of colocalization are marked with arrows. Bar = 10μm

We also determined if Tf colocalized with IgA-labeled ARE elements (labeled by pulsing with ligand for 2.5 min followed by a 7.5 min chase). While little colocalization was observed between IgA and Tf in the fine vesicular punctae at the apex of the cell (Figure 1-9C), some colocalization was observed between Tf and IgA in the large supranuclear structures that were deeper in the apical cytoplasm (Figure 1-9F). These large supranuclear IgA- and Tf-positive vesicles were reminiscent of the AEE elements described above.

To determine if Tf was present in AEE we analyzed the distribution of IgA-labeled AEE and Tf (Figure 1-10). The relationship of these markers and Rab11 was also assessed. Significant colocalization between IgA (internalized from the apical pole of the cell for 2.5 min at 37˚ C) and basolaterally internalized Tf was observed (see arrows in Figure 1-10 F-H and J-L). These data indicate that Tf had access to the AEE. We also observed that Tf colocalized to some extent with apically internalized FITC-dextran (data not shown), again confirming that Tf had access to the AEE. There were Tf-labeled endosomes that did not overlap with the AEE marker and these were found in supranuclear sections (Figure 1-10H), in sections directly above the nucleus (Figure 1-10L). These presumably represent elements of the Tf-rich CE. Tf was also found along the lateral margins of the cell (Figure 1-10P) and at the base of the cell (data not shown). As described above, the staining of the Tf-labeled structures or the IgA-labeled AEE did not overlap with that of the Rab11-positive ARE elements (Figure 1-10 D & H). Because localization of Tf with apically internalized fluid phase marker was surprising we confirmed this finding biochemically using the density shift assay described above. When [^{125}I]Tf was internalized basolaterally and fluid-phase HRP was cointernalized from the apical pole of the cell, colocalization of these two markers was observed. However, the percent of total internalized Tf present in the HRP-labeled AEE was modest (11.8 ± 1.9 %).

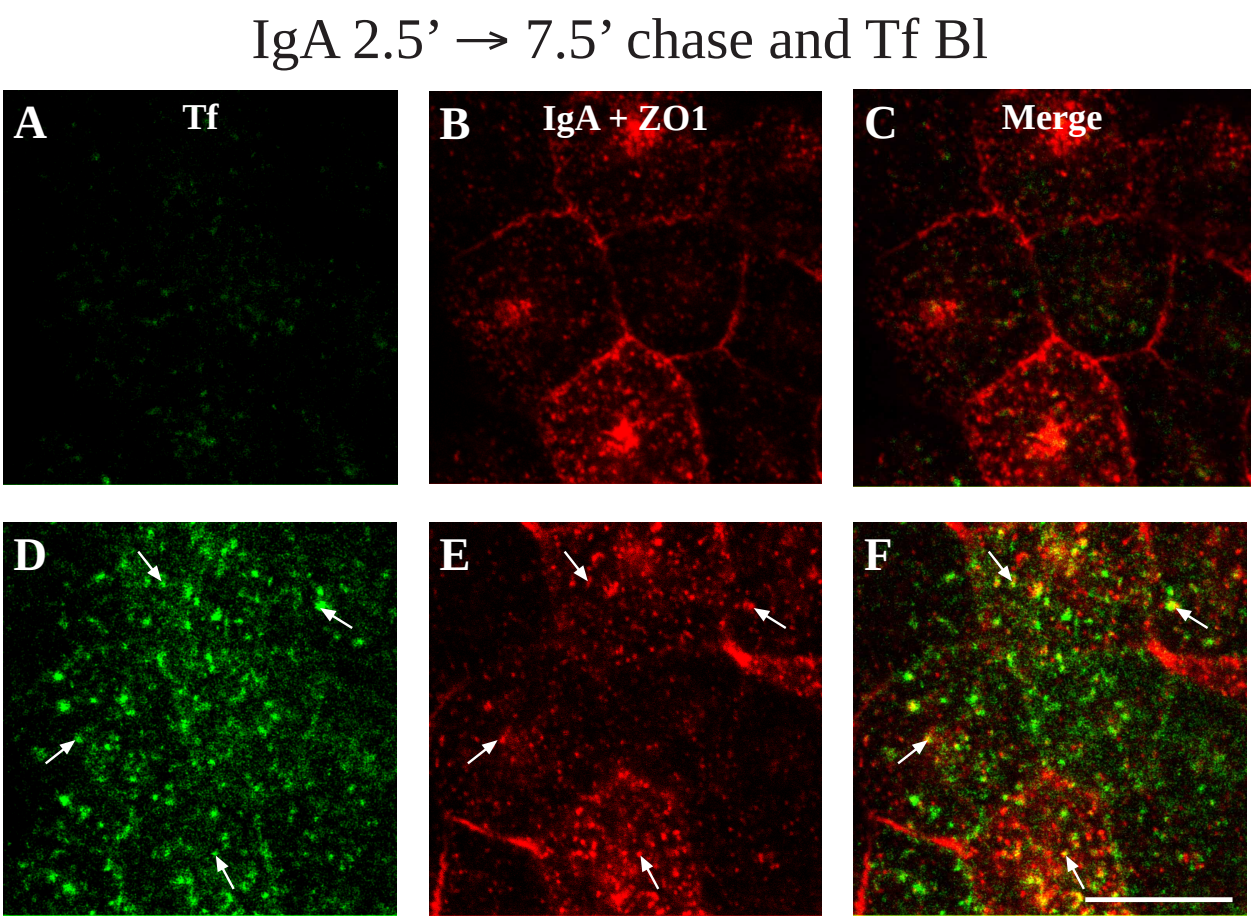

Figure 1-9. Distribution of Tf and IgA. IgA was internalized from the apical pole of the cell for 2.5 min at 37˚ C and then incubated in marker free medium for 7.5 min at 37˚ C. The cells were then rapidly chilled, cell surface IgA was removed by trypsin treatment, and the cells were fixed using a pH-shift protocol. The fixed cells were incubated with primary antibodies directed against IgA, ZO1, or Tf and then reacted with either CY5- or FITC-labeled secondary antibodies. The FITC signal is shown in the left panels, the CY5 signal is shown in the center panels, and merged images of the FITC and CY5 signals are shown in the right panels. ZO1 appears as a thin red line at the periphery of the cell. Optical sections are shown from the apical region of the cell just below the apical plasma membrane (**A-C**) or in sections near the level of the tight junctions (**D-F**). Representative regions of colocalization are marked with arrows. Bar = 10μm

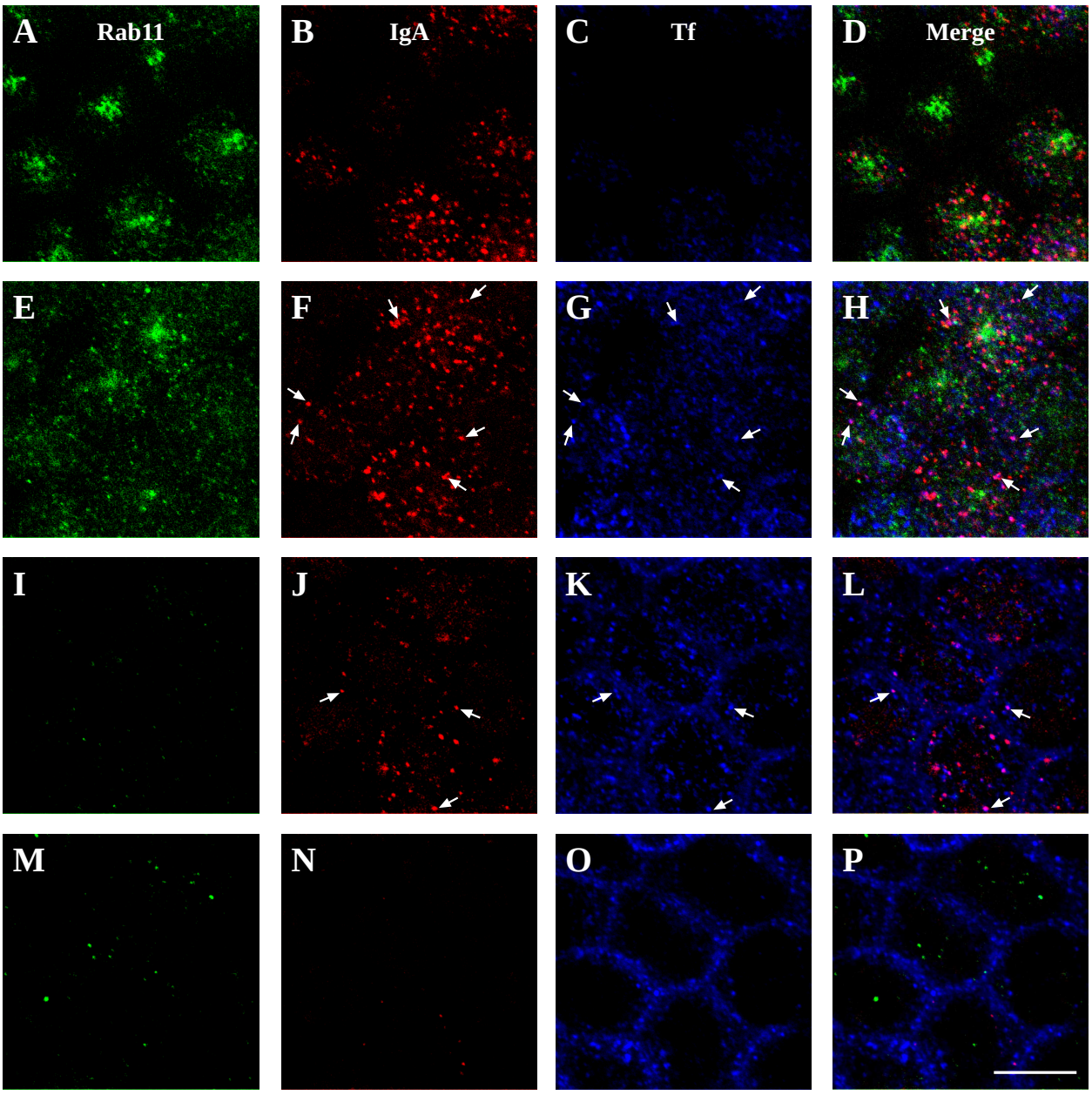

Figure 1-10. Distribution of Tf, IgA-labeled AEE, and Rab11 in polarized MDCK cells. Tf was internalized from the basolateral pole of the cell for 30 min at 37˚ C. During the last 2.5 min of this internalization period IgA was added to the apical pole of the cell. At the end of the experiment, the cells were rapidly chilled, cell surface IgA was removed by trypsin treatment, and the cells were fixed using a pH-shift protocol. The cells were incubated with primary antibodies directed against Rab11, IgA, or Tf and then reacted with either CY5-, CY3, or FITC-labeled secondary antibodies. The FITC signal (in green) is shown in the left panels, the CY3 signal (in red) is shown in the center left panels, the CY5 signal (in blue) is shown in the center right panels, and merged images of the FITC, CY3, and CY5 signals are shown in the right panels. Single optical sections, obtained with a confocal microscope, are shown from the apex of

the cell (**A-D**), at or near the level of the tight junctions (**E-H**), directly above the nucleus (**I-L**), or along the lateral margins of the cell near its base (**M-P**). Note that the cells in the lower right corner of panels **A-P** are taller than the cells in the upper left hand corner of these panels. Regions of colocalization between IgA and Tf appear magenta in the merged images, and representative regions of colocalization are indicated by arrows. Bar = 10μm

DISCUSSION

Understanding how polarized membrane domains are established and maintained requires an intimate knowledge of the membrane and solute trafficking pathways of the cell, the sites of sorting, and the mechanisms used to acutely and developmentally regulate these pathways. Past attempts at delineating the endocytic pathways of polarized cells were complicated by the use of either fluid or membrane markers, lack of agreement on what to call the labeled compartments, disagreements on the sites of sorting, and lack of compartment specific markers (Apodaca et al., 1994; Barroso and Sztul, 1994; Bomsel et al., 1989; Knight et al., 1995; Odorizzi et al., 1996; Parton et al., 1989; Sheff et al., 1999).

Sorting at the Apical Pole of Polarized MDCK Cells

We have carefully analyzed the pathways accessed by fluid and membrane markers at the apical pole of the MDCK cell and have defined potential sites for sorting and recycling. Moreover, we have identified markers that are associated with these compartments. We find that when fluid-phase FITC-dextran and receptor-bound IgA (a membrane marker) are cointernalized for short periods of time they are delivered to an apically distributed endosomal compartment, where they colocalize, and are then rapidly sorted from one another. Morphologically, this early compartment is comprised of relatively large vesicles that primarily reside in a supranuclear position. Because of its location, rapid filling with endocytosed fluid and membrane, and putatative role in sorting, we refer to this compartment as the AEE. Moreover, EEA1, an antigen associated with early endosomes is also localized to this compartment (see below).

While FITC-dextran (internalized from the apical pole of the cell for up to 10 min at 37˚ C) is only detected in the AEE, a significant fraction of internalized IgA is delivered to a downstream "recycling" compartment comprised of fine vesicular elements. Many of these small vesicles are in the same plane as the AEE, while the majority of them are found to accumulate directly under the

apical plasma membrane in a pericentriolar subapical distribution. This morphological finding was confirmed by cell fractionation and density shift assays. By convention we refer to this downstream subapical compartment as the ARE; it is apically distributed and receives apical recycling IgA from an upstream sorting compartment. Like many recycling compartments the ARE is Rab11 positive (Casanova et al., 1999; Chen et al., 1998; Green et al., 1997; Ren et al., 1998; Ullrich et al., 1996). As described below, some of the IgA may be delivered from the AEE to the CE. We note that the definition of ARE used in this manuscript is more restrictive than in our previous work in which we defined ARE as the endosomal compartment labeled with a 10-min pulse of an apically internalized membrane marker (Apodaca et al., 1994). As originally defined, the ARE would include the AEE and perhaps elements of the CE.

The mechanism of membrane and fluid sorting is unknown but might reflect the geometries of sorting endosomes. Membranous markers are thought to partition with the tubular aspects of the sorting endosome, while fluid is retained in the volume-rich vesicular portions of the endosome (reviewed in Mukherjee et al., 1997). By budding off the tubular portions of these endosomes in an iterative process it is possible to achieve high fidelity sorting of membrane and fluid (Dunn et al., 1989). In addition to sorting apical recycling molecules from fluid-phase molecules, we also observed that basolateral recycling Tf was delivered to the AEE. This was a surprising observation as it has not been shown previously that apically internalized fluid-phase markers mix with basolaterally internalized Tf. In fact, the presence of basolaterally internalized Tf and apical recycling IgA in this compartment suggests that it may in fact be a subdomain of the CE (Odorizzi et al., 1996). If so, the AEE may also play a role in recycling of basolaterally internalized proteins. Recycling may be via 60 nm vesicles that are coated with AP1 adaptor complexes (Futter et al., 1998). An alternative possibility is that the Tf found in the AEE is *en route* to the apical plasma membrane; approximately 5% of Tf is transcytosed and released at the apical pole of the cell (Fuller and Simons, 1986). This may explain why only a small fraction of the total cellular Tf colocalizes with HRP-labeled AEE in the density shift assays.

While our present results, and those of others, do not rule out that some sorting may occur in the ARE, they do suggest that much of the sorting of fluid and basolateral recycling markers occurs in compartments upstream of the ARE (e.g., in the AEE or CE). There is evidence that in hepatocytes sorting of membrane markers occurs in the so-called subapical compartment (Ihrke et al., 1998; van IJzendoorn and Hoekstra, 1998; van IJzendoorn et al., 1997). The relationships of the AEE and ARE to this compartment are unclear although they are likely to be related. In fact, the distribution of the hepatocyte subapical compartment and its lack of basolateral recycling markers suggests that it may be comprised in part of AEE- and/or ARE-like elements (Hemery et al., 1996; Ihrke et al., 1998; van IJzendoorn and Hoekstra, 1999). We previously suggested that the ARE is the polarized cell equivalent of the paracentriolar recycling endosome observed in non-polarized cells (Apodaca et al., 1994). This was based in part on the observations that both compartments are comprised of tubular elements, are organized about the centrosome, and receive cargo from upstream compartments. It is apparent from our current analysis that the ARE is in fact depleted of Tf and is therefore distinct from the Tf-rich recycling endosome observed in non-polarized cells.

Role for Microtubules in Delivery of Cargo to the ARE

In non-polarized cells, delivery of cargo from early endosomes to late endosomes requires an intact microtubule cytoskeleton (Gruenberg et al., 1989). Likewise, in polarized cells movement of cargo from the BEE to the apical pole of the cell requires microtubules (Apodaca et al., 1994; Brown et al., 2000; Hunziker et al., 1990). We report that traffic between the ASE and the ARE is blocked in cells treated with nocodazole. It was previously reported that apical recycling of IgA is slowed in cells treated with nocodazole (Breitfeld et al., 1990b). That IgA recycling is not completely inhibited by microtubule depolymerization indicates that passage through the ARE is not an obligatory step in the recycling process. In such cases, recycling may occur directly from the ASE, or some intermediate compartment. Similarly, recycling of Tf in non-polarized cells is apparently unaffected by nocodazole treatment (McGraw et al., 1993), possibly the result of direct recycling from early

sorting endosomes, as has been suggested recently (Sheff et al., 1999). If cargo can recycle directly from early endosomes then why deliver cargo to these recycling compartments at all? As described below the primary function of recycling compartments such as the ARE may be to modulate traffic flow to the cell surface. In the case of polarized epithelial cells, traffic to and from the apical cell surface must be highly regulated to preserve normal cellular function and maintenance of a polarized phenotype (Mostov and Cardone, 1995).

EEA1 is Associated with the AEE and Rab11 with the ARE

One of the most difficult challenges facing cell biologists studying endocytic traffic in polarized epithelial cells has been to descriminate between the various endosomal subcompartments. In the present study we have utilized antibodies that recognize endogenous EEA1 and Rab11. In MDCK cells, EEA1 is primarily associated with a population of large supranuclear vesicles in the apical cytoplasm of the cell. However, it is also found on the occasional basolateral vesicle. Notably, we observe that many of these supranuclear EEA1-positive vesicles receive membrane and fluid internalized from the apical pole of the cell for short pulses, consistent with these structures being AEE. The basolaterally distributed EEA1-positive vesicles are presumably performing a similar function at the basolateral pole of the cell. While EEA1 is not exclusively associated with the AEE, it is a convenient marker to discriminate between markers in the AEE, and those *en route* to or delivered to the ARE.

Our results further indicate that Rab11 may be a useful marker of the MDCK ARE. In non-polarized cells, Rab11 is primarily associated with the recycling endosome and, to a lesser extent, with the TGN (Casanova et al., 1999; Chen et al., 1998; Green et al., 1997; Ren et al., 1998; Ullrich et al., 1996). We find no evidence that Rab11 is associated with the TGN of polarized MDCK cells (our unpublished observations). Consistent with observations made in gastric parietal cells and recent reports in MDCK cells, we observe that Rab11 is associated with small tubulo-vesicles localized under the apical membrane (Brown et al., 2000; Casanova et al., 1999; Goldenring et al.,

1994). In MDCK cells these Rab11-positive endosomal elements receive apical recycling and transcytosing cargo from upstream sorting compartments (the AEE and CE, respectively)(this work and Brown et al., 2000; Casanova et al., 1999). We do not observe that endogenous Tf and Rab11 colocalize to any notable extent in polarized MDCK cells. It has been observed that Rab11 is associated with sucrose gradient fractions enriched in Tf-labeled recycling compartments (prepared from MDCK cells overexpressing the human Tf receptor)(Sheff et al., 1999). However, consistent with our observations, <<1 % of the total cellular Rab11 was associated with these gradient fractions; the vast majority of Rab11 had dissociated from the membrane and was found in other fractions in the gradient (Sheff et al., 1999). Moreover, colocalization of Rab11 and Tf is not observed in non-polarized MDCK cells (Brown et al., 2000).

In addition to Rab11, there is evidence that Rab17 and Rab25 may be associated with the ARE or a subdomain of this compartment (Casanova et al., 1999; Hunziker and Peters, 1998; Zacchi et al., 1998). Rab25 labels a subapical compartment directly below the apical plasma membrane (Casanova et al., 1999). Expression of a dominant active mutant of this protein slows transcytosis and apical recycling of IgA, but has no effect on basolateral recycling of Tf (Casanova et al., 1999). This result is consistent with our observation that Tf is largely excluded from the subapical elements of the ARE. There are light microscopy data that suggest that the distribution of Rab25 and Rab11 significantly overlap, but their distributions are not identical (Casanova et al., 1999). The relationship of the Rab17 compartments to those associated with Rab25 and Rab11 has not been assessed. The presence of multiple Rabs with overlapping distribution on subapical elements suggest that the ARE may in fact contain subdomains with specialized functions that remain to be described.

Model for Sorting at the Apical Pole of Polarized MDCK Cells

In summary, we propose the following model for endocytic traffic in polarized MDCK cells (Figure 1-11). Membrane and fluid, internalized from the apical pole of the cell, are rapidly delivered

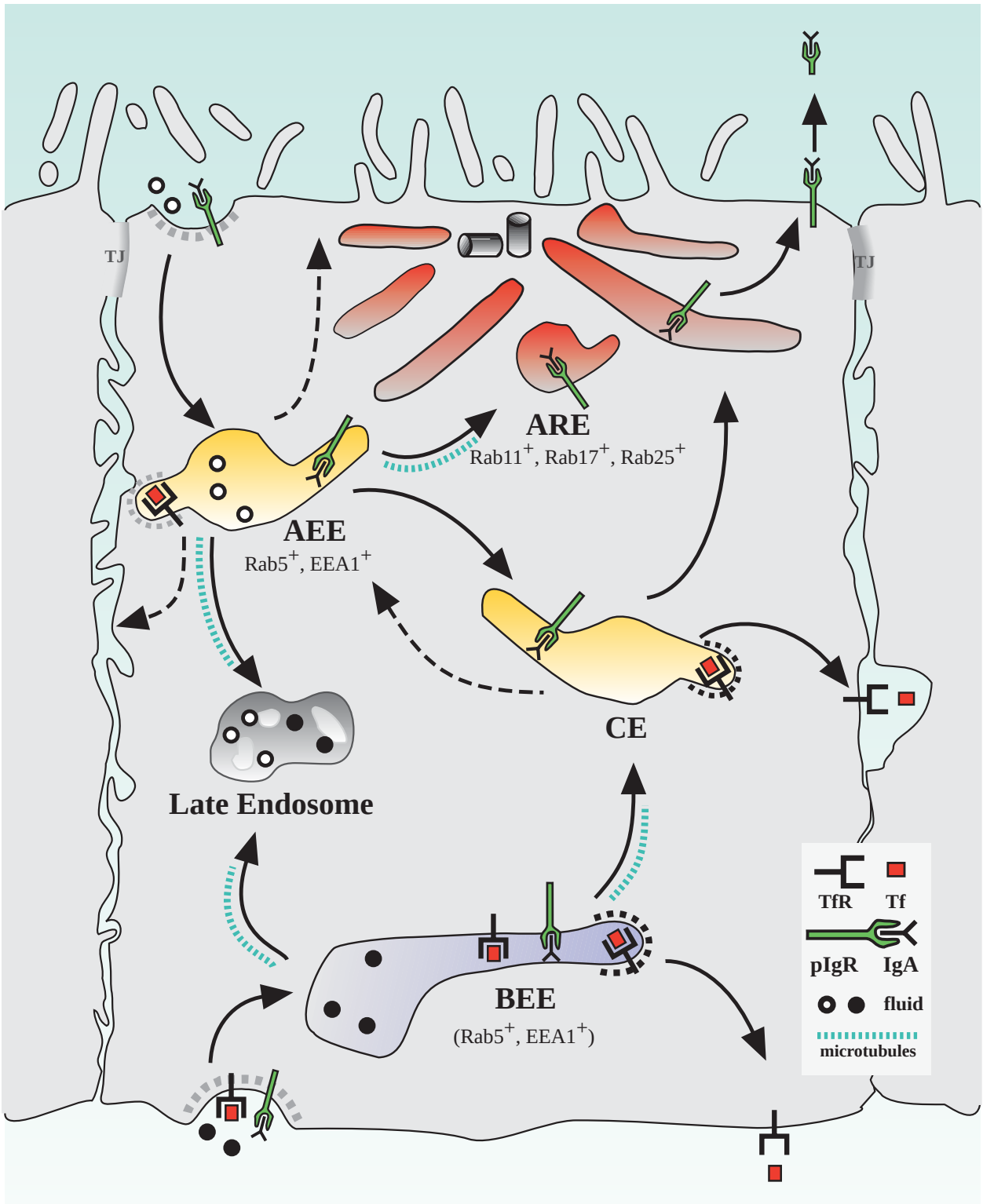

Figure 1-11. Model for endocytic traffic in polarized MDCK cells. Upon internalization, fluid and membrane are delivered to distinct AEE (step 1A) or BEE (step 1B). While some fluid can recycle or transcytose from these compartments, some is also delivered in a microtubule

dependent step to late endosomes (step 2A & 2B) and ultimately lysosomes (not shown). Apical recycling proteins are delivered to the ARE (step 3B) or the CE (step 3C) before their ultimate release from the apical pole of the cell (step 4). Some membrane/fluid may recycle directly from the AEE (step 3A). Basolateral recycling proteins (i.e. receptor bound-Tf) as well as proteins transcytosing in the basolateral to apical direction (i.e. pIgR-IgA) enter a shared BEE (step 1B). Although some receptor bound-Tf may recycle directly from this compartment (step 5B), a significant fraction is delivered to the CE along with the majority of the pIgR-IgA (step 5A). This translocation step is thought to require microtubules. The majority of the receptor bound-Tf is thought to recycle from the CE (step 6B), however, a fraction is delivered to the AEE (step 6C) and may recycle from this compartment (step 7). The transcytosing pIgR-IgA complexes, as well as apical recycling pIgR-IgA complexes, are delivered from the CE to the ARE (step 6A) and are ultimately released at the apical pole of the cell (step 4).

to the EEA1-positive AEE (Figure 1-11, step 1A). It is in this compartment that sorting of apical recycling and fluid-phase markers is thought to occur. While apically internalized fluid is thought to primarily recycle or transcytose (Bomsel et al., 1989), a fraction is delivered to late endosomes (step 2A) and ultimately to lysosomes. It is presently unclear if fluid markers recycle from the AEE or through the ARE. As little fluid is observed in the ARE, it is likely that recycling occurs directly from the AEE (step 3A). Likewise, some membrane proteins may recycle directly from the AEE. However, a significant fraction of recycling membrane proteins are delivered to the rab11-positive ARE (step 3B), or to the Tf-rich CE (step 3C). Delivery to the ARE apparently requires an intact microtubule cytoskeleton. The pathways taken by proteins transcytosing in the apical to basolateral direction is not well understood, but is likely to involve initial passage through the AEE.

In addition to receiving apical recycling proteins, the Rab11-, Rab17-, and Rab25-positive ARE also receives cargo transcytosing in the basolateral to apical direction (step 6A) (Apodaca et al., 1994; Barroso and Sztul, 1994). The presence of multiple Rab proteins on this compartment indicates that it may in fact be comprised of multiple subcompartments with specialized function. Exit from the ARE (step 4) may be via C-shaped vesicles (Gibson et al., 1998). While the ARE may have some role in sorting, we suggest that one of its primary functions may be to fine tune or regulate endocytic traffic specifically directed toward the apical pole of the cell. There is evidence in fact that multiple regulatory phenomena act at the level of the ARE. For example, ligand-stimulated transcytosis of basolaterally internalized pIgR, and protein kinase C-stimulated transcytosis and apical recycling are thought to occur at the level of the ARE (Cardone et al., 1994; Song et al., 1994). Future studies will delineate the role of Rab11, Rab 17, and Rab25 in ARE subcompartmentalization and function.

The basolateral recycling marker, Tf, has access to multiple compartments including the BEE, CE, and AEE. However, it is excluded from the ARE. Recycling of receptor-bound Tf may occur from BEE (step 5B) as well as from the CE (step 6B) (Brown et al., 2000; Gibson et al., 1998;

Odorizzi et al., 1996; Sheff et al., 1999). In addition, we observe that a small fraction of basolaterally internalized Tf has access to the AEE (step 6C). As such, the AEE may be a subdomain of the CE and may play a role in directing proteins to the basolateral pole of the cell (step 7). However, we can not rule out that the small amount of Tf found in the AEE represents ligand-receptor complexes that are trafficking towards the apical plasma membrane. At present it is difficult to define the boundries of the CE as there are no specific markers for this compartment. It has been hypothesized recently that the newly described AP1-B adaptor complex may play a role in basolateral delivery of proteins from both the TGN as well as endosomes (Fölsch et al., 1999; Mostov et al., 1999). By comparing the distribution of AEE and ARE markers with AP1-B positive endosomes (labeled with Tf), the relationship of these compartments may become clarified. Our analysis is a first step to dissecting the complex endosomal sorting events and subcompartmentalization that occurs at the apical pole of polarized MDCK cells.

CHAPTER 2

Selective Alterations in Biosynthetic and Endocytic Protein Traffic in Madin-Darby Canine Kidney Epithelial Cells Expressing Mutants of the Small GTPase Rac1*

ABSTRACT

MDCK cells expressing constitutively active Rac1 (Rac1V12) accumulate a large central aggregate of membranes beneath the apical membrane that contains filamentous actin, Rac1V12, rab 11, and the resident apical membrane protein GP-135 (Jou and Nelson, 1998, *J. Cell Biol*. 142: 85-100). To examine roles of Rac1 in membrane traffic and formation of this aggregate, we analyzed endocytic and biosynthetic trafficking pathways in MDCK cells expressing Rac1V12 and dominant inactive Rac1 (Rac1N17). Rac1V12 expression decreased the rates of apical and basolateral endocytosis, while Rac1N17 expression increased those rates from both membrane domains. Basolateral to apical transcytosis of IgA (a ligand for the polymeric immunoglobulin receptor, pIgR), apical recycling of pIgR-IgA, and accumulation of newly synthesized GP-135 at the apical plasma membrane were all decreased in cells expressing Rac1V12. These effects of Rac1V12 on trafficking pathways to the apical membrane were the result of delivery and trapping of these proteins in the central aggregate. In contrast to abnormalities in apical trafficking events, basolateral recycling of transferrin, degradation of epidermal growth factor internalized from the basolateral membrane, and delivery of newly synthesized pIgR from the Golgi to the basolateral membrane were all relatively unaffected by Rac1V12 expression. Rac1N17 expression had little or no effect on these post-endocytic or biosynthetic trafficking pathways. These results show that in polarized MDCK cells

activated Rac1 may regulate the rate of endocytosis from both membrane domains, and that expression of dominant active Rac1V12 specifically alters post-endocytic and biosynthetic membrane traffic directed to the apical, but not basolateral membrane.

* Reprinted from *Molecular Biology of the Cell*, (2000, volume 11, pg. 287-304), with permission by the American Society for Cell Biology

INTRODUCTION

The compartmentalized nature of the eukaryotic cell requires a highly regulated protein trafficking system to establish and maintain membrane, organellar, and cellular identity (Mostov and Cardone, 1995). As a result, the quality and quantity of biosynthetic and endocytic traffic must be capable of changing in response to extracellular signals. The Rho family of small GTPases represents an important class of molecules that can adjust cellular functions in response to a variety of extracellular signals (Van Aelst and D'Souza-Schorey, 1997). This family is presently comprised of at least seven members and their isoforms (Mackay and Hall, 1998): Rho (A, B, isoforms), Rac (1 and 2 isoforms), Cdc42 (Cdc42Hs and G25K isoforms), RhoD, RhoG, RhoE, and TC10. Initially, Rho family members were shown to regulate formation of specialized actin structures in the cell: RhoA controls the formation of stress fibers and focal adhesion (Ridley and Hall, 1992a), Rac1 directs lamellipodia formation (Ridley et al., 1992a), and Cdc42 modulates the assembly of filopodia (Kozma et al., 1995). In addition, it is now clear that the Rho family of GTPases controls diverse cellular events including transcription, cell growth, development, and membrane traffic (Hall, 1998; Van Aelst and D'Souza-Schorey, 1997; Vojtek and Cooper, 1995).

Multiple membrane trafficking events appear to be modulated by Rho family members, including phagocytosis of *Shigella* by RhoA (Adam et al., 1996; Watarai et al., 1997) and *Salmonella* by Cdc42 (Chen et al., 1996), pinocytosis by Rac1 (Schmalzing et al., 1995) and receptor-mediated by RhoA and Rac1 (Lamaze et al., 1996; Leung et al., 1999). RhoA may also regulate transcytosis and recycling in polarized MDCK cell (Leung et al., 1999). RhoB is localized to early endosomes and synaptic micro-vesicles (Adamson et al., 1992; Cussac et al., 1996), and RhoD is found on early endosomes and the plasma membrane (Murphy et al., 1996). Expression of constitutively active RhoD decreases endosome motility (Murphy et al., 1996). Rho family members also regulate secretion. In mast cells RhoA, Rac1, and Cdc42 stimulate exocytosis of secretory granules, while C-3 transferase and dominant inactive RhoA and Rac1 inhibit GTPγS-stimulated secretion (Brown et al., 1998; Mariot et al., 1996; Norman et al., ; Norman et al., 1996; O'Sullivan et al., 1996; Price

et al., 1995). New evidence indicates that Cdc42 may be important in regulating delivery of newly synthesized proteins to the basolateral domain of polarized Madin-Darby canine kidney (MDCK) epithelial cells (Kroschewski et al., 1999).

Recently, we analyzed the effect of expression of RhoA and Rac1 mutants on the development of polarity of MDCK cells (Jou and Nelson, 1998). Establishment and maintenance of epithelial cell polarity requires cell-cell and cell-substratum interactions, remodeling of the cytoskeleton, and the development of directionality in membrane trafficking pathways to the apical and basolateral membrane domains (Drubin and Nelson, 1996). During development of cell polarity, Rac1V12 expression caused the re-distribution of GP-135, an apical membrane protein, to a large central aggregate of membranes located beneath the apical membrane domain (Jou and Nelson, 1998). This aggregate contained Rac1V12 and filamentous actin. Significantly, we also detected the small GTPase rab11 in the aggregate; rab11 is normally found on the trans-Golgi network (TGN) and recycling endosomes, and is known to regulate endosome function (Casanova et al., 1999; Green et al., 1997; Ren et al., 1998; Ullrich et al., 1996; Urbé et al., 1993). The presence of rab11 on this central aggregate indicated that the aggregate may be an endosomal compartment and, therefore, Rac1 might have a previously unappreciated role in regulating endocytic membrane traffic. The goals of our current analysis were several-fold: to determine the origin of the large central aggregate in Rac1V12 expressing cells; to analyze the effects of Rac1V12 and dominant inactive Rac1 (Rac1N17) expression on biosynthetic traffic in MDCK cells; and to determine if constitutively active or dominant inactive Rac1 regulate endocytic traffic.

RESULTS

Induction of Rac1 Overexpression in Polarized MDCK Cells

Previously we established the T23 clone of MDCK cells that stably expresses the tetracycline transactivator (Barth et al., 1997). Subsequently, we generated clones of T23 cells in which expression

of either NH_2-terminal myc-tagged dominant active Rac1V12 or dominant inactive Rac1N17 was controlled by a tetracycline transactivator (Jou and Nelson, 1998). The T23 clone of MDCK cells also express pIgR.

Expression levels of Rac1V12 or Rac1N17 were controlled by addition of doxycycline (DC) to the growth medium. In the presence of 20 ng/ml of DC, neither western blotting (Figure 2-1) nor immunofluorescence microscopy (Figure 2-2) detected expression of either Rac1V12 or Rac1N17. However, in the absence of DC, western blotting showed that the amount of Rac1V12 expressed in cells 18h after plating on Transwells was ~80% of the level of endogenous Rac1, and after 36-48 h was ~50% (Figure 2-1). By 72 h, the amount of Rac1V12 expressed was undetectable (S.-M. Leung, unpublished results). This latter observation is consistent with our previous observations that the levels of these exogenous proteins is down regulated over time (Jou and Nelson, 1998). In the biochemical experiments described below we used cells 18-48 h after plating and obtained similar results; at these times polarized trafficking of proteins to apical and basolateral membrane domains occurs (Grindstaff et al., 1998b). The level of Rac1N17 expression was ~500% of that of endogenous Rac1, and remained at that level >48 h after plating cells on Transwells (Figure 2-1).

The Central Aggregate Observed in Rac1V12-Expressing MDCK Cells Primarily Contains Markers of the Early Endosomal System

To determine the origin of the membranous aggregate, we examined whether marker proteins of the ER, Golgi, TGN, early endosome, or late endosome/lysosome co-localized with Rac1V12 in this structure. The presence of any of these marker proteins in the aggregate might identify which membrane trafficking pathway(s) was affected by Rac1V12 expression.

Because the central aggregate contained rab11, a marker of endosomal recycling compartments (Casanova et al., 1999; Green et al., 1997; Ren et al., 1998; Ullrich et al., 1996), we

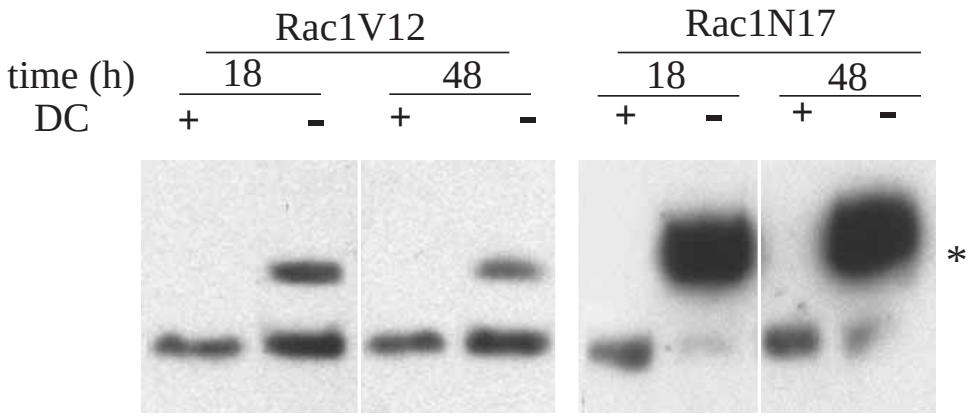

Figure 2-1. Inducible expression of myc-tagged Rac1V12 and Rac1N17 in polarized MDCK cells. Rac1V12 or Rac1N17 cells were plated at low density in medium lacking DC (-) or containing DC (+), incubated for 16-20h (Rac1N17) or 36h (Rac1V12), and then plated on Transwell filter supports (± DC). At the designated time point the filter-grown cells were solubilized in SDS lysis buffer and processed for Western blotting with an anti-Rac1 monoclonal antibody to detect induction of the myc-tagged mutant proteins as well as endogenous Rac1. * The addition of the myc tag to Rac1V12 and Rac1N17 causes these proteins to migrate slower than endogenous Rac1.

first examined the distribution of several marker proteins of the endocytic pathway in Rac1V12 and Rac1N17 expressing cells, including: (i) basolaterally internalized IgA (a pIgR ligand), which is transported to the apical cell surface via a series of endosomal compartments including basolateral early endosomes, the common endosome (Odorizzi et al., 1996), and the apical recycling endosome (ARE) (Apodaca et al., 1994); (ii) basolaterally internalized transferrin, which recycles back to the basolateral membrane (Fuller and Simons, 1986) from the basolateral early endosomes and the common endosome (Sheff et al., 1999); (iii) apically internalized IgA, which primarily recycles back to the apical membrane (Apodaca et al., 1994); and (iv) the Ac17 antigen, which recognizes a lysosomal membrane protein that is found primarily in late endosomes, lysosomes and basolateral early endosomes (Nabi et al., 1991).

To determine if IgA is delivered to the central Rac1V12 aggregate, we followed the fate of IgA internalized from the basolateral membrane of control cells and cells expressing Rac1V12. In control cells grown in the presence of DC, IgA was rapidly delivered to the apical pole of the cell where it was found in punctate membrane structures that lie above the nucleus and at the level of the tight junction (Figure 2-2A & B). These structures have previously been characterized as elements of the common endosome/ARE (Apodaca et al., 1994; Barroso and Sztul, 1994; Odorizzi et al., 1996). As expected, we did not detect myc-tagged Rac1V12 in these cells (Figure 2-2A-D, left panels). In contrast, in cells expressing Rac1V12 (grown in the absence of DC), IgA was found not only in a centralized distribution characteristic of the ARE (Figure 2-2E), but also in the Rac1V12-positive aggregate (Figure 2-2F). In a kinetic analysis we determined that basolaterally internalized IgA reached the central aggregate in as little as 5 min at 37˚ C (S.-M. Leung, unpublished results). Moreover, entry of IgA into the central aggregate did not require passage through the apical plasma membrane (S.-M. Leung, unpublished results). Little IgA was found concentrated at either the lateral or basal membranes (Figure 2-2G & H), indicating that internalized ligand had not been trapped in basolateral early endosomes. Rac1V12 was distributed at the lateral membrane, and in a cluster at the very apex of the cell. In many, but not all cells, Rac1V12 was also associated with the

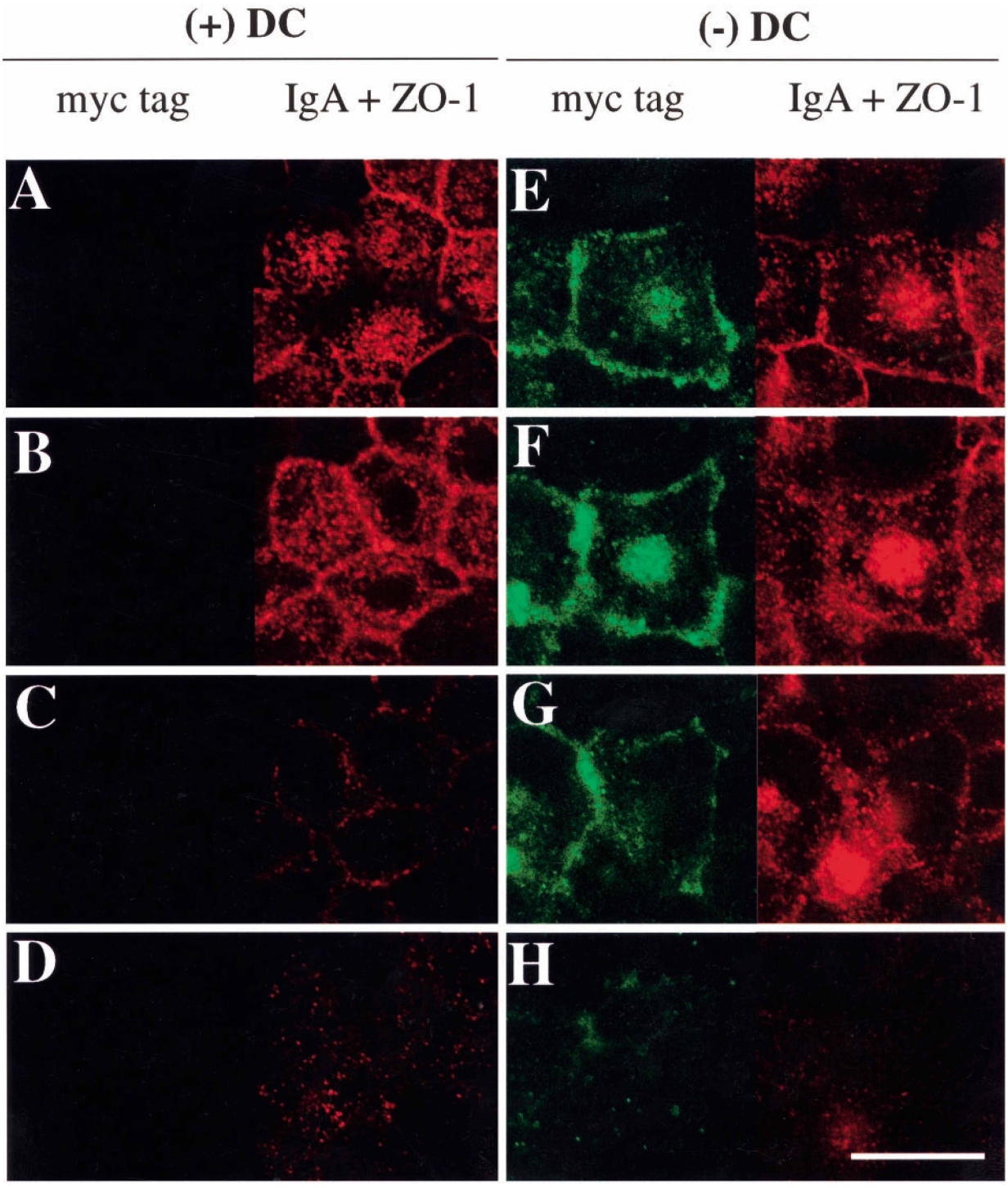

Figure 2-2. Distribution of basolaterally internalized IgA and myc-tagged Rac1V12 in cells grown in the absence or presence of DC. IgA was internalized from the basolateral surface for 10 min at 37˚ C in Rac1V12 cells grown in the presence (panels **A-D**) or absence (panels **E-H**) of DC, and then washed and chased for 5 min at 37˚ C. Cells were fixed with paraformaldehyde, stained with the appropriate antibodies, and FITC and CY5 emission (which are displayed in the

left and right halves of each panel, respectively) captured using a scanning laser confocal microscope. Shown are optical sections from the base of the cells (**D&H**), along the lateral surface of the cells (**C&G**), above the nucleus (**B&F**), and at or above the level of the tight junctions (**A&E**). Note that there is at least 2-3μm between each optical section. The tight junctions are the thin red lines that surround the cell. Bar=10μm

central aggregate where it overlapped with punctate structures containing IgA (Figure 2-2E). Rac1V12 was also found in small punctate structures at the base of the cell (Figure 2-2H, left panel). There was no effect of Rac1N17 expression on the distribution of internalized IgA.

In addition to basolaterally internalized IgA, we observed that basolaterally internalized Tf was also highly concentrated in the central aggregate of Rac1V12-expressing cells (Figure 2-3A-C). In fact, after a short pulse (10 min) the majority of the internalized Tf appeared within the central aggregate. Much, but not all of the Tf within the aggregate colocalized with membranous elements containing basolaterally internalized IgA (see arrows in Figure 2-3A-C). Apically internalized IgA, a marker for the apical recycling pathway, was also delivered to the central aggregate within 15 min of being internalized (data not shown). In contrast to these early endosomal markers, the Ac17 positive compartments (predominantly late endosomes and lysosomes) were found to surround the IgA-positive central aggregate but were rarely seen to be incorporated into this structure (Figure 2-3D-F). The distributions of these markers were unaltered in cells expressing Rac1N17.

Next, we assessed the distribution of marker proteins of the ER, Golgi, and TGN in cells expressing Rac1V12. In both control and Rac1V12 expressing cells, the ER resident protein mp30/ BAP31 (Annaert et al., 1997) was distributed throughout the cell cytoplasm, but in cells expressing Rac1V12 the ER was excluded from the region of the central aggregate (Figure 2-3G-I). In control cells, giantin, a resident Golgi protein (Lindstedt and Hauri, 1993), was distributed in a ribbon-like structure that localized between the nucleus and apical membrane. In Rac1V12 expressing cells giantin-labeled Golgi appeared to be excluded from, and generally surrounded the central aggregate (data not shown). In many cells Furin, a marker protein of the TGN (Molloy et al., 1994), was excluded from the central aggregate (Figure 2-3J-L). Although, an occasional furin positive TGN ribbon was found within the central aggregate of some Rac1V12-expressing cells. The distributions of marker proteins of the ER and Golgi were unaffected in cells expressing Rac1N17.

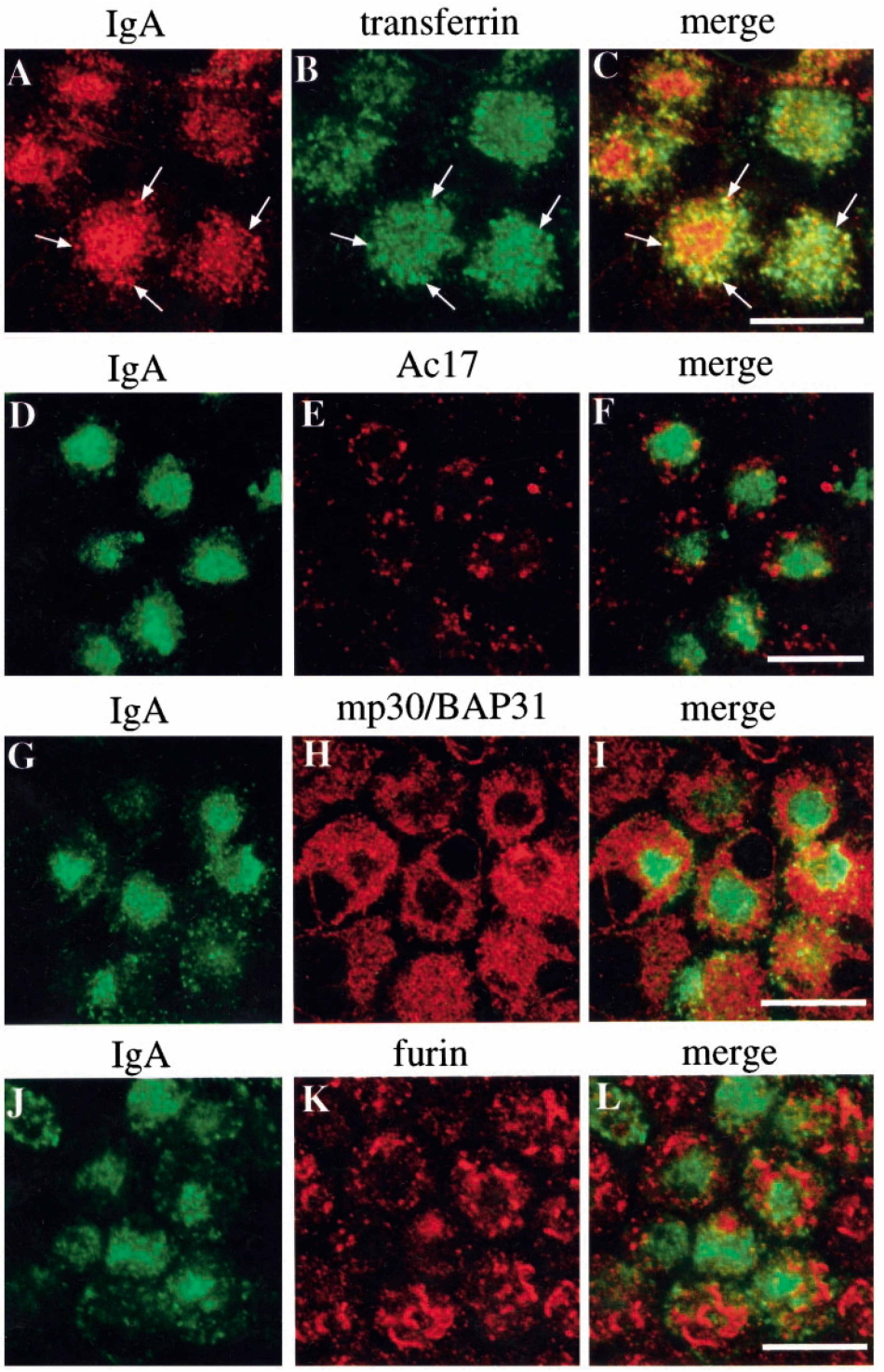

Figure 2-3. Distribution of IgA, Tf, the Ac17 antigen, mp30/BAP31, and furin in cells expressing Rac1V12. IgA was internalized from the basolateral surface of the cell for 10 min at 37˚ C, washed, and then chased for 60 min at 37˚ C. (**A-C**) Tf was internalized during the last 10 min of the 60-min chase. The cells were fixed, incubated with antibodies against IgA and Tf (**A-**

C), IgA and Ac17 antigen (**D-F**), IgA and mp30/BAP31 (**G-I**), or IgA and furin (**J-L**) and then reacted with the appropriate secondary antibody coupled to FITC or CY5. Small arrows indicate regions of colocalization. A single optical section at the level of the central aggregate was obtained with a scanning laser confocal microscope. Bar=10μm

The Central Aggregate is Comprised of Tubulovesicular Endosomal Elements

Ultrastructure of the central aggregate was examined at high resolution by electron microscopy. To mark the central aggregate, we internalized Fab fragments, derived from affinity purified antibodies to secretory component, coupled to horseradish peroxidase (HRP) (Breitfeld et al., 1989b). Like IgA, these Fab fragments move by transcytosis from the basolateral to apical membrane (Breitfeld et al., 1989b). In the presence of H_2O_2 and diaminobenzidine, HRP catalyzes the formation of a product that fills intracellular compartments and appears electron dense when examined by electron microscopy. In control cells, Fab-HRP was primarily localized to small tubulovesicular membrane elements in the apical cytoplasm, often beneath the apical membrane (Figure 2-4A). Note that the electron micrographs also show that control cells were relatively uniform in shape, with apical microvilli and few plasma membrane interdigitations of the lateral membrane.

In many cells expressing Rac1V12, Fab-HRP was located in tubulovesicular elements beneath the apical membrane, similar to those in control cells (Figure 2-4B). However, in contrast to control cells, ligand was also found in the central aggregate (Figure 2-4B&C). This is consistent with our confocal immunofluorescence analysis presented above (see Figure 2-2). In some Rac1V12-expressing cells, Fab-HRP labeled only the central aggregate and little ligand was found underneath the apical membrane (Figure 2-4C). In electron micrographs, the central aggregate appeared as a heterogeneous cluster of small vesicular elements, tubules, signet ring shaped structures, and occasionally a multivesicular body (see insets in Figure 2-4B & C). Many of these structures were labeled with the Fab-HRP, suggesting that they are endosomal in nature. This is consistent with our observation that these structures contain the endocytic marker rab11 (see Figure 2-8 below, as well as reference Jou and Nelson, 1998). In some sections, we found a centriole at the center of the aggregate (inset in Figure 2-4B). The presence of a centriole this deep in the cytoplasm is aberrant, as they are usually located beneath the apical membrane, one of which forms the basal body for a single cilium that projects from the apical surface of the MDCK cell (Bacallao et al., 1989). While

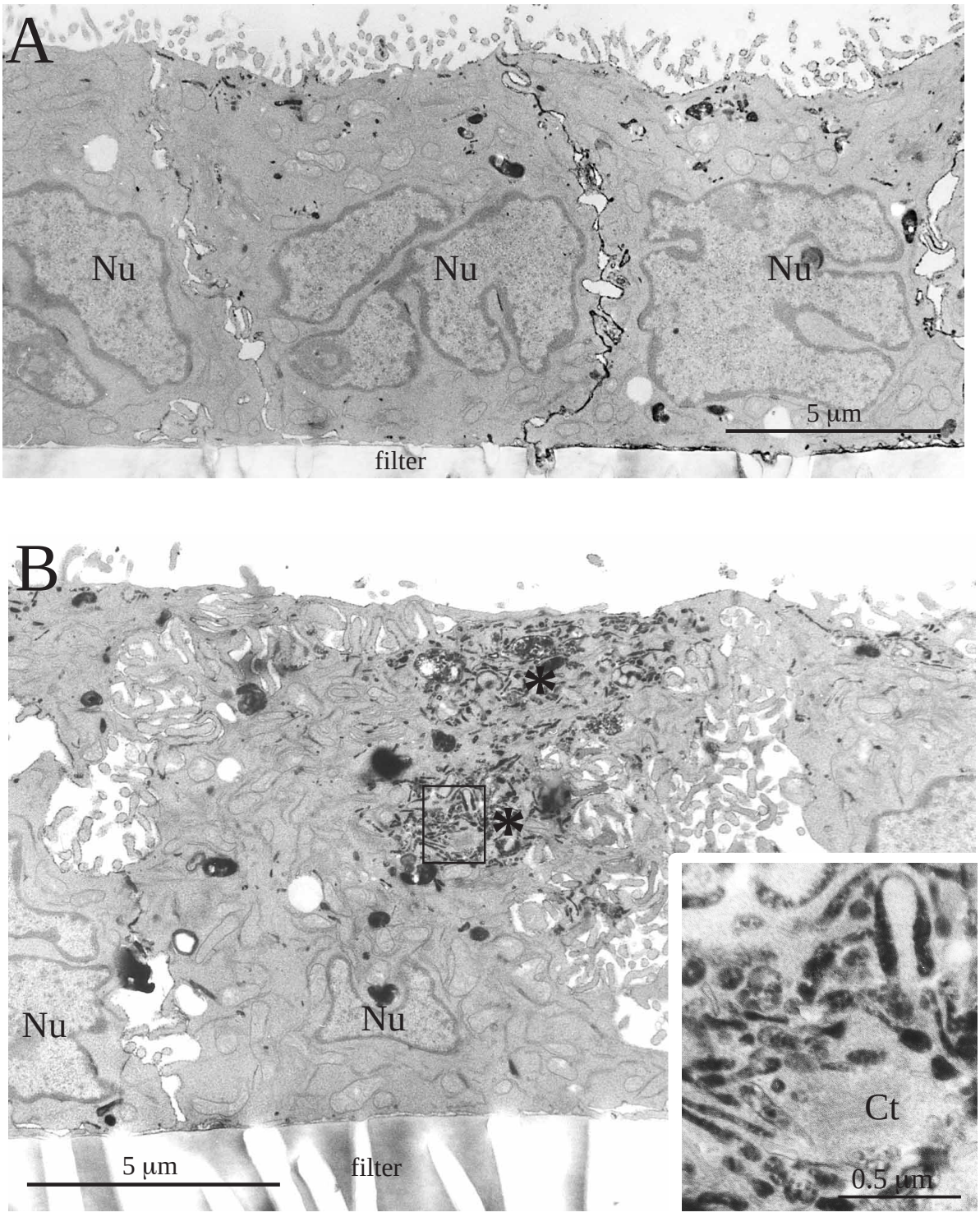

Figure 2-4

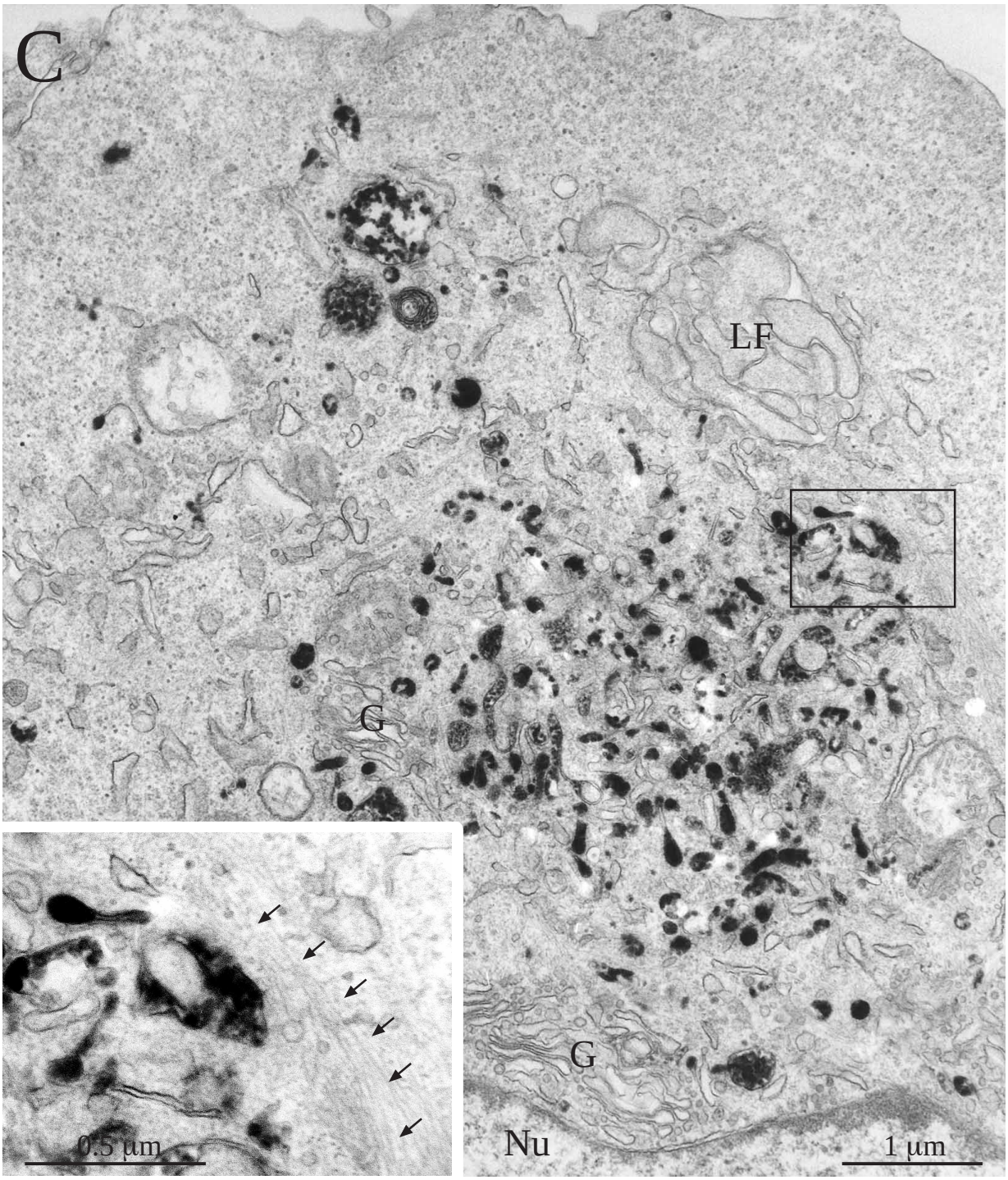

Figure 2-4. Ultrastructural analysis of Rac1V12 cells grown in the presence or absence of DC. Fab-HRP was internalized from the basolateral pole of the cell, the cells were fixed, a DAB reaction was performed, and the cells were processed for electron microscopy. (**A**) Cells grown in the presence of DC. (**B**) Cells grown in the absence of DC. Clusters of Fab-HRP-labeled structures are labeled with an "✶". The upper cluster represents ligand present in the common

endosome/ARE, while the bottom cluster represents ligand present in the central aggregate. Inset: a magnified view of the endosomal elements that comprise the central aggregate. Ct = centriole. (**C**) Cells grown in the absence of DC. A juxtanuclear central aggregate is shown. Inset: a magnified view of the 10-nm filaments surrounding the endosomal elements of the central aggregate (marked with arrows). G, Golgi stacks; LF, infoldings of the lateral membrane; Nu, nucleus.

the localization of the central aggregate is aberrant, it is important to note that the organization (paracentriolar) and morphology of endosomal elements is similar to that previously observed in control cells (Apodaca et al., 1994; Parton et al., 1989).

In cells expressing Rac1V12, the Golgi apparatus was generally dispersed, and small Golgi stacks often surrounded the central aggregate (Figure 2-4C). This is consistent with our confocal immunofluorescence analysis of giantin and furin distributions (see Figure 2-3J-L). However, Golgi were rarely found within the aggregate. Several other structural features of Rac1V12 cells were different from control cells (Figure 2-4B). Occasionally, we observed that the aggregate was surrounded by bundles of thin 10 nm filaments (Figure 2-4C), presumably intermediate filaments. In cross-section, the profile of Rac1V12 cells was tortuous, with a small diameter at the apex of the cell and a progressively wider diameter at the base of the cell, or vice-versa. There was an occasional cell that grew on top of its neighbors. In general, cells had few microvilli, and those present were sometimes fused with adjacent microvilli. One of the most pronounced effects of Rac1V12 expression was the dramatic increase in membrane interdigitations in the lateral membranes between adjacent cells.

Rates of Apical and Basolateral Endocytosis are Affected by Mutant Rac1 Expression

Rac1 is known to affect pinocytosis in oocytes and receptor-mediated endocytosis in Hela cells (Lamaze et al., 1996; Schmalzing et al., 1995). To determine whether Rac1 mutants affected endocytosis in MDCK cells, we measured the rate of [^{125}I]IgA internalization from either the apical or basolateral membrane. In cells expressing Rac1V12, the rate of both apical and basolateral endocytosis of [^{125}I]IgA was decreased by ~30% (Figure 2-5A and C). In contrast, Rac1N17 expression increased the rate of apical and basolateral endocytosis (Figure 2-5B and D). The Rac1N17 effect on apical endocytosis were especially pronounced with a 2-3-fold increase in the rate at early times. The rate of basolateral endocytosis was enhanced by Rac1N17 expression at all time points.

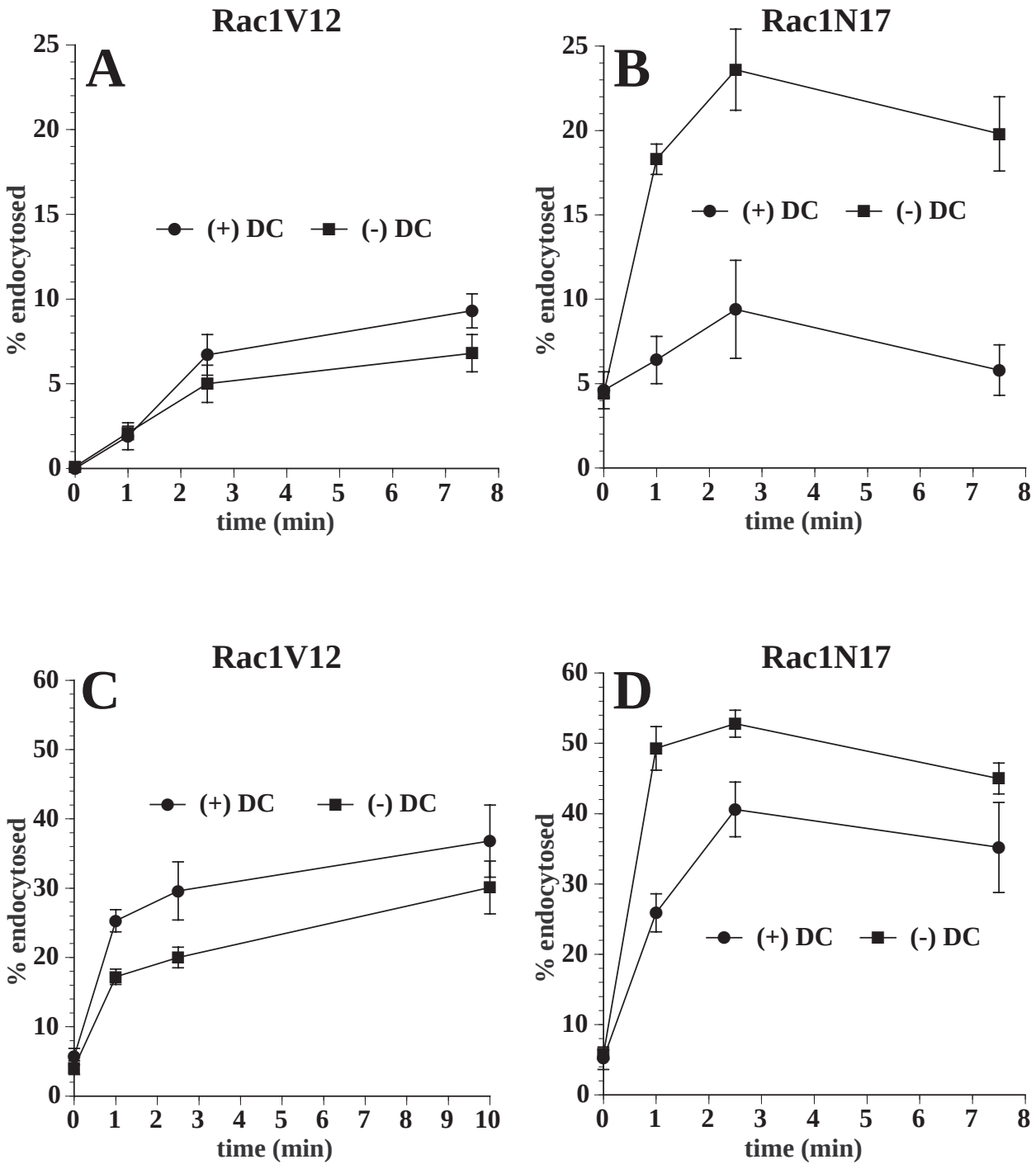

Figure 2-5. Apical and basolateral endocytosis in Rac1V12 and Rac1N17 cells. [^{125}I]IgA was bound to the apical (**A&B**) or basolateral (**C&D**) surface of cells for 60 min at 4˚ C. The Rac1V12 (**A&C**) or Rac1N17 (**B&D**) cells were washed and then incubated at 37˚ C for the times indicated. The media were collected and the cells were then rapidly cooled on ice. [^{125}I]IgA was stripped from the cell surface by a sequential treatment with trypsin and acid at 4˚ C and the filters were cut out of their holders. Total [^{125}I]IgA initially bound to the cells included

ligand released into the medium, ligand stripped from the cell surface with trypsin and acid, and cell associated ligand not sensitive to stripping (endocytosed), and was quantified in a gamma counter. Shown is the percent of total endocytosed ligand from a representative experiment (mean ± SD; n=3)

Apically Directed Postendocytic Traffic is Impaired in Rac1V12 Expressing Cells

The finding that endocytosed ligands were delivered to the central aggregate in Rac1V12 expressing cells prompted us to explore whether postendocytic traffic was altered in these cells, and in cells expressing Rac1N17. In the assays described below, we measured transcytotic delivery of ligands from the basolateral to apical membrane by sampling medium in the appropriate compartment of confluent monolayers grown on Transwell filters. However, we had demonstrated previously that tight junction function is altered in cells expressing Rac1V12 and Rac1N17, and as a result the paracellular flux of several markers is increased (Jou et al., 1998). Because large scale paracellular diffusion of ligands between the apical and basolateral compartments could significantly alter the interpretation of our results, we determined the extent of [^{125}I]IgA and [^{125}I]Tf flux in Rac1V12-expressing cells. While there was an increase in paracellular flux, less than 1.2% of apically added [^{125}I]IgA or [^{125}I]Tf appeared in the basolateral compartment of the cells after 60 min at 37˚C (data not shown). This small increase in flux was insufficient to alter the outcome of the postendocytic fate assays described below. Similar results were observed in cells expressing Rac1N17.

The fates of basolaterally internalized [^{125}I]IgA in control and Rac1V12-expressing cells are shown in Figure 2-6A. In control cells, ~85% of ligand was transcytosed and released into the apical medium during a 2-h chase, ~8% of ligand was released back into the basolateral compartment, ~5% was degraded, and ~2% remained in the cell. These results are similar to those published previously (Apodaca et al., 1994). In cells expressing Rac1V12, transcytosis of internalized [^{125}I]IgA to the apical compartment was decreased by 45-50% (Figure 2-6A). This decrease was not accounted for by the small changes in amount of ligand released basolaterally and amount of ligand degraded. However, the decrease could be accounted for by the ~15-fold increase in the amount of ligand that

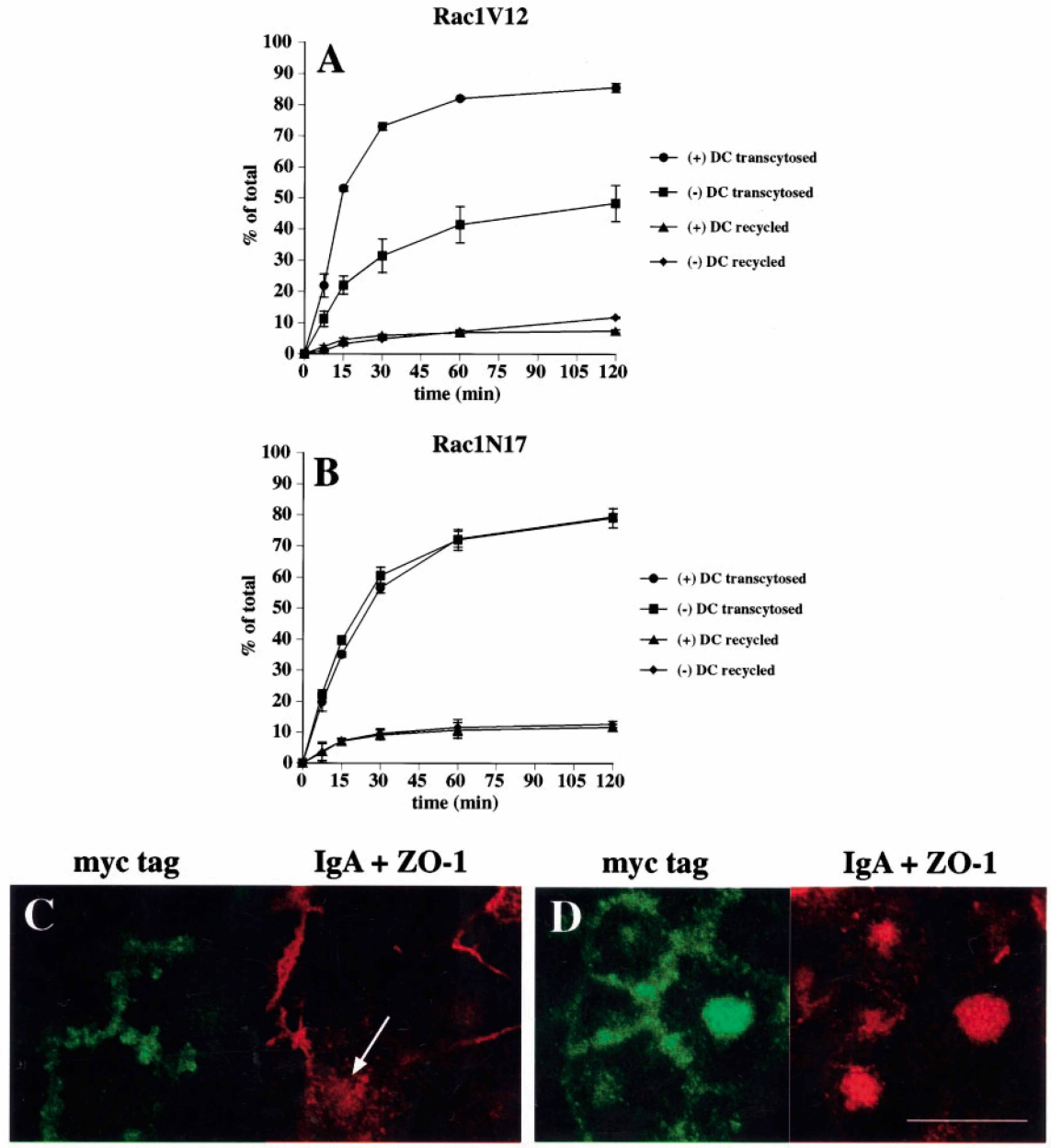

Figure 2-6. Postendocytic fate of basolaterally internalized IgA in Rac1V12- and Rac1N17-expressing cells. [^{125}I]IgA was internalized from the basolateral surface of the cells for 10 min at 37˚ C, the cells were washed, and then chased for 120 min. The percent of total ligand released apically (transcytosed) or basolaterally (recycled) in cells expressing Rac1V12 (**A**) or Rac1N17 (**B**) is shown. Values for degradation were as follows: Rac1V12 +DC, 5.0±0.7%; Rac1V12 –DC, 10.6±0.7%; Rac1N17 +DC, 5.6±0.3; Rac1N17 – DC, 4.4±0.5. Values for ligand remaining cell associated were as follows: Rac1V12 +DC, 2.0±0.7%; Rac1V12 –DC, 29.1±6.7%; Rac1N17 +DC, 3.1±0.2; Rac1N17 – DC, 3.8±1.0. Values (mean ± SD; n=3) are from a representative experiment. (**C&D**) IgA was internalized from the basolateral cell surface for 10 min at 37˚ C, the cells were washed, and then chased 60 min at 37˚ C in ligand-free medium. The cells were

fixed, incubated with antibodies against myc-tagged Rac1V12, IgA, and ZO-1 and then reacted with the appropriate secondary antibody coupled to FITC or CY5. Single optical sections at the level of the tight junctions (**C**) or the central aggregate (**D**) were obtained with a scanning laser confocal microscope. The arrow in (**C**) demarks a cell in which some IgA is seen accumulating at the apical pole of the cell. Bar=10μm

remained cell-associated (29% in Rac1V12 expressing cells, compared to 2% in control cells). Rac1N17 expression had little or no effect on the postendocytic fate of basolaterally internalized [^{125}I]IgA (Figure 2-6B).

To determine the compartment(s) in which cell-associated IgA was trapped in Rac1V12-expressing cells, IgA was internalized for 10 min and then chased for 60 min at 37˚C, during which time most of the ligand is released into the apical secretions of control cells. Cells were processed for immunofluorescence and the samples examined by confocal microscopy. In control cells, the amount of detectable, cell-associated ligand was very little. In cells expressing Rac1V12, however, internalized IgA strongly labeled the central aggregate (Figure 2-6C&D). In some cells, IgA was also found under the apical plasma membrane in the ARE (see arrow in Figure 2-6C). Taking these kinetic and morphological data together, we conclude that in the presence of Rac1V12 delivery of ligand to the central aggregate is efficient, but that exit of IgA from this compartment is inefficient.

The fate of apically internalized [^{125}I]IgA was also assessed in cells expressing Rac1V12 or Rac1N17. Although pIgR is efficiently cleaved at the apical pole of MDCK cells to produce secretory component, a fraction of the receptor escapes cleavage and can be internalized with ligand from the apical cell surface (Breitfeld et al., 1989b). The majority of this apically internalized pool of pIgR-IgA is then recycled back to the apical membrane. In Rac1V12 cells, of the amount of internalized ligand that was recycled to the apical membrane was reduced by ~30% (Figure 2-7A). We detected little or no effects on either apical to basolateral transcytosis, nor intracellular degradation of apical internalized ligand. However, we detected a 5–6-fold increase in the amount of cell-associated ligand in Rac1V12 cells compared to controls. Confocal microscopy confirmed that cell-associated ligand was trapped in the central aggregate of cells expressing Rac1V12. There was no effect of Rac1N17 expression on postendocytic traffic of apically internalized [^{125}I]IgA (Figure 2-7B).

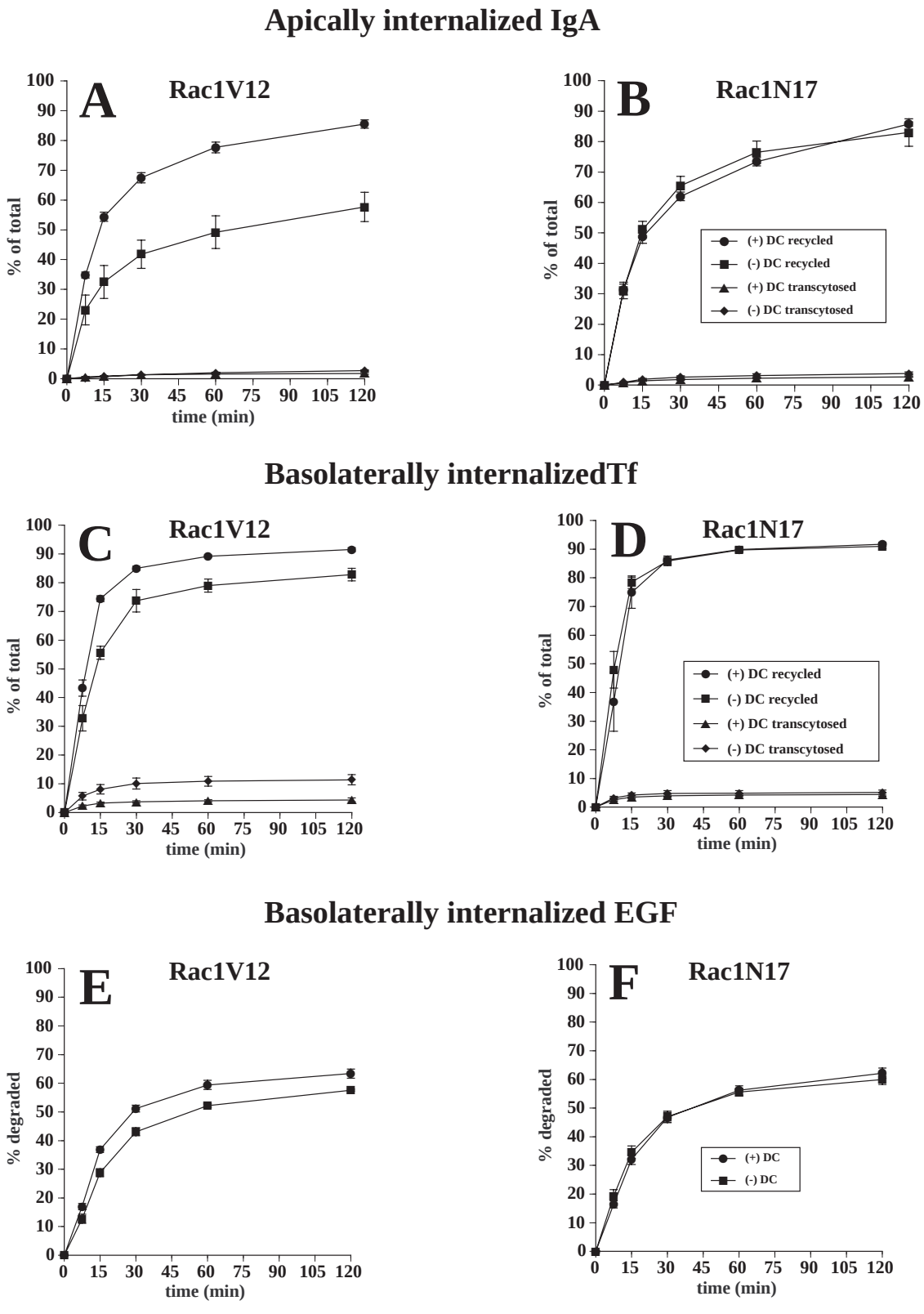

Figure 2-7. Postendocytic fate of apically internalized IgA, basolaterally internalized Tf, or

basolaterally internalized EGF in cells expressing Rac1V12 or Rac1N17. (**A&B**) [^{125}I]IgA was internalized from the apical surface of the cells for 10 min at 37˚ C, the cells were washed, and then chased for 120 min. The percent of total ligand released apically (recycled) or basolaterally (transcytosed) in cells expressing Rac1V12 (**A**) or Rac1N17 (**B**) are shown. Values for degradation were as follows: Rac1V12 +DC, 7.6±0.7%; Rac1V12 –DC, 11.3±1.1%; Rac1N17 +DC, 7.3±0.3; Rac1N17 – DC, 5.2±0.4. Values for ligand remaining cell associated were as follows: Rac1V12 +DC, 5.1±0.9%; Rac1V12 –DC, 28.3±4.8%; Rac1N17 +DC, 4.3±0.7; Rac1N17 – DC, 7.8±3.9. Values (mean ± SD; n=3) are from a representative experiment.(**C&D**) [^{125}I]Tf was internalized from the basolateral surface of the cells for 30 min at 37˚ C, the cells were washed, and then chased for 120 min at 37˚ C. The percent of total ligand released apically (transcytosed) or basolaterally (recycled) in cells expressing Rac1V12 (**C**) or Rac1N17 (**D**) are shown. Values for degradation were as follows: Rac1V12 +DC, 2.8±0.1%; Rac1V12 –DC, 2.8±0.1%; Rac1N17 +DC, 2.2±0.3; Rac1N17 – DC, 1.7±0.2. Values for ligand remaining cell associated were as follows: Rac1V12 +DC, 1.8±0.2%; Rac1V12 –DC, 3.1±0.4%; Rac1N17 +DC, 1.8±0.6; Rac1N17 – DC, 2.3±0.6. Values (mean ± SD; n=4) are from a representative experiment. (**E&F**) [^{125}I]EGF was internalized from the basolateral surface of the cells for 10 min at 37˚ C, the cells were washed, and then chased for 120 min. The percent of total degraded ligand in cells expressing Rac1V12 (**E**) or Rac1N17 (**F**) is shown. Values for transcytosis were as follows: Rac1V12 +DC, 8.7±0.7%; Rac1V12 –DC, 11.5±0.8%; Rac1N17 +DC, 10.0±1.2; Rac1N17 – DC, 12.1±1.0. Values for ligand recycling were as follows: Rac1V12 +DC, 22.8±1.7%; Rac1V12 –DC, 24.6±0.8%; Rac1N17 +DC, 21.5±0.8; Rac1N17 – DC, 22.6±1.1. Values for ligand remaining cell associated were as follows: Rac1V12 +DC, 5.2±0.5%; Rac1V12 –DC, 6.6±0.5%; Rac1N17 +DC, 5.3±1.0; Rac1N17 – DC, 5.4±1.0. Values (mean ± SD; n=4) are from a representative experiment.

Next, we examined whether the postendocytic fates of a basolateral recycling marker (Tf) and a marker of the degradative pathway (EGF) were affected in Rac1V12 or Rac1N17 expressing cells. Recycling of basolaterally internalized [^{125}I]Tf was slightly decreased in cells expressing Rac1V12 (Figure 2-7C), and was coupled with an increase in the amount of ligand released from the apical membrane (~11% in Rac1V12 expressing cells compared to ~5% in control cells). In contrast to basolaterally internalized IgA, there was little difference in the amount of [^{125}I]Tf degraded (~3%) or cell-associated (2-3%) between control cells and cells expressing Rac1V12. These results indicate that proteins that recycle to the basolateral membrane may be able to efficiently exit the central aggregate. To confirm this observation we cointernalized Tf and IgA for 10 min at 37˚ C and then followed the kinetics of Tf exit from the IgA-labeled central aggregate using indirect immunofluorescence. As shown in Figure 2-3, we observed colocalization of the two markers after the pulse. However, within 30 min of chase there was no detectable Tf associated with the IgA-labeled central aggregate (data not shown). There was no effect of Rac1N17 expression on [^{125}I]Tf recycling (Figure 2-7D).

When [^{125}I]EGF was internalized from the basolateral surface of control cells, ~60% of ligand was degraded (Figure 2-7E), ~25% was recycled to the basolateral membrane, ~10% was transcytosed, and the remainder was cell-associated. Rac1V12 expression slightly decreased the amount of [^{125}I]EGF that was degraded (Figure 2-7E), and slightly increased the amounts of ligand released from the apical and basolateral membranes. There was no increase in the amount of [^{125}I]EGF that was cell-associated in cells expressing Rac1V12. Rac1N17 expression had no effect on the post-endocytic traffic of [^{125}I]EGF (Figure 2-7F).

Protein Exit from the Central Aggregate in Rac1V12 Cells Is Unaffected by Nocodazole, but Enhanced by Disruption of the Actin Cytoskeleton by Cytochalasin D

The paracentriolar distribution of the central aggregate indicated that its organization might be dependent on the integrity of the microtubule cytoskeleton. To test this possibility, we treated

cells with nocodazole, a microtubule depolymerizing agent. This treatment resulted in a complete dispersion of the central aggregate; immunofluorescence showed that rab11 and myc-tagged Rac1V12 were localized to small puncta that were dispersed throughout the apical cytoplasm (compare Figure 2-8A&B with Figure 2-8C&D).

Because ligand that was delivered to the central aggregate in Rac1V12 cells did not efficiently exit this structure, we asked whether dispersal of the aggregate with nocodazole would restore normal protein trafficking from the central aggregate to the apical membrane. To load the central aggregate with [^{125}I]IgA, Rac1V12-expressing cells were pulse-labeled with [^{125}I]IgA for 10 min, followed by a 60-min chase to allow [^{125}I]IgA to accumulate in the central aggregate (as shown above). The cells were then chilled to 4˚ C and either left untreated or incubated in the presence of nocodazole. The fate of this intracellular cohort of ligand was then measured over a 2-h chase period at 37˚ C in the continued presence of nocodazole (Figure 2-8E). Exit of [^{125}I]IgA from the central aggregate was similarly slow in untreated cells or those treated with nocodazole. These results indicate that dispersal of the central aggregate with nocodazole is not sufficient to restore normal endocytic function in Rac1V12-expressing cells.

We next tested the effect of disruption of the actin cytoskeleton with cytochalasin D (CD) on protein trafficking out of the central aggregate. Although there appeared to be little effect of CD on the organization or distribution of the central aggregate, CD treatment caused the release of trapped ligand and a significant increase in the amount of IgA that was released into the apical compartment (Figure 2-8F) This observation suggests that the trapping function of this aberrant compartment may due in part to Rac1V12-induced changes in the actin cytoskeleton.

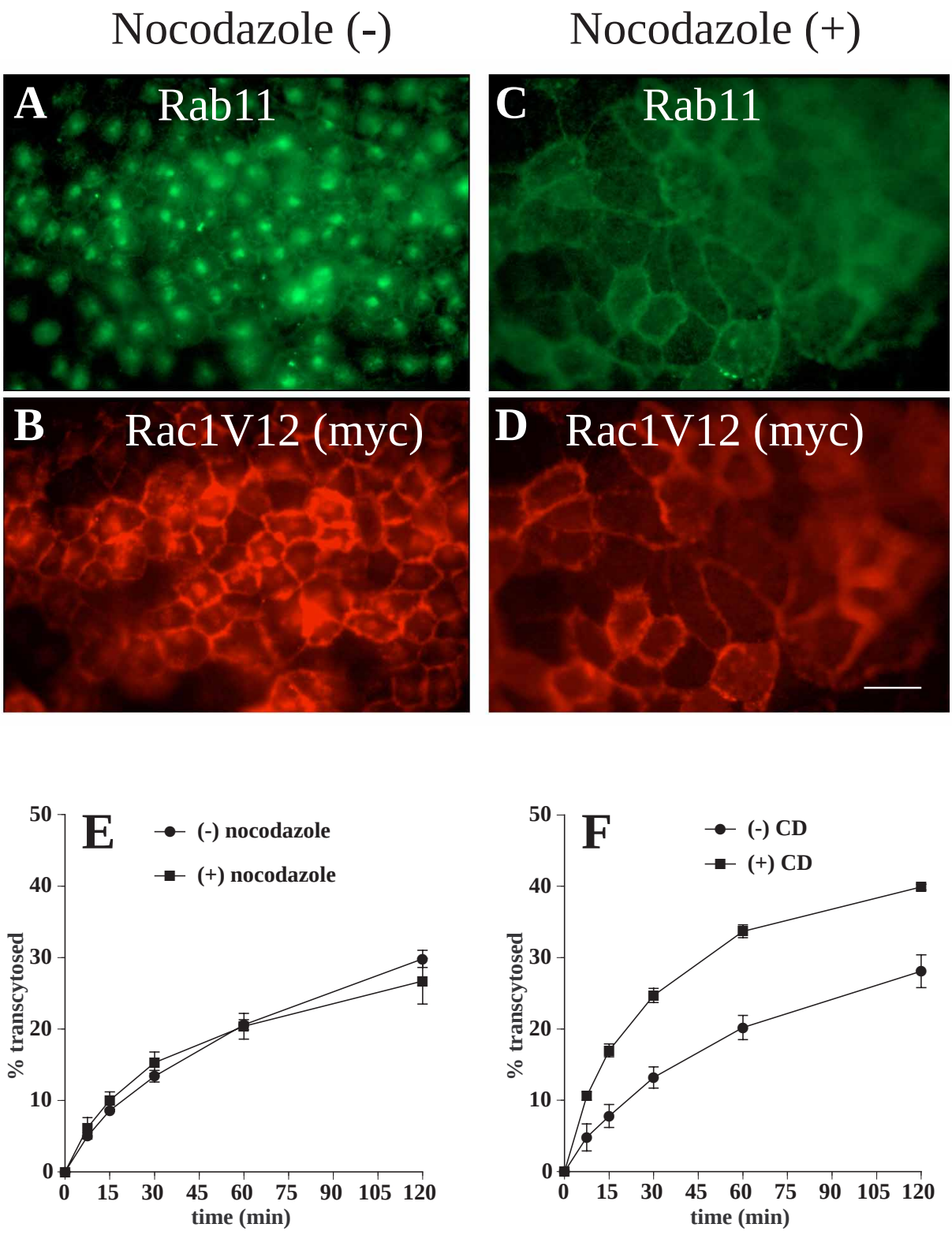

Figure 2-8. Effects of nocodazole and CD on the distribution and exit of proteins from the central aggregate. (**A-D**) Cells were mock-treated or treated with nocodazole, fixed, incubated

with antibodies against Rab11 and the myc tag, and then reacted with the appropriate secondary antibody coupled to FITC or Texas red. Bar=10μm. (**E**) [^{125}I]IgA was internalized from the basolateral surface of the cells for 10 min at 37˚ C, the cells were washed, and then chased for 60 min. Cells were rapidly chilled to 4˚C for 60 min (± nocodazole), and the postendocytic fate of ligand assessed in a subsequent 120-min incubation at 37˚ C (±nocodazole). The percent of total ligand released apically (transcytosed) or basolaterally (recycled) is shown. Values for degradation were as follows: - nocodazole, 21.0±1.2%; + nocodazole, 21.9±0.8%. Values for ligand remaining cell associated were as follows: - nocodazole, 36.1±5.5%; + nocodazole, 37.2±1.5%. (**F**) [^{125}I]IgA was internalized from the basolateral surface of the cells for 10 min at 37˚ C, the cells were washed, and then chased for 45 min at 37˚ C. Following a 15-min treatment, ± 25 μg/ml CD, the postendocytic fate of ligand was assessed in a 120-min incubation at 37˚ C (± CD). The percent of total ligand released apically (transcytosed) or basolaterally (recycled) is shown. Values for degradation were as follows: - CD, 10.2±0.5%; + CD, 14.0±1.1%. Values for ligand remaining cell associated were as follows: - CD, 46.7±2.2%; + CD, 35.7±1.1%. Values (mean ± SD; n=3) are from a representative experiment.

Delivery of Newly Synthesized Membrane Proteins to the Apical, but not Basolateral Membrane is Decreased in Rac1V12 Expressing MDCK Cells.

Previously, we showed that the apical membrane protein GP-135 was present in the central aggregate in cells expressing Rac1V12 (Jou and Nelson, 1998). Therefore, we explored whether this aberrant localization was the result of a block in biosynthetic traffic of GP-135 between the Golgi and the apical membrane. Cells were pulse-labeled with [^{35}S]met/cys for 15 min, chased for different times up to 240 min, and plasma membrane delivery of newly synthesized GP-135 was assessed by cell surface biotinylation. In control cells, newly synthesized GP-135 was rapidly delivered to the apical membrane (Figure 2-9A and B). In cells expressing Rac1V12, initial delivery of GP-135 to the apical membrane was identical to that observed in control cells, but the amount of GP-135 that accumulated at the apical plasma membrane was decreased by ~75% (Figure 2-9A and B). Under both conditions, GP-135 was completely solubilized in buffer containing Triton X-100, suggesting that it had not become aggregated into a detergent insoluble complex. By following the internalization of a biotinylated cohort of GP-135 we determined that the lack of accumulation of GP-135 at the apical plasma membrane was not the result of increased endocytosis of GP-135 from the apical pole of the cell; in control and Rac1V12-expressing cells, <5% of cell surface GP-135 was internalized per hour (data not shown). These data indicate that a small fraction of GP-135 was rapidly delivered to the apical cell surface of Rac1V12 expressing cells while the remainder was retained inside the cell, presumably in the central aggregate. Note that as in our previous studies (Grindstaff et al., 1998a) we found that <5% of newly-synthesized GP-135 was delivered to the basolateral membrane in either control cells or cells expressing Rac1V12, and these data are not shown here.

We also measured delivery of newly synthesized pIgR to the basolateral membrane of control and cells expressing Rac1V12 or Rac1N17. As previously described, the majority of newly synthesized pIgR is delivered directly to the basolateral membrane (Aroeti et al., 1993; Casanova et

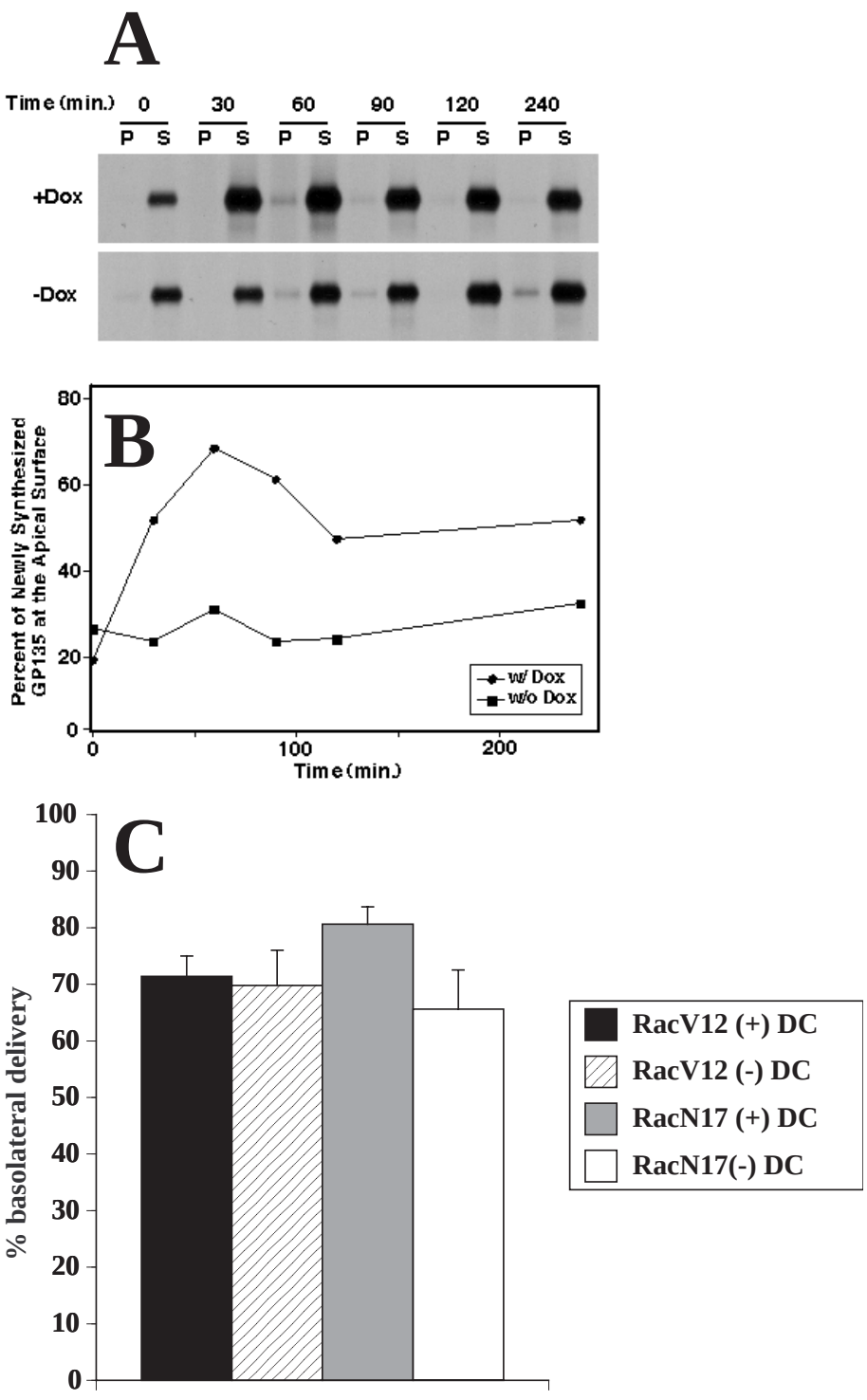

Figure 2-9. Effect of Rac1V12 expression on trafficking of newly-synthesized apical proteins from the Golgi complex to the cell surface. (**A&B**) MDCK cells were grown in the presence (+) or absence (-) of DC on Transwell filters. Cells were metabolically labeled for 15 min with [^{35}S] met/cys, and then chased for different times in medium containing an excess of unlabeled met/

cys. For analysis of GP-135 trafficking, pairs of filters were processed for apical (A) and basolateral (B) cell surface biotinylation, respectively. Cells were extracted with buffer containing Triton X-100 to yield a soluble (S) and insoluble (P) fraction from which the biotinylated fraction of GP-135 was isolated by sequential GP-135 antibody and streptavidin-agarose precipitation. A separate filter for each time point was extracted with SDS lysis buffer, and GP-135 was immunoprecipitated directly to obtain the total amount of [^{35}S] met/cys-labeled GP-135 in the cells. Proteins were separated by SDS-PAGE and detected subsequently using a Molecular Dynamics PhosphoImager (see Materials and Methods and reference Grindstaff et al., 1998a). Kinetics of GP-135 (**A & B**) trafficking to the apical membrane domain are presented. Data is from a representative experiment. As shown by us previously, <5% of GP-135 is delivered to the basolateral membrane in control cells (Grindstaff et al., 1998a) and Rac1V12 cells (L. Fung, unpublished results), and these data are, therefore, not presented. To determine the proportion of GP-135 on the apical membrane, the amount of apical biotinylated GP-135 was divided by the total amount of labeled GP-135 in the cell, and the fraction was plotted against the time of the chase (see panel **B**). (**C**) Cells were metabolically labeled with [^{35}S]cys for 15 min at 37˚ C and then chased in the presence or absence of basolateral trypsin for 60 min at 37˚ C as described previously (Apodaca et al., 1993; Aroeti and Mostov, 1994). In the presence of trypsin newly synthesized pIgR delivered to the basolateral cell surface is rapidly proteolyzed. By comparing the amount of immunoprecipitable pIgR in non trypsin-treated cells and those treated with trypsin it is possible to quantify the extent of pIgR delivery to the basolateral cell surface(Apodaca et al., 1993; Aroeti and Mostov, 1994). The percent of basolateral delivery is shown (mean ± SD; n=4).

al., 1991). We did not observe a significant difference in basolateral delivery of the pIgR between control and cells expressing Rac1V12 (Figure 2-9C). However, Rac1N17 expression decreased delivery of the pIgR to the basolateral membrane by ~20%.

DISCUSSION

An initial characterization of cells expressing Rac1V12 revealed that a central aggregate formed beneath the apical membrane (Jou and Nelson, 1998). To investigate the nature of this aggregate, we have performed a detailed analysis of endocytic and biosynthetic trafficking pathways in these cells. We have found that activation of Rac1 has multiple downstream effects on many membrane trafficking events in polarized cells, including apical and basolateral endocytosis, basolateral to apical transcytosis, apical recycling, as well as accumulation of newly synthesized membrane proteins at the apical cell surface.

Rac1 Regulates the Plasma Membrane Endocytic Rate

Recent evidence indicates that Rho family members are important regulators of endocytosis, as mutants of either RhoA or Rac1 alter fluid-phase and receptor-mediated endocytosis in non-polarized cells (Lamaze et al., 1996; Schmalzing et al., 1995). In MDCK cells RhoA appears to be an important modulator of both apical and basolateral endocytosis (Leung et al., 1999). Our current results show that endocytosis from both plasma membrane domains of polarized MDCK cells was decreased by Rac1V12, and increased by Rac1N17. These observations indicate that Rac1 may act as a throttle on the rate of endocytosis, with the GTP-bound form decreasing the rate and the GDP form increasing the rate. These results are consistent with Rac1-mediated regulation of receptor-mediated endocytosis reported in non-polarized Hela cells by Lamaze et al (1996), but in contrast to those of Li et al. (1997) who found no effect of dominant active Rac1 expression on fluid-phase

endocytosis in baby hamster kidney cells. This discrepancy may reflect differences in cell type, or the use of a fluid phase marker by Li et al. and ligands that undergo receptor-mediated endocytosis in our study and that of Lamaze et al.

Expression of Rac1V12 Alters Delivery of Proteins to the Apical Membrane of MDCK Cells

While there have been several reports of Rho family members regulating endocytosis and exocytosis (Brown et al., 1998; Kroschewski et al., 1999; Lamaze et al., 1996; Mariot et al., 1996; Norman et al., 1994; Norman et al., 1996; O'Sullivan et al., 1996; Price et al., 1995; Schmalzing et al., 1995), little is known about the roles of these proteins in post-endocytic or biosynthetic traffic. In cells expressing Rac1V12, we observed that apically directed membrane protein traffic was selectively impaired compared with traffic directed toward the basolateral membrane. Both basolateral to apical transcytosis and the apical recycling pathway were significantly altered in cells expressing Rac1V12. Significantly, alterations of these apically directed pathways appeared to be the direct result of the delivery to, and retention of these proteins in the central aggregate. In contrast, basolateral recycling of Tf and delivery of EGF to late endosomes/lysosomes was less perturbed by Rac1V12 expression. While Tf was delivered to the central aggregate, it was not retained in this compartment and was recycled reasonably efficiently to the basolateral pole of the cell. This observation indicates that sorting machinery in the aggregate for basolaterally-targeted proteins remained intact in these Rac1V12 expressing cells.

To determine if TGN to cell surface delivery was altered in Rac1V12 cells we measured the appearance of newly synthesized GP-135 and the pIgR at the apical and basolateral plasma membrane, respectively. Delivery of the pIgR to the basolateral membrane was unimpaired in Rac1V12 expressing cells. However, accumulation of newly-synthesized GP-135 at the apical plasma membrane domain was decreased by ~75%. Note that the remaining GP-135 was not delivered to the basolateral membrane, but was retained inside the cells. Presumably, this intracellular pool of GP-135 was delivered to and/or retained in the central aggregate where the protein accumulated to

high levels. At present we do not know whether delivery of GP-135 to the central aggregate is a result of direct delivery from the TGN and trapping, or a result of aberrant redistribution of GP-135 from another cellular membrane as a consequence of Rac1V12 expression. We do not believe that increased apical endocytosis accounts for decreased accumulation of GP-135 at the apical surface of cells expressing Rac1V12, as less than 5.0% of cell surface GP-135 was endocytosed per hour in these cells.

Rac1V12 expression had dramatic effects on slowing apically directed biosynthetic or postendocytic traffic, while Rac1N17 expression had little effect on these trafficking pathways. This was surprising as it was expected that Rac1N17 expression would act as an antagonist to the effects of Rac1V12, as we found in the case of the rate of endocytosis (see above). We have observed previously that this level of Rac1N17 expression (~5x greater than that of endogenous Rac1) is sufficient to alter cellular polarity (Jou and Nelson, 1998), decrease trans-epithelial resistance (Jou et al., 1998), and increase the rate of endocytosis (see above). As such, the role of Rac1 in the normal function of these postendocytic trafficking pathways is presently unclear. It has been observed recently that other dominant negative mutants of small GTPases (e.g., rab25) have little effect on endocytic traffic out of the ARE (Casanova et al., 1999) and a dominant negative mutant of the early endosome associated GTPase RhoD has no effect on endosome morphology or function. Perhaps traffic of proteins from the ARE to the apical surface is only modulated by changes in the activation of these small GTPases. This would be similar to the effects of protein kinase C and protein kinase A on postendocytic traffic; when activated, these kinases modulate apically-directed traffic, while inactivation of these kinases is apparently without effect (Cardone et al., 1994; Hansen and Casanova, 1994).

Membrane and Protein Accumulation in the Central Aggregate Is Due, In Part, to Alterations in the Actin Cytoskeleton

Although the role of Rac1 in normal postendocytic traffic is somewhat unclear, our data indicate that the central aggregate observed in Rac1V12 expressing cells does not comprise a random assortment of membranes from different organelles or trafficking pathways. Instead, it contains specific membranes and proteins that are blocked in their exit to the apical membrane. Marker proteins of late endosomes/lysosomes, the Golgi, the TGN, and the ER were not found within the aggregate. Electron microscopy revealed that it is comprised of membranous structures including vesicular elements, tubules, and signet ring-shaped structures that are redolent of early endosomes. Rab11, a marker of recycling endosomes in general, and the ARE in particular (Casanova et al., 1999; Ren et al., 1998; Ullrich et al., 1996) (an early endosomal compartment) was found associated with the central aggregate. The presence of TF in the central aggregate indicates that the central aggregate is comprised in part of common endosomal elements. Under normal conditions, the balance between membrane entry into, and exit from the endosome results in the maintenance of a small resident pool of membranes in this structure. Inhibition of membrane exit from the ARE/common endosome by Rac1V12 may result in a proportional increase in the amount of resident membrane and formation of the central aggregate. As such, Rac1V12 expression may be a useful tool to understand the normal requirements for protein exit from the ARE/common endosome.

What is the underlying mechanism for the retention of apical directed cargo in cells expressing Rac1V12? One possible explanation is that apically directed traffic is prevented from exiting the central aggregate because of interactions between endosomes or endocytic transport vesicles with the surrounding cytoskeletal cage of filamentous actin and cytokeratin intermediate filaments. Although elements of the central aggregate were organized around a centriole, dispersal of the central aggregate by nocodazole did not relieve the block in protein exit to the apical membrane. In

contrast, CD-induced disruption of the actin cytoskeleton restored the ability of some ligand to exit the cell. This observation suggests that some of the defects in post-endocytic traffic may be the result of Rac1V12-promoted actin polymerization.

An alternative or additional possibility is that Rac1V12 exerts its effects by acting on effector pathways that are independent of its action on the actin cytoskeleton. Potential downstream effectors that are activated by Rac1 include, RhoA, phospholipase D, phosphoinositol-4-phosphate 5-OH kinase, phosphatidylinositol-3-kinase (PI-3-K), PAK, and POR1 (reviewed in Van Aelst and D'Souza-Schorey, 1997). We believe that the effects we observe are not due to activation of RhoA, because constitutively active RhoAV14 primarily affects traffic through the basolateral early endosomes, and a central aggregate is not formed (Leung et al., 1999). Through modifications of the lipid bilayer, both phospholipase D and phosphoinositol-4-phosphate 5-OH kinase are known to affect the ability of coat proteins to bind to organellar membranes (De Camilli et al., 1996; Liscovitch and Cantley, 1995; Liskovitch, 1996). Perhaps the coats that specify apical targeting are selectively disrupted in cells expressing Rac1V12. Activation of PI-3-K is especially intriguing as transcytosis of the pIgR is inhibited by wortmannin, a potent inhibitor of PI-3-K (Hansen et al., 1995). Uncontrolled activation of PI-3-K and its effectors may have dramatic effects on postendocytic traffic. The target(s) of Rac1 will have to await additional studies as the signals that specify apical sorting in the endocytic pathway of polarized epithelial cells are largely unknown, and the apical sorting/budding machinery is undescribed.

The defects in apical membrane traffic observed in Rac1V12 expressing cells may be relevant to understanding cellular physiology in cancerous cells where cellular polarity is highly disorganized (Schoenenberger and Matlin, 1991; Schoenenberger et al., 1991). Rho family members have been implicated in cancer progression and RhoA and Rac1 are required for Ras-mediated transformation (Olson, 1996; Qiu et al., 1995a; Qiu et al., 1995b; Vojtek and Der, 1998). Moreover, all of the more than 20 guanine nucleotide exchange factors for members of the Rho family are potentially oncogenic,

and this oncogenicity is apparently the result of their inappropriate activation of Rho-family members (Olson, 1996; Van Aelst and D'Souza-Schorey, 1997). Uncontrolled Rac1 activation could therefore lead to disruption of apically directed membrane traffic, loss of cell polarity, and ultimately to cellular dysfunction.

CHAPTER 3

Modulation of Endocytic Traffic in Polarized Madin-Darby Canine Kidney Cells by the Small GTPase RhoA*

ABSTRACT

Efficient postendocytic membrane traffic in polarized epithelial cells is thought to be regulated in part by the actin cytoskeleton (Maples et. al., *J. Biol. Chem*. 272: 6741-6751). RhoA modulates assemblies of actin in the cell and it has been shown to regulate pinocytosis and phagocytosis; but its effects on postendocytic traffic are largely unexplored. To this end, we expressed wild type RhoA (RhoAWT), dominant active RhoA (RhoAV14) and dominant inactive RhoA (RhoAN19) in Madin-Darby canine kidney (MDCK) cells expressing the polymeric immunoglobulin receptor (pIgR). RhoAV14 expression stimulated the rate of apical and basolateral endocytosis, while RhoAN19 expression decreased the rate from both membrane domains. Polarized basolateral recycling of transferrin was disrupted in RhoAV14-expressing cells due to increased ligand release at the apical pole of the cell. Degradation of basolaterally internalized epidermal growth factor was slowed in RhoAV14-expressing cells. While apical recycling of IgA was largely unaffected in cells expressing RhoAV14, transcytosis of basolaterally internalized IgA was severely impaired. Morphological and biochemical analyses demonstrated that a large proportion of IgA internalized from the basolateral pole of RhoAV14-expressing cells remained within basolateral early endosomes and was slow to exit these compartments. RhoAN19 and RhoAWT expression had little effect on

these postendocytic pathways. These results indicate that in polarized MDCK cells activated RhoA may modulate endocytosis from both membrane domains and postendocytic traffic at the basolateral pole of the cell.

* Reprinted from *Molecular Biology of the Cell*, (1999, volume 10, pg. 4369-4384), with permission by the American Society for Cell Biology

INTRODUCTION

Endocytosis comprises a diverse set of mechanisms used by the cell to internalize extracellular fluid as well as small patches of the cell plasma membrane (Mukherjee et al., 1997). Once internalized, endocytosed fluid and membrane have several postendocytic fates including return to the cell surface (recycling), delivery to lysosomes, or delivery to the trans-Golgi network (Mukherjee et al., 1997). In polarized epithelial cells, endocytosis occurs at both the apical and basolateral surfaces of the cell, and internalized macromolecules have the additional option of delivery to the opposite pole of the cell in a process termed transcytosis (Apodaca et al., 1991). Because of the highly compartmentalized nature of the eukaryotic cell, protein and membrane sorting in these endocytic pathways must be constantly modified during development or in response to changes in the extracellular environment (Mostov and Cardone, 1995).

One mechanism used to regulate endocytic pathways involves changes in the dynamics of the cytoskeleton. Microtubules, for example, are known to be required for transport of contents between early sorting endosomes, late endosomes and the recycling endosome (Bomsel et al., 1990; Gruenberg et al., 1989; McGraw et al., 1993). In polarized Madin-Darby canine kidney (MDCK) cells, microtubules are necessary for the movement of transcytotic cargo between the basolateral early endosomes and apical pole of the cell (Breitfeld et al., 1990b; Hunziker et al., 1990; Maples et al., 1997). In addition to microtubules, there is increasing evidence that the actin cytoskeleton is required for not only endocytosis (Geli and Riezman, 1996; Gottlieb et al., 1993; Jackman et al., 1994; Kübler and Riezmann, 1993; Lamaze et al., 1997), but also postendocytic traffic (Durrbach et al., 1996; Maples et al., 1997). We have previously observed that there is a requirement for the actin cytoskeleton early in the transcytotic pathway of polymeric immunoglubulin receptor (pIgR)-IgA complexes (Maples et al., 1997).

The above results indicate that modulation of the actin cytoskeleton may be an important mechanism for regulating endocytic and postendocytic traffic. One class of macromolecules that couple changes in the external environment to alterations in the actin cytoskeleton is the Rho family of GTPases (Hall, 1998; Van Aelst and D'Souza-Schorey, 1997). This family is comprised of at least seven members and their isoforms (Mackay and Hall, 1998): Rho (A and B isoforms), Rac (1 and 2 isoforms), Cdc 42 (Cdc42Hs and G25K isoforms), RhoD, RhoG, RhoE, and TC10. One well known aspect of Rho family function is to regulate the formation of specialized actin structures in the cell. Rac1 directs lamellipodia formation (Ridley et al., 1992a), Cdc-42 modulates the assembly of filopodia (Kozma et al., 1995), and RhoA controls the formation of stress fibers and focal adhesions (Ridley and Hall, 1992a). Further experimentation has revealed that Rho family GTPases control a variety of cellular events including: development, cell growth control, transcription, and membrane trafficking events including endocytosis (reviewed in Hall, 1998; Van Aelst and D'Souza-Schorey, 1997; Vojtek and Cooper, 1995).

Multiple endocytic pathways are modulated by Rho family members including phagocytosis (Adam et al., 1996; Chen et al., 1996; Watarai et al., 1997) and pinocytosis (Ridley et al., 1992a; Schmalzing et al., 1995). RhoA and Rac1 may also be important regulators of receptor-mediated endocytosis. Dominant active mutants of these proteins inhibit endocytosis of transferrin receptor in intact as well as perforated cells (Lamaze et al., 1996). We have recently observed that Rac1 modulates endocytosis from both the basolateral and apical poles of MDCK cells (Jou et al., 2000). In addition, a dominant active mutant of Rac1 (Rac1V12) selectively alters apically directed postendocytic traffic including apical recycling and basolateral to apical transcytosis (Jou et al., 2000). Recent evidence indicates that Cdc42 may be important in regulating delivery of newly synthesized proteins to the basolateral domain of MDCK cells (Kroschewski et al., 1999). While the role of RhoB in endocytic traffic is not established, it has been localized to early endosomes and synaptic microvesicles (Adamson et al., 1992; Cussac et al., 1996). RhoD, a recently described member of the Rho family, is found on early endosomes as well as the plasma membrane (Murphy

et al., 1996). Overexpression of dominant active RhoD causes endosomal scattering, and in time-lapse video microscopy endosomes are observed to have decreased motility (Murphy et al., 1996).

We analyzed endocytic traffic in MDCK cells expressing mutant and wild-type RhoA (RhoAWT). We find that RhoA regulates the rate of endocytosis at both poles of polarized MDCK cells. In addition, expression of dominant active RhoA (RhoAV14) dramatically slows basolateral to apical transcytosis of pIgR-IgA, due to trapping of ligand in basal endosomes. While basolateral recycling of transferrin (Tf) was slowed, apical recycling of IgA was unaffected. This analysis reveals previously undescribed functions for activated RhoA in regulating endocytic rates at both cell surfaces and postendocytic traffic at the basolateral pole of the MDCK cell.

RESULTS

Induction of RhoA Overexpression in Polarized MDCK Cells

We used the T23 clone of MDCK cells that stably expresses the tetracycline transactivator (Barth et al., 1997), and either NH_2-terminal myc-tagged wild-type RhoA, dominant active RhoAV14 or dominant inactive RhoAN19. These cells also express pIgR. The level of expression of wild-type and mutant RhoA was regulated by the addition of DC. In the presence of 20 ng/ml of DC expression of neither wild-type nor mutant RhoA was detected by Western blotting (Figure 3-1A), nor was expression detected by immunofluorescence using the 9E10 monoclonal antibody that specifically recognizes the myc tag (Figure 3-1B-E). The data shown in Figure 3-1B-E are for RhoAV14 cells grown in the presence of 20 ng/ml of DC. Identical results were obtained with RhoAWT and RhoAN19 cells grown in the presence of 20 ng/ml DC.

The tetracycline repressible system allows the level of transgene expression to be regulated by altering the amount of DC added to the cell cultures. When RhoAWT cells were cultured on Transwells in the absence of DC for 18 h, the amount of RhoAWT was determined to be

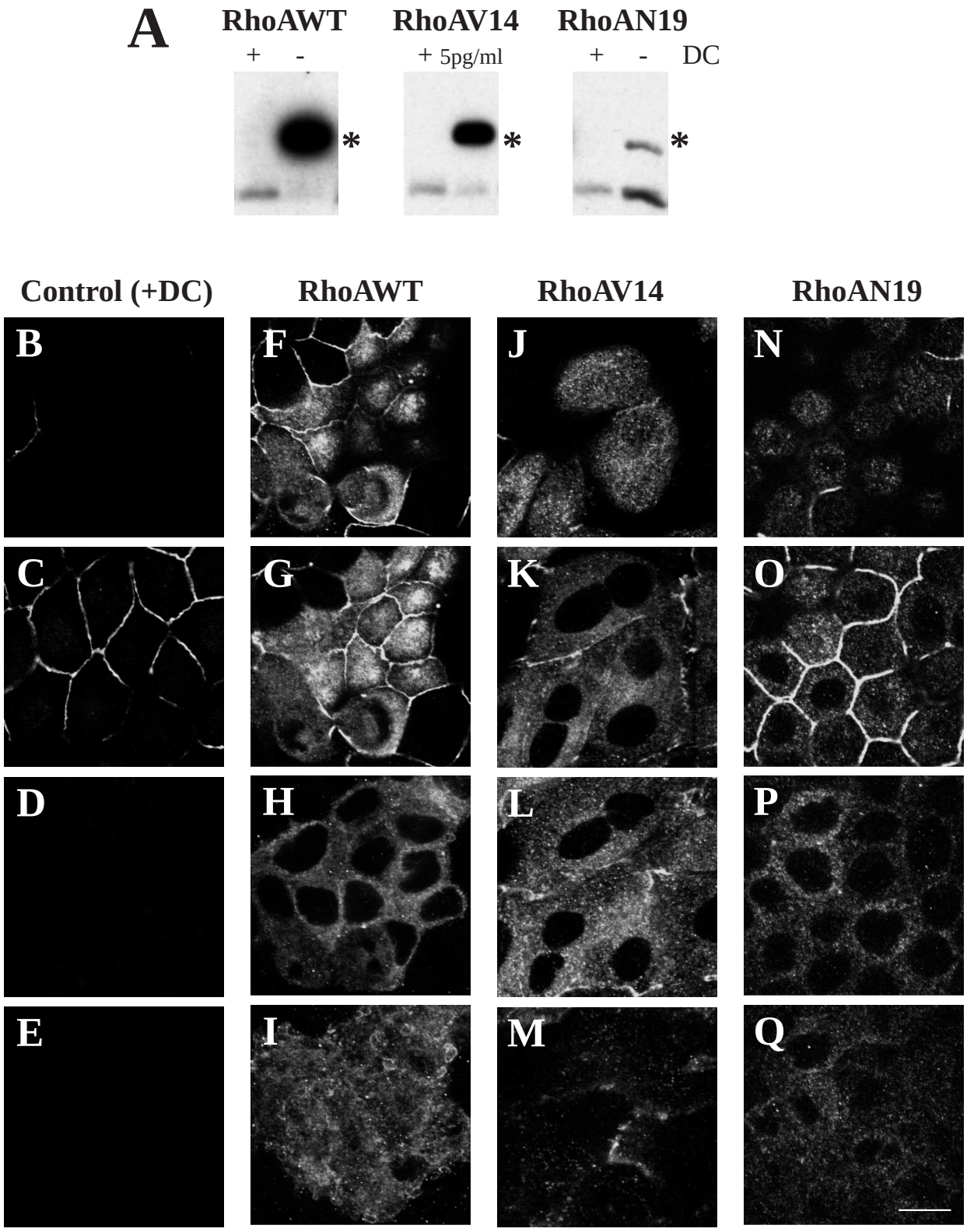

Figure 3-1. Inducible expression and distribution of myc-tagged RhoAWT, RhoAV14 and RhoAN19 in polarized MDCK cells. (**A**) RhoAWT, RhoAV14 and RhoAN19 cells were plated at

low density in medium containing 0-5 pg/ml DC (- or 5pg/ml) or containing 20 ng/ml DC (+), incubated for 36-48 h, and then plated on Transwell filter supports (± DC). After 18 h, the filter-grown cells were solubilized in SDS lysis buffer, 10 μg of lysate was resolved by PAGE, and Western blots were probed with an anti-RhoA monoclonal antibody to detect induction of the myc-tagged mutant proteins as well as endogenous RhoA. * The addition of the myc tag to RhoAWT, RhoAV14, and RhoAN17 causes these proteins to migrate slower than endogenous RhoA. (**B-Q**) Distribution of ZO-1 and myc-tagged proteins in RhoAV14 cells grown in the presence of 20 ng/ml of DC (B-E), RhoAWT cells grown in the absence of DC (**F-I**), RhoAV14 cells grown in the presence of 5 pg/ml DC (**J-M**) or RhoAN19 cells grown in the absence of DC (**N-Q**). Cells were fixed with paraformaldehyde, stained with antibodies that recognize the tight junction protein ZO-1 or the myc tag, and emission from FITC-conjugated secondary antibodies captured using a scanning laser confocal microscope. Shown are optical sections from the base of the cells (**E, I, M, Q**), along the lateral surface of the cells (**D, H, L, P**), at the level of the tight junctions (**C, G, K, O**), and at the very apex of the cell (**B, F, J, N**). The tight junctions are the thin, brightly stained lines that surround each cell. IgA was internalized at the basolateral pole of these cells, but staining for this marker is not shown. Bar=10μm

approximately 12-fold greater than the level of endogenous RhoA (Figure 3-1A). A similar level of expression was observed 48-h post-plating on Transwells. When examined by immunofluorescence, myc-tagged RhoAWT was distributed throughout the cell in a diffuse cytoplasmic staining pattern as well as in punctate structures (Figure 3-1F-I). We costained the cells for the tight-junction associated protein ZO-1, as this structure serves as a convenient landmark to identify the border between the apical and basolateral plasma membrane domains. Moreover it has been shown that tight junction morphology and function is altered in cells expressing mutants of RhoA (Jou et al., 1998). ZO-1 staining in RhoAWT-expressing cells was similar to that observed in control cells (compare Figure 3-1C and 1G; ZO-1 is the thin bright line that surrounds each cell).

Because expression of RhoAV14 has dramatic consequences on the tight junction function and integrity of cells monolayers (Jou et al., 1998), we determined in a preliminary set of experiments that derepression of RhoAV14 transcription in the presence of 5 pg/ml of DC allowed for a ~10.6-fold level of overexpression while maintaining an acceptable level of barrier function (see below). Similar levels of expression were observed 48 h post plating on Transwells. The distribution of RhoAV14 was cytosolic or punctate in appearance (Figure 3-1 J-M). The punctate structures at the base of the cell are apparently endocytic in nature (see Figure 3-8 below). As previously described (Jou et al., 1998), ZO-1 staining was irregular and penetrated down the lateral membranes of the cell (Figure 3-1J-L).

The amount of RhoN19 expression was ~40% of the endogenous RhoA level 18 h after plating on Transwells and was similar to the level of expression described previously (Jou and Nelson, 1998). This level of overexpression was maintained for up to 48 h after plating on Transwells. While this level was much less than that obtained for RhoAWT and RhoAV14, we were unable, after several attempts, to obtain stably transfected cells that had higher levels of expression (see

also Jou and Nelson, 1998; Takaishi et al., 1997). The distribution of myc-tagged RhoAN19 and ZO-1 was similar to the myc-tagged wild-type RhoA and ZO-1 staining observed in RhoAWT cells (Figure 3-1N-Q).

In biochemical experiments described below we used RhoAWT, RhoAV14, or RhoAN19 cells 18-48 h after plating and obtained similar results. It has previously been observed that at these times polarized trafficking of proteins to both apical and basolateral membrane domains occurs (Grindstaff et al., 1998a).

Apical and Basolateral Endocytosis Are Altered by Mutant RhoA Expression

To determine whether RhoA regulated endocytosis in MDCK cells, we measured internalization of [^{125}I]IgA from either the apical or basolateral pole of cells expressing either RhoAWT, RhoAV14, or RhoAN19. RhoAWT expression has no clear-cut effect on either apical (Figure 3-2A) or basolateral (Figure 3-2B) endocytosis. In cells expressing RhoAV14, the rate and extent of both apical and basolateral endocytosis was significantly stimulated by expression of dominant active RhoAV14 protein (Figure 3-2C & D). The effect was especially pronounced at the apical pole of the cell where endocytosis was stimulated ~ 2- fold at each time point relative to control. In contrast, both the rate and/or extent of apical and basolateral endocytosis was decreased by RhoAN19 expression (Figure 3-2E & F). The significant decrease (~25-50%) in apical endocytosis was observed at the 1 and 7.5 min time points. A decrease (~25-40%) in basolateral endocytosis was apparent at all time points. In summary, the results indicate that in polarized MDCK cells endocytosis may be modulated by RhoA; activation of RhoA increases the rate of endocytosis, while inactivation of RhoA decreases the rate of endocytosis.

Postendocytic Traffic is Altered in RhoAV14 Expressing Cells

Previously, we observed that efficient postendocytic traffic requires an intact actin cytoskeleton (Maples et al., 1997). Therefore, we next explored the effect of RhoAWT, RhoAV14,

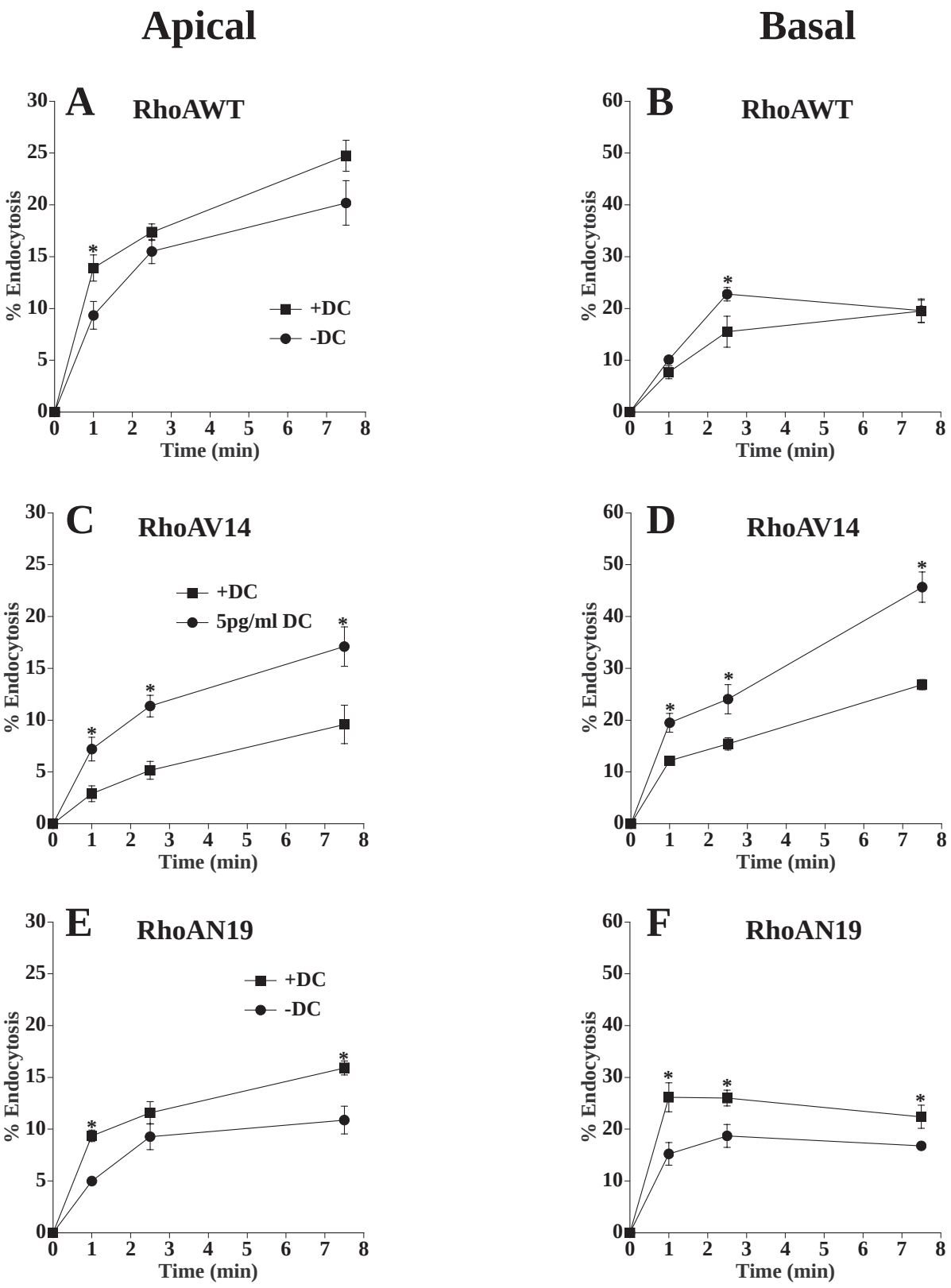

Figure 3-2. Apical and basolateral endocytosis in RhoAWT, RhoAV14 or RhoAN19 cells.

[^{125}I]IgA was bound to the apical (**A, C, E**) or basolateral (**B, D, F**) surface of the cells for 60 min at 4^{o}C. The RhoAWT (**A-B**), RhoAV14 (**C-D**) or RhoAN19 (**E-F**) cells, cultured in the presence of 20 ng/ml DC (+DC) or 0-5pg/ml DC (-DC or 5 pg/ml DC), were washed and then incubated at 37^{o}C for the times indicated. Medium was collected and the cells were then rapidly cooled on ice. [^{125}I]IgA was stripped from the cell surface by a sequential treatment of trypsin and acid at 4^{o}C and the filters were then cut out of their holders. Total [^{125}I]IgA initially bound to the cells included ligand released into the medium, ligand stripped from the cell surface with trypsin and acid, and cell associated ligand not sensitive to stripping (endocytosed). Shown is the percent of total ligand endocytosed (mean $\pm$ SEM; n $\geq$ 4). Statistical significance was assessed using a t-test. Values where $p<0.05$ are marked with an "*". Endocytosis values from filters that were never warmed up to 37˚ C were subtracted from the endocytosis values of cells that were allowed to internalize ligand at 37˚ C.

or RhoAN19 expression on these pathways. We followed markers of the basolateral recycling pathway, the apical recycling pathway, the degradative pathway, or the basolateral to apical transcytotic pathway. As described above, and reported previously, cells expressing RhoAV14 and RhoAN19 have disrupted tight junctions with altered "gate" and "fence" functions (Jou et al., 1998). In the assays described below, we measure movement of ligand between the apical and basolateral compartments of the Transwell. Because large scale diffusion of ligands would significantly alter the interpretation of the results, we determined the extent of [^{125}I]IgA and [^{125}I]Tf flux in cells expressing wild-type and mutant RhoA. Less than 0.5% of apically added [^{125}I]IgA or [^{125}I]Tf appeared in the basolateral compartment of RhoAWT, RhoAV14, or RhoAN19 cells after 60 min at 37˚ C (our unpublished results). We deemed this small increase in flux insufficient to alter the outcome of the postendocytic fate assays described below.

We used Tf as a marker of the basolateral recycling pathway. In control cells, Tf is internalized almost exclusively from the basolateral pole of the cell, and rapidly recycles back to this cell surface (Fuller and Simons, 1986). Recycling of basolaterally internalized [^{125}I]Tf was not significantly altered in cells expressing RhoAWT (Figure 3-3A). However, Tf recycling was significantly slowed in cells expressing RhoAV14 (Figure 3-3B). This decrease was coupled with an increase in the amount of ligand released from the apical pole of the cell (~10% in control vs ~30% in cells expressing RhoAV14). There was little difference in the amount of [^{125}I]Tf degraded (~2-3%), but there was a small increase in the amount of ligand remaining cell associated (~2% in control vs ~10% in RhoAV14 expressors). There was only a slight effect of RhoAN19 expression on polarized Tf traffic (Figure 3-3C). These observations indicate that RhoAV14 expression alters the efficient sorting of Tf into the basolateral recycling pathway of polarized MDCK cells.

Epidermal growth factor (EGF) is primarily delivered to late endosomes/lysosomes where it is degraded (reviewed in Mukherjee et al., 1997; Schmid, 1997). In MDCK cells, a fraction of the ligand (~20-25%) also recycles at the basolateral pole of the cell or is released at the apical pole of

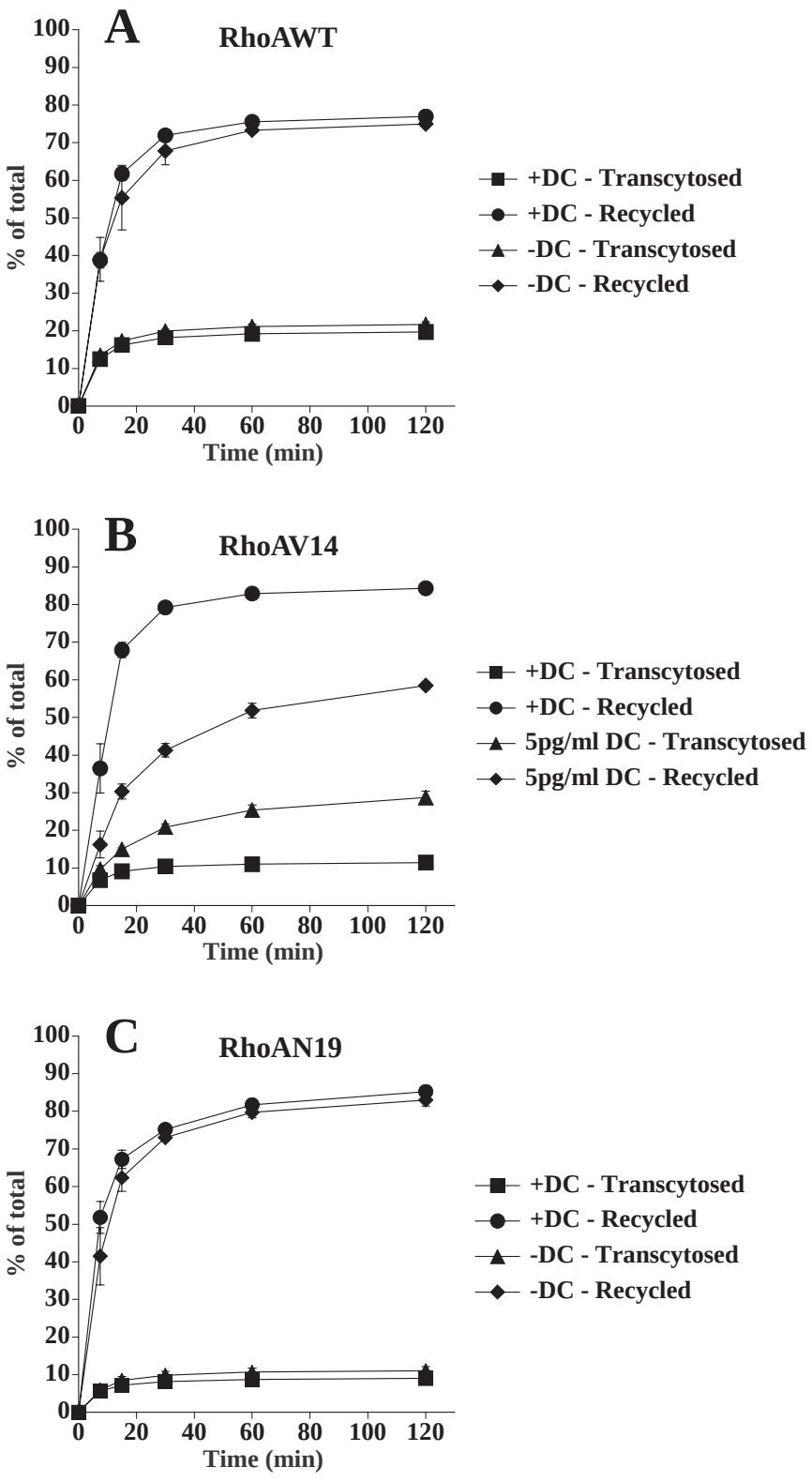

Figure 3-3. Postendocytic fate of basolaterally internalized Tf in RhoAWT, RhoAV14 or RhoAN19 cells. [^{125}I]Tf was internalized from the basolateral pole of the cell for 45 min at 37° C.

The cells were then washed at 4°C, warmed up for 2.5 min at 37° C to allow for receptor internalization, and the postendocytic fate of internalized [^{125}I]Tf was determined in a 120 min chase at 37° C. The percent of ligand released basolaterally (recycled) or released apically (transcytosed) in RhoAWT (**A**), RhoAV14 (**B**) or RhoAN19 (**C**) cells is shown. Values for degradation were as follows: RhoAWT +DC, 1.9±0.2%; RhoAWT –DC, 1.9±0.1%; RhoAV14 +DC, 1.9±0.4; RhoAV14 + 5 pg/ml DC, 2.6±0.2; RhoAN19 + DC, 2.6±0.3; RhoAN19 – DC, 3.0±0.2. Values for ligand remaining cell associated were as follows: RhoAWT +DC, 1.5±0.2%; RhoAWT –DC, 1.4±0.1%; RhoAV14 +DC, 2.3±0.5; RhoAV14 + 5 pg/ml DC, 10.3±2.1; RhoAN19 + DC, 3.1±0.3; RhoAN19 – DC, 3.0±0.8. Values (mean ± SD; n=3) are from a representative experiment.

the cell (~5-10%) (Brandli et al., 1991). The majority of [^{125}I]EGF internalized from the basolateral surface of cells expressing RhoAWT was degraded (~60%)(Figure 3-4A), ~20% was recycled to the basolateral surface, ~10% was transcytosed, and the balance remained cell associated. RhoAV14 expression slowed the degradation of [^{125}I]EGF (Figure 3-4B) and reduced the maximal levels of degradation by ~15%. There was no significant effect on the amount of ligand released at the apical or basolateral pole of the cell, but the amount of ligand remaining cell associated was increased from 3% in control cells to 7% in RhoAV14-expressing cells. RhoAN19 expression did not affect EGF degradation (Figure 3-4C).

IgA internalized from the apical pole of pIgR-expressing cells was used as a marker of the apical recycling pathway. Although the pIgR normally moves by transcytosis from the basolateral to apical pole of the cell where it is cleaved to secretory component (Apodaca et al., 1991), a fraction of the receptor escapes cleavage and can be internalized from the apical cell surface (Breitfeld et al., 1989b). This apically internalized pool of IgA primarily recycles to the apical membrane (Apodaca et al., 1994). In cells expressing RhoAWT, the majority of apically internalized ligand was rapidly recycled to the apical pole of the cell and there was no difference between RhoAWT cells grown in the presence or absence of DC (Figure 3-5A). In RhoAV14 expressing cells, there was a small increase in the kinetics of apical recycling vs control cells, but there was no effect on the extent of IgA recycling (Figure 3-5B). Compared to control cells there was no difference in the amount of ligand that was degraded (~5%) or remaining cell associated (~7%) in RhoAV14-expressing cells. Finally, RhoAN19 expression increased the kinetics of apical [^{125}I]IgA recycling in a reproducible manner. No effect on degradation was observed, but there was a small decrease in the amount of cell associated ligand (~9% in control vs ~4% in RhoAN19-expressing cells).

Next, we measured the effect of wild-type and mutant RhoA expression on the postendocytic fate of basolaterally internalized [^{125}I]IgA. When internalized basolaterally pIgR-IgA complexes move sequentially between basolateral early endosomes, a common endosomal compartment, and

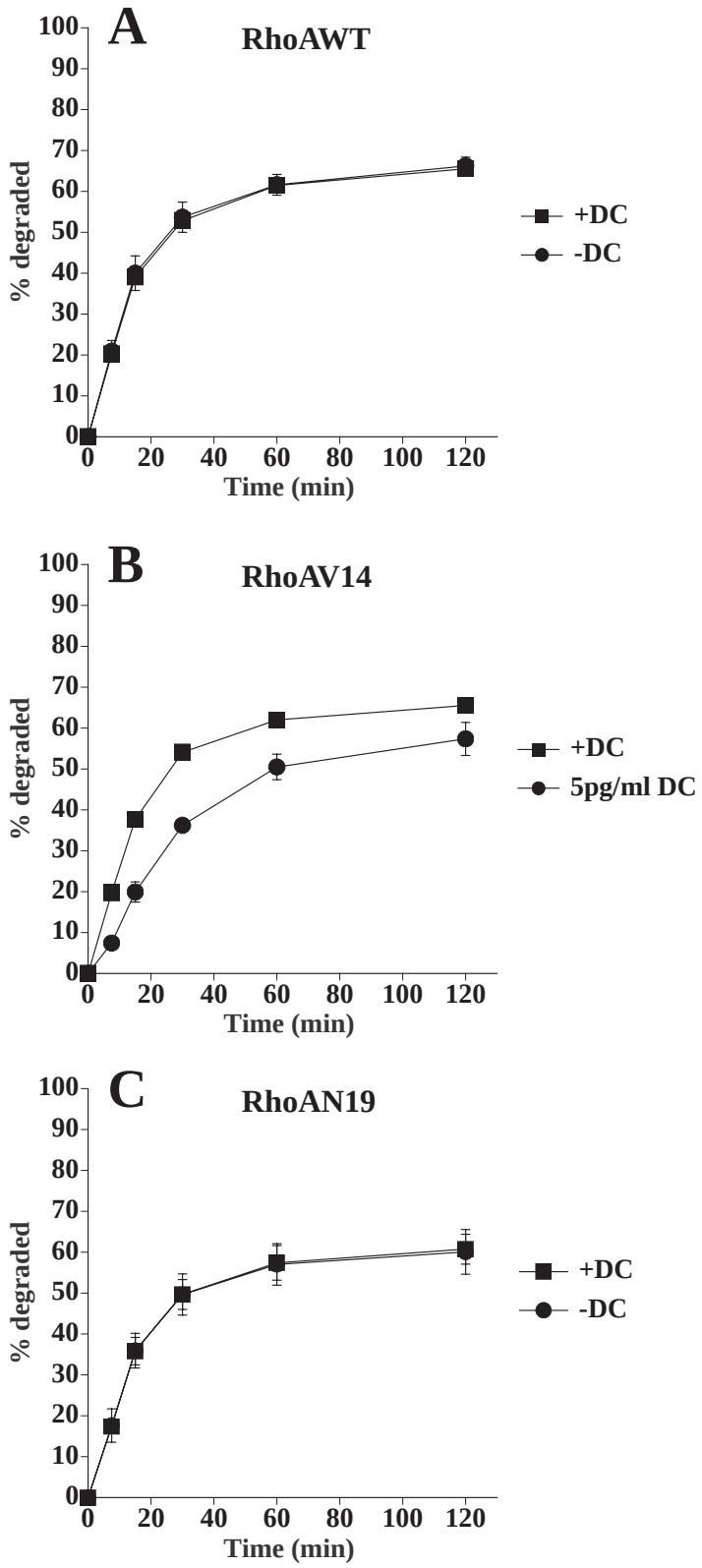

Figure 3-4. Postendocytic fate of basolaterally internalized EGF in RhoAWT, RhoAV14 or

RhoAN19 cells. [^{125}I]EGF was internalized from the basolateral surface of cells for 10 min at 37^{o}C, the cells were quickly washed and then chased for 120 min. The percent of total degraded ligand released from RhoAWT (**A**), RhoAV14 (**B**) or RhoAN19 (**C**) cells is shown. Values for transcytosis were as follows: RhoAWT +DC, 10.1±0.4%; RhoAWT –DC, 11.1±1.0%; RhoAV14 +DC, 9.0±1.0; RhoAV14 + 5 pg/ml DC, 11.5±2.3; RhoAN19 + DC, 9.2±0.7; RhoAN19 – DC, 12.5±3.3. Values for ligand recycling were as follows: RhoAWT +DC, 19.4±1.2%; RhoAWT – DC, 17.9±1.3%; RhoAV14 +DC, 22.7±0.5; RhoAV14 + 5 pg/ml DC, 24.6±2.8; RhoAN19 + DC, 16.8±0.7; RhoAN19 – DC, 17.1±0.9. Values for ligand remaining cell associated were as follows: RhoAWT +DC, 5.0±0.8%; RhoAWT –DC, 4.8±0.3%; RhoAV14 +DC, 2.8±0.5; RhoAV14 + 5 pg/ml DC, 6.6±1.2; RhoAN19 + DC, 13.2±5.1; RhoAN19 – DC, 10.3±3.0. Values (mean ± SD; n=3) are from a representative experiment.

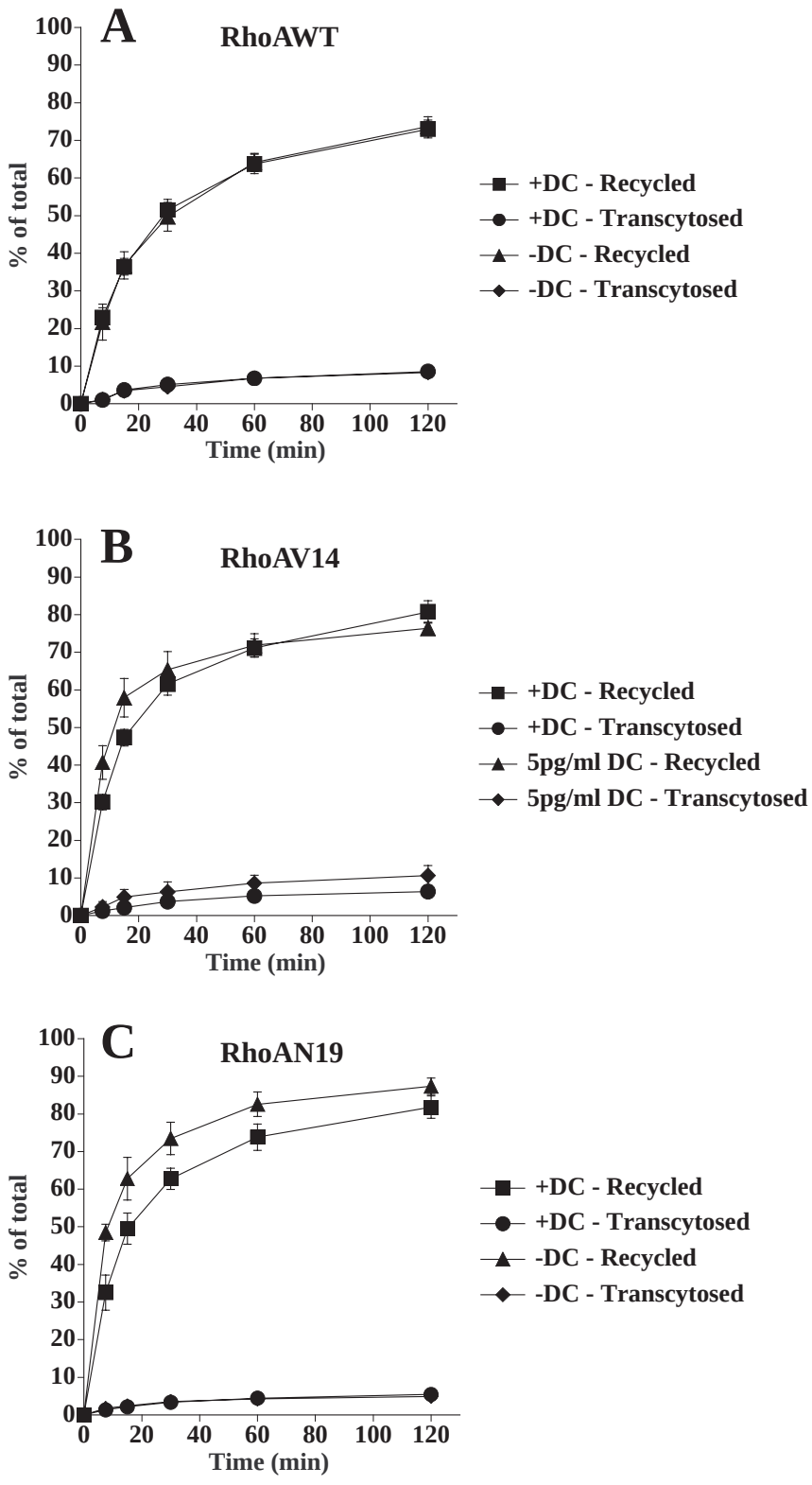

Figure 3-5. Postendocytic fate of apically internalized IgA in RhoAWT, RhoAV14 or RhoAN19 cells. [^{125}I]IgA was internalized from the apical surface of cells for 10 min at 37^{o}C, the cells were

quickly washed and then chased for 120 min. The percent of total ligand released apically (recycled) or basolaterally (transcytosed) in RhoAWT (**A**), RhoAV14 (**B**) or RhoAN19 (**C**) cells is shown. Values for degradation were as follows: RhoAWT +DC, 5.9±0.5%; RhoAWT –DC, 5.3±0.3%; RhoAV14 +DC, 5.0±0.8; RhoAV14 + 5 pg/ml DC, 5.7±1.3; RhoAN19 + DC, 4.2±0.8; RhoAN19 – DC, 3.5±1.6. Values for ligand remaining cell associated were as follows: RhoAWT +DC, 12.6±2.1%; RhoAWT –DC, 12.7±1.3%; RhoAV14 +DC, 7.9±2.0; RhoAV14 + 5 pg/ml DC, 7.3±0.3; RhoAN19 + DC, 8.5±1.9; RhoAN19 – DC, 4.2±0.5. Values (mean ± SD; n=3) are from a representative experiment.

the apical recycling endosome prior to release at the apical pole of the cell (Apodaca et al., 1994). There was little effect of RhoAWT expression on the postendocytic fate of basolaterally internalized IgA (Figure 3-6A). In contrast, in cells expressing RhoAV14 there was a significant slowing of basolateral to apical transcytosis (Figure 3-6B); transcytosis was inhibited by ~ 70%. This inhibition of transcytosis was coupled with a large increase in the amount of ligand that recycled back to the basolateral pole of the cell (~10% in control vs ~40% in cells expressing RhoAV14; Figure 3-6B). Moreover, RhoAV14 expression resulted in an increase in the release of degraded ligand (~6% in control vs 14% in cells expressing RhoAV14) and that remaining cell associated (~6% in control vs 19% in cells expressing RhoAV14). Expression of RhoAN19 did not alter the postendocytic fate of basolaterally internalized IgA (Figure 3-6C).

IgA is Trapped at the Basolateral Pole of RhoAV14-Expressing Cells

The large increase in basolateral recycling of IgA observed in RhoAV14-expressing cells is symptomatic of a block early in the transcytotic pathway. A similar phenotype is observed in pIgR-expressing cells treated with reagents that slow IgA exit from the basolateral early endosomes (e.g. nocodazole or cytochalasin D) (Breitfeld et al., 1990b; Hunziker et al., 1990; Maples et al., 1997). To determine if IgA was trapped in the basolateral early endosomes of RhoAV14-expressing cells, IgA was internalized for 10 min, the cells were washed, and then chased for 5 min at 37˚ C. The cells were then processed for immunofluorescence and the samples examined by confocal microscopy. Figure 3-7 shows a series of optical sections (obtained with a confocal microscope) from the apical (A, E), lateral (B, F, C, G), and basal (D, H) regions of the cell. In control cells (+ DC), IgA was rapidly delivered to the apical pole of the cell where it was found in punctate membrane structures (Figure 3-7A & B). These structures have previously been characterized as elements of the common endosome/apical recycling endosome (Apodaca et al., 1994; Barroso and Sztul, 1994; Odorizzi et al., 1996). Less ligand was found along the lateral surfaces of the cell (Figure 3-7C), or at the base of the cells (Figure 3-7D).

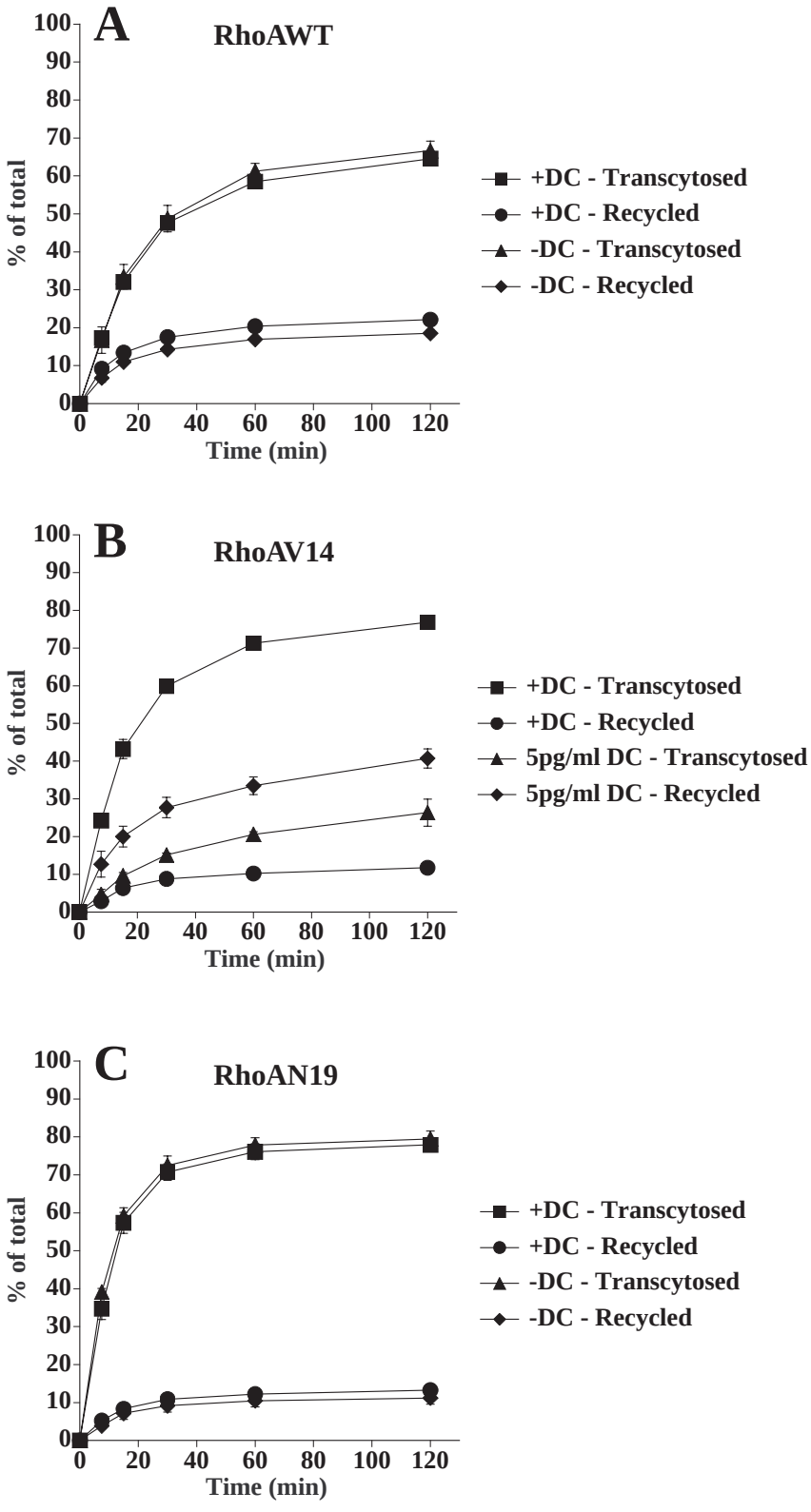

Figure 3-6. Postendocytic fate of basolaterally internalized IgA in RhoAWT, RhoAV14 or

RhoAN19 cells. [^{125}I]IgA was internalized from the basolateral surface of cells for 5 min at 37^{o}C, the cells were quickly washed and then chased for 120 min. The percent of total ligand released basolaterally (recycled) or apically (transcytosed) in RhoAWT (**A**), RhoAV14 (**B**) or RhoAN19 (**C**) cells is shown. Values for degradation were as follows: RhoAWT +DC, 5.3±0.7%; RhoAWT –DC, 5.8±0.5%; RhoAV14 +DC, 5.8±0.5; RhoAV14 + 5 pg/ml DC, 13.6±0.8; RhoAN19 + DC, 6.3±0.6; RhoAN19 – DC, 6.4±0.5. Values for ligand remaining cell associated were as follows: RhoAWT +DC, 8.1±0.2%; RhoAWT –DC, 9.1±1.3%; RhoAV14 +DC, 5.7±1.0; RhoAV14 + 5 pg/ml DC, 19.4±1.0; RhoAN19 + DC, 2.5±0.2; RhoAN19 – DC, 3.0±0.4. Values (mean ± SD; n=3) are from a representative experiment.

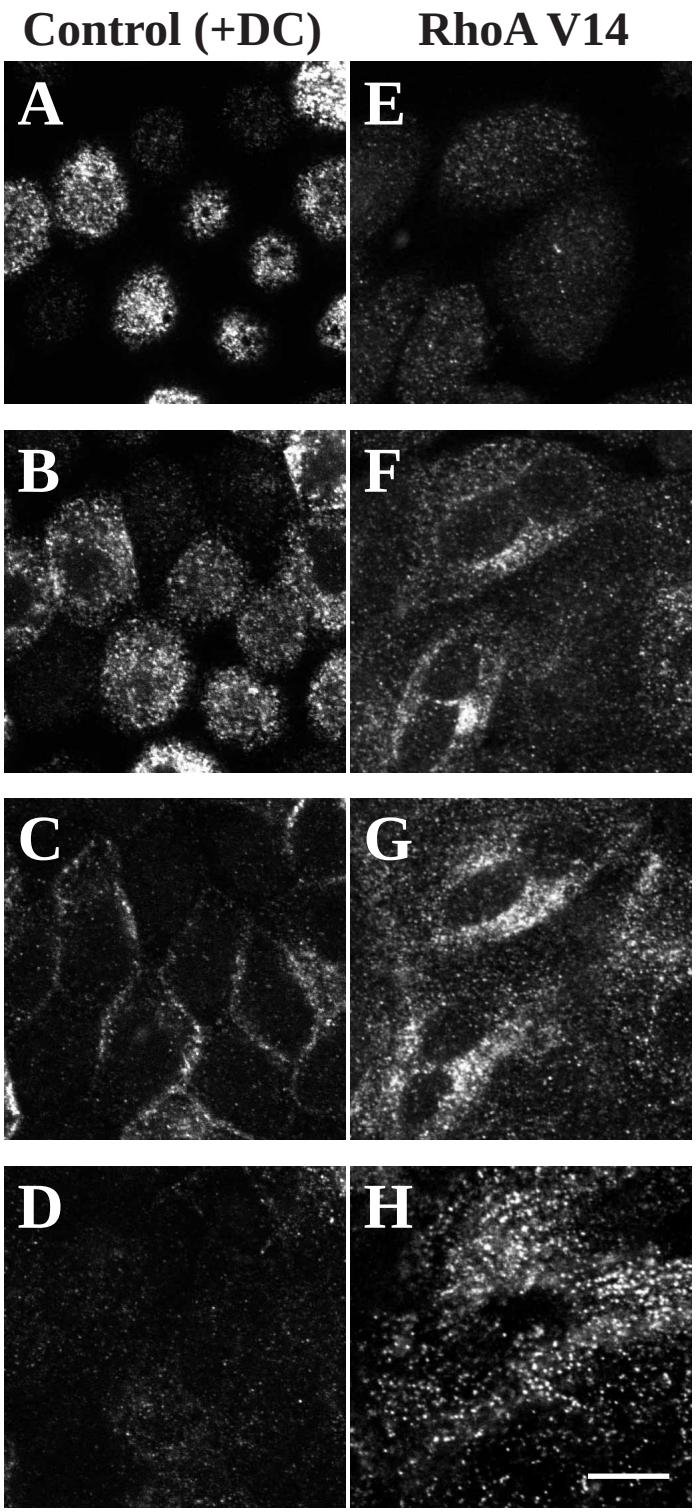

Figure 3-7. Distribution of basolaterally internalized IgA in RhoAV14 cells. RhoAV14 cells were grown in the presence of 20 ng/ml DC (**A-D**) or 5 pg/ml DC (**E-H**). IgA was internalized from the basolateral pole of the cell for 10 min at 37˚ C, the cells were washed quickly, and then

chased in ligand-free medium for 5 min at 37˚ C. The cells were fixed with paraformaldehyde, incubated with rabbit anti-IgA antibody and a myc tag specific monoclonal antibody, and then reacted with fluorescently labeled secondary antibodies. Only staining for IgA is shown. Single optical sections, obtained with a confocal microscope, are shown from the base of the cell (**D &H**), the lateral surfaces of the cell at the level of the nucleus (**C & G**), 2 μm above the previous section (**B & F**), or at the apex of the cell (**A & E**). bar = 10μm

In contrast, in RhoAV14-expressing cells IgA was not concentrated at the apical pole of the cell (Figure 3-7E), but was concentrated in vesicular elements at the base of cell (Figure 3-7H). These IgA-labeled basal endosomes often appeared to be aligned in parallel rows that ran the width of the cell. As noted in Figure 3-1J-M, RhoAV14 was found in a cytosolic distribution as well as in punctate stuctures. Some of the RhoAV14-labeled punctae at the base of the cells colocalized with IgA (Figure 3-8A-C), indicating that these RhoAV14 positive structures were endosomal in nature. The other RhoAV14 positive punctate structures found in the lateral and apical cytoplasm did not colocalize with IgA and their identity is presently unknown. Endogenous, wild-type RhoA had a similar intracellular distribution to that of RhoAV14, and was associated with numerous punctate structures in the cell cytoplasm including ones at the base of the cell, some of which colocalized with IgA (Figure 3-8D-F). This observation indicates that a fraction of endogenous RhoA is normally associated with basolateral endosomes.

To determine if RhoAV14 expression resulted in association of F-actin with the limiting membrane of basal endosomes, we colocalized IgA and F-actin using confocal microscopy. At the very base of the cell, below the level of the stress fibers, a high degree of colocalization was observed between IgA and F-actin (Figure 3-9C, F, I). Small, punctate F-actin-rich structures were also seen associated with, or sandwiched between, F-actin cables (Figure 3-9B, E, H). These F-actin-labeled punctate structures often colocalized with IgA indicating that many were endosomal in nature (Figure 3-9B, E, H). However, we also observed IgA-labeled endosomes that were not actin positive and appeared in the same optical plane where the actin-labeled stress fibers appeared maximally in focus (Figure 3-9D). These IgA-containing endosomes often appeared to be aligned next to or sandwiched between adjacent actin-labeled stress fibers (Figure 3-9G). Similar results were obtained when F-actin was colocalized with basolaterally internalized TF (our unpublished results). There was little colocalization of F-actin with IgA-labeled lateral and apical endosomes (our unpublished results).

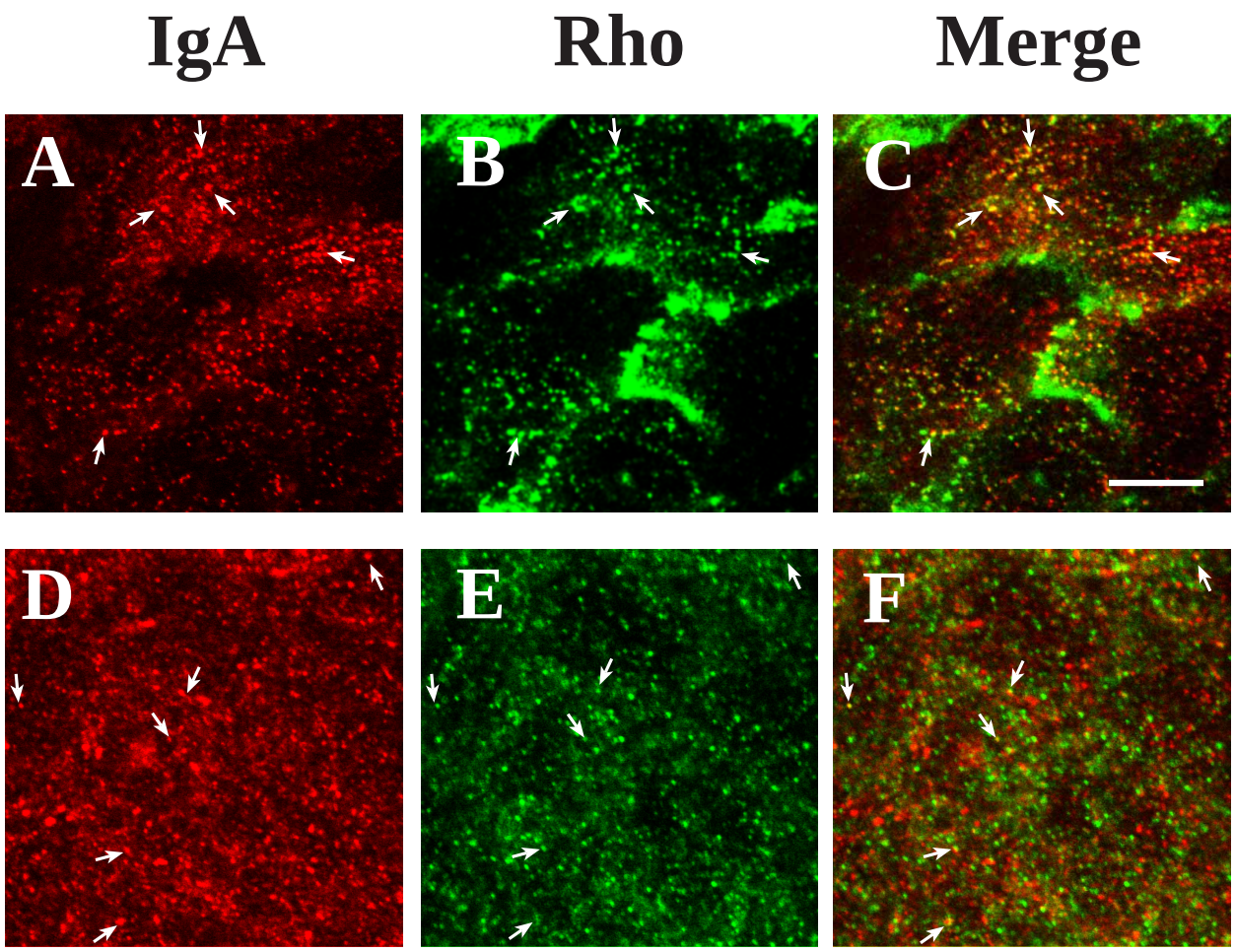

Figure 3-8. Distribution of basolaterally internalized IgA and endogenous RhoA or myc-tagged RhoAV14. RhoAV14 cells were grown in the presence of 5 pg/ml DC (**A-C**) or 20 ng/ml DC (**D-F**). IgA was internalized from the basolateral pole of the cell for 10 min at 37˚ C and cell-surface ligand was removed by chasing in ligand-free medium for 5 min at 37˚ C (**A-C**) or by trypsin treatment at 4˚ C (**D-F**). The cells were fixed with paraformaldehyde, incubated with rabbit anti-IgA antibody (**A-F**) and a myc tag specific monoclonal antibody (**A-C**) or a monoclonal anti-RhoA antibody (**D-F**), and then reacted with goat anti-rabbit-Cy5 and goat anti-mouse-FITC secondary antibodies. Panel A is identical to panel H in Figure 7 and Panel B is identical to panel M in Figure 1. In the latter case the contrast was enhanced and the image brightened to demonstrate colocalization of myc-tagged RhoAV14 and IgA. Examples of IgA and myc-tagged RhoAV14 colocalization are marked with arrows. Bar = 10 μm

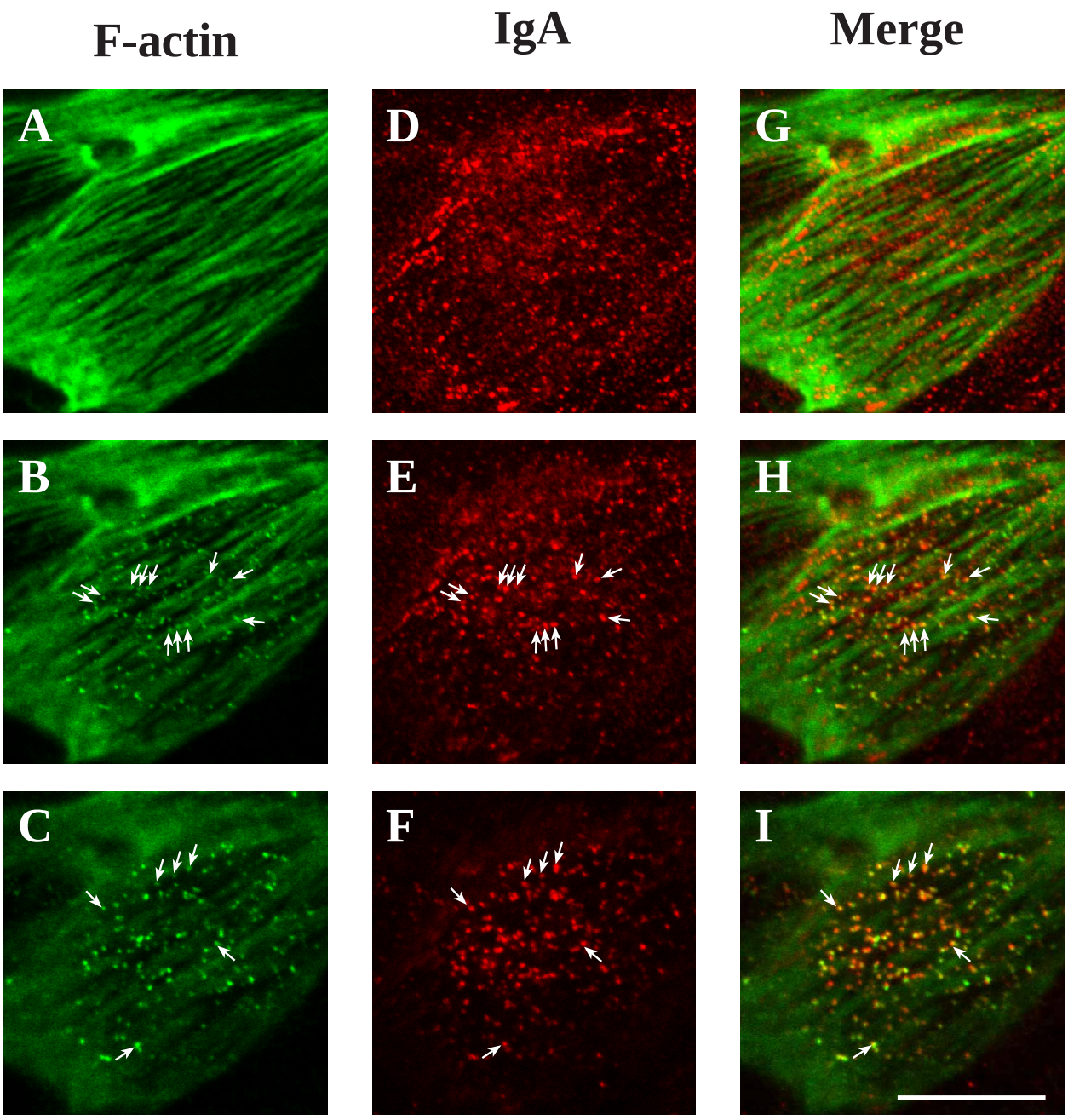

Figure 3-9. Distribution of IgA and F-actin in cells expressing RhoAV14. IgA was internalized for 10 min at 37˚ C from the basolateral surface of RhoAV14 cells grown in the presence of 5 pg/ml DC, and then washed and chased for 5 min at 37˚C. Cells were fixed with paraformaldehyde, incubated with rabbit anti-IgA antibody, and then reacted with goat anti-rabbit-CY5 secondary antibody and FITC-phalloidin. The FITC and CY5 emission was simultaneously captured using a scanning laser confocal microscope. Single optical sections were taken at the very base of the cell (**C, F, I**), 1 μm above the previous section (**B, E, H**), or at a focal plane where the phalloidin-labeled stress fibers appeared maximally in focus (**A, D, G**). Examples of IgA and F-actin colocalization are marked with arrows. Bar=10μm

To determine if association of endosomes with F-actin was particular to cells expressing RhoAV14, we performed the same experiment in control cells (RhoAV14 cells grown in the presence of 20 ng/ml DC). In these experiments, IgA was internalized from the basolateral pole of the cell for 5 min at 37˚ C, and cell-surface ligand removed by trypsin stripping prior to processing the samples for confocal microscopy. The normal wash and chase following ligand internalization was omitted because, in control cells, IgA does not accumulate at the base of the cell and is rapidly delivered to the apical pole of the cell (Apodaca et al., 1994). The distribution of IgA and F-actin was similar to what was observed in RhoAV14 expressing cells. However, as previously described the amount of F-actin associated with stress fibers was decreased in these control cells (Jou and Nelson, 1998). IgA and F-actin were found to colocalize at the base of the cell (Figure 3-10C, F, I). In addition, there were F-actin positive, IgA-labeled endosomes that were associated with or sandwiched between the F-actin-labeled stress fibers (Figure 3-10B, E, H). Actin-negative, but IgA-positive endosomes were also observed in a slightly higher plane of focus (Figure 3-10A, D, G). Often these IgA-positive endosomes appeared in linear arrays.

Exit from Basolateral Endosomes Is Slow in RhoAV14-Expressing MDCK Cells

The above morphological analysis indicated that the significant slowing of IgA transcytosis in RhoAV14-expressing cells was in part the result of a defect in IgA movement towards the apical pole of the cell. To determine if this was the case, we used a previously described density-shift assay that measures the movement of IgA from the basal endosomes to apical endosomes loaded with an apically internalized marker conjugated to HRP (Apodaca et al., 1994). [^{125}I]IgA was internalized basolaterally, while WGA-HRP was cointernalized from the apical pole of the cell for 10 min at 37˚ C. Ligand was removed from the cell surface and the cells were treated with DAB and H_2O_2 to crosslink [^{125}I]IgA present in the WGA-HRP filled apical endosome into a dense, detergent-insoluble complex that can be recovered by centrifugation. When normalized to the maximum amount of [^{125}I]IgA found in the apical endosomal compartment, we estimated that approximately

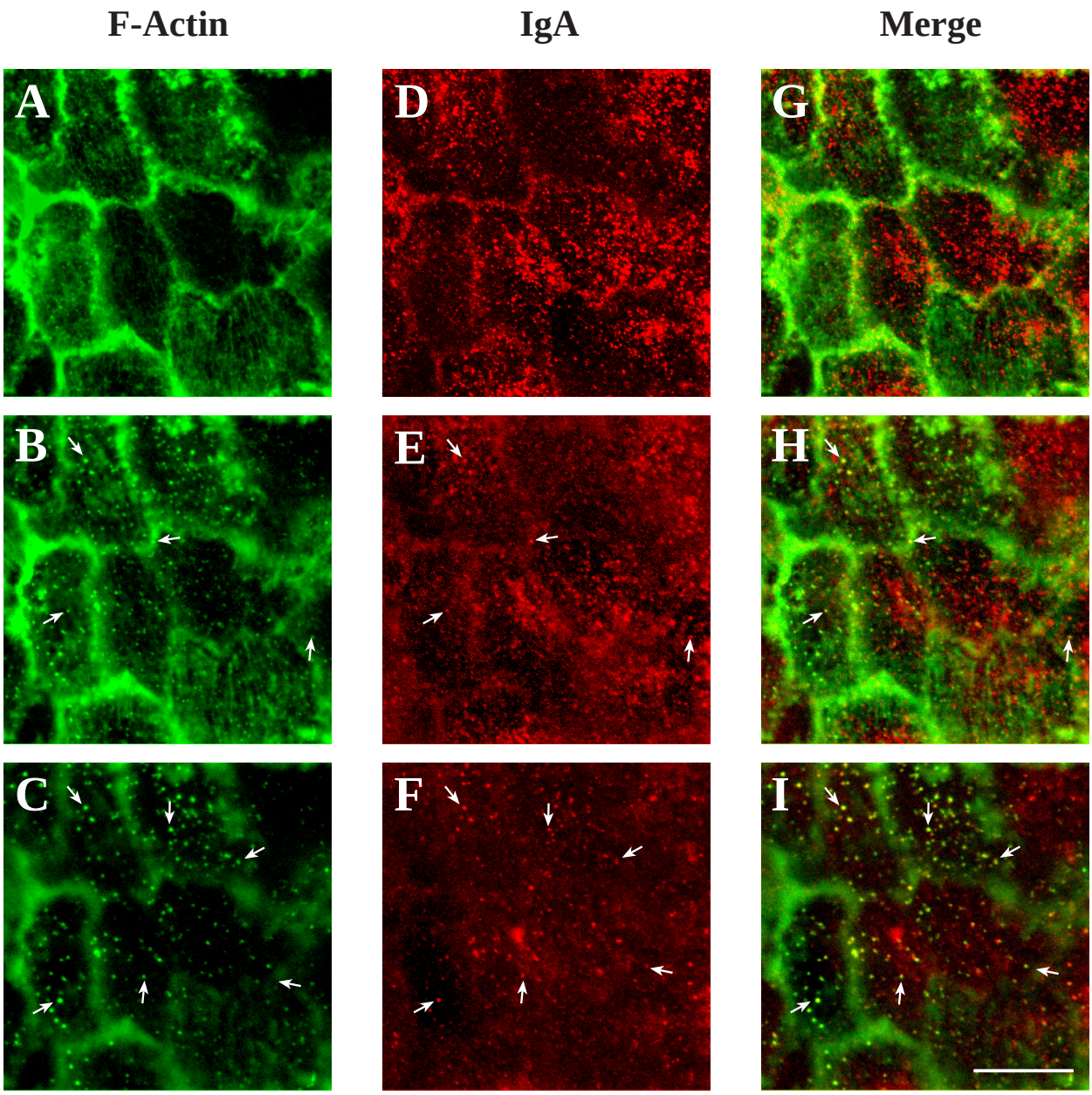

Figure 3-10. Distribution of IgA and F-actin in RhoAV14 grown in the presence of 20 ng/ml DC. IgA was internalized for 10 min at 37˚ C from the basolateral surface of RhoAV14 cells grown in the presence of 20 ng/ml DC, and cell surface ligand removed by trypsin treatment at 4˚ C. Cells were fixed with paraformaldehyde, incubated with rabbit anti-IgA antibody, and then reacted with goat anti-rabbit-CY5 secondary antibody and FITC-phalloidin. The FITC and CY5 emission was simultaneously captured using a scanning laser confocal microscope. Single optical sections were taken at the very base of the cell (**C, F, I**), 1 μm above the previous section (**B, E, H**), or at a focal plane where the phalloidin-labeled stress fibers appeared maximally in focus (**A, D, G**). Examples of IgA and F-actin colocalization are marked with arrows. Bar=10μm

70% of [^{125}I]IgA internalized for 10 min at 37˚ C resides in an apical endosomal compartment of control cells (Figure 3-11). In contrast, in cells expressing RhoAV14 delivery of [^{125}I]IgA to these apical compartments was significantly inhibited by ~70% (Figure 3-11).

DISCUSSION

RhoA is known to regulate numerous cellular functions including: stress fiber formation, focal adhesion assembly, stimulation of mitogen-activated protein kinase cascades, phagocytosis, secretion, and receptor-mediated endocytosis (Hall, 1998; Van Aelst and D'Souza-Schorey, 1997). We now report that activation of RhoA can have multiple downstream consequences on several polarized cell membrane trafficking events including apical and basolateral endocytosis, basolateral recycling, and transcytosis in the basolateral to apical direction.

Regulation of Apical and Basolateral Endocytosis by RhoA

There is increasing evidence that Rho family members may be important regulators of endocytosis. Mutant RhoA and Rac1 alter fluid-phase as well as receptor-mediated endocytosis in non-polarized cells (Lamaze et al., 1996; Li et al., 1997; Ridley et al., 1992a; Schmalzing et al., 1995). Lamaze *et al*. (1996) have reported that, in Hela cells, dominant active RhoA inhibits endocytosis while RhoA inactivation stimulates receptor-mediated endocytosis. In our current analysis, we observe that RhoA has the opposite effect; apical and basolateral endocytosis were accelerated in RhoAV14-expressing cells, while apical and basolateral endocytosis were inhibited in RhoAN19-expressing cells. These observations indicate that in polarized epithelial cells RhoA activation stimulates endocytosis, while RhoA inactivation inhibits endocytosis. The discrepancy between these two studies may reflect inherent differences in how nonpolarized and polarized cells regulate endocytosis. We have recently observed that a dominant active mutant of Rac1 (Rac1V12) decreases apical and basolateral endocytosis, while a dominant negative mutant (Rac1N19) stimulates endocytosis from both poles of the MDCK cell (Jou et al., 2000). The opposing actions of Rac1 and

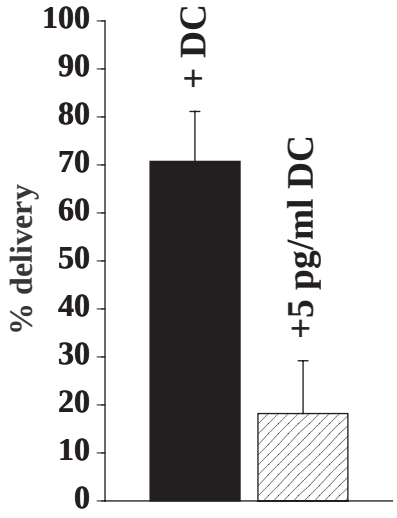

Figure 3-11. Quantification of IgA delivery to apical endosomes in RhoAV14 cells. [^{125}I]IgA was internalized basolaterally for 10 min at 37˚ C, while WGA-HRP was cointernalized from the apical surface of RhoAV14 cells grown in the presence of 20 ng/ml DC (+DC) or 5 pg/ml DC (+5 pg/ml DC). Details of the DAB reaction and quantitation are given in the Materials and Methods. Values (mean ± SD; n=3) are from a representative experiment.

RhoA suggest a mechanism whereby different extracellular cues could differentially regulate endocytosis in polarized epithelial cells; agents that signal through Rac1 (e.g. the insulin receptor or EGF receptor) would inhibit endocytosis, whereas activation of RhoA (e.g. via the lysophosphatidic acid receptor) could lead to increases in receptor-mediated endocytosis.

RhoAV14 Primarily Alters Postendocytic traffic at the Basolateral Pole of MDCK Cells

While there have been several reports of Rho family members regulating endocytosis and exocytosis (reviewed in Van Aelst and D'Souza-Schorey, 1997), little is known about the roles of these proteins in postendocytic or biosynthetic traffic. We have recently observed in Rac1V12-expressing cells that apically directed membrane traffic is more severely impaired than traffic directed toward the basolateral pole of the cell (Jou et al., 2000). This inhibition was largely the result of trapping of endocytosed markers in a central membranous aggregate.

In contrast, we observed here that RhoAV14 expression had little effect on apical recycling of IgA. Instead, RhoAV14 primarily altered basolateral recycling of Tf, slowed degradation of basolaterally internalized EGF, and inhibited basolateral to apical transcytosis of IgA. Tf recycling was markedly slowed and there was a large increase (3-fold) in the amount of Tf ligand released from the apical pole of the cell. The increase in Tf transcytosis was surprising as transcytosis of basolaterally internalized IgA was severely impaired in RhoAV14-expressing cells. Moreover, we observed that significant amounts of Tf were retained in basal endosomes (S.M. Leung, unpublished observations), although, some Tf was also observed in the apical cytoplasm of these cells. Overexpression of RhoAV14 may alter the normally efficient basolateral sorting/targeting machinery in endosomes and/or at the basolateral cell surface, resulting in apical release of Tf ligand from, most likely, the apically distributed endosomal elements. The increase in Tf release at the apical pole of the cell was not simply a result of paracellular diffusion, as we cultured cells under conditions where RhoAV14-mediated changes in tight junction formation were moderate.

Degradation of basolaterally internalized EGF was also slowed by RhoAV14 expression. However, this was primarily a kinetic effect as inhibition of EGF degradation was only 15%, which may reflect alterations in basal endosome function (see below). The largest effect of RhoAV14 expression was a 70% inhibition of basolateral to apical transcytosis of IgA. This was coupled with a significant increase in the amount of IgA that was released at the basolateral pole of the cell. As described below, alterations in basolateral endosome dynamics may explain some of these defects in transcytosis.

While RhoAV14 expression altered postendocytic traffic, expression of RhoAN19 or RhoAWT had little effect on these trafficking pathways. This was unexpected as RhoAN19-expression inhibited endocytosis and one might predict that RhoAN19 expression would alter postendocytic traffic. This lack of effect may be the result of poor RhoAN19 expression. Experimentally it has been challenging to generate stable cell lines that express dominant negative forms of RhoA (Jou and Nelson, 1998; Takaishi et al., 1997). While this level of RhoAN19 expression was sufficient to decrease trans-epithelial resistance as well as inhibit endocytosis (this study, Jou and Nelson, 1998; Jou et al., 1998) it may be insufficient to alter endocytic traffic. Other systems have been described where only the dominant active forms of small GTPases (e.g. Rab25 and Rac1) have effects on postendocytic traffic (Casanova et al., 1999; Jou et al., 2000). Perhaps these trafficking pathways only respond to the activation of these particular small GTPases. An alternative possibility is that RhoA is not absolutely required for normal postendocytic traffic to occur. However, the presence of endogenous RhoA on a subpopulation of basolateral endosomes might suggest otherwise. Additionally, failure to observe an effect with a dominant negative mutant does not rule out involvement of the wild-type protein. Ras activity can be induced directly by nitric oxide and can be modulated by decreases in the activity of guanine nucleotide exchange factors (Downward et al., 1990; Mott et al., 1997). As noted previously, neither of these mechanisms of Ras activation would be sensitive to expression of a dominant negative mutant (Feig, 1999).

The Transcytotic Pathway is Blocked at an Early Step in RhoAV14-Expressing Cells

The significant decrease in transcytosis of basolaterally internalized IgA may reflect altered endosomal function and dynamics at the base of the RhoAV14-expressing cells. Normally, transcytosing IgA moves rapidly from the basolateral early endosomes to the apical pole of cells where it mixes with apically internalized membrane cargo (Apodaca et al., 1994). We have measured this translocation step in RhoAV14-expressing cells and found that it was significantly slowed. While this slowing could reflect an inhibition of fusion between basolateral and apical cargo, we observed that in RhoAV14-expressing cells a significant fraction of the internalized IgA was found in basal endosomes. Moreover, myc-tagged RhoAV14 was localized to these basolateral endosomes and F-actin was found associated with the limiting membrane of these endosomes.

The association of actin and RhoA with basolateral endosomes was not particular to cells expressing RhoAV14, but was also observed in control cells. These results indicate that a fraction of endogenous RhoA is normally associated with a subpopulation of basolateral endosomes, and could therefore regulate the function/dynamics of these endosomes. RhoA, for example, could be important in modulating the actin cytoskeleton and/ or association of myosin motors with these basolateral endosomes. In fact, there is evidence that an unconventional myosin motor (Myr5) contains a GTPase activating domain for RhoA (Reinhard et al., 1995). In some respects RhoA functions similarly to RhoD. This member of the Rho family is associated with endosomes. In cells expressing a dominant active mutant of RhoD ($RhoD^{G26V}$) the endosomes are found to lack tubular extensions, lose their dynamic properties, are associated with actin, and often appear in linear arrays (Murphy et al., 1996). Unlike RhoAV14-expressing cells, those expressing $RhoD^{G26V}$ have only a minimal effect on the internalization and recycling of Tf. A dominant negative mutant of

RhoD ($RhoD^{T31N}$) has no observable effects on the actin cytoskeleton or endosome dynamics/function. This lack of effect is consistent with our observation that RhoAN19 did not alter postendocytic traffic.

In addition to its ability to modulate the actin cytoskeleton, RhoA is known to activate multiple downstream effectors including: phospholipaseD, phosphoinositol-4-phosphate-5-kinase, ROKa/Rho kinase, p160 ROCK, p140mDia, PKN, Rhotekin, Rhophilin, and citron (reviewed in Mackay and Hall, 1998; Van Aelst and D'Souza-Schorey, 1997). While many of these effectors are known to induce changes in the actin cytoskeleton, phospholipase D and phosphoinositol-4-phosphate-5-kinase have the additional effect of controlling coat binding to organellar membranes (De Camilli et al., 1996; Liscovitch and Cantley, 1995; Liskovitch, 1996). As such, the efficient formation or inclusion of cargo into vesicles involved in postendocytic traffic could be altered by RhoAV14. Perhaps the coats that recognize basolateral targeting information are disrupted in cells expressing RhoAV14 and as a result depolarized secretion of Tf occurs. In addition to potential defects in endosome/actin interactions, alterations in coat binding may also play a role in producing the large inhibition of transcytosis observed in RhoAV14-expressing cells. We are currently exploring the role of these various Rho effectors on postendocytic traffic.

In summary, our observations indicate that RhoA has a previously unappreciated role in modulating endocytic traffic in polarized MDCK cells. These findings are not only relevant in understanding normal cellular physiology but in conditions where normal cellular function is altered. Rho family members have been implicated in cancer progression and of the more than 20 guanine nucleotide exchange factors for members of the Rho family all of them are potentially oncogenic, presumably as a result of their uncontrolled activation of Rho family members (Olson, 1996; Qiu et al., 1995b; Van Aelst and D'Souza-Schorey, 1997; Vojtek and Der, 1998). Uncontrolled RhoA activation could therefore lead to disruption of membrane traffic, loss of cell polarity, and progression into a malignant phenotype.

CHAPTER 4

Localization of Proteins involved in Actin Polymerization Based Propulsion and Myosin Motors at the Basal Pole of Polarized Madin-Darby Canine Kidney Cells

ABSTRACT

Madin-Darby canine kidney (MDCK) cells expressing dominant active RhoA (RhoAV14) trap basal to apical transcytosing IgA in basolateral early endosomes (BEE) below the level of the stress fibers. These endosomes are associated with filamentous actin (f-actin). Examination of control cells reveals that a subset of BEE was also f-actin associated. The function of the BEE associated f-actin is not known. Transcytosis of IgA has been shown to be dependent on both actin and microtubule based transport and step-wise experiments demonstrated that the actin-dependent transport precedes the microtubules-based transport. Therefore, one hypodissertation of the role for the BEE associated f-actin is to transport the endosome to the level of the stress fibers where the endosome can switch to a microtubule based transport. There are two models of actin-based transport: actin polymerization based propulsion (APBP) and myosin motor based propulsion. In order to examine whether either model is possible, the localization of various components involved in either model was determined. While the APBP was not found to colocalize with BEE, MIc, a type I myosin, was found to colocalize with a subset of BEE. These results demonstrate that one possible function of the BEE associated f-actin is as part of a MIc based transport mechanism to carry the BEE to the level of the stress fibers.

INTRODUCTION

The cytoskeleton is important for many eukaryotic cellular functions including cell motility, cell structure maintenance, muscle contraction, mitosis, endocytosis and organelle localization (Brown and Stow, 1996; Kelly, 1990; Mays et al., 1994). Polarized epithelial cells have separate apical and basolateral plasma membrane domains. Both microtubules and the actin cytoskeleton are involved in transport to these domains (Mays et al., 1994). Recently, Maples et al. demonstrated that basal to apical transcytotic transport in MDCK cells utilizes both actin filaments and microtubules and furthermore the actin dependent step precedes transport along microtubules (Maples et al., 1997). This suggests that initial transport through the cortical actin utilizes an actin based mechanism which then shifts to microtubule transport further in the cell.

The Rho family of small GTPases couples extracellular signals to changes in the actin cytoskeleton (Hall, 1998; Van Aelst and D'Souza-Schorey, 1997). Expression of dominant active RhoA (RhoAV14) in MDCK cells results in basolaterally internalized ligand being trapped in basal endosomes (Leung et al., 1999). These endosomes are associated with RhoAV14 and filamentous actin (F-actin) (Leung et al., 1999). The association of F-actin with basolateral endosomes is not restricted to cells expressing RhoAV14. In control cells, a subset of basolateral endosomes is associated with endogenous RhoA and F-actin (Leung et al., 1999). The function of this associated F-actin is unknown. One hypothesis is that the associated F-actin is used for transport of the endosomes to the level of the stress fibers where the endosomes can link with the ends of microtubules. This would explain the stepwise requirement for the actin and microtubule cytoskeleton in basal to apical transcytosis. Two possible endosome transport mechanisms using F-actin have been described. One is actin polymerization based propulsion (APBP) (Borisy and Svitkina, 2000; Condeelis, 2001; Machesky, 1999; Theriot, 2000) and the other is myosin based motility (Baker and Titus, 1998; DePina and Langford, 1999; Tuxworth and Titus, 2000; Wu et al., 2000).

Initially, APBP was observed as a mechanism for motility of certain intracellular microorganisms . Bacteria (*Listeria, Shigella* and *Rickettsia*) and at least one virus (Vaccinia) have been shown to use APBP to move through the cell cytoplasm (Gouin et al., 1999; Lasa et al., 1998; Steele-Mortimer et al., 2000). Actin polymerization is induced at one pole of the bacteria forming an actin tail. As actin continues to polymerize, the tail remains stationary and the polymerized actin pushes the bacteria through the cytoplasm (Cameron et al., 2000; Gouin et al., 1999). This requires both specialized proteins found in the bacteria coat and proteins co-opted from within the infected cell cytoplasm.

The proteins involved in APBP include Arp2 and Arp3, and five Arp 2/3 complex (Arc) proteins (p41-Arc, p34-Arc, p21-Arc, p-20-Arc and p16-Arc in mammalian cells)(Borisy and Svitkina, 2000; Dramsi and Cossart, 1998). The Arp 2/3 complex is involved in actin polymer nucleation. *In vitro* studies have shown that the Arp2/3 complex is capable of nucleating F-actin but this nucleation is weak compared to that observed at the barbed end of filaments (Machesky and Gould, 1999; Mullins et al., 1998). Mullins et al. has demonstrated that the Arp2/3 complex can bind the pointed end of F-actin with high affinity (Mullins et al., 1998). This binding inhibits both disassembly and growth at the pointed end of the actin filament and promotes extension from the barbed end (Mullins et al., 1998). In addition, the Arp2/3 complex binds to the sides of F-actin crosslinking them into a branching structure (Mullins et al., 1998). Together, these actions form a highly dynamic, dendritic network of F-actin. Studies have shown that actin tail formation for *Listeria* and *Shigella* APBP requires the Arp2/3 complex (Gouin et al., 1999; Welch et al., 1998). In fact, the *Listeria* protein ActA has been shown to interact with the Arp2/3 complex enhancing its ability to nucleate F-actin (Welch et al., 1998).

Similarly, the WASP family of proteins has been shown to activate the Arp2/3 complex enhancing its weak intrinsic ability to nucleate F-actin (Blanchoin et al., 2000; Machesky et al., 1999). The *Shigella* protein IcsA has been shown to interact with neuronal WASP (N-WASP) (Suzuki

et al., 1998). WASP is one member of a family of proteins that includes WASP, N-WASP, Scar/ WAVE and Bee1p (a yeast homolog) (Caron, 2002). The C-terminus of WASP has two conserved domains. The first is a WASP homology 2 (WH2) domain, which binds to actin monomers (Mullins, 2000). The other is an Arp2/3 complex interacting region (Mullins, 2000). The mechanism by which WASP activates the Arp2/3 complex is not known but it is postulated that WASP binding induces a conformational change in the Arp2/3 complex leading to enhanced F-actin nucleation (Mullins, 2000).

In addition to Arp2/3 complex and its activator, several other cellular proteins have been shown to be involved in actin tail formation and motility. *In vitro* reconstitution of either *Listeria* or *Shigella* APBP has demonstrated that the only cellular proteins required for actin tail formation are actin, Arp2/3 complex, capping protein and cofilin (Loisel et al., 1999). Capping protein binds the majority of barbed ends stopping filament growth . Therefore, capping controls actin filament growth by limiting actin polymerization to either new sites of actin nucleation or regions where capping is inhibited (Borisy and Svitkina, 2000). Cofilin acts as an F-actin severing protein and it is also thought to increase filament turnover by increasing the off-rate of actin monomers from the pointed end (Cooper and Schafer, 2000; Rosenblatt et al., 1997). The latter function is thought to increase actin treadmilling in conjunction with profilin, a protein which binds actin monomers and adds them to the barbed end (Borisy and Svitkina, 2000). Profilin is not required for actin tail formation but enhances motility efficiency (Frischknecht and Way, 2001). VASP family proteins bind profilin, ActA and F-actin (Cameron et al., 2000). It is hypothesized that VASP helps link the bacteria to the forming actin tail and induces movement by a ratchet-like mechanism (Steele-Mortimer et al., 2000). *In vitro* reconstitution of *Listeria* APBP, but not *Shigella* APBP, requires VASP for maximal efficiency (Loisel et al., 1999). In addition, α-actinin, an actin crosslinking protein, has been implicated in providing directionality of *Listeria* APBP but it does not seem to be required for tail formation or motility (Gouin et al., 1999). Finally, other proteins have been localized with actin tails but their functions are not as well understood.

In contrast to *Listeria* and *Shigella*, *Rickettsia* actin tail formation may not require the Arp2/3 complex (Gouin et al., 1999). Structural analysis of *Rickettsia* tails show that it is composed of longer parallel actin filaments when compared to *Listeria* or *Shigella* tails (Gouin et al., 1999). In addition, Arp2/3 complex, cofilin, capping-protein and N-WASP are not associated with *Rickettsia* tails but VASP and α-actinin are found throughout the actin tail (Gouin et al., 1999). This suggests that an alternative mechanism for actin tail formation exist.

Currently, it is thought that bacterial-based APBP is exploiting cellular machinery used for lamellipodia and filopodia formation (Rohatgi et al., 1999; Welch et al., 1997). Recent evidence has linked the Rho family GTPase Cdc42 (which induces filopodia formation) to Arp2/3 activation (Rohatgi et al., 1999). Evidence suggests that Cdc42 and phosphatidlyinositol 4,5-bisphophate (PIP_2) localizes N-WASP to the membrane and activates it (Ma et al., 1998; Miki et al., 1996). N-WASP can then bind and activate the Arp2/3 complex leading to the formation of a dendritic network at the nascent filopodia (Rohatgi et al., 1999).

There is evidence that suggests cells may use APBP for organelle transport. Merrifeld et al. demonstrated that pinosomes in cultured mast cells are pushed away from the plasma membrane by short-lived actin tails (Merrifield et al., 1999). The pinosomes also showed a preference in direction relative to the plasma membrane (Merrifield et al., 1999). The majority moved away from the plasma membrane at an angle between 45^{o} and 90^{o} (Merrifield et al., 1999). Another study by Tauton et al. showed that a subset of vesicles formed actin tails minutes after Phorbol 12-myristate 13-acetate (PMA) treatment of *Xenopus* eggs (Taunton et al., 2000). PMA is an activator of protein kinase C (PKC). The vesicles are associated with PKC and treatment with PMA stimulated actin tail formation (Taunton et al., 2000). These endosomes could form actin tails in an *in vitro* system.

Similar results were observed with vesicle preparations from HeLa cells (Taunton et al., 2000). In addition, N-WASP colocalized with HeLa cell derived vesicles and N-WASP distribution on the vesicles was polarized (Taunton et al., 2000).

Finally, Rozelle et al. demonstrated that increases in PIP_2 promote actin tail formation on vesicles in Swiss 3T3 fibroblasts (Rozelle et al., 2000). Injection or transfection of dominant negative WASP constructs inhibited the tail formation (Rozelle et al., 2000). This suggests that formation of a comet tail requires the Arp2/3 complex. Analysis of the tails showed that 26% were associated with endocytic vesicles and 61% associated with Golgi-derived vesicles (Rozelle et al., 2000). These studies suggest that cells may have machinery to form endogenous comet tails for vesicle and organelle transport.

Therefore, one hypothesis is that actin polymerization is induced on basolateral endosomes thus forming an actin tail. Continuous actin polymerization propels the endosomes away from the plasma membrane and through the cytoplasm in a rocket-like fashion to the level of the stress fibers. The endosome associated F-actin is a small actin tail oriented perpendicular to the basal plasma membrane. This would account for the early actin dependent step in basal to apical transcytosis. Once the endosome is propelled above the stress fibers, it switches to the microtubules for transport to the apical pole of the cell.

A second potential model for the transport of the endosomes through the actin-rich cortex of the cell is a myosin motor-based endosome transport mechanism. Currently, there are at least 13 distinct classes of unconventional (nonmuscle) myosins (Mermall et al., 1998). At least five classes (I, V, VI, VII and conventional or class II myosin) have been implicated in membrane trafficking(DePina and Langford, 1999; Mermall et al., 1998; Tuxworth and Titus, 2000).

The strongest evidence for myosin-based organelle motility involves class V myosins. In yeast, two class V myosins, Myo2p and Myo4p, are thought to be involved in organelle transport(Wu et al., 2000). Myo2p accumulates at the bud tip and this accumulation requires the actin cytoskeleton(Wu et al., 2000). A temperature sensitive mutant of Myo2p results in cells that are unable to form a bud and the cells accumulate many cytoplasmic vesicles (Pruyne et al., 1998). It has been hypothesized that Myo2p is required for polarized delivery of these vesicles to the forming bud tip. Myo4p, which has a similar sequence to Myo2p, has been implicated in establishing the polarized distribution of ASH1, a particular mRNA, at the bud tip (Bertrand et al., 1998). This polarized distribution also requires an intact actin cytoskeleton. In mammalian cells, studies using melanocytes from wild type and myosin Va null (*dilute*) mice demonstrated that melanosome transport uses both actin and microtubules (Wu et al., 1998). The melanosomes use the microtubules for long-range transport and actin-based transport for short distances (Wu et al., 1998). Wu et al. showed that *dilute* melanocytes were capable of long-range melanosome transport in a fast, bi-directional manner using microtubules but were unable to capture the melanosomes at the peripheral dendritic tips (Wu et al., 1998). This suggests that myosin Va is required to trap melanosomes at the dendritic tips using the actin cytoskeleton. In addition, slower short-ranged actin-based transport could be seen in wild type but not *dilute* melanocytes (Wu et al., 1998). This suggests that local melanosome movement may be due to myosin Va.

Shaker-1 mice also have altered melansome distributions in retinal pigment epithelial (RPE) cells due to a myosin VIIa deficiency (Liu et al., 1998). Melanosomes again fail to reach the outer periphery of the RPE cells (Liu et al., 1998). This suggests that myosin VIIa may play a role in the transport of the melanosomes or in the organization of actin at the outer periphery that may impair melanosome distribution. Furthermore, opsin distribution in the photoreceptors of *shaker-1* mice is also altered (Liu et al., 1999). Opsin is synthesized in the inner segment of the photoreceptor and then transported through the connecting cilia to the outer segment. (Liu et al., 1999) Myosin VIIa has been localized to the connecting cilia of the photoreceptor. In *shaker-1* mice, some opsin remains

in the connecting cilia that suggests myosin VIIa may play a role in opsin transport (Liu et al., 1999). In the outer and inner cochlear hair cells of mice, aminoglycosides are internalized through an undefined endocytic pathway (Richardson et al., 1997). Uptake of aminoglycosides in *shaker-1* mice is severely inhibited (Richardson et al., 1997). Similarly, Myosin VIIa null mutants of *Dictyostelium* exhibit significantly reduced levels of phagocytosis (Tuxworth and Titus, 2000). This suggests a role for myosin VIIa in endocytosis.

Class VI myosins are hypothesized to be involved in transport of vesicles and endosomes from the plasma membrane, through the cortical actin and to microtubules. Myosin VI, unlike all other myosins, moves toward the pointed end of actin filaments (Schliwa, 1999; Wells et al., 1999). Therefore, it may transport vesicles through the cortical actin, which are primarily organized with the barbed end facing the membrane. Analysis of polarized epithelial cells has shown that myosin VI colocalizes with clathrin-coated pits and vesicles (Buss et al., 2001). Myosin VI is enriched in purified clathrin-coated vesicles. Co-immunoprecipitation of myosin VI shows that it interacts with adaptor protein-2 and clathrin (Buss et al., 2001). Finally, overexpression of the tail domain of myosin VI in fibroblasts inhibits transferrin uptake by >50% (Buss et al., 2001). This data suggests that myosin VI is involved in clathrin mediated endocytosis. In addition, myosin VI has been shown to interact with CLIP-170, a microtubule-binding protein. CLIP-170 is localized to the distal ends of dynamic microtubules in the cell periphery and both dynactin and dynein have been colocalized with this distal CLIP-170 (Lantz and Miller, 1998; Vaughan et al., 1999). A model has been suggested in which myosin VI is responsible for inward vesicle movement by initially using the cortical actin and then transferring the vesicles to microtubules via CLIP-170. The vesicles are then carried further into the cell using a dynein motor.

Evidence suggests that class I myosins in yeast, Myo3p and Myo5p, are part of the endocytic machinery. Myo5p null cells are defective in the rate of receptor-mediated endocytosis and, if Myo3p is also deleted, the defect becomes more severe (Geli and Riezman, 1996). In vertebrate

cells, myosin-Iα associates with tubulovesicular endosomes (Raposo et al., 1999). Overexpression of a nonfunctional truncated form of myosin-Iα disperses the tubulovesicular endosomal compartment and impairs fluid-phase marker delivery to lysosomes. Finally, expression of truncated, non-functional form of brush border myosin I (BBMI) affected basolateral transferrin recycling and basal to apical transcytosis of dipeptidyl-peptidase IV (Durrbach et al., 2000).

Class II or conventional myosins are primarily associated with their role in skeletal muscle function but recent evidence supports a role for myosin II in vesicle transport. Studies of mammalian cells suggest that myosin II is involved in vesicle budding from the *trans*-Golgi network (TGN) (Musch et al., 1997; Stow et al., 1998). Myosin II has been localized to the Golgi complex by immunofluorescence using several different antibodies and it has been shown to associate with a population of TGN-derived vesicles. In addition to its role in vesicle budding, DePina and Langford have demonstrated that vesicles in clam oocyte extracts use F-actin for transport and have associated myosin II (DePina and Langford, 1999). Treatment of the extracts with ML-7, a myosin light chain kinase inhibitor, resulted in inhibited vesicle transport. This suggests that myosin II is responsible for clam vesicle transport. Therefore in an alternative hypothesis, a myosin motor would attach to the endosome and subsequently would use the associated F-actin to carry the endosome through the cortical actin to the level of the stress fiber. Then an undefined mechanism would result in transfer of the endosome to microtubules for transport deeper into the cell.

To examine whether basolateral endosomes with associated F-actin are propelled by either model, we examined the localization the several proteins involved in APBP or myosin motors at the basal pole of polarized MDCK cells using confocal microscopy.

RESULTS

The Arp2/3 complex, WASP and cofilin do not colocalize with basal early endosomes

To determine if the machinery utilized in APBP was associated with the basolateral endosomes, we examined the basolateral localization of several proteins involved in APBP using confocal microscopy. In these experiments, IgA was internalized from the basolateral pole of MDCK cells for 5 min at 37^{o} C then the cells were rapidly cooled and trypsin-treated to remove any cell-surface ligand. Finally the cells were processed for confocal microscopy. IgA labeled endosomes were observed at the base of the cell similar to previous reports (Leung et al., 1999). The sections shown correspond to the region at or below the level of the stress fibers.

We examined the distribution of two members of the Arp2/3 complex, Arp3 and p21 Arc, by immunofluorescence. Large accumulations of Arp3 were found along the lateral borders of the cells particularly at junctions of three or more cells (Figure 4-1A & D). Arp3 colocalized with a few IgA-labeled endosomes at these accumulations but the majority of the IgA-labeled endosomes were not associated with Arp3 (Figure 4-1C & F). Similarly, p21Arc was also found in large accumulations at the lateral border and it was also in a small number of punctate basal structures (Figure 4-1G & J). Very few p21Arc-positive structures colocalized with IgA-labeled endosomes (Figure 4-1I & L). This suggests that the Arp2/3 complex is not associated with IgA-labeled basolateral endosomes.

We examined the distribution of two WASP-family proteins, WASP and N-WASP, in MDCK cells by immunofluorescence. No staining of WASP was seen in these cells (data not shown) but this is not unexpected because WASP is exclusively expressed in haematopoietic cells (Ramesh et al., 1999). Next, we examined N-WASP, which is more ubiquitously expressed (Ramesh et al., 1999). N-WASP was found in several punctate structures at the base of the cells and in larger accumulations at the lateral border particularly at junctions of three or more cells (Figure 4-2A &

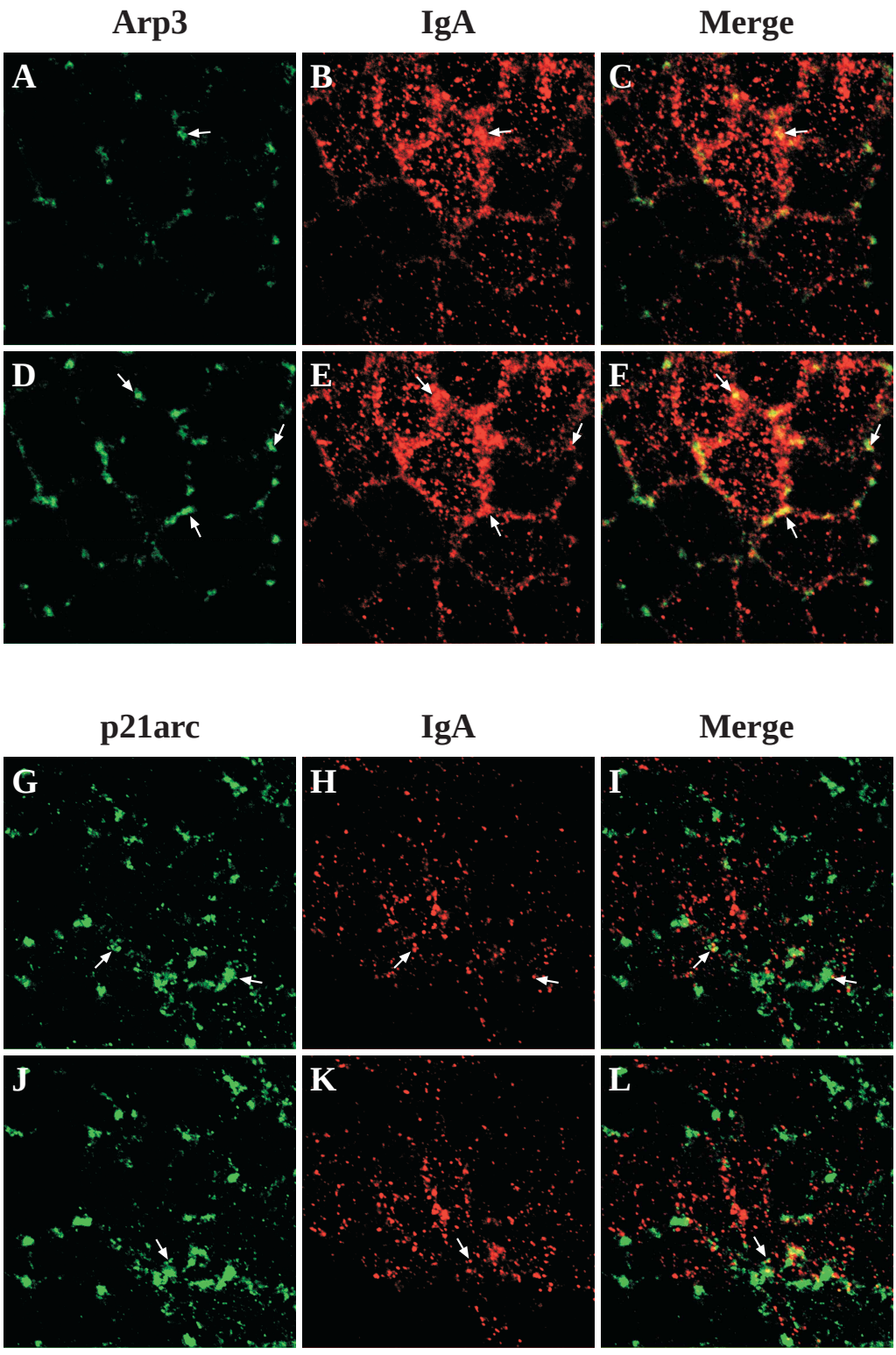

Figure 4-1. Distribution of Arp3, p21arc and IgA in MDCK cells. IgA was internalized for 10 min at 37˚ C from the basolateral surface of MDCK cells, and cell surface ligand removed by

trypsin treatment at 4˚ C. Cells were fixed with paraformaldehyde, incubated with rabbit anti-Arp3 (**A, B, C, D, E, F**) or rabbit anti-p21arc (**G, H, I, J, K, L**) and then reacted with goat anti-hIgA-CY5 and goat anti-rabbit-FITC secondary antibodies. The FITC and CY5 emission was simultaneously captured using a scanning laser confocal microscope. Single optical sections were taken at the very base of the cell (**D, E, F and J, K, L**), 1 μm above the previous section (**A, B, C and G, H, I**). Examples of Arp3 or p21arc and IgA colocalization are marked with arrows. Bar=10μm

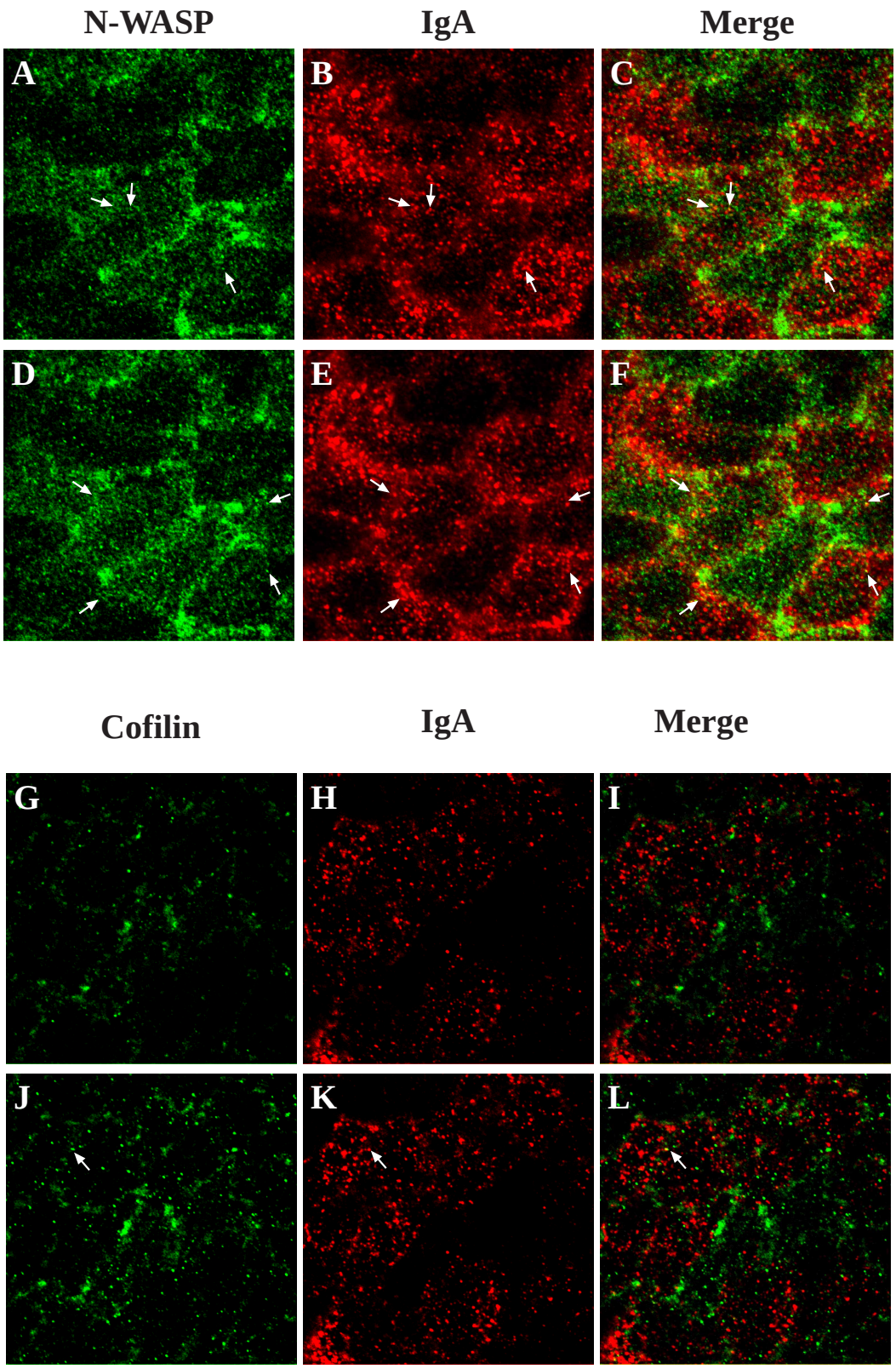

Figure 4-2. Distribution of NWASP, cofilin and IgA in MDCK cells. IgA was internalized for 10

min at 37˚ C from the basolateral surface of MDCK cells, and cell surface ligand removed by trypsin treatment at 4˚ C. Cells were fixed with paraformaldehyde, incubated with rabbit anti-NWASP (**A, B, C, D, E, F**) or rabbit anti-cofilin (**G, H, I, J, K, L**) and then reacted with goat anti-hIgA-CY5 and goat anti-rabbit-FITC secondary antibodies. The FITC and CY5 emission was simultaneously captured using a scanning laser confocal microscope. Single optical sections were taken at the very base of the cell (**D, E, F and J, K, L**), 1 μm above the previous section (**A, B, C and G, H, I**). Examples of NWASP or cofilin and IgA colocalization are marked with arrows. Bar=10μm

D). A moderate number of the smaller punctate structures did colocalize with IgA-labeled endosomes (Figure 4-2C & F). However, further repetition of this experiment did not result in N-WASP staining and the cause of this is not known. Therefore, N-WASP may or may not be expressed in MDCK cells and it is inconclusive whether IgA-labeled endosomes are associated with N-WASP.

Cofilin has also been shown to associate with *Listeria* and *Shigella* comet tails (Gouin et al., 1999). We examined the distribution of cofilin in MDCK cells by immunofluorescence. Cofilin was found on small punctate structures at the base of the cells and some larger accumulations that are possibly at the lateral borders (Figure 4-2G & J). Little colocalization of cofilin with IgA-labeled endosomes was seen (Figure 4-2I & L).

PKCα is not localized to basal early endosomes

The PKC family has been demonstrated to play a role in many transport processes including endocytosis, postendocytic transport and APBP. PMA is an activator of many PKC isoforms. *In vivo* experiments on *Xenopus* oocytes showed that PMA treatment induced PKCα association with cytoplasmic vesicles and some of these vesicles exhibited the formation of comet-like actin tails (Taunton et al., 2000). Another PKC isoform, PKCε, has been demonstrated to regulate basolateral endocytosis by inducing remodeling of filamentous actin (Song et al., 1999). Furthermore, PKC activation increases basolateral endocytosis, basal to apical transcytosis and apical recycling in MDCK cells. This suggests that PKC may be involved in regulating endosome trafficking and this regulation may be through F-actin remodeling including the formation of comet tails. We examined the distribution of PKCα and PKCε in MDCK cells by immunofluorescence. No PKCε staining was seen (data not shown). PKCα was found in small punctate structures at the base of MDCK cells (Figure 4-3A & D). No colocalization of PKCα with IgA-labeled endosomes was seen (Figure 4-3C & F),

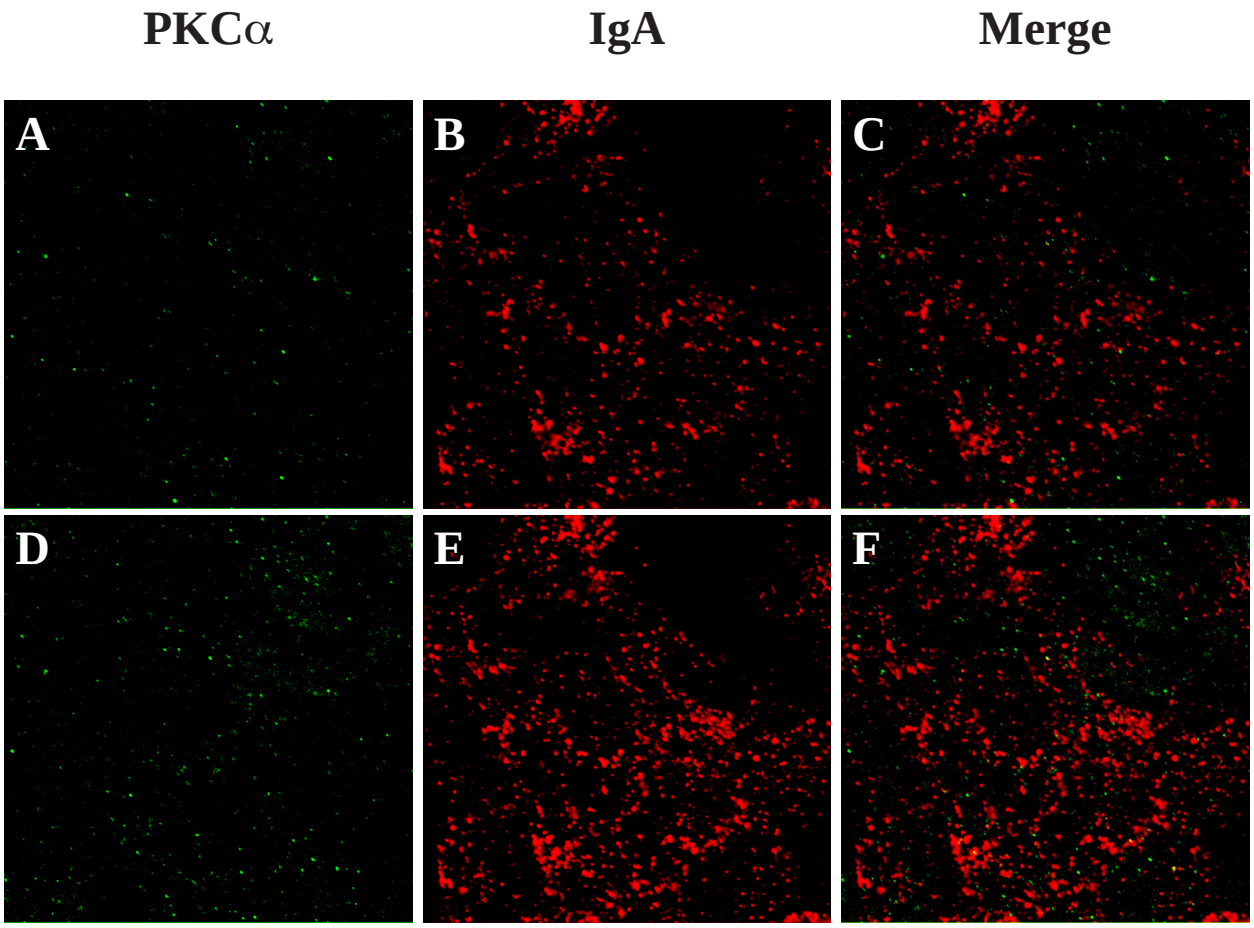

Figure 4-3. Distribution of PKCα and IgA in MDCK cells. IgA was internalized for 10 min at 37˚ C from the basolateral surface of MDCK cells, and cell surface ligand removed by trypsin treatment at 4˚ C. Cells were fixed with paraformaldehyde, incubated with mouse anti- PKCα (**A, B, C, D, E, F**) and rabbit anti-IgA antibodies, and then reacted with goat anti-rabbit-CY5 and goat anti-mouse-FITC secondary antibodies. The FITC and CY5 emission was simultaneously captured using a scanning laser confocal microscope. Single optical sections were taken at the very base of the cell (**D, E, F**), 1 μm above the previous section (**A, B, C**). Examples of PKCα and IgA colocalization are marked with arrows. Bar=10μm

MIc but not BBMI colozalizes with basal early endosomes

An alternative mechanism for endosome motility via the actin cytoskeleton is through the association of myosin motors. Several classes of unconventional myosins have been implicated in vesicle and organelle transport. In order to narrow down the number of unconventional myosins to be analyzed by immunofluorescence, we first examined expression of several myosins in MDCK cells by Western blot. We probed both an MDCK lysate and an early endosome enriched fraction from a discontinuous sucrose gradient. Only two myosins were found to be expressed in MDCK cells, brush border myosin I (BBMI) and MIc (MIc) (Figure 4-4B lanes 1 & 2). Therefore we examined the distribution of these two myosins using confocal microscopy after labeling the basolateral endosomes with IgA as described above.

The distribution of BBMI and MIC in MDCK cells was examined by immuno-fluorescence. BBMI was found in punctate structures at the base of MDCK cells (Figure 4-5A & D). However, there was little colocalization of BBMI-associated structures with IgA-labeled endosomes (Figure 4-5C & F). MIc was associated with the lateral plasma membrane and also small punctate structures at the base of the cell (Figure 4-5G & J). There was some colocalization of MIc with IgA-labeled endosomes at both the lateral accumulations and the smaller punctate structures (Figure 4-5I & L). This suggests that MIc maybe involved in trafficking of the IgA-labeled basolateral endosomes.

Expression of RhoAV14 does not significantly alter BBMI or MIc localization

In MDCK cells expressing the dominant-active form of RhoA (RhoAV14), there is an accumulation of IgA-labeled endosomes (Leung et al., 1999). In addition, expression of RhoAV14 increases the level of F-actin associated with these endosomes. It is therefore possible that cells expressing RhoAV14 may also exhibit a significant increase in myosin association with IgA-labeled endosomes. In RhoAV14 cells, BBMI was still found on small punctate structures at the base of the cell (Figure 4-6A &D). There was a slight increase in the number of BBMI-associated structures at the base of these cells but this was difficult to determine due to drastic changes in the cell morphology.

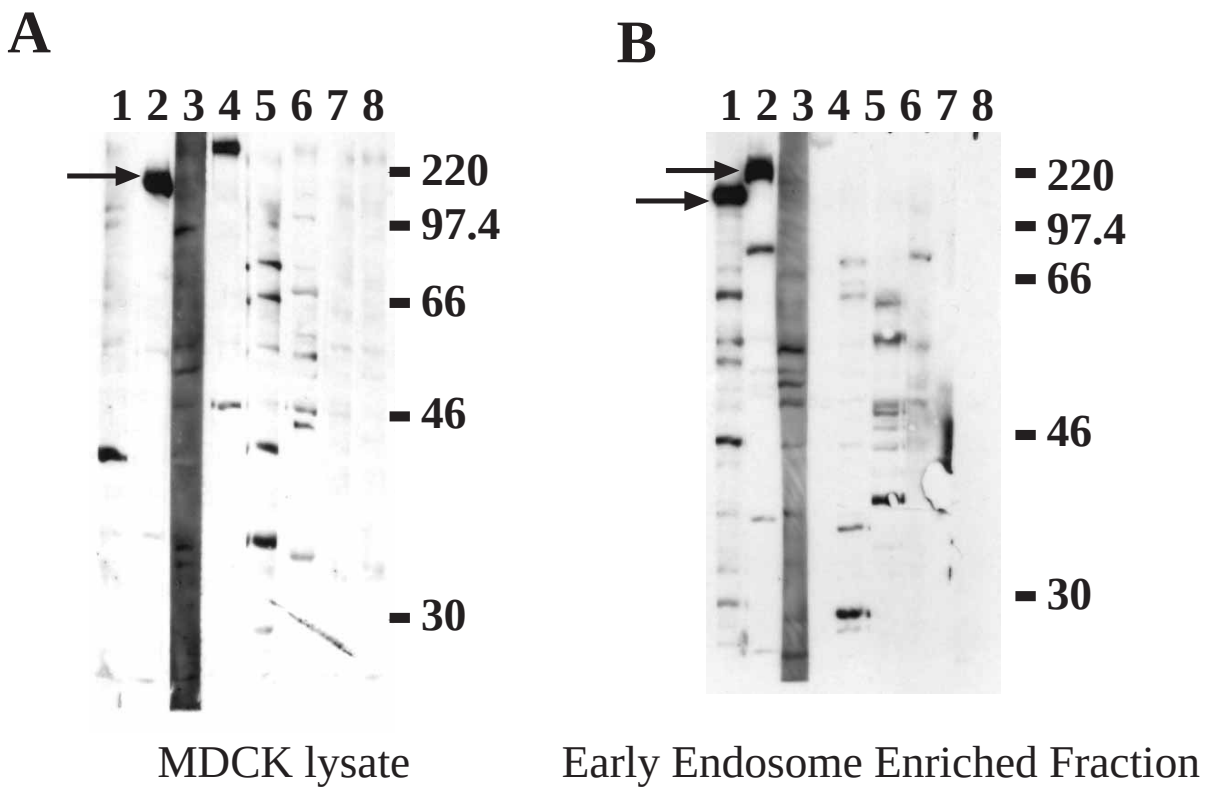

Figure 4-4. Expression of myosin isoforms in MDCK cells. Filter grown MDCK cells were lysed with SDS lysis buffer and then vortex shaken to shear the DNA (**A**). Cells were homogenized and a postnuclear supernatant was generated, the postnuclear supernatant (adjusted to 40.2% sucrose) was overlaid with 35, 25, and 8.5% (wt/wt) sucrose solutions and then centrifuged. The early endosome enriched fraction at the 35% and 25% sucrose solution interface was collected (**B**). MDCK whole cell lysates (**A**) or an early endosome enriched fraction (**B**) were resolved using PAGE and Western blots probed by antibodies. 1 - BBMI, 2 - MIc, 3 - Myosin V tail, 4 - Myosin VI tail, 5 - Myosin VIIa, 6 - Myosin IXb, 7 - Myosin II and 8 - nonimmune rabbit IgG. Positive expression of myosin isoform indicated by arrow.

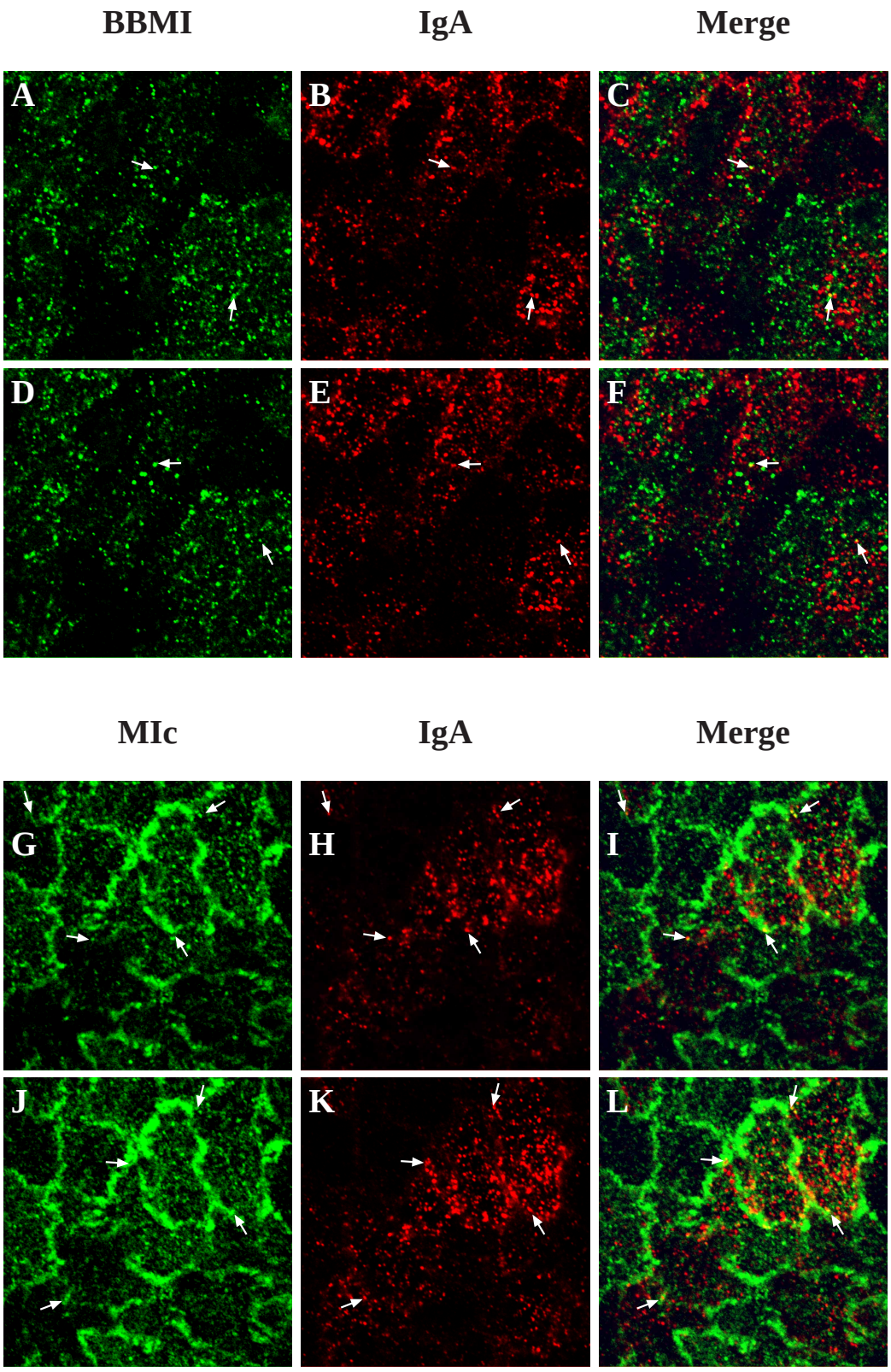

Figure 4-5. Distribution of BBMI, MIc and IgA in MDCK cells. IgA was internalized for 10 min

at 37˚ C from the basolateral surface of MDCK cells, and cell surface ligand removed by trypsin treatment at 4˚ C. Cells were fixed with paraformaldehyde, incubated with rabbit anti-BBMI (**A, B, C, D, E, F**) or rabbit anti-MIc (**G, H, I, J, K, L**) antibodies, and then reacted with goat anti-hIgA-CY5 and goat-anti-rabbit-FITC secondary antibodies. The FITC and CY5 emission was simultaneously captured using a scanning laser confocal microscope. Single optical sections were taken at the very base of the cell (**D, E, F and J, K, L**), 1 μm above the previous section (**A, B, C and G, H, I**). Examples of BBMI or MIc and IgA colocalization are marked with arrows. Bar=10μm

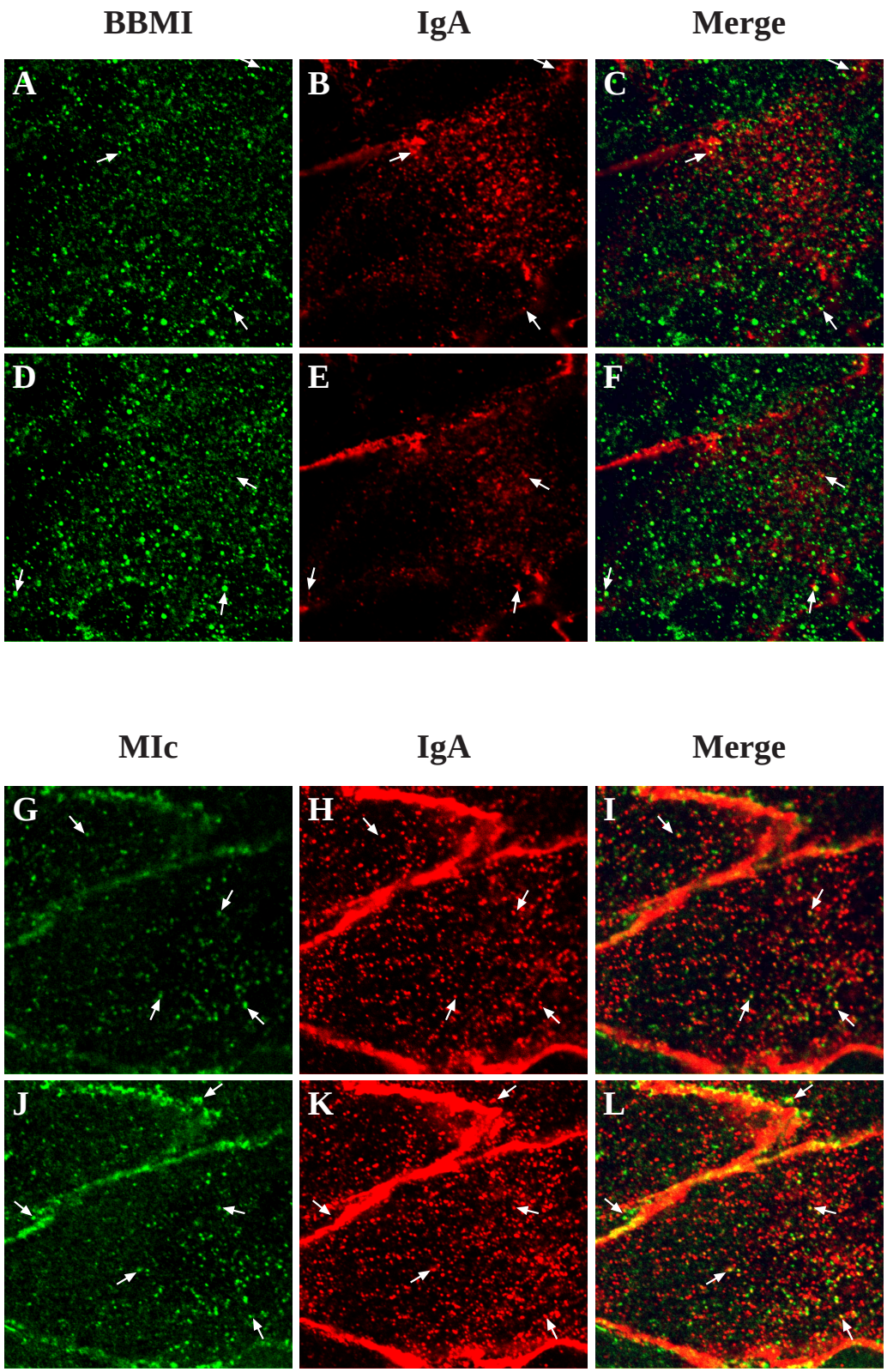

Figure 4-6. Distribution of BBMI, MIc and IgA in RhoAV14 cells grown in the presence of 20

ng/ml DC. IgA was internalized for 10 min at 37˚ C from the basolateral surface of RhoAV14 cells grown in the presence of 20 ng/ml DC, and cell surface ligand removed by trypsin treatment at 4˚ C. Cells were fixed with paraformaldehyde, incubated with rabbit anti-BBMI (**A, B, C, D, E, F**) or rabbit anti-MIc (**G, H, I, J, K, L**) antibodies, and then reacted with goat anti-rabbit-CY5 and goat anti-mouse-FITC secondary antibodies. The FITC and CY5 emission was simultaneously captured using a scanning laser confocal microscope. Single optical sections were taken at the very base of the cell (**D, E, F and J, K, L**), 1 μm above the previous section (**A, B, C and G, H, I**). Examples of BBMI or MIc and IgA colocalization are marked with arrows. Bar=10μm

There was little change in the amount of colocalization of BBMI and IgA-labeled endosomes in RhoAV14 cells (Figure 4-6C & F). MIc in RhoAV14 cells was still found at the lateral plasma membrane and in small punctate structures at the base of the cell (Figure 4-6G & J). The level of colocalization between IgA-labeled endosomes and MIc was slightly increased but a large population of IgA-labeled endosomes does not associate with MIc (Figure 4-6I & L). Although, expression of RhoAV14 does not trap MIc on IgA-labeled endosomes, it is still possible that MIC is involved in the movement of IgA-labeled endosomes.

Hip1R and APC do not colocalize with basal early endosomes

In addition to the proteins involved in APBP and the unconventional myosins, we examined a number of other proteins that have been shown to link the endocytic system with the cytoskeleton. Hip1R has a talin-like actin-binding domain and colocalizes with F-actin. Hip1R has been shown to associate with clathrin-coated vesicles and colocalizes with clathrin, AP-2 and endocytosed transferrin (Engqvist-Goldstein et al., 1999). Therefore Hip1R is thought to link the endocytic machinery to the actin cytoskeleton. It is therefore possible that Hip1R is associated with IgA-labeled endosomes. Analysis of the distribution of Hip1R in MDCK cells shows that Hip1R was found on small punctate structures at the base of the cell (Figure 4-7A & D) but there was little colocalization between Hip1R and the IgA-labeled endosomes (Figure 4-7C & F).

The protein CLIP170 is associated with the plus-end of microtubules and in *Drosophila* it has been shown to associate with Myosin VI. However, there was no CLIP-170 staining in MDCK cells. The Adenomatous Polyposis Coli (APC) protein has been shown to express in epithelial cells and is also concentrated at the plus-end of microtubules (Mimori-Kiyosue et al., 2000). Therefore we examined the basolateral distribution of APC protein and its colocalization with IgA-labeled endosomes. APC protein was associated with punctate structures at the very base of the cell (Figure 4-7G & J). However, no colocalization of APC protein and IgA-labeled endosomes was observed (Figure 4-7I & L).

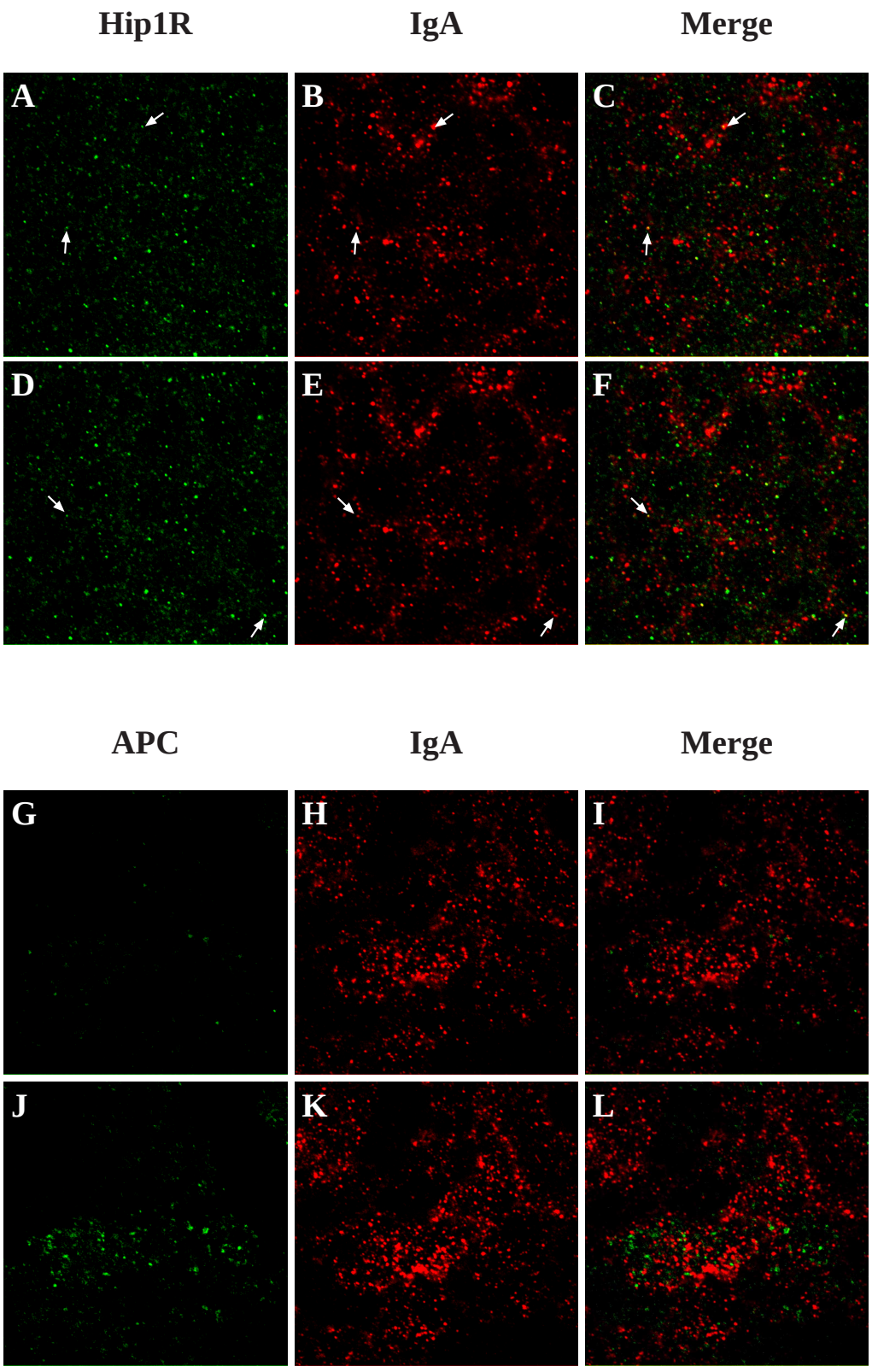

Figure 4-7. Distribution of Hip1R, APC and IgA in MDCK cells. IgA was internalized for 10

min at 37˚ C from the basolateral surface of MDCK cells, and cell surface ligand removed by trypsin treatment at 4˚ C. Cells were fixed with paraformaldehyde, incubated with guinea pig anti-Hip1R (**A, B, C, D, E, F**) or rabbit anti-APC (**G, H, I, J, K, L**) antibodies, and then reacted with goat anti-hIgA-CY5 and goat anti-rabbit-FITC or goat-anti-guinea pig-FITC secondary antibody. The FITC and CY5 emission was simultaneously captured using a scanning laser confocal microscope. Single optical sections were taken at the very base of the cell (**D, E, F and J, K, L**), 1 μm above the previous section (**A, B, C and G, H, I**). Examples of Hip1R or APC and IgA colocalization are marked with arrows. Bar=10μm

DISCUSSION

Role of APBP in basal early endosome transport

APBP has primarily been described as a method of bacterial motility using co-opted cellular machinery. Many of the proteins involved in this process have been described as part of the machinery for lamellipodia and filopodia formation. However, there is growing evidence that APBP is used in mammalian cells as a method of moving vesicles, endosomes and lysosomes (Borisy and Svitkina, 2000; Merrifield et al., 1999; Rozelle et al., 2000; Taunton et al., 2000).

The Arp2/3 complex is required for *Listeria* and *Shigella* comet tail formation and is localized with the actin tail (Gouin et al., 1999; Steele-Mortimer et al., 2000). The lack of colocalization of the Arp 2/3 complex proteins with the basolateral IgA-labeled endosomes suggests that the endosomes do not use some form of APBP. In addition, the lack of Arp3-positive punctate structures at the base of the cell suggests that no internalized vesicles from the basal membrane use APBP. There is an alternative method of APBP that does not seem to require the Arp2/3 complex. The comet tails of *Rickettsia* are structurally different from that of *Listeria* or *Shigella* (Gouin et al., 1999). These tails are much more linear rather than a branched network and the Arp2/3 complex is absent. *Rickettsia* comet tails also lack several other proteins found in *Listeria* or *Shigella* tails including cofilin, capZ (a barbed end actin capping protein) and N-WASP (Gouin et al., 1999). Therefore *Rickettsia* comet tails are likely to use a different mechanism but the proteins involved in this are not known. It is still possible that the IgA-labeled endosomes could move by a *Rickettsia*-type APBP mechanism.

Examination of the protein N-WASP suggests that it colocalizes with a subset of basolateral endosomes. However, repetition did not result in N-WASP staining. It is not clear whether this is due to loss of a functional antibody or if the initial experiment was faulty. It is of interest to note however that the Rho family protein Cdc42 is known to bind and activate N-WASP. Expression of

the dominate-active mutant of Cdc42, Cdc42V12, in MDCK cells inhibits transport of basolaterally internalized ligands (Rojas et al., 2001). In addition, confocal microscopy reveals that Cdc42V12 can be found on several basolateral endosomes. This supports the possibility that N-WASP may be located on basolateral endosomes, but this will require further examination.

Endogenous APBP machinery may regulate cell shape

Although it does not seem likely from our data that the APBP machinery is involved in transport of the basolateral endosomes, one interesting observation is many of the proteins involved in APBP are localized to the corners (where three or more cells meet) of the lateral membrane. The reason for this association is not known but it is possible that the APBP machinery may play a structural role. The actin cytoskeleton is known to play a critical role in cell shape maintenance. Examination of migratory cells has shown that many APBP proteins including the Arp2/3 complex can be found within lamellipodia (Welch et al., 1997). Interestingly, expression of dominant active Rac1, the Rho family protein associated with lamellipodia formation, in polarized MDCK cells results in a dramatic increase of lateral membrane interdigitations as seen by transmission electron microscopy (Jou et al., 2000).

Role of myosin in basal early endosome transport

Several unconventional myosins have been linked to the transport of intracellular organelles. Analysis of MDCK cells by Western blot shows that MIc and BBMI are expressed but results of our studies indicate that only MIc exhibits any association with the IgA-labeled endosomes. The sparse level of colocalization of MIc with the endosomes does not rule out the possibility that they represent a transient step of the transport mechanism. In normal cells, only a subset of the endosomes is actin associated and therefore it is not surprising that only a subset of endosomes is MIc associated. In cells expressing dominant active RhoA, IgA is trapped in basolateral endosomes that are all associated with F-actin (Leung et al., 1999). MIc in these cells exhibits a slight increased association with IgA-labeled basal endosomes. RhoA activation probably does not induce MIc association

with the endosomes although the limited population of MIc may not be capable of labeling all the basolateral endosomes. Recently, Durrbach et al. have demonstrated that BBMI is involved in basolateral recycling of transferrin in Caco-2 cells (Durrbach et al., 2000). Expression of a truncated non-functional dominant negative BBMI effects transferrin recycling and basal to apical transcytosis of dipeptidyl-peptidase IV. Whether the dominant negative BBMI is competing with endogenous BBMI or some other related myosin I is not known. We do not see any association of BBMI with IgA-labeled endosomes. IgA and Tf have been shown to be internalizaed together and then delivered to BEE. This suggests that BBMI plays no role in Tf recycling in MDCK cells.

It is possible that other myosins may be expressed in MDCK cells. At least five classes of myosins have been shown to express in polarized epithelial cells (Mermall et al., 1998; Tuxworth and Titus, 2000). Although the Western blot probe only revealed two myosins, several other myosin isoforms may still be expressed in MDCK cells. Furthermore, many of the antibodies used to probe the Western blot are not created for the canine version of the myosins. The exact role myosin plays in membrane traffic at the actin cortex is not known, but evidence suggests that it may be used for both short local movements and as a mechanism for protein localization by anchoring it to the actin cytoskeleton (Wu et al., 1998). In addition, myosin VI has been shown to play a role in clathrin-mediated endocytosis (Buss et al., 2001) and myosin VII has been linked to two distinct methods of internalization (Richardson et al., 1997; Tuxworth and Titus, 2000). This supports a role for myosins in endocytosis.

Function of basal early endosome associated F-actin

Another possible role of the associated F-actin is that it is part of the endocytic machinery in polarized epithelial cells. Treatment of MDCK cells with the actin disrupting agent cytochalasin D blocks apical endocytosis of vesicular stomatitis virus G-protein and ferritin (both endocytosed via clathrin coated vesicles) and the fluid-phase marker lucifer yellow (Gottlieb et al., 1993). In addition, treatment with jasplakinolide, an actin stabilizing agent, stimulates endocytosis of fluid-phase markers

from the basolateral pole but apical endocytosis is unaffected (Shurety et al., 1998). This suggests that actin plays transient a role in the mechanism of endocytosis. The associated F-actin could play a role in endocytosis by associating with coated pits. However, this is not likely since the IgA cell surface labeling is removed by trypsin treatment and only sealed or highly constricted vesicles should be labeled. In addition, Fujimoto et al. have shown using electron microscopy that plasma membrane regions of clathrin coated pits are in fact devoid of actin filaments (Fujimoto et al., 2000).

In conclusion, vesicle transport requires actin based transport and then microtubule based transport. Similar sequential transport events have been observed. For example, melanosome transport in melanocytes is initially moved through the dendrite by fast long-ranged transport via microtubules. Then melasomes shift to the actin cytoskeleton for short-ranged movement and anchoring at the cell periphery using myosin V (Wu et al., 1998). This study demonstrated that MIc is localized to F-actin-associated basolateral endosomes. Based on these other systems, basolateral endosomes may use the actin cytoskeleton and a myosin motor for short-ranged transport at the cell periphery.

CHAPTER 5

SNAP-23 Requirement for Transferrin Recycling in Streptolysin-O-permeabilized Madin-Darby Canine Kidney Cells*

ABSTRACT

Fusion of recycling and transcytotic vesicles with the apical and basolateral plasma membrane domains of Madin-Darby canine kidney (MDCK) cells requires the N-ethylmaleimide (NEM) sensitive factor (NSF) and is sensitive to botulinum neurotoxin serotype E (BoNT/E). BoNT/E is thought to selectively proteolyze the 25,000 D synaptosomal associated protein (SNAP-25), a protein found in neurons or cells of neuroendocrine origin. However, SNAP-25 is not found in MDCK cells. One possible target for BoNT/E in MDCK cells is SNAP-23, a newly described SNAP-25 homolog that is found in several organs including kidney. Currently, the function of SNAP-23 is unknown. We have reconstituted transferrin (Tf) recycling in permeabilized MDCK cells to assess the role of SNAP-23 in the endocytic traffic of this protein. We find that: (i) SNAP-23 is expressed in MDCK cells and is found both at the basolateral plasma membrane and associated with apical and basolateral vesicles, (ii) canine SNAP-23 is cleaved by BoNT/E, (iii) Tf recycling is NSF dependent and BoNT/E sensitive and (iv) addition of either exogenous SNAP-23 or anti-SNAP-23 antibodies inhibits ligand recycling. Our observations suggest that SNAP-23 may be required for fusion of recycling vesicles with the basolateral membrane of polarized MDCK cells.

* Reprinted from *Journal of Biological Chemistry*, (1998, volume 273, pg. 17732-17741), with permission by the American Society for Biochemistry & Molecular Biology

INTRODUCTION

Membrane trafficking is mediated by transport vesicles that bud from a donor membrane and then fuse with an acceptor membrane (Wilson et al., 1991). An important regulatory step in this process is controlling the vesicle target specificity and subsequent fusion event. In many systems, the vesicle targeting/fusion machinery is composed of both cytosolic and membrane bound proteins (Pevsner and Scheller, 1994). The cytosolic components are the N-ethyl maleimide sensitive factor (NSF) (Block et al., 1988; Glick and Rothman, 1987), and the soluble NSF attachment protein (SNAP) that binds NSF to the fusion complex (Clary et al., 1990; Whiteheart and Kubalek, 1995). The membrane bound components, the SNAP receptors (SNAREs), are divided into two types — vesicle membrane associated (v-SNAREs) and target membrane associated (t-SNAREs). The v-SNAREs are thought to dock vesicles to the appropriate target membranes via interactions with cognate t-SNAREs (Sollner et al., 1993). Recent evidence suggests that the v-SNARE/t-SNARE complex may also be the minimal machinery needed for vesicle fusion to occur with the target membrane (Weber et al., 1998). Interactions between v-SNAREs/t-SNAREs are regulated by Rab proteins, N-sec-1/Munc-18 homologs (Lupashin and Waters, 1997; Pevsner et al., 1994; Rothman and Söllner, 1997; Rybin et al., 1996), as well as hydrolysis of ATP by NSF, which may act to dissociate v-SNARE/t-SNARE complexes priming them for another round of fusion (Mayer et al., 1996; Nichols et al., 1997; Ungermann et al., 1998a).

In neurons, SNAREs are thought to control synaptic vesicle docking and fusion. One v-SNARE, vesicle-associated membrane protein (VAMP, also known as synaptobrevin), and two t-SNAREs, syntaxin and SNAP-25 (not related to the SNAP of the cytosolic component) have been isolated and characterized from synaptosomal membranes (Sudhof, 1995). Clostridial neurotoxins inhibit synaptic vesicle fusion by acting as specific proteinases of a single SNARE component without cleaving the others (Jahn and Niemann, 1994). For example, VAMP is cleaved by tetanus toxin, BoNT/B, D, F, and G, while syntaxin is cleaved by BoNT/C1 and SNAP-25 is cleaved by

BoNT/A and E. It has now been shown that many trafficking reactions require SNARE-mediated targeting and fusion including ER to Golgi transport and trans-Golgi to basolateral plasma membrane transport (Bennett and Scheller, 1993; Ikonen et al., 1995; Protopopov et al., 1993). In other cases, SNAREs have been identified but their exact role in trafficking is unknown (Gaisano et al., 1996; Low et al., 1996; Peng et al., 1997).

Previously, we analyzed the role of the vesicle fusion machinery in the exit of IgA from the apical recycling endosome (ARE) and fusion with the apical and basal plasma membrane in streptolysin-O (SLO) permeabilized MDCK cells expressing the polymeric Ig receptor (pIgR) (Apodaca et al., 1996). The ARE is a tubulovesicular compartment that receives molecules transcytosing in the basolateral to apical direction and those recycling from the apical and basolateral poles of the cell (Apodaca et al., 1994; Barroso and Sztul, 1994; Mostov and Cardone, 1995). The pIgR protein transports polymeric Igs (IgA and IgM) across epithelial cells and into secretions. Both transcytosis in the basolateral to apical direction and recycling of pIgR ligand is dependent on NSF and inhibited by BoNT/E (which cleaves SNAP-25) (Apodaca et al., 1996). Surprisingly, BoNT/A has no apparent effect on either pathway. In contrast, transport of a newly synthesized protein from the trans-Golgi network to the apical surface is apparently independent of NSF/SNAP/SNAREs while transport from the trans-Golgi network to the basolateral surface requires these complexes (Ikonen et al., 1995). The above observations suggest that fusion with the apical plasma membrane of MDCK cells may occur by multiple mechanisms, one of which may require NSF/SNAP/SNAREs (basal to apical transcytosis) and one which may not (trans-Golgi network to apical cell surface delivery). While studies have found several isoforms of VAMP and syntaxin are expressed within MDCK cells (Ikonen et al., 1995; Low et al., 1996), attempts to identify SNAP-25 in MDCK cells have failed (Apodaca et al., 1996). This led us to hypothesize that a BoNT/E sensitive SNAP-25 homolog(s) may exist in MDCK cells and may be required for transcytosis and recycling (Apodaca et al., 1996).

A SNAP-25 homolog, called SNAP-23, has recently been cloned and characterized from human B lymphocytes (Ravichandran et al., 1996). Moreover, a mouse isoform of SNAP-23 (also known as syndet) has been cloned from 3T3 L1 adipocytes and is 98.6 % similar and 86.7% identical to human SNAP-23 (Araki et al., 1997; Wang et al., 1997). Unlike SNAP-25, which is distributed along axons, SNAP-23 is concentrated on nerve cell bodies with only limited staining of the axons and syntaptosomes (Deng and Whiteheart, submitted). In addition, SNAP-23 is expressed in several non-neuronal tissues including heart, lung, liver, muscle, pancreas and kidney (where it is expressed at high levels)(Ravichandran et al., 1996; Wong et al., 1997). It has been shown to bind various syntaxins (isoforms 1,2,3 and with high affinity to 4) and VAMP (Araki et al., 1997; Ravichandran et al., 1996)(Deng and Whiteheart, submitted). While SNAP-23 is localized to the plasma membrane and in vesicular structures, little is known presently about its role in membrane trafficking. Our goal was to determine if SNAP-23 was required for endocytic traffic in polarized epithelial cells.

We find that SNAP-23 is expressed in MDCK cells, both at the basolateral plasma membrane and in apical and basolateral vesicles. Tf recycling is NSF dependent and BoNT/E sensitive and addition of either exogenous SNAP-23 or anti-SNAP-23 antibodies inhibits ligand recycling. Our observations suggest that SNAP-23 may regulate fusion of recycling vesicles with the basolateral domain of polarized MDCK cells. These findings further our understanding of some of the underlying fusion mechanisms used in polarized MDCK cells and may ultimately lead to a better understanding of how polarized cells achieve and maintain their distinct plasma membrane domains.

RESULTS

MDCK cells express SNAP-23

We previously hypothesized that a SNAP-25 homolog exists in polarized MDCK cells (Apodaca et al., 1996). One possible candidate is SNAP-23, a widely distributed SNAP-25 homolog

that has recently been found in several organs including kidney (Araki et al., 1997; Ravichandran et al., 1996; Wang et al., 1997; Wong et al., 1997). Initially, we determined if SNAP-23 was expressed in MDCK cell by probing western blots of lysates from SLO-permeabilized MDCK cells with an affinity-purified rabbit polyclonal antibody against SNAP-23. A major protein band was observed at approximately 28 kD (Figure 5-1, left lane), and is slightly larger than the predicted molecular weight of 23 kD. The slower than expected mobility has been reported previously (Wong et al., 1997). There were additional protein bands at 60 kD and 90 kD. The 60 kD protein was susceptible to BoNT/E treatment (see below; Figure 5-1, right lane), and may represent dimers of SNAP-23. The faint 90 kD band was not susceptible to toxin treatment, and may be nonspecific.

SNAP-25 is specifically cleaved by BoNT/E at the Arg180-Ile181 peptide bond (Schiavo et al., 1993), and SNAP-23 was predicted to be susceptible to BoNT/E since it retains the identical cleavage sequence (Arg186-Ile187), although, at a different position. Surprisingly, recent reports determined that rat and human SNAP-23 are not cleaved by BoNT/E (Low et al., 1998; Macaulay et al., 1997). To determine whether canine SNAP-23 is susceptible to BoNT/E, we treated SLO-permeabilized MDCK cells with BoNT/E and analyzed the effects of toxin treatment on SNAP-23 immunoreactivity. In cells treated with 650 nM of reduced di-chain BoNT/E there was a large reduction (approximately a 70% loss) in the amount of the 28 kD band (Figure 5-1, right lane) and the appearance of an additional faint band at 25 kD (marked with an asterisk in Figure 5-1). These results are consistent with earlier observations that BoNT/E cleavage of SNAP-25 removes an approximately 3 kD fragment from the C-terminus of this protein (Schiavo et al., 1993) and is predicted to remove a similar size fragment from SNAP-23 (Wong et al., 1997). This cleavage is consistent with a recent report that canine SNAP-23, unlike human SNAP-23, is susceptible to BoNT/E cleavage (Low et al., 1998).

The amount of cleaved fragment and uncleaved SNAP-23 following toxin treatment did not add up to the amount of SNAP-23 found in untreated cells. One possible explanation is that the

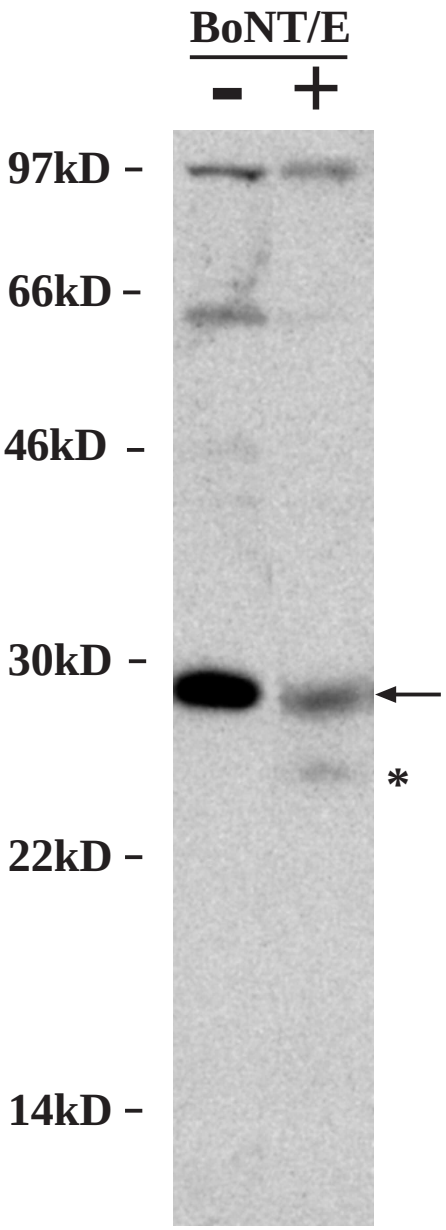

Figure 5-1. Expression of SNAP-23 in MDCK cells and effect of BoNT/E treatment. MDCK cells expressing the pIgR were SLO permeabilized and either left untreated (left lane, -) or treated with 650 nM reduced di-chain BoNT/E for 10 min at 37˚ C (right lane, +). The cells were lysed in detergent, the proteins resolved by SDS PAGE and transferred to immobilon P membranes. The membranes were reacted sequentially with affinity purified anti-SNAP-23 antibodies and goat anti-rabbit horseradish peroxidase, and SNAP-23 (small arrow) was detected by chemiluminescence. Molecular weight markers are shown to the left and the asterisk to the right indicates the 25 kD cleavage product of SNAP-23 found upon BoNT/E treatment.

cleaved fragment is only inefficiently recognized by our polyclonal antibody (i.e., as a result of loss of epitopes). Another possibility is the cleaved SNAP-23 fragment is susceptible to other proteinases that rapidly degrade it into small peptides. The significant fraction of uncleaved SNAP-23, following BoNT/E treatment most likely represents SNAP-23 bound in SNARE complexes since, as previously demonstrated, BoNT/E is only weakly effective on assembled fusion complexes (Hayashi et al., 1994). 650 nM BoNT/E causes a significant inhibition of recycling in our permeabilized cell system (see below), and we have previously shown that this concentration of toxin gives maximal inhibition of IgA transcytosis and recycling (Apodaca et al., 1996).

SNAP-23 Is Found at the Basolateral Cell Surface and in Small Intracellular Vesicles

The distribution of SNAP-23 has been analyzed in several non-polarized cell lines and is found at the plasma membrane and in intracellular vesicles (Wang et al., 1997; Wong et al., 1997). In addition, SNAP-23 has recently been localized to the basolateral surface of pancreatic acinar cells and when human SNAP-23 is overexpressed in MDCK cells it is found at both the apical and basolateral cell surfaces (Gaisano et al., 1997; Low et al., 1998). We localized endogenous canine SNAP-23 within MDCK cells using confocal microscopy which allows visualization of individual optical planes through the three-dimensional MDCK monolayer. Our goal was to identify if endogenous SNAP-23 was associated with the plasma membrane and might therefore act (in a manner analagous to SNAP-25) as a t-SNARE for endocytic traffic. The cells were co-stained with a monoclonal antibody that recognizes ZO-1, a marker for the tight junction which separates the apical and basolateral plasma membrane (Figure 5-2B). At the level of the brightest ZO-1 staining, SNAP-23 was found in small vesicles across the apical pole of the cell (Figure 5-2D). It was not possible to determine whether SNAP-23 was present at the apical plasma membrane because the signal was low and at the light level it is hard to discriminate microvillar staining (which also gives a punctate staining pattern) from SNAP-23 found in sub-apical vesicles. The brightest SNAP-23

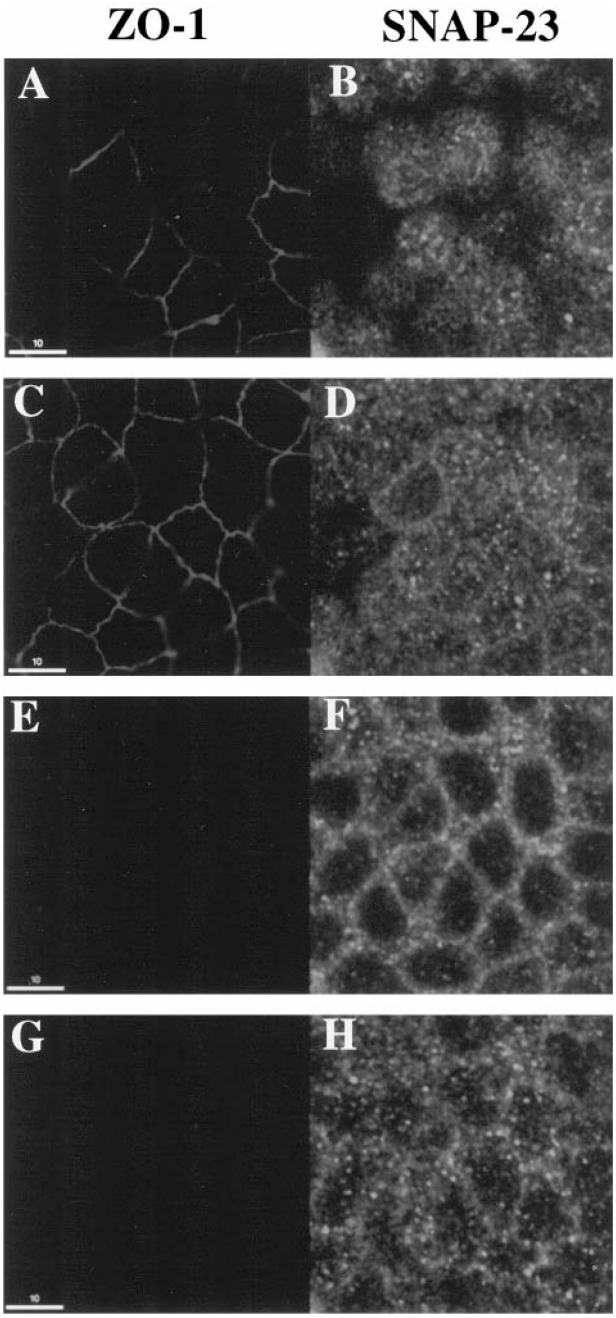

Figure 5-2. Distribution of SNAP-23 in polarized MDCK cells. MDCK cells were fixed with paraformaldehyde, and ZO-1 (panels **A**, **C**, **E**, **G**) and SNAP-23 (panels **B**, **D**, **F**, **H**) simultaneously detected by indirect immunofluorescence. Individual optical sections, obtained with a scanning laser confocal microscope, are shown from the apical pole of the cell at or above the level of the tight junctions (**A**, **B**), at the level of the tight junctions (**C, D**), from the lateral surface of the cell at the level of the nucleus (**E, F**), or from the basal portion of the cell below the nucleus (**G, H**). All images are at the same magnification. Bar = 10 μm

staining was observed in small vesicles along the lateral and basal surfaces and also on what appeared to be the basolateral plasma membrane (Figure 5-2F & H). The specificity of the antibody labeling was confirmed by the addition of exogenous SNAP-23 protein which competitively inhibited binding of SNAP-23 antibodies to the cells and completely eliminated the signal (data not shown).

In order to confirm the localization of SNAP-23 at the basolateral plasma membrane, we performed double labeling with an antibody against E-cadherin (Figure 5-3A, D, G, J) and anti-SNAP-23 (Figure 5-3B, E, H, K). At steady-state E-cadherin was found predominantly at the lateral plasma membrane. Figure 5-3 G, H, and I demonstrate that SNAP-23 and E-cadherin were colocalized along the lateral membrane surfaces, but there were distinct, SNAP-23 containing vesicles that lacked E-cadherin. The presence of SNAP-23 on the plasma membrane and intracellularly is consistent with previous observations on the localization of this protein in other cell types (Wang et al., 1997; Wong et al., 1997); however, in MDCK cells there seemed to be an extensive amount of vesicular staining.

Tf Recycling in Permeabilized MDCK Cells Requires ATP, Cytosol, and NSF

The exit of pIgR-IgA complexes from the ARE and fusion with the apical and basolateral plasma membrane were previously shown to require NSF and were BoNT/E sensitive (Apodaca et al., 1996). However, basolateral recycling of IgA ligand was more sensitive to BoNT/E than transcytosis (50% inhibition of recycling versus 30% inhibition of transcytosis). Coupled with the above observations that SNAP-23 was found predominantly on the basolateral plasma membrane and in basolateral vesicles, we determined whether basolateral recycling of Tf (the classical basolateral recycling marker) could be reconstituted in a permeabilized cell system. Our objective was to use this system to determine if Tf recycling was susceptible to BoNT/E and required SNAP-23. In addition, we hoped to confirm and extend our original observations and gain insight into the molecular requirements for the basolateral recycling pathway.

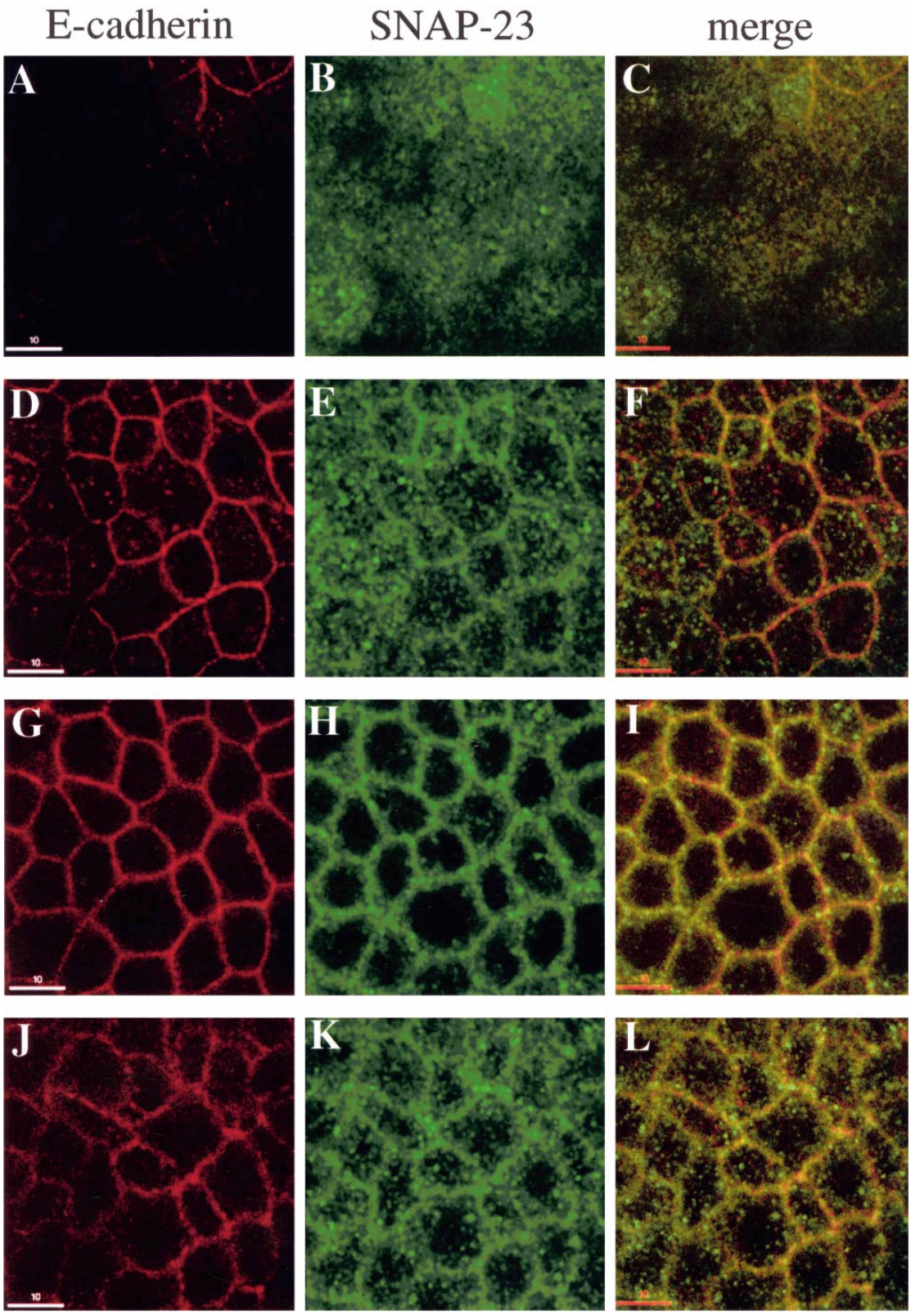

Figure 5-3. Distribution of SNAP-23 and E-cadherin in polarized MDCK cell**s.** Filter-grown

MDCK cells were fixed with paraformaldehyde, and E-cadherin (panels **A**, **D**, **G**, **J**) and SNAP-23 (panels **B**, **E**, **H**, **K**) simultaneously detected by indirect immunofluorescence. Individual optical sections, obtained with a scanning laser confocal microscope, are shown from the apical pole of the cell (**A**, **B, C**), at the level of the tight junctions (**D, E, F**), from the lateral surface of the cell at the level of the nucleus (**G, H, I**), or from the basal portion of the cell below the nucleus (**J, K, L**). Merged images of adjacent panels are shown in **C, F, I, L**. Areas of colocalization are yellow. All images are at the same magnification. Bar = 10 μm

Because MDCK cells do not express the appropriate receptors for BoNT/E binding, we have reconstituted Tf recycling traffic in SLO permeabilized MDCK cells. SLO forms pores in the plasma membrane which are sufficiently large enough to allow BoNT/E to enter the cells. In this assay [^{125}I]Tf was internalized from the basolateral surface for 45 min at 37^{o} C (upon which all the Tf containing compartments were maximally loaded with ligand). The cells were washed at 4^{o} C to remove non-specifically bound ligand and then they were incubated for 2.5 min at 37^{o} C to allow for cell surface bound Tf to be internalized, as previously described (Apodaca et al., 1994; Podbilewicz and Mellman, 1990). Under these internalization conditions Tf was found in small vesicles in the basal region of the cell and underlying the lateral borders (data not shown). In addition, Tf was found at the apical pole of the cell, both at and above the level of the tight junctions, in a vesicular compartment that has previously been characterized as a subdomain of the ARE (Apodaca et al., 1994).

Following [^{125}I]Tf internalization, the cells were rapidly cooled and SLO bound to the basolateral surface. Free SLO was washed from the cell surface, the cells were warmed up to 37^{o} C to allow permeabilization to occur and then re-cooled to 4^{o} C for extended cytosol washout. When permeabilized cells were incubated in the presence of an ATP regenerating system and exogenous rat liver cytosol, approximately 45 - 50% of the pre-internalized ligand was released basolaterally (recycled) over a 90 min incubation period at 37˚ C (Figure 5-4). This is an efficiency of 50-55% (approximately 90% of ligand is recycled basolaterally in non-permeabilized cells during the same time course). Basolateral recycling of [^{125}I]Tf required both ATP and cytosol (Figure 5-4). These observations are consistent with a previous analysis of the energy and cytosol requirements for Tf recycling in mechanically perforated MDCK cells (Podbilewicz and Mellman, 1990). In the absence of ATP there was a 4- to 5-fold reduction in recycling and cytosol depletion resulted in a 3-fold reduction.

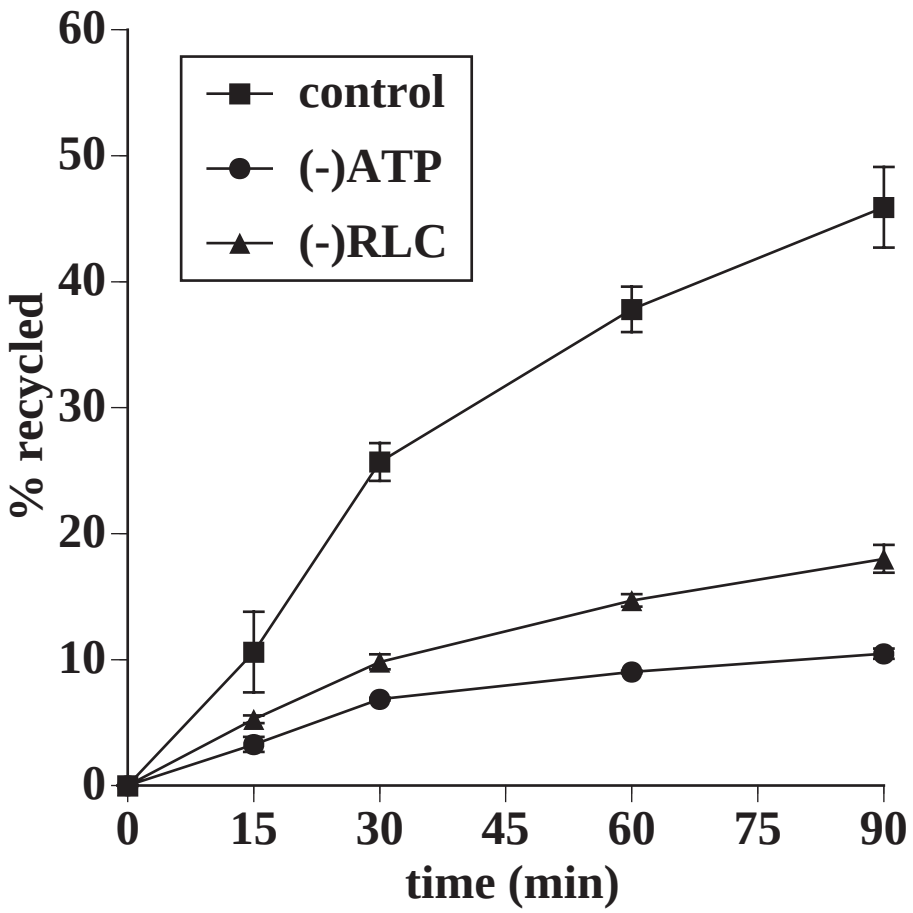

Figure 5-4. ATP and cytosol requirements for Tf recycling in permeabilized MDCK cells. Following ligand internalization, SLO permeabilization, and cytosol wash-out cells were incubated in the presence of an ATP regenerating system and rat liver cytosol (control). Alternatively, the ATP regenerating system was left out of the transport buffer (-ATP), or exogenous cytosol was omitted from the reaction (-RLC). The percent of total ligand released basolaterally (recycled) during a 90 min chase at 37˚ C is shown. The percent of total ligand released apically was as follows: control, 18.2±3.6%; (-RLC), 7.8±0.6%; (-ATP), 3.5±0.9%. The remainder of the counts remained intracellular. Mean and SD of values from a representative experiment are given (n=3).

In this cell system, there was a fraction of Tf (approximately 18-19%) that was released apically (transcytosed). This is more than has been observed in nonpermeabilized cells (typically 5-8%) and may reflect some loss of cytosolic machinery that controls the amount of Tf transcytosis. Because this signal is relatively small, and because Tf is generally considered a marker of the basolateral recycling pathway we have not included the apical release of this marker in the subsequent figures. However, for the sake of completeness the amount of Tf released apically is included in each of the subsequent figure legends. In general, all treatments affected Tf recycling and transcytosis in a similar manner.

As an additional control, we also determined if Tf recycling requires NSF. If so, it would suggest that a *bona fide* membrane fusion event(s) was occurring. In fact, NEM treatment (which inactivates NSF) reduced recycling by 82% (Figure 5-5). No inhibition was observed if both NEM and DTT were added simultaneously, confirming that NEM treatment is the cause of the inhibition. More importantly, exogenous NSF added subsequent to NEM treatment restored much of the recycling activity (72% of the control value)(Figure 5-5). This observation confirmed that Tf recycling is NSF dependent and likely requires use of an NSF/SNAP/SNARE complex. The inability of NSF to completely restore activity has been reported previously and probably reflects the inactivation of other NEM sensitive proteins other than NSF (Apodaca et al., 1996; Beckers et al., 1989).

The primarily basolateral release, high efficiency, and the requirements for energy, cytosol, and NSF confirm that we have faithfully reconstituted the Tf basolateral recycling pathway in MDCK cells. Previous investigators have permeabilized the plasma membrane domain opposite of the cell surface from which trafficking will be explored (Ikonen et al., 1995; Pimplikar et al., 1994). However, we find that basolateral recycling in apically permeabilized cells is inefficient and the large amount of SLO toxin required is cost prohibitive. Permeabilizing the same membrane that is

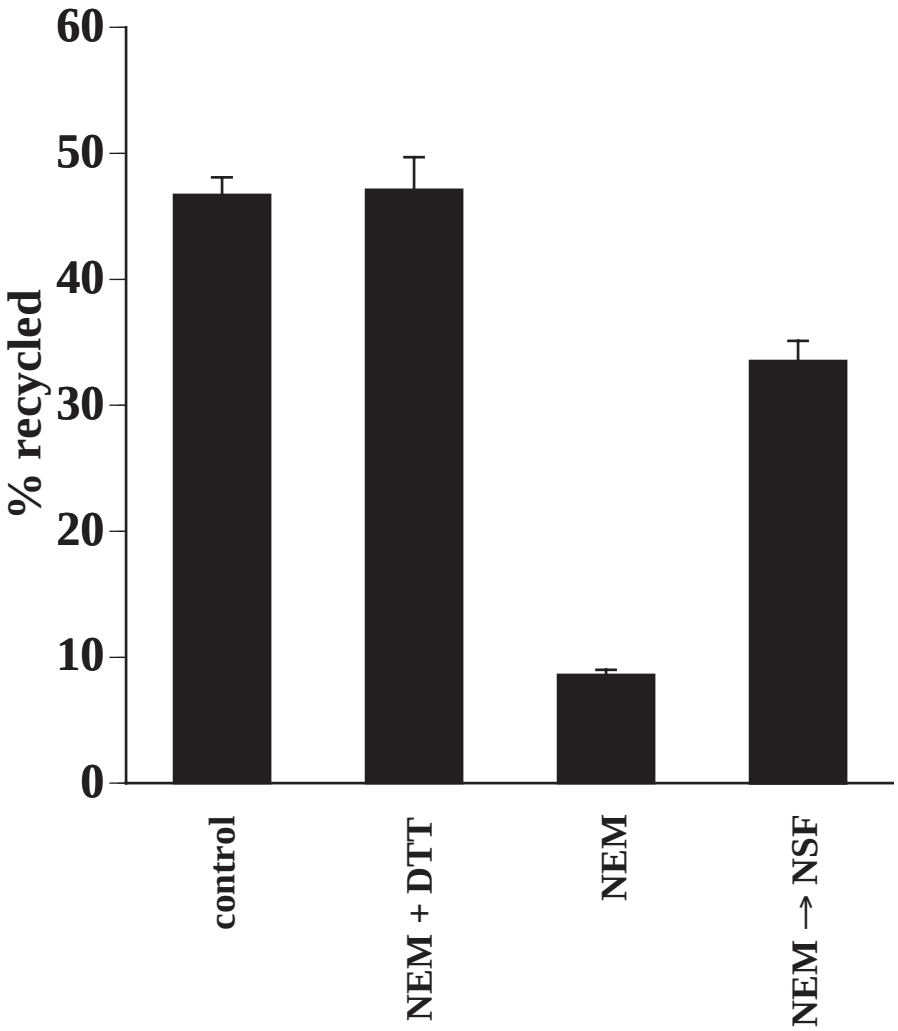

Figure 5-5. NSF requirement for Tf traffic in permeabilized MDCK cells. Permeabilized cells were either left untreated (control), or incubated in the presence of 0.1 mM NEM and 2 mM DTT (NEM + DTT), or 0.1 mM NEM alone (NEM and NEM → NSF) for 15 min on ice. Cells were then washed and incubated 5 min on ice with 2 mM DTT to quench free NEM. The percent of ligand recycled during a 90 min incubation at 37˚ C in the presence of an ATP regenerating system, cytosol, and ± 200 μg/ml of recombinant NSF (NEM → NSF) is shown. The percent of total ligand released apically was as follows: control, 18.5±1.0%; NEM+DTT, 18.7±1.2%; NEM, 5.9±0.5%; NEM → NSF, 15.1±1.5%. Mean and SD of values from a representative experiment are given (n=3).

the chief target for fusion is not inherently different from other SLO permeabilized cell systems involving nonpolarized cells in which there is only one plasma membrane domain that is both permeabilized and the target of fusion (for example see Galli et al., 1994; Martyst et al., 1996; Miller and Moore, 1991).

Basolateral Recycling of Tf is BoNT/E Sensitive

The dependence of Tf recycling on NSF and the expression of SNAP-23 at the basolateral plasma membrane suggests that SNAP-23 may be a t-SNARE involved in Tf delivery to the basolateral cell surface. In order to determine the involvement of SNAP-23 in Tf traffic, SLO permeabilized cells were treated with reduced di-chain BoNT/E. Tf recycling was inhibited by reduced di-chain BoNT/E in a concentration dependent fashion (Figure 5-6). Maximal inhibition was observed at 650 nM which inhibited ~80% of the cytosol-dependent basolateral release. The cytosol dependent release was calculated by subtracting the percent release that occurred in the absence of cytosol from the percent release that occurred in the presence of cytosol. This is similar to the reporting technique used by Simons and coworkers (Ikonen et al., 1995; Pimplikar et al., 1994). BoNT/E had little effect on the fraction of basolateral recycling that occurred in the absence of cytosol (Figure 5-6). These cytosol independent reactions may represent SNAP-23 that is already bound in fusion complexes. As described above, these complexes are thought to be toxin insensitive. These results support the conclusion that the majority of the cytosol dependent reaction is sensitive to BoNT/E and therefore may require SNAP-23.

The neurotoxicity of single chain neurotoxins is enhanced by proteolytic cleavage (nicking) into a di-chain form (Simpson and DasGupta, 1983), and the inhibitory activity of the di-chain form is further enhanced after reduction of its disulfide bond (DasGupta, 1990; Lomneth et al., 1991). For example, proteolysis of synthetic peptides of SNAP-25 and VAMP-2 by BoNT/E, BoNT/A and BoNT/B are stimulated by reduction with DTT (Schmidt and Bostian, 1995; Shone et al., 1993). We therefore examined the inhibitory activity of either single chain or di-chain BoNT/E (+/

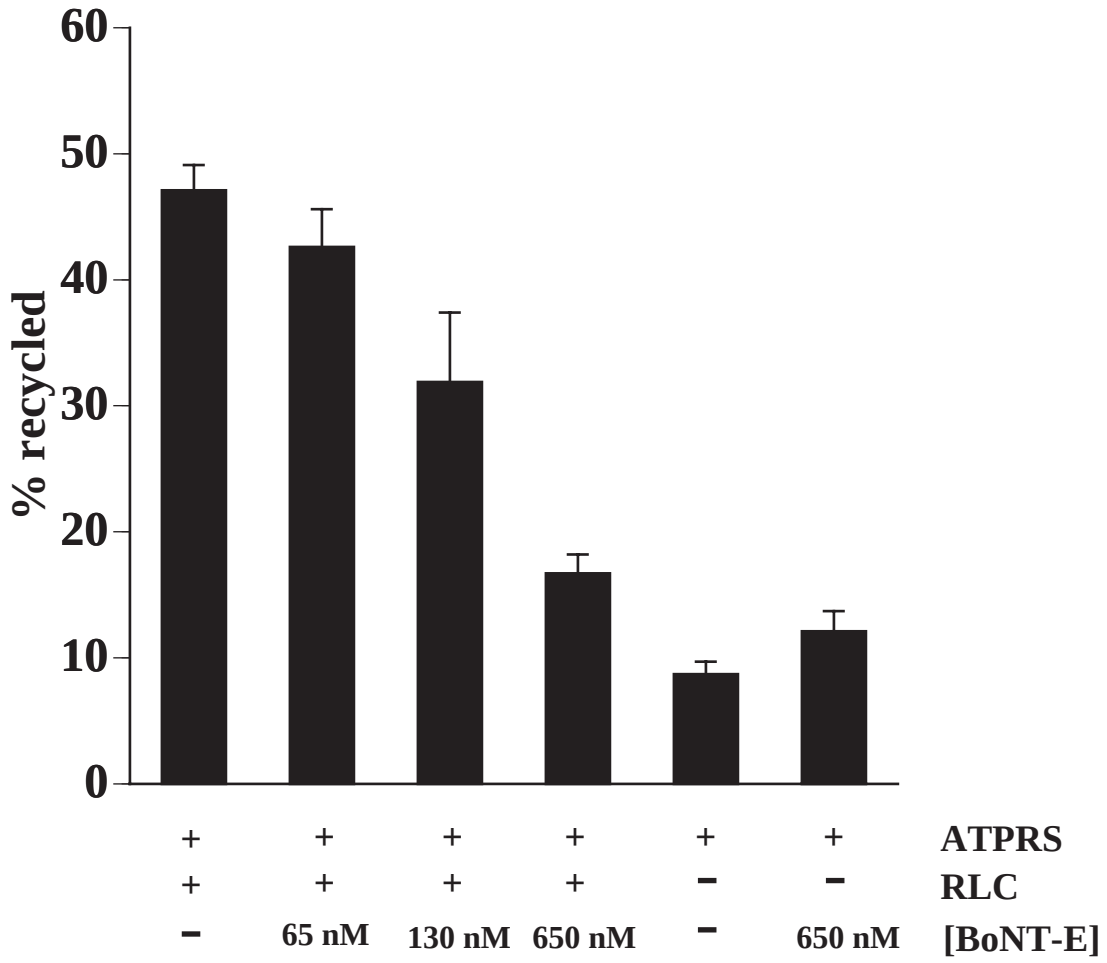

Figure 5-6. Effect of reduced di-chain BoNT/E on transcytosis and recycling of Tf. Ligand was internalized, SLO bound to the basolateral cell surfaces, and cells permeabilized for 10 min at 37˚ C in the presence of 0 (control), 65, 130, or 650 nM of di-chain BoNT/E reduced with DTT. Following the cytosol wash-out, the percent of total ligand released basolaterally (recycled) during a 90 min incubation at 37˚ C in the presence of an ATP-regenerating system (ATPRS) and in the presence or absence of rat liver cytosol (RLC) was quantified. The percent of total ligand released apically was as follows: ATPRS + RLC, 19.3±0.2%; ATPRS + RLC + 65 nM toxin, 18.9±1.9%; ATPRS + RLC + 130 nM toxin, 13.5±1.5%; ATPRS + RLC + 650 nM toxin, 4.3±3.4 %; ATPRS - RLC, 5.5±0.5%; ATPRS - RLC + 650 nM toxin 8.6±1.0%. Mean and SD of values from a representative experiment are given (n=3).

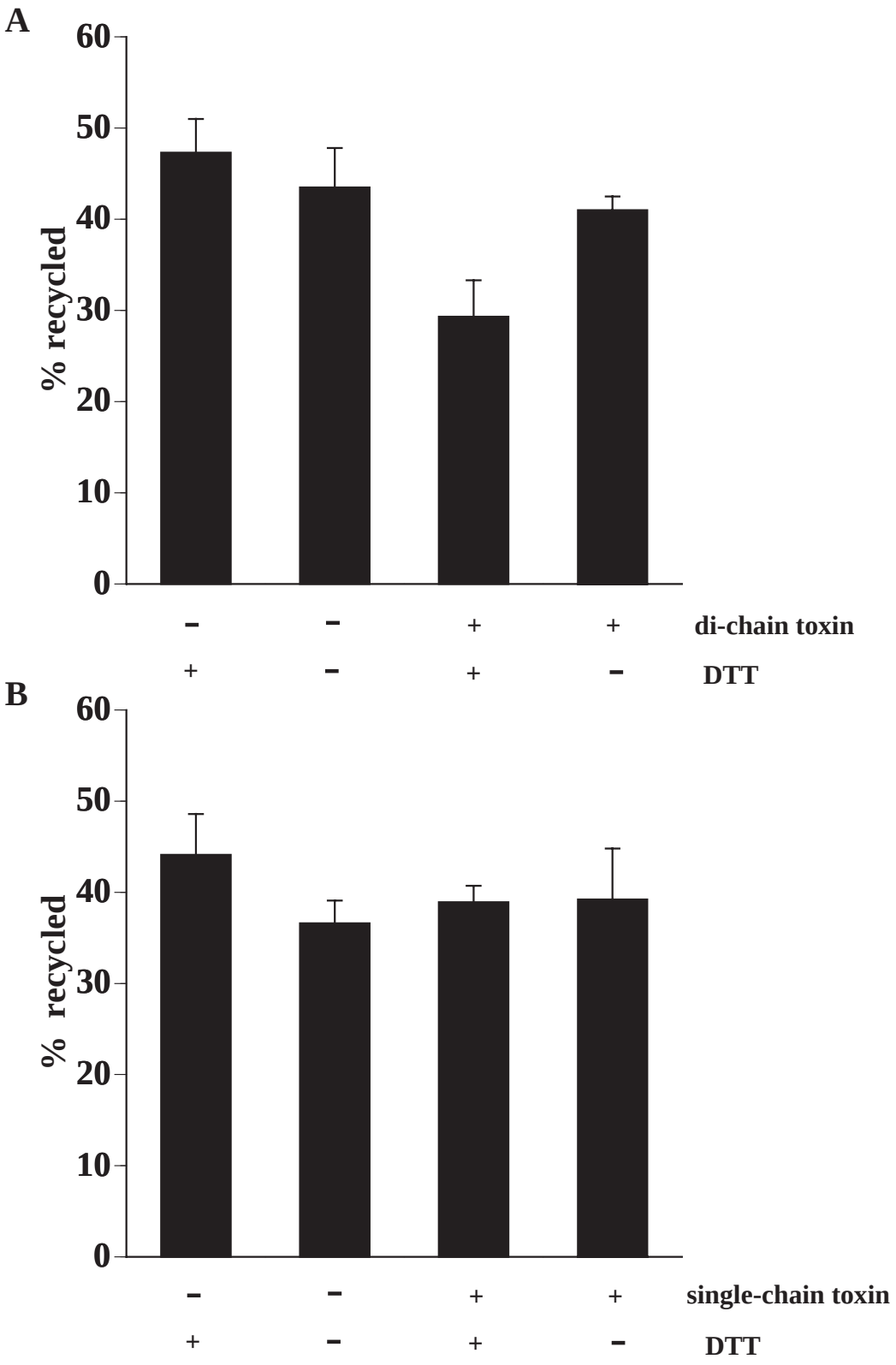

Figure 5-7. Inhibitory activity of di-chain and single-chain BoNT/E (± reduction) on Tf release. Ligand was internalized, SLO bound to the basolateral cell surfaces, and cells permeabilized for

10 min at 37˚ C in the absence or presence of 300 nM di-chain (panel **A**) or 600 nM single-chain toxin (panel **B**). BoNT/E that was either sham treated or reduced with DTT. Following a cytosol washout in the absence of DTT the percent of ligand recycled during a 90 min incubation at 37˚ C was determined. Neurotoxin and DTT were not included in the final incubation at 37˚ C. The percent of total ligand released apically was as follows: - dichain toxin + DTT, 17.9±1.0%; - dichain toxin - DTT, 18.0±1.3%; + dichain toxin + DTT, 9.4±1.6%; + dichain toxin - DTT, 15.7±1.0 %; - single-chain toxin + DTT, 18.2±0.3%; - single-chain toxin - DTT, 16.5±1.6%; + single-chain toxin + DTT, 19.4±1.1%; + single-chain toxin - DTT, 19.2±2.2 %; The mean and SD of values are given (n=3).

- reduction) (Figure 5-7). As expected, only reduced di-chain toxin inhibited basolateral release of Tf (Figure 5-7A); single chain toxin had little effect both before and after reduction (Figure 5-7B). Note that only 300 nM concentration of toxin was used in the experiment described in Figure 5-7A as our toxin supply was limited. These results demonstrate that inhibition of Tf recycling by BoNT/E is only observed following nicking and reduction of the toxin, and confirms that the inhibition we have observed is not due to some contaminating inhibitory activity present in the toxin preparation.

Tf Recycling is SNAP-23 dependent

Although BoNT/E is believed to specifically proteolyze SNAP-25 and SNAP-25 homologs (in our case SNAP-23), it cannot be excluded that it may be proteolyzing some unknown substrate that is required for Tf recycling. Since endogenous SNAP-23 is believed to be membrane bound (probably via palmitoylation of one of its internal cysteine residues)(Ravichandran et al., 1996; Wang et al., 1997) and part of the SNARE complex for vesicle fusion, addition of exogenous SNAP-23 might act as a competitive inhibitor of basolateral recycling by forming nonproductive interactions between exogenous SNAP-23 and endogenous syntaxin or VAMP. Earlier studies have shown that a 20 amino acid peptide derived from the C-terminus of SNAP-25 can inhibit SNAP-25-dependent exocytosis in chromaffin cells (Gutiérrez et al., 1995). In this system, addition of recombinant SNAP-23 inhibited approximately 45% of cytosol dependent Tf recycling (Figure 5-8A), but had no effect on the cytosol independent reactions.

As additional evidence, we tested the effect of anti-SNAP-23 antibody addition on the assay (Figure 5-8B). This is expected to inhibit endocytic traffic by binding SNAP-23 and sterically hindering its ability to interact with other proteins. Antibody treatment resulted in an approximately 35% inhibition of the cytosol dependent recycling reaction (Figure 5-8B). A nonspecific antibody against human IgA (used as a control) had no effect on Tf recycling. These results confirm that SNAP-23 is required for a fraction of Tf recycling.

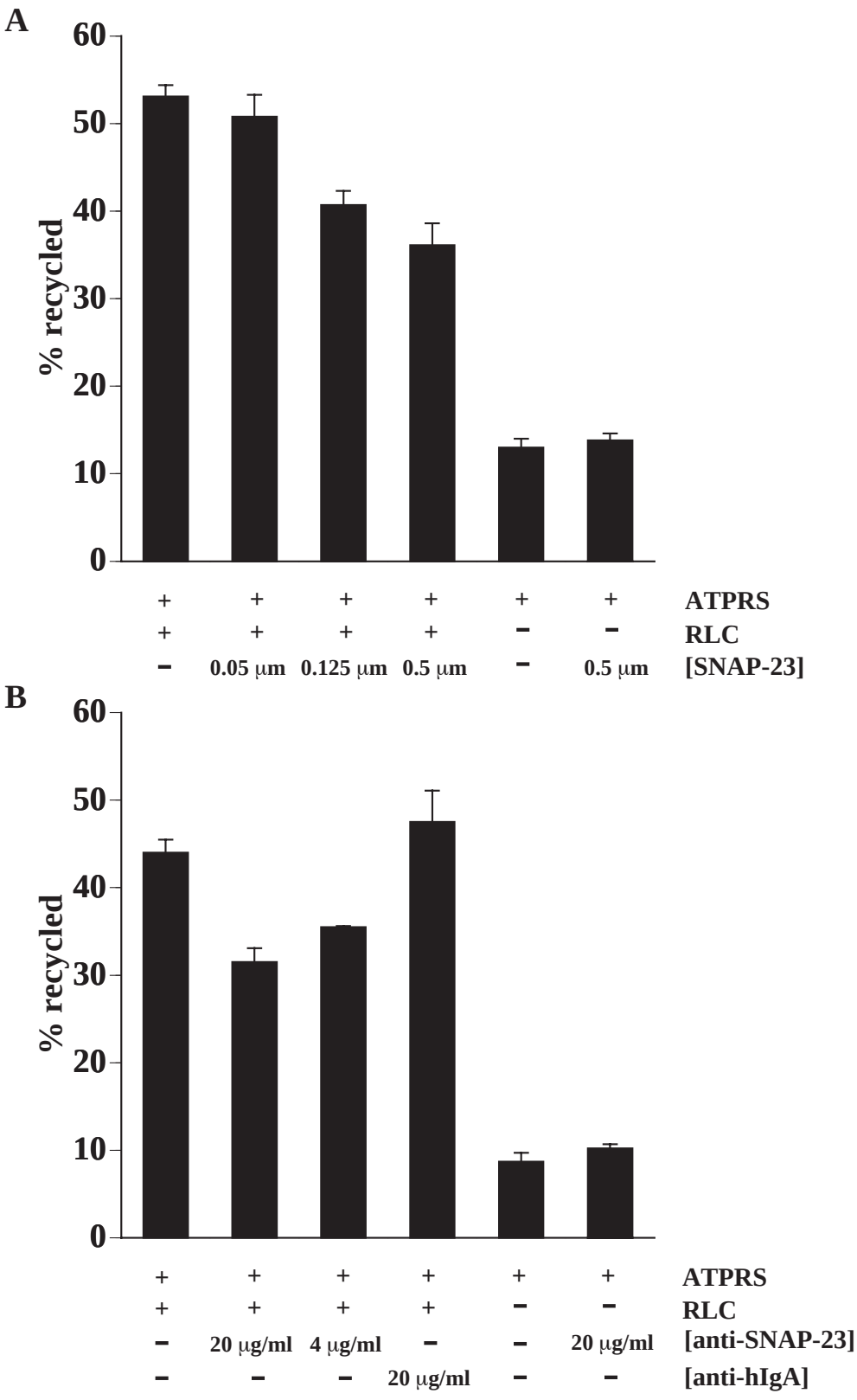

Figure 5-8. Effect of SNAP-23 and anti-SNAP-23 antibodies on Tf transcytosis and recycling in

permeabilized MDCK cells. (**A**) SNAP-23 (0.05-0.5 μM) was included during the 90 min transport reaction at 37˚ C. The percent of total ligand released basolaterally in the presence of an ATP-regenerating system (ATPRS) and in the presence or absence of rat liver cytosol (RLC) was quantified. The percent of total ligand released apically was as follows: ATPRS + RLC, 19.9±1.9%; ATPRS + RLC + 0.05 μM SNAP-23, 18.9±1.0%; ATPRS + RLC + 0.125 μM SNAP-23, 13.6±1.8%; ATPRS + RLC + 0.5 μM SNAP-23, 11.8±3.3 %; ATPRS - RLC, 6.9±1.3%; ATPRS - RLC + 0.5 μM SNAP-23, 7.5±1.4%. Mean and SD of values from a representative experiment are given (n=3). (**B**) Ligand was internalized, SLO bound to the basolateral cell surfaces, and cells permeabilized for 10 min at 37˚ C in the absence (control) or presence of anti-SNAP-23 or anti-human IgA (hIGA) antibodies. Antibodies were included during the cytosol wash-out and during the 90 min transport reaction at 37˚ C. The percent of ligand released basolaterally during a 90 min incubation at 37˚ C in the presence of an ATP-regenerating system (ATPRS) and in the presence or absence of rat liver cytosol (RLC) was quantified. The percent of total ligand released apically was as follows: ATPRS + RLC, 13.7±0.6%; ATPRS + RLC + 20 μg/ml anti-SNAP-23, 10.4±1.0%; ATPRS + RLC + 4 μg/ml anti-SNAP-23, 10.5±0.6%; ATPRS + RLC + 20 μg/ml of anti-hIgA, 15.1±1.6 %; ATPRS - RLC, 1.0±0.5%; ATPRS - RLC +20 μg/ml of anti-SNAP-23, 0.5±0.9%. Mean and SD of values from a representative experiment are given (n=3).

DISCUSSION

The SNARE hypothesis predicts that the specificity of vesicle targeting and fusion is mediated through specific interactions between v-SNAREs and t-SNAREs (Sollner et al., 1993). If true, then each membrane trafficking event would require distinct isoforms or homologs of the various SNARE components. Until recently, however, only isoforms of syntaxin and VAMP, but no mammalian isoforms of SNAP-25 have been identified (Bennett et al., 1993; McMahon et al., 1993). In the last two years, Ravichandran et al. identified a SNAP-25 homolog with a predicted molecular weight of 23 kD called SNAP-23 (Ravichandran et al., 1996). This protein, expressed in several tissues, is able to bind various syntaxins and VAMPs. A mouse isoform of SNAP-23, also known as syndet, has recently been cloned from an adipocyte 3T3 L1 cDNA library (Araki et al., 1997; Wang et al., 1997), and has a similar cellular distribution to human SNAP-23. Munc 18c, an N-sec-1 homolog and putative regulator of the NSF/SNAP/SNARE complex, has been shown to inhibit SNAP-23 and syntaxin 4 binding *in vitro* (Araki et al., 1997). While these observations identify some of the potential binding partners of SNAP-23, the role of SNAP-23 in membrane trafficking remains largely uncharacterized.

Previous work is consistent with the hypothesis that SNAP-23 plays a role in exocytosis. Banerjee et al. have shown that exocytosis of large core granules in permeabilized PC12 cells is inhibited completely by BoNT/E but not BoNT/A, even though SNAP-25 is efficiently cleaved by both toxins (Banerjee et al., 1993)[Banerjee, 1996 #1323]. However, when PC12 cells are treated with nerve growth factor, release of granules became BoNT/A sensitive. It is now known that these cells express both SNAP-25 and SNAP-23 (Wong et al., 1997). It is therefore possible that SNAP-23, which is sensitive to E-toxin and predicted to be insensitive to A-toxin, may be required for release of PC12 storage granules in untreated cells, while in nerve growth factor-treated cells SNAP-25 (and possibly SNAP-23) is required. These observations also suggest that usage and expression of SNARE components may change with the development of any particular cell or tissue.

In the present study we have demonstrated that SNAP-23 is not only present in MDCK cells, and cleaved by BoNT/E, but is required for basolateral recycling of Tf. Our observation that canine SNAP-23 is succeptible to toxin cleavage is consistent with work by Low et. al which have shown that the canine isoform of SNAP-23 is sensitive to BoNT/E cleavage while the human isoform of SNAP-23 is insensitive (Low et al., 1998). Even though BoNT/E is thought to specifically cleave SNAP-25 and SNAP-25 homologs, other proteins in the cell may be susceptible. In order to examine SNAP-23 involvement more directly, we added either exogenous SNAP-23 or anti-SNAP-23 antibodies to the assay. Addition of either resulted in an inhibition of recycling; however, the level of inhibition was less than that attained with BoNT/E treatment. The added SNAP-23 and anti-SNAP-23 antibodies might only compete at steps prior to SNARE complex formation and only ineffectively compete or sterically hinder already formed SNARE complexes. This possibility would be consistent with recent observations by Weber et al. (Weber et al., 1998) who have reconstituted v- and t-SNAREs into separate lipid bilayer vesicles which fuse with one another in a SNARE dependent reaction. This fusion reaction can be inhibited when soluble VAMP or t-SNAREs are included in a preincubation reaction (during which fusion complex formation is occurring). However they have no effect when added to reactions in which fusion complexes have already formed. Another possibility is that there are additional BoNT/E sensitive SNAP-23/SNAP-25 homologs in MDCK cells. These unidentified homologs could account for the higher level of BoNT/E inhibition observed than when SNAP-23 or anti-SNAP-23 antibodies were added exogenously to the permeabilized cell system.

Localization of SNAP-23 reveals that it is present along the basolateral plasma membrane. It was not possible to determine unequivocally if SNAP-23 was present at the apical cell surface. Ultrastructural localization of SNAP-23 is currently under way. There was extensive localization of endogenous SNAP-23 within intracellular vesicular structures. This is contrary to findings by Low et. al. - who found little intracellular SNAP-23 in MDCK cells (Low et al., 1998). However,

this group examined the distribution of overexpressed human SNAP-23, whereas, we have examined the endogenous distribution of this protein. The amount of intracellular SNAP-23 is not unexpected since SNAP-23 localization in non-polarized cells is both at the plasma membrane and in intracellular vesicles (Wang et al., 1997; Wong et al., 1997). Some of the intracellular vesicles we observed could be endocytic in nature, a possibility we are actively exploring. In neurons, SNAP-25 and syntaxin 1 are found not only at the plasma membrane but are also abundant constituents of both synaptic vesicles and clathrin coated vesicles (Walch-Solimena et al., 1995). While the function of these proteins in this setting are unknown, it has been suggested that SNAP-25 and syntaxin 1 may reside in these structures as a result of incomplete dissociation from the v-SNARE VAMP, or that t-SNAREs may be reactivated by recycling (Walch-Solimena et al., 1995). Alternatively, these t-SNAREs may be involved in synaptic vesicle fusion with already docked synaptic vesicles in a process termed compound exocytosis (Walch-Solimena et al., 1995).

In MDCK cells it is thought that the final step of recycling and transcytosis is direct transport from endosomes to the cell surface. An alternative possibility is that several vesicles may fuse with one another prior to fusion with the cell surface. SNAP-23 could function in these intermediate steps of recycling or transcytotic vesicle fusion, and therefore may be acting at steps prior to or in addition to vesicle fusion with the plasma membrane. In fact, the differential effects we observe between BoNT/E treatment and either SNAP-23 or anti-SNAP-23 addition may reflect the differential sensitivity of these agents on homotypic fusion of recycling vesicles or fusion of these vesicles with the plasma membrane.

At present it is not clear if SNAP-23 is also required for fusion of vesicles with the apical plasma membrane domain of MDCK cells. The apical release of Tf has a similar sensitivity to BoNT/E and requirement for SNAP-23, and as such basolateral to apical transcytosis of Tf may also require SNAP-23. In addition, our previous observations that transcytosis of IgA in MDCK cells is inhibited by BoNT/E is consistent with there being a SNAP-23 requirement for fusion with

the apical plasma membrane (Apodaca et al., 1996). If we assume that SNAP-23 is a SNARE required for fusion at both cell surfaces, then the specificity of fusion must be regulated by additional factors. One possibility is that distinct v-SNAREs are present on basolateral recycling versus transcytosing vesicles or that additional t-SNAREs, present on each of the plasma membrane domains, are required for fusion. VAMP-2, for example, interacts with syntaxin 1 and 4 but not with syntaxin 2 and 3 (Calakos et al., 1994). Syntaxin 4 is found primarily at the basolateral surface of MDCK cells (Low et al., 1996) and is known to bind with high affinity to SNAP-23 (Araki et al., 1997). It is therefore possible that VAMP-2 will be found on basolateral recycling vesicles and will be required for fusion with the basolateral cell surface. Syntaxin 3, in contrast, is found at both the apical membrane and in apical vesicles and may be involved in fusion of vesicles with the apical pole of the cell (Low et al., 1996; Peng et al., 1997). Additional work is required to identify the binding partners of SNAP-23 and which components are required for the targeting specificity of recycling and transcytotic vesicles. The existence of fusion events that occur in the absence of NSF-SNAP-SNARE complexes further extends the possible types of fusion events possible in the cell (Ikonen et al., 1995; Wilson, 1995). The present work suggests that SNAP-23 may be one component of a complex required for vesicle fusion with at least the basolateral plasma membrane domain of MDCK cells.

CONCLUSIONS

The experiments presented in this dissertation analyzed several aspects of regulation of endocytosis and post endocytic traffic in polarized epithelial cells. Although trafficking of fluid and membrane endocytosed from the basolateral plasma membrane was already well understood, little was known about sorting of apically endocytosed fluid and membrane. Chapter 1 analyzed the sorting of membrane and fluid internalized from the apical pole of polarized epithelial cells. Fluid remained with the larger vesicular AEE while apically internalized membrane was rapidly removed and delivered to the more punctate ARE (Figure 1-1 and 1-2). Transport of membrane from the AEE to the ARE was microtubule-dependent (Figure 1-6 and 1-7). Access to these compartments from the basolateral recycling pathway was limited to the AEE (Figure 1-8, 1-9 and 1-10). Furthermore, biochemical markers of these compartments were identified. The AEE is EEA-1-positive and the ARE is Rab-11-positive (Figure 1-3, 1-4 and 1-5). Therefore the ARE was redifined as the subapical Rab-11-positive compartment that is distinct from the transferrin-rich CE and the fluid-rich AEE.

At the basolateral pole, fluid also remains in BEE while membrane is rapidly removed (Apodaca et al., 1994) and the BEE is also EEA-1-positive. Several differences exist between the AEE and BEE, however. The majority of fluid within the BEE is eventually degraded while in contrast most fluid in the AEE is recycled back to apical plasma membrane or transcytosed to the basolateral plasma membrane (Bomsel et al., 1989). In addition, the AEE and BEE are biochemically distinct structures and are incapable of heterotypic fusion *in vitro* (Bomsel et al., 1990) even though both are EEA-1-positive (and presumably rab5-positive). EEA-1 and rab5 have both been linked to

endosome homotypic fusion (Bucci et al., 1992; Chistoforidis et al., 1999; Gorvel et al., 1991b) but the data above suggests that a more complex level of regulation must exist. One possible explanation is that rab5 and EEA-1 provide the intial tether (Zerial and McBride, 2001) but fusion between AEE and BEE is not possible due to lack of proper SNARE complementation (McNew et al., 2000; Scales et al., 2000). Analysis of SNARE localization to the AEE and BEE may demonstrate the reason why these compartments are distinct. Furthermore, this would also help to demonstrate that SNAREs may be the final check in vesicle targeting.

Analysis of the organization of the apical endosomes also revealed that basolaterally recycling transferrin is largely excluded from the ARE. Basolaterally recycling transferrin and basal to apical transcytosing IgA are initially found within the same compartments (Brown et al., 2000). Sorting of these two markers must occur prior to the ARE. The CE is the most likely site for sorting of these elements to occur. Currently there is no biochemical marker for the CE. The exact localization of rab17 and rab25 has not been determined. It is possible that one of these two may label at least in part the CE. Furthermore, if a marker for the CE can be found then it may be possible to isolate the CE. Further analysis of the CE may reveal the mechanism for sorting of apically targeted membrane markers from basolaterally targeted membrane markers. This would be a major step in understanding how polarity is maintained along the endocytic pathway.

In chapters 2 and 3, the role of the Rho family of small GTPases in endocytosis and postendocytic trafficking was analyzed. Expression of mutants of both Rac1 and RhoA were shown to alter endocytosis from both plasma membrane domains (Figure 2-5 and 3-2). It is likely that both of the proteins play a direct role in regulating endocytosis but at distinct steps. RhoA activation stimulates endocytosis (Figure 3-2) while Rac1 activation inhibits it (Figure 2-5). The markers examined in these studies are those which are primarily internalized via clathrin-dependent endocytosis. Several studies have suggested, however, that clathrin-independent endocytosis may also be regulated by RhoA and Rac1 (Dharmawardhane, 1997; Ellis and Mellor, 2000; Gingras et

al., 1998; Ridley et al., 1992b; Senda et al., 1997; Stahlhut and van Deurs, 2000; West et al., 2000) (Ridley et al., 1992a). One way of determining whether or not clathrin-independent endocytosis in polarized MDCK cells involves Rac1 or RhoA is to block clathrin-dependent uptake and examine if expression of mutant forms of RhoA or Rac1 alter subsequent internalization. In addition, expression of mutant forms of RhoA and Rac1 alter the cell on a global level. This makes it difficult to distinguish direct effects of the Rho proteins compared with indirect effects. Several Rho effectors have been identified (Takai et al., 2001; Van Aelst and D'Souza-Schorey, 1997) and examination of their distribution in the cell would hint at the location of their actions. This information would help to define what effectors are responsible for RhoA and Rac1 regulation of endocytosis, and thereby link RhoA and Rac1 to regulation of endocytosis.

In addition, Rac1V12 expression results in the formation of a central aggregate that traps apically targeted markers from both the endocytic and biosynthetic pathways (see chapter 2 and Jou et al., 2000). This aggregate is composed in part of both the ARE and CE and is surrounded by intermediate filaments (Figure 2-3, 2-4 and 2-6). The global changes resulting from the expression of the dominant active Rac1 in polarized MDCK cells makes it difficult to understand the full extent of Rac1 regulation along the apically targeted transport pathway. Rac1V12 expression has a very minor effect on trafficking along the basolateral recycling and degratory pathways while blocking apically targeted transport it also does not missort traffic to the basolateral plasma membrane (Figure 2-6, 2-7 and 2-8). This suggests that Rac1 may have a direct role in apically targeted transport. Although, it is possible that Rac1 effects the cytoskeleton, this may explain the block (Figure 2-4C and 2-8). Identification of Rac1 effectors could help isolate if the block of apically targeted transport is independent of Rac1's effect on the actin cytoskeleton.

Similar to Rac1, RhoAV14 expression in polarized MDCK cells also blocks a transport step. Several markers endocytosed from the basolateral plasma membrane are trapped in BEE (Figure 3-3, 3-4, 3-6, 3-7, 3-8, 3-9 and 3-10). Traffic of basal to apical transcytosis of IgA (Figure

3-6), degradation of EGF (Figure 3-4) and basolateral recycling of transferrin (Figure 3-3) are all altered by expression RhoAV14. Unlike Rac1V12, RhoAV14 does cause missorting. Not surprisingly, trapping of transcytosing IgA in BEE results in an increased delivery to the basolateral plasma membrane (Figure 3-6 and 3-11). What is surprising, however, is that transport of transferrin to the apical plasma membrane is increased (Figure 3-3). This suggests that RhoA may play a role in regulating sorting of basolaterally targeted and apically targeted proteins. Once again, an important first step in analyzing the role of RhoA in postendocytic traffic is the localization of its effectors both under normal and mutant conditions.

RhoAV14 expression traps several markers in BEE and in part this is likely due to alterations of the actin cytoskeleton. Examination of the actin cytoskeleton in RhoAV14 cells revealed that a majority of IgA-labeled BEE below the level of the stress fibers are associated with F-actin (Figure 3-9). Furthermore, examination of control cells showed that a population of IgA-labeled BEE is again associated with F-actin (Figure 3-10). This suggests that dynamic regulation of this F-actin is important in transport. Previous studies have demonstrated that basal to apical transcytotic transport requires both an intact actin and microtubule cytoskeleton (Maples et al., 1997). More in-depth analysis showed that the actin based transport preceded the microtubules requirement (Maples et al., 1997). In chapter 4, the possible role of the BEE associated F-actin as a mechanism for endosome transport was examined. APBP and myosin motor based propulsion are two models of transport via the actin cytoskeleton. Examination of the distribution of the proteins involved in either model showed that myosin motor transport is the more likely. Proteins involved in APBP were not found to colocalize with BEE and instead shown to localize to peripheral areas of the cell (Figure 4-1, 4-2 and 4-3). Of the myosin isoforms examined, only MIc was shown to colocalize with BEE (Figure 4-5 and 4-6). One study using Caco-2 cells demonstrated that expression of a dominant negative mutant of BBMI inhibited transferrin recycling (Durrbach et al., 2000). However, BBMI did not colocalize with BEE in our hands (Figure 4-5 and 4-6). One alternative is that dominant negative BBMI may interfere with protein interactions meant for MIc. The use of mutant forms of MIc could

determine whether or not it plays a role in transport of BEE deeper into the cell. Furthermore, analysis of proteins that may interact with MIc or dominant negative BBMI could also reveal the role of myosins in BEE transport.

In chapter 5, the requirement for SNAP-23 in transferrin recycling was examined. SNAP-23 was distributed in vesicles throughout the cell and located on the basolateral plasma membrane (Figure 5-2 and 5-3). Treatment of permeabilized MDCK cells with BoNT/E, which cleaves SNAP-23 (Figure 5-1), inhibited transferrin recycling (Figure 5-6) and addition of exogenous SNAP-23 or anti-SNAP-23 antibodies also resulted in inhibited transferrin recycling (Figure 5-8). Results of recent studies have renewed interests in SNAREs. There is now a growing body of evidence that SNAREs may be the minimum fusion machinery (Chen et al., 1999; Nickel et al., 1999; Weber et al., 1998). In addition, SNAREs may be the final check for vesicle targeting (McNew et al., 2000; Scales et al., 2000). The analysis of SNAREs in polarized epithelial cells is rather sparse. The localization of many SNAREs in nonpolarized cells has been identified but this localization in polarized epithelial cells may dramatically differ. Proper evaluation of SNAREs based on new classification methods and identification of SNARE localization should help the understanding of the final step in targeting and fusion through out the endocytic pathway.

Finally, proper traffic along the endocytic pathway is likely to require several different regulatory proteins. Traffic along these pathways requires several stages of transport via vesicle carriers. For example, basal to apical transcytosis of IgA involves many steps. First, IgA bound to pIgR is internalized into a vesicle and delivered the BEE. The IgA is sorted from fluid into tubular sections, are transported deeper into the cell to the CE. IgA is then sorted from basolaterally targeted markers, such as Tf, and delivered to the ARE, possibly via the AEE. Finally, IgA is transported from the ARE to the apical plasma membrane where pIgR is cleaved by a protease releasing it as secretory component into the apical medium. It is appealing to hypothesize that each vesicle transport step is under general control by a single protein. One family of proteins that have been shown to

regulate many of individual steps in vesicle transport is the rab family of small GTPases. Proper understanding of rabs and their effectors may reveal a more global picture of how the large number of regulating proteins can be drawn together on a single platform to drive vesicle transport.

APPENDICES

APPENDIX A

ABBREVIATIONS

AEE	Apical Early sorting Endosome
APBP	Actin Polymerization Based Propulsion
AP	Adaptor protein
APC	Adenomatous Poylposis Coli
Arc	Arp 2/3 Complex
ARE	Apical Recycling Endosome
BBMI	Brush Border Mysoin I
BEE	Basolateral Early sorting Endosome
BoNT	Botulinum Neurotoxin
BSA	Bovine Serum Albumin
CAPS	3-(cyclohexylamino)-1-propanesulfonic acid
CD	Cytochalasin D
CE	Common recylcing Endosome
CR	Complement Receptor
DAB	Diaminobenzidine
DC	Doxycycline
DTT	Dithiothreitol
EE	Early Endosome
EEA1	Early Endosome Antigen 1
ER	Endoplasmic Reticulum
F- Actin	Filamentous Actin
GAP	GTPase-activating protein
GDF	GDI Displacement Factor

GDI	GDP Dissociation Inhibitor
GEF	Guanine Nucleotide Exchange Factor
IgA	Immunoglobulin A
LE	Late Endosome
LPA	Lysophosphatidic Acid
MDCK	Madin Darby Canine Kidney
MEM	Minimum Essential Medium
MIc	Myosin Ic
NSF	N-Ethylmaleimide-Sensitive Factor
N-WASP	Neuronal WASP
pIgR	polymeric Immunoglobin receptor
PIP_2	Phosphatidylinositol 4,5-bisphosphate
PIP_3	Phosphatidylinositol 3,4,5-triphosphate
PI-3-K	Phosphatidylinositol-3-kinase
PKC	Protein Kinase C
PMA	Phorbol 12-myristate 13-acetate
RE	Recycling Endosome
RPE	Retinal Pigment Epithelial
SAC	SubApical Compartment
SNAP	Soluble NSF Attachment Protein
SNAP-23	23000 Dalton SNAP-25 homolog
SNAP-25	25000 Dalton Synaptosomal associated protein
SNARE	SNAP Receptor
Tf	Transferrin
Tf-R	Transferrin Receptor
TGN	Trans-Golgi Network
t-SNARE	Target membrane-associated SNARE

v-SNARE	Vesicle-associated SNARE
WASP	Wiskott Aldrich Syndrome Protein
WGA-HRP	Wheat Germ Agglutinin conjugated to Horseradish Peroxidase
WH2	WASP Homology 2

APPENDIX B

Materials and Methods

Antibodies, Proteins, and Other Markers

The following reagents were used: mouse anti-myc hybridoma 9E10 (Dr. Gordan Cann, Stanford University, Stanford, CA); mouse anti-GP135 hybridoma 3F2/D8 (Dr. G. Ojakian, SUNY, Brooklyn, NY); rabbit polyclonal anti-mp30/BAP31, an ER resident protein (Dr. P. Walter, University of California, San Francisco, CA); rabbit polyclonal anti-mouse furin, a TGN resident protein (Alexis Biochemicals Inc., San Diego, CA); mouse monoclonal anti-giantin, a Golgi resident protein (Dr. A. Lindstedt, Carnegie Mellon University, Pittsburgh, PA); guinea pig anti-Hip1R (Dr. D. Drubin, University of California, Berkeley, CA); rabbit anti-1 Arp3 and rabbit anti-p21Arc (Dr. M. D. Welch, University of California, Berkeley, CA); mouse anti-PKC∝ and mouse anti-PKCε (Santa Cruz Biotechnology Inc., Santa Cruz, CA); rabbit anti-cofilin (Cytoskeleton, Inc., Denver, CO); rabbit anti-WASP (Santa Cruz Biotechnology Inc., Santa Cruz, CA); rabbit anti-NWASP anti-serum (Dr. M. W. Kirschner, Harvard Medical School, Boston, MA); rabbit anti-APC (Santa Cruz Biotechnology Inc., Santa Cruz, CA); rabbit anti-BBMI and rabbit anti-Mic (Dr. M. S. Mooseker, Yale University, New Haven, CT); mouse monoclonal anti-lysosomal membrane protein hybridoma Ac17 (Dr. E. Rodriguez-Boulan, Cornell University, New York, NY); mouse anti-myc hybridoma 9E10 ascites (Dr. S.W. Whiteheart, University of Kentucky, Lexington, KY);); purified mouse anti-RhoA monoclonal antibody (Santa Cruz Biotechnology Inc., Santa Cruz, CA); mouse anti-Rac1 (Transduction Laboratories, Lexington, KY); rhodamine- and FITC- phalloidin (Molecular Probes, Eugene, OR); Fab fragments of affinity purified polyclonal sheep anti-secretory component conjugated to horseradish peroxidase (Dr. K. Mostov, University of California, San Francisco, CA); canine apo-Tf (Sigma Chemical, St. Louis, MO) which was loaded with iron as previously described (Apodaca et al., 1994); rat anti-ZO-1 monoclonal antibody ascites (Chemicon, Temecula, CA); mouse anti-E-cadherin monoclonal antidoby supernatant hybridoma rr1 (Dr. K. Simons, EMBL, Heidelberg, Germany); affinity purified rabbit anti-Rab11 polyclonal antibodies (Zymed, South San Francisco, CA); purified mouse monoclonal anti-EEA1 antibody (Transduction Laboratories, San Diego, CA); rat anti-ZO1 hybridoma R40.76 (Dr. D.A. Goodenough, Harvard University, Cambridge, MA); affinity-purified rabbit polyclonal anti-human IgA antibodies (Jackson Immunoresearch Laboratories, West Grove, PA); affinity purified rabbit or mouse polyclonal anti-canine Tf antibodies (Apodaca et al., 1994); affinity-purified and minimal cross reacting HRP-,

fluorescein-, Texas red- and Cy5-conjugated secondary antibodies (Jackson Immunoresearch Laboratories); human polymeric IgA (Dr. K. Mostov, University of California, San Francisco, CA); lysine-fixable 10,000 Dalton FITC- or Texas red-dextran; IgA was conjugated to horseradish peroxidase (HRP) using an Actizyme Peroxidase conjugation kit (Zymed; South San Francisco, CA) as detailed in the included protocol. Conjugates containing 1-2 HRP molecules were separated from overly-conjugated IgA-HRP and free HRP by chromatography on an S-200 column using phosphate buffered saline containing 0.01% (w/v) thimerosol as eluant. Biochemical assays confirmed that conjugated IgA-HRP was efficiently transcytosed.

Preparation of affinity purified antiserum to SNAP-23 was as described (Araki et al., 1997; Ravichandran et al., 1996). A human SNAP-23 cDNA was obtained by PCR from a human platelet cDNA library using primers (cgggatccATGGATAATCTGTCATCAG and cccaagcttTTAGCTGTC AATGAGTTTC) based on the human B cell SNAP-23 sequence (Ravichandran et al., 1996) The sequence was confirmed by dideoxyribose nucleic acid sequencing. The human platelet cDNA encoding SNAP-23 is identical to that reported (Ravichandran et al., 1996). This human SNAP-23 cDNA was inserted into pQE-9 vector using BamH1 and Hind III. Recombinant His_6-SNAP-23 was prepared from *Escherichia coli* and purified by Ni^{2+}NTA affinity chromatography. Rabbits were immunized with purified His_6-SNAP-23. The serum was first purified by affinity chromatography using GST-SNAP-23 covalently coupled by BS^3 crosslinking to GSH-agarose beads. This antibody (ab23) was further purified by passing it through an affinity column using GST-SNAP-25 covalently coupled beads. The His_6-SNAP-25 construct was a generous gift of Dr. Thomas Söllner. The flow-through antibody, termed affinity purified anti-SNAP-23, showed no detectable cross reactivity to His_6-SNAP-25.

Generation of Cell Lines Expressing Wild-type and Mutant RhoA

pEXVmyc-RhoAWT and pEXV myc-RhoV14 cDNAs were generously provided by Dr. A. Hall (MRC Laboratory of Molecular Cell Biology, London, GB) (Ridley and Hall, 1992b).The vectors were digested with EcoRI to remove the insert containing myc-RhoAWT or myc-RhoAV14 DNA and then ligated into EcoRI digested and dephosphorylated pTRE vector (Clontech, Palo Alto, CA). *Escherichia coli* were transfected with the vector constructs and selected for ampicillin resistance. Plasmid DNAs were purified from bacterial cells expressing pTRE-myc-RhoAWT or pTRE-myc-RhoAV14 cDNAs in the appropriate orientation (assessed by DNA sequencing). The T23 clone of MDCK cells (which express a tetracycline-repressible transactivator and the pIgR) (Barth et al., 1997) were cotransfected with 20 μg of pTRE-myc-RhoAWT or pTRE-myc-RhoAV14 and 2 μg of the pCB7 vector that contains a hygromycin resistance gene using $CaPO_4$ precipitation as previously described (Breitfeld et al., 1989a). Following a 2-3-day incubation in the presence of 20 ng/ml of doxycycline (DC; Sigma, St. Louis, MO), the cells were diluted into selection medium

containing Minimal Essential Medium (MEM), 10% v/v FBS, 250 μg/ml of hygromycin and 20 ng/ml of DC. The DC stock solution (20 μg/ml in 95% ethanol) was stored at –20˚ C and was diluted 1:1000 just prior to use. After selection for 10 days, surviving colonies were isolated using cloning rings and RhoAWT or RhoAV14 expression assessed by Western blotting and immunofluorescence 36 h after removal of DC. Positive clones were expanded in the presence of DC, aliquoted, and stored in liquid nitrogen. Several clones of each type were selected and then screened for polarized secretion of GP-80 (Urban et al., 1987), and a transepithelial resistance of >120 Ωcm^2 when cultured on Transwells in the presence of 20 ng/ml DC. The data presented are from an individual, representative clone that uniformally expressed high levels of either myc-RhoAWT or myc-RhoV14 when cells were cultured in the absence of DC. However, similar results were obtained with other clones expressing these mutant proteins. T23 MDCK cells expressing dominant negative myc-tagged RhoAN19 have been described previously (Jou and Nelson, 1998).

Cell Culture

MDCK strain II cells expressing the wild-type rabbit pIgR have been described (Breitfeld et al., 1989a). Cells were maintained in Minimal Essential Medium (MEM; Cellgro, Fischer Scientific, Pittsburgh, PA) supplemented with 10% fetal bovine serum (FBS; Hyclone, Logan, UT), 100 U/ml penicillin and 100 μg/ml streptomycin in 5% CO_2/95% air. In order to maintain a high level of receptor expression, new cells were thawed every 2 weeks, and were split 1:10 and passaged once weekly. For experiments, cells were cultured on 12-mm or 75-mm diameter, 0.4 μm pore size Transwells (Costar; Cambridge, MA) as described (Breitfeld et al., 1989a). Cells were fed each day following the second day of plating and used 3-4 days post culture.

The RhoAWT, RhoAV14 and RhoAN19 cell lines were routinely cultured in MEM medium (MEM/FBS) containing 10% (v/v) FBS, penicillin/streptomycin/fungizone and 20 ng/ml of DC at 37˚ C in a humidified atmosphere containing 5% CO_2. Expression of RhoAWT, RhoAV14, or RhoAN19 was induced by plating cells in 15-cm dishes at low density into MEM/FBS medium containing 0-5pg/ml DC and incubating them for 36-48 h at 37˚ C. At the end of this incubation period the cells had reached approximately 30% confluency. Cells treated in an identical fashion, but in the presence of 20 ng/ml DC, served as controls. The cells were trypsinized, washed with culture medium containing 5 μM calcium chloride (LCM), and 1 x 10^6 cells (resuspended in 0.5ml of LCM) were added to the apical chamber of rat-tail collagen-coated 12-mm diameter Transwells (Corning-Costar Corp., Cambridge, MA) in LCM containing either 20 ng/ml DC (control) or 0-5 pg/ml DC. Cells were incubated in LCM for 3-4 h (± DC), rinsed twice with PBS, and then incubated in MEM/FBS containing either 20 ng/ml DC (control) or 0-5 pg/ml DC and normal amounts of calcium chloride (1.8 mM) for 18-48 h.

MDCK cells (T23 clone) expressing dominant active myc-tagged Rac1V12 or dominant negative myc-tagged Rac1N17 under the control of a tetracycline-repressible transactivator have been described previously (Jou and Nelson, 1998). The cells were routinely cultured in DME medium containing 10% (v/v) FBS (DME/FBS), penicillin/streptomycin and 20 ng/ml of doxycycline (DC)(Sigma, St. Louis, MO) at 37˚ C in a humidified atmosphere containing 5% CO_2. The DC stock solution (20 μg/ml in 95% ethanol) was stored at –20˚ C and was diluted 1:1000 just prior to use. Expression of Rac1V12 or Rac1N17 was induced by plating cells in 15-cm dishes at low density into DME/FBS medium lacking DC and incubating them for 16-20h (Rac1N17) or 36h (Rac1V12) at 37˚ C. At the end of this incubation period the cells had reached approximately 30% confluency. Cells treated in an identical fashion, but in the presence of 20 ng/ml DC, served as controls. The cells were trypsinized, washed with culture medium containing 5 μM calcium chloride (LCM), and 1 x 10^6 cells (resuspended in 0.5ml of LCM) were added to the apical chamber of rat-tail collagen-coated 12-mm diameter Transwells (Corning-Costar Corp., Cambridge, MA) in LCM (± 20 ng/ml DC). Cells were incubated in LCM for 3-4 h, rinsed twice with Dulbecco's phosphate buffered saline (PBS) lacking calcium and magnesium, and then incubated in DME/FBS containing normal amounts of calcium chloride (1.8 mM) for 18-48 h (±20 ng/ml DC).

Apical Internalization of Ligands and Fluid-Phase Markers and Stripping of Cell-Surface Ligands

Ligands and fluid-phase markers were internalized from the apical and/or basolateral surface of filter-grown MDCK cells. Prior to Tf internalization the cells were incubated for 1 h at 37˚ C in MEM/BSA (MEM, Hank's balanced salt solution, 0.6% w/v BSA, 20 mM HEPES, pH 7.4) to deplete intracellular stores of Tf and to allow for cell surface and filter-bound Tf to dissociate. All incubations in MEM/BSA were performed in a circulating water bath. For basolateral uptake of Tf the cells were rinsed with MEM/BSA at 37˚ C and the bottom edge of the filter was carefully blotted to remove excess media. The 12-mm Transwell unit was placed on a 50 μl drop of MEM/BSA containing the ligand. For apical uptake, the cells were rinsed with MEM/BSA at the appropriate temperature, excess fluid was aspirated from the cell-side of the 12-mm Transwell and 150 μl of ligand or fluid-phase marker, diluted in MEM/BSA, was added. All incubations were performed in a humid chamber. At the end of the experiment cells were either rapidly chilled to 4˚ C or, if appropriate, fixed immediately.

In many of the experiments cell-surface receptors and their ligands were stripped from the cell surface as follows: cells were treated for 30 min at 4˚ C with 25 μg/ml of TPCK-treated trypsin. Subsequently, the cells were washed twice with ice cold MEM/BSA and once for 10 min with

either 125 μg/ml soybean trypsin inhibitor or 2 mM phenylmethylsulfonyl fluoride dissolved in MEM/BSA. For morphological analysis the cells were subsequently rinsed with PBS containing 0.5 mM $MgCl_2$ and 0.9 mM $CaCl_2$ (PBS^+), and immediately fixed.

Treatment with Nocodazole or Cytochalasin D (CD)

Nocodazole (Calbiochem) was dissolved in DMSO at 33 mM and stored at -20˚ C. In all experiments in which this drug was used, cells were pretreated 60 min at 4˚ C in the presence of 33 μM nocodazole. The drug was included in subsequent incubations. In some experiments 25 μg/ml of CD was included in the MEM/BSA. Both nocodazole and CD were prepared in DMSO as 1000-fold concentrated stocks and stored at –20 ˚ C

Immunofluorescent Labeling and Scanning-Laser Confocal Microscopy

Cells were fixed using a pH shift protocol (Apodaca et al., 1994) or periodate-lysine-paraformaldehyde (Brown and Farquhar, 1989) and then processed as previously described (Apodaca et al., 1994). Photomicrographs were obtained by photographing epifluorescence images aquired with an Axioplan fluorescence microscope (Carl Zeiss, Thornwood, NY) fitted with 40x or 63x oil immersion lenses or by capturing digital images with a krypton-argon laser coupled to a Multiprobe 2001 confocal (Molecular Dynamics, Mountain View, CA), attached to a Diaphot microscope (Nikon, Melville, NY) or by capturing digital images a TCS confocal microscope equipped with krypton, argon, and helium-neon lasers (Leica, Dearfield, IL). Images obtained with the Multiprobe 2001 confocal were acquired using a Plan Apo 60x objective (NA 1.4) with appropriate filter combinations. Collection parametes wew as follows: laser output, 60 mW, PMT-1 and PMT-2 set to 700-800 mV, laser attenuation at 10%, 100 μm slit. The images (512 x 512 pixels, 0.8 μm pixel size) were acquired using ImageSpace software. The images were converted to tag-information-file-format and the contrast levels of the images adjusted in the Photoshop program (Adobe Co., Mountain View, CA) on a Power PC Macintosh 9500 (Apple, Cupertino, CA). The contrast-corrected images were imported into Freehand (Macromedia; San Francisco, CA) and printed from a Kodak (Rochester, NY) 8650PS dye sublimation printer. Images obtained with the TCS confocal microscope were acquired using a 100x plan-apochromat objective (NA 1.4) and the appropriate filter combination. Settings were as follows: photomultipliers set to 600-800 mV, 1.5 μm pinhole, zoom = 2.0-3.5, Kalman filter (n=4). The images (1024 x 1024 pixels) were saved in a tag-information-file-format (TIFF) and the contrast levels of the images adjusted in the Photoshop program (Adobe Co.; Mountain View, CA) on a Power PC G-3 Macintosh (Apple; Cupertino, CA). The contrast-corrected images were imported into Freehand (Macromedia; San Francisco, CA) and printed from a Kodak (Rochester, NY) 8650PS dye sublimation printer.

Electron Microscopic Analysis of Cells Expressing Rac1V12

Following internalization of Fab-HRP, Rac1V12 cells were washed three times quickly with MEM/BSA (MEM containing 0.25 g/l of $NaHCO_3$, 0.6% BSA, and 20 mM HEPES, pH 7.4) and one time with ice cold PBS^+ (PBS containing 0.5 mM $MgCl_2$ and 0.9 mM $CaCl_2$). The cells were immediately fixed by adding ice-cold 0.5% (v/v) gluteraldehyde in 200 mM Na cacodylate, pH 7.4, 1 mM $CaCl_2$, 0.5 mM $MgCl_2$ and incubating the cells for 30 min at room temperature. Cells were rinsed three times with 200 mM Na cacodylate buffer, pH 7.4, and 0.1% (w/v) DAB (dissolved in 200 mM cacodylate buffer) was added for 2 min at room temperature. The DAB solution was aspirated and replaced with fresh DAB solution containing 0.01% (v/v) H_2O_2 and incubated 30 min at room temperature in the dark. Samples were rinsed with 200 mM Na cacodylate, pH 7.4, and osmicated with 1% OsO_4 (w/v), 200 mM Na cacodylate, pH 7.4, 1% (w/v) $K_4Fe(CN)_6$, for 90 min at 4˚ C. After several rinses with H_2O, samples were *en bloc* stained overnight with 0.5% (w/v) uranyl acetate in H_2O. Filters were dehydrated in a graded series of ethanol, embedded in the epoxy resin LX-112 (Ladd; Burlington, VT), and sectioned with a diamond knife (Diatome; Fort Washington, PA). Sections, pale gold in color, were mounted on butvar-coated nickel grids and viewed at 80 kV in a JEOL (Japan) 100 CX electron microscope without further contrasting.

Immunoperoxidase Electron Microscopy and Immunogold Labeling of Rab-11

Following internalization of IgA-HRP from the apical pole of MDCK cells, plasma membrane bound ligand was stripped with trypsin and the cells fixed using a pH shift protocol as described above. The cells were rinsed three times with 200 mM Na cacodylate buffer, pH 7.4, and then incubated with 0.1% (w/v) DAB dissolved in 200 mM cacodylate buffer for 2 min at room temperature. The DAB solution was aspirated and replaced with fresh DAB solution containing 0.01% (v/v) H_2O_2 and incubated 30 min at room temperature in the dark. Cells were then washed with ice-cold KTM buffer (115 mM potassium acetate, 2.5 mM magnesium acetate, 4 mM EGTA, 2 mM calcium carbonate, 20 mM Hepes, pH 7.4, and 1 mM dithiothreitol), and the plasma membrane permeabilized with 200 μg/ml digitonin (dissolved in KTM) for 20 min at 4˚ C. The cells were washed three times for 5 min with KTM buffer. Unreacted fixative was quenched with 40 mM glycine dissolved in PBS, and non-specific protein binding sites were blocked with PBS containing 2% (w/v) BSA (PBS-BSA) for 15 min at room temperature. The cells were incubated with anti-Rab11 antibodies, diluted 1:100 in PBS-BSA, for 60 min at room temperature. The cells were washed three times 5 min with PBS-BSA and then incubated with Protein A-5 nm gold (diluted in PBS-BSA) for 60 min at room temperature. Following three 5-min washes with PBS-BSA, the cells were fixed with 2.0% (v/v) gluteraldehyde in 100 mM Na cacodylate, pH 7.4, containing 1 mM $CaCl_2$, 0.5 mM $MgCl_2$ for 30 min at room temperature. Samples were rinsed with 100 mM Na cacodylate, pH 7.4, and osmicated with 1.5% OsO_4 (w/v), 100 mM Na cacodylate, pH 7.4, 1% (w/

v) $K_4Fe(CN)_6$, for 30 min at room temperature. After several rinses with H_2O, the samples were *en bloc* stained overnight with 0.5% (w/v) uranyl acetate in H_2O. Filters were dehydrated in a graded series of ethanol, embedded in the epoxy resin LX-112 (Ladd; Burlington, VT), and sectioned with a diamond knife (Diatome; Fort Washington, PA). Sections, green in color (approximately 250 nm), were mounted on butvar-coated nickel grids and viewed at 100 kV in a JEOL (Japan) 100 CX electron microscope without further contrasting.

Homogenization of MDCK Cells and Sucrose Flotation Gradient.

Following internalization of marker, the cells (grown on 75 mm Transwells) were gently scraped in phosphate buffered saline (PBS), centrifuged for 5 min at 400 x *g*, and the pellet resuspended in HB (250 mM sucrose, 10 mM HEPES, pH 7.4, 0.5 mM EDTA, containing proteinase inhibitors), recentrifuged, and then homogenized by 3-5 passages through a 22 gauge needle as previously described (Bomsel et al., 1990). The resulting homogenate was centrifuged at 1000 x *g* for 15 min at 4˚ C to generate a post-nuclear supernatant (PNS). Under these gentle conditions of homogenization >95% of the fluid-phase marker (HRP) was retained in membrane bound "vesicles" which were pelleted when centrifuged at 100,000 x *g*. The PNS was brought to 40.6% (w/w) sucrose in a 1 ml volume and loaded into 12-ml polycarbonate tubes and then overlaid successively with 3 ml of 35% (w/w) sucrose, 3 ml of 25% (w/w) sucrose, and 3 ml of 8.5% (w/w) sucrose (the sucrose solutions contained 0.5 mM EDTA and 10mM HEPES, pH 7.4 as buffer). The gradients were then centrifuged for 60 min at 4˚ C in a TH641 swinging bucket rotor (Sorvall) at 35,000 rpm. 450 μl fractions were collected from the top of the gradient. HRP activity was measured using 0.1 mg/ml of tetramethyl-benzidine dihydrochloride substrate (Sigma, catalog number T-3405) dissolved in phosphate-citrate-perchlorate buffer (Sigma, catalog number P4922). The reaction was stopped by the addition of 1/5 volume of 2 M H_2SO_4, the time noted, and the A_{450} recorded. One unit of HRP activity increased the A_{450} by 0.01 absorbance units/min. Protein was measured using the Pierce BCA kit with bovine serum albumin as a standard.

Diaminobenzidine (DAB) Density-Shift Assay

We have used a modified version of the DAB density-shift assay previously described [Apodaca, 1994 #715]. [^{125}I]IgA (5μg/ml) and 5-10 mg/ml of HRP (Pierce) or 25-50 μg/ml wheat germ agglutinin conjugated to HRP (WGA-HRP) (Vector Laboratories, Burlingame, CA) were cointernalized from the apical pole of the cells. The concentration of HRP was adjusted so that equivalent amounts of HRP were retained by the cell at the end of the 2.5 min pulse or 2.5 min pulse followed by a 7.5 min chase. The concentrations WGA-HRP was adjusted so that equivalent amounts of WGA-HRP were internalized by control and RHoAV14-expressing cells. Following internalization, the cells were washed with ice-cold MEM/BSA. [^{125}I]IgA was stripped from the

apical cell surface with 100 μg/ml of tosyl-phenylmethyl-chloromethyl ketone-treated trypsin (Worthington, Freehold, NJ)(in MEM/BSA) for three times for 10 min at 4˚ C. Cell surface WGA-HRP was simultaneously removed by treating the apical cell surface for 3x 10 min with 100 mM *N*-acetyl-D-glucosamine (dissolved in MEM/BSA). Alternatively, [^{125}I]Tf was internalized from the basolateral cell surface for 30 min at 37˚ C and HRP (5-10 mg/ml) was cointernalized from the apical pole of the cell during the last 7.5 min of the Tf pulse. These Tf-loaded cells were rapidly chilled and washed three times for 10 min. To allow for internalization of cell surface bound Tf the cells were warmed up to 37˚ C for 2.5 min. HRP was included in the apical medium during this 2.5 min chase.

Following ligand internalization and cell surface stripping, cells with internalized HRP were washed twice with ice-cold Hank's balanced salt solution containing 0.9 mM $CaCl_2$, 0.5 mM $MgCl_2$, and 20 mM HEPES, pH 7.4 ($HBSS^+$). DAB reaction buffer (0.5 ml) was added to both apical and basal compartments of the Transwell. DAB reaction buffer was prepared by adding 3.3 ml of 3 mg/ml of DAB (dissolved in $HBSS^+$, pH adjusted to 7.4 with NaOH, and filtered), and 20 μl of 30% (v/v) H_2O_2 to 20 ml of $HBSS^+$. In control reactions H_2O_2 was omitted from the DAB reaction buffer. Following a 45 min incubation at 4˚ C the cells were washed 2 times with $HBSS^+$, the filters were carefully excised from their holders, boiled in 0.4 ml of SDS lysis buffer (0.5 % [w/v] SDS, 100 mM triethanolamine, pH 8.6, 5 mM EDTA, 0.02 % [w/v] NaN_3) for 90 sec, and vortex-shaken for 15 min at 4˚ C. Under these conditions less than 5 % of the total counts were associated with the detergent-treated filter. The supernatants were then centrifuged at 100,000 x *g* in a RP70AT rotor (Sorvall, Wilmington, DE) for 25 min at 20˚ C in a RCM100 centrifuge (Sorvall). Radioactivity was quantified in a gamma counter. Values were normalized to reactions in which [^{125}I]IgA and IgA-HRP were cointernalized from the apical pole of the cell as described previously (Apodaca et al., 1994).

Following ligand internalization and cell surface stripping, cells with internalized WGA-HRP were then washed twice with ice-cold 200 mM sodium cacodylate, pH 7.4 buffer, and DAB reaction buffer (0.5 ml) was added to both apical and basal compartments of the Transwell. DAB reaction buffer was prepared by adding 40 mg of DAB to 40 ml H_2O and then adding 1.8 g of solid sodium cacodylate. The buffer was pH adjusted to 7.4 with NaOH, the buffer was filtered, and 1 μl of 30% (v/v) H_2O_2 was added to each ml of DAB reaction buffer. In control reactions H_2O_2 was omitted from the DAB reaction buffer. Following a 45 min incubation at 4˚ C, the cells were washed 2 times with 200 mM sodium cacodylate buffer, the filters were carefully excised from their holders, boiled in 0.4 ml of SDS lysis buffer (0.5 % [w/v] SDS, 100 mM triethanolamine, pH 8.6, 5 mM EDTA, 0.02 % [w/v] NaN_3) for 90 sec, and vortex-shaken for 15 min at 4˚ C. Under these conditions less

than 5 % of the total radioactivity was associated with the filter. The supernatants were then centrifuged at 100,000 x *g* in a RP70AT rotor (Sorvall, Wilmington, DE) for 30 min at 20˚ C in a RCM100 centrifuge (Sorvall). Radioactivity present in the pellet and supernatant was quantified in a gamma counter. Values were normalized to reactions in which [^{125}I]IgA and WGA-HRP were cointernalized from the apical pole of the cell as described previously (Apodaca et al., 1996; Apodaca et al., 1994).

Western Blot Analysis

Filter-grown cells were lysed in 0.2 ml of 0.5% SDS lysis buffer (100 mM triethanolamine, pH 8.6, 5 mM EDTA, 0.5% SDS), boiled for 3 min, and then vortex shaken for 15 min at 4˚ C to shear the DNA. The samples were centrifuged at 13,000 x *g*, and 10 μl of the sample was mixed with an equal volume of 2x Laemmli sample buffer containing 100 mM DTT, heated to 100˚ C for 3 min, and then resolved by SDS-PAGE in 10% or 15% (w/v) polyacrylamide gels. Rainbow markers (Amercham, Arlington Heights, IL) were loaded in adjacent lanes as molecular weight standards. The gels were then equilibrated in 10 mM 3-[cyclohexylamino]-1-propanesulfonic acid – NaOH buffer (CAPS buffer) for 10 min at room temperature before the proteins were transferred to Immobilon-P membranes (Millipore, Bedford, MA) for 75 min at 375 mAmps constant current in CAPS buffer. The membrane was blocked for 30 min at room temperature or overnight at 4º C in 10% (w/v) BSA dissolved in Dulbecco's phosphate buffered saline (PBS). Blotted proteins were reacted with primary antibodies (diluted in PBS containing 1% dehydrated non-fat milk) for 2 hours at room temperature with rotation. The membrane was then washed with TBS-Tween (2.68 mM KCl, 0.5M NaCl, 25mM Tris-HCl, pH 8.0, and 0.05% v/v Tween-20) three times for 15 min each, and then incubated in the appropriate secondary antibody conjugated to HRP diluted 1:25,000 in PBS-milk for 1 hour with rotation. The membrane was washed with 3 times 15 min with TBS-Tween, and then incubated for 1 min in Super Signal (Pierce, Rockford, IL) and exposed to XAR-5 film (Kodak). Relative intensities of the protein bands were quantified by densitometry.

Endocytosis of [^{125}I]IgA

Endocytosis of [^{125}I]IgA was measured as described (Breitfeld et al., 1990a). [^{125}I]IgA was iodinated using the ICl method to a specific activity of 1.0-2.0 x 10^7 cpm/μg (Breitfeld et al., 1989a). Cells were rapidly cooled and washed three times with ice-cold MEM/BSA. [^{125}I]IgA diluted in MEM/BSA was bound to either the apical or basolateral surface of the cells for 60-90 min at 4˚ C. Cells were washed three times quickly and then three times for 10 min with MEM/BSA (the final washes were performed by incubating the cells on a rotator). Cells were then either left on ice or warmed up to 37˚ C for periods up to 10 min. At the conclusion of the experiment, [^{125}I]IgA was stripped from the cell surface by incubating the cells for 60 min at 4˚ C with 100 μg/ml of trypsin followed by an

acid treatment with 750 mM glycine, pH 2.5 diluted 1:5 with PBS^+. The Transwells were rinsed with PBS^+ and the filters were cut out of their holders. Total [^{125}I]IgA initially bound to the cells included ligand dissociated from the cell surface, ligand stripped from the cell surface with trypsin and acid, and cell associated ligand not sensitive to trypsin and acid stripping (endocytosed), and was quantified in a gamma counter.

Measurement of Paracellular Diffusion of [^{125}I]IgA and [^{125}I]Tf

Filter-grown cells were washed three times with MEM/BSA and [^{125}I]IgA or [^{125}I]Tf, diluted in 0.5 ml of MEM/BSA containing a 100-fold excess of unlabeled IgA or Tf, were added to the apical chamber of the Transwell. Cold competing ligand was added to prevent receptor-mediated internalization and apical to basolateral transcytosis. MEM/BSA (0.5 ml) was placed in the basolateral chamber. At the designated time points, the basolateral MEM/BSA medium (0.5 ml) was collected and replaced with fresh MEM/BSA. After the final time point, filters were washed twice with ice-cold PBS, cut out of the insert, and the amount of [^{125}I]IgA or [^{125}I]Tf that remained in the apical medium, that had diffused into the basolateral chamber, or that remained cell associated was quantified in a gamma counter. The results are expressed as percent of [^{125}I]IgA or [^{125}I]Tf initially added to the apical chamber that was released basolaterally.

Analysis of [^{125}I]IgA Postendocy°tic Fate

The postendocytotic fate of a preinternalized cohort of [^{125}I]IgA (at 5-10 μg/ml) was analyzed as described (Breitfeld et al., 1989b). In brief, [^{125}I]IgA, diluted in MEM/BSA, was internalized from either the apical or basolateral pole of the cells for 10 min at 37˚ C. Subsequently, the cell surface from which ligand was internalized was washed rapidly three-times with MEM/BSA, the apical and basolateral media aspirated, and replaced with fresh MEM/BSA. The cells were then incubated for 3 min at 37˚ C. This total wash procedure took 5 min at 37˚ C. Fresh MEM/BSA was added to the cells, which were chased for up to 2 h at 37˚ C. At the designated time points, the apical and basolateral MEM/BSA media (0.5 ml) were collected and replaced with fresh MEM/BSA. After the final time point, filters were cut out of the insert and the amount of [^{125}I]IgA quantified with a gamma counter. The MEM/BSA samples were precipitated with 10% trichloroacetic acid (TCA) for 30 min on ice, and then centrifuged in a microfuge for 15 min at 4˚ C. The amount of [^{125}I]IgA in the TCA-soluble (degraded) and insoluble fractions (intact) was quantified with a gamma counter. In the original description of the assay, values for untransfected MDCK cells were subtracted from those of MDCK cells expressing the pIgR as a correction for fluid-phase internalization (Breitfeld et al., 1989b). In preliminary experiments, we performed assays in the presence of a 100-fold excess of cold competing IgA. We found that the amount of fluid-phase internalization was less that 5% of the signal observed in pIgR expressing cells. Because this correction for fluid-phase

internalization did not alter the results significantly, this step was omitted in subsequent experiments.

Analysis of [^{125}I]Tf Recycling

Iron saturated Tf was iodinated to a specific activity of 5.0-9.0 x 10^6 cpm/μg using ICl as described [Apodaca, 1994 #715]. The cells were washed with warm (37˚ C) MEM/BSA three times and unlabeled Tf allowed to dissociate from the cell surface and filter for 60 min in MEM/BSA. [^{125}I]Tf (5 μg/ml) was internalized from the basolateral surface of the cells for 45 min at 37˚ C in a humid chamber. The cells were washed 3-times for 5-min each with ice-cold MEM/BSA, and then warmed up to 37˚ C for 2.5 min to allow for receptor internalization as described previously (Apodaca et al., 1994). The medium was aspirated, fresh medium was added, and the postendocytic fate of [^{125}I]Tf assessed as described above. Alternatively after the 2.5 min 37° C warm up, cells were then SLO permeabilized (see below). [^{125}I]Tf uptake was inhibited >95% when the radioactive ligand was internalized in the presence of a 100-fold excess of cold ligand.

Analysis of [^{125}I]EGF Degradation

[^{125}I]epidermal growth factor (EGF) was purchased from NEN Life Science Products Inc. (Boston, MA; 150-200 μCi/ug) and used at final concentration of 40 ng/ml. The cells were washed with warm (37˚ C) MEM/BSA three times, and [^{125}I]EGF was internalized from the basolateral surface of the cells for 10 min at 37˚ C. The cells was washed rapidly three-times with MEM/BSA, the apical and basolateral medium aspirated and replaced with fresh MEM/BSA, and the cells were then incubated for 3 min at 37˚ C. The media was aspirated, fresh media was added, and the postendocytic fate of [^{125}I]EGF, and TCA precipitations of media samples performed as described above.

Cell-Surface Delivery Assays

Basolateral delivery of the polymeric immunoglobulin receptor (pIgR) was assessed as previously described (Aroeti and Mostov, 1994). Delivery of newly synthesized GP-135 from the Golgi to apical membrane was determined as described previously (Grindstaff et al., 1998a).

Preparation of SLO, SLO Permeabilization of MDCK Cells, LDH Release, and Assessment of Monolayer Integrity.

SLO was prepared and MDCK cells permeabilized with this toxin as described previously (Apodaca et al., 1996), however, 35 U/ml of SLO was used instead of 40 U/ml to permeabilize the cells. Briefly, cells were washed twice with ice cold $KOAc^+$ buffer (115 mM potassium acetate, 2.5 mM magnesium acetate, 25 mM HEPES, pH 7.4, 0.9 mM $CaCl_2$, and 0.5 mM $MgCl_2$), and once with ice-cold KTM buffer [115 mM potassium acetate, 2.5 mM Mg acetate, 25 mM HEPES, pH 7.4, 2

mM K_2CaEGTA (prepared as described in Tsien and Pozzan, 1989), pH 7.4, 2 mM EGTA-KOH, pH 7.4, and 1 mM DTT]. The Transwell was placed on a 15 μl drop of SLO, and the cells were incubated for 10 min on ice, and then washed twice quickly and once for 5 min with ice-cold KTM. To induce permeabilization of the cells and wash out cytosol, the cells were incubated 7.5 min at 37˚ C in KTM buffer. Subsequently, the KTM buffer was aspirated, replaced with ice-cold KTM, and the cells incubated for an additional 30-45 min on ice to further wash out cellular cytosol.

These permeabilized MDCK monolayers remain functionally intact by several previously described criteria (Apodaca et al., 1996): > 90% of the cellular LDH activity is released into the basolateral medium of permeabilized cells; when permeabilized from the basolateral surface no LDH activity is released apically; antibodies against cytoplasmic epitopes do not stain cells unless their basolateral surfaces have been SLO-permeabilized; and when examined by electron microscopy, the monolayers are found to be intact and junctional complexes are readily observable. In addition, when [^{125}I]Tf was added directly to the buffer bathing the apical side of permeabilized cells ≤ 0.8% of the marker was found in the opposite chamber following a 90 min incubation at 37˚ C in cytosol-free transport buffer (standard assay conditions/ buffers are given below). All of these observations confirm that the apical membrane remained unpermeabilized in these preparations and there was little leakage or transcytosis of unbound [^{125}I]Tf from one chamber of the Transwell to the opposite in the time frame of the experiments presented in this work.

Preparation of Rat Liver Cytosol and Reconstitution of [^{125}I]Tf Recycling in Permeabilized MDCK Cells

Preparation of rat liver cytosol has been described previously (Apodaca et al., 1996). Reconstituting traffic in the permeabilized cells requires an exogenous source of both energy and cytosol, hence 0.5 ml of KTM containing 8-10 mg/ml of rat liver cytosol, 1 mM ATP, 80 mM creatine phosphate, and 50 μg/ml creatine kinase (transport buffer) was added to the basolateral surface of the cells as described previously (Apodaca et al., 1996), and 0.5 ml of KTM alone was added to the apical cell surface. The cells were then incubated for periods up to 90 min at 37˚ C. At the end of the incubation the amount of [^{125}I]Tf released basolaterally (recycled), released apically (transcytosed), or that remained cell associated was quantified in a Cobra II Auto-Gamma counter from Packard (Downers Grove, IL). Cytosol was not added in some experiments, and in other initial experiments the ATP regenerating system was replaced with 40 U/ml of the ATP depleting enzyme apyrase (grade VI, Sigma). However, we later found that in this permeabilized cell system there is no difference between adding apyrase or not adding it, therefore, the addition of this enzyme was omitted in later experiments.

BoNT/E Treatment of Permeabilized MDCK Cells

The 150 KDa single-chain BoNT/E was produced and purified as described (DasGupta and Rasmussen, 1983). BoNT/E was treated with trypsin to convert the single-chain protein into the 150 KDa di-chain BoNT/E as previously described (Sathyamoorthy and DasGupta, 1985). Neurotoxins (1 mg/ml stocks, stored on ice) were diluted 1:10 in KTM buffer containing 10 mM DTT (freshly dissolved in degassed buffer), and incubated at room temperature for 60 min. The neurotoxins were further diluted in KTM containing 1 mM DTT and then added to the cells during their permeabilization at 37˚C. One difference from the normal assay condition described above was that following SLO binding the permeabilization step was extended to 10 min at 37˚ C to allow for maximal proteolytic action of the neurotoxins on SNAREs. No additional inhibition was observed in this permeabilized cell system when neurotoxin was included in the 90 min transport reaction at 37˚ C so this step was omitted.

In one set of experiments single chain or di-chain BoNT/E was reduced with DTT as described above or sham treated. Following SLO binding, cells were washed with DTT-free KTM and then warmed up for 10 min at 37˚ C in the presence of neurotoxin reduced or unreduced with DTT. The cells were then washed once with ice-cold DTT-free KTM and then incubated 30 min in ice-cold DTT-free KTM. Transcytosis and recycling of ligand in these neurotoxin-treated cells was assayed as described above except the transport buffer did not contain DTT.

NEM Treatment of Permeabilized MDCK Cells and NSF, SNAP-23, and anti-SNAP-23 Addition

NEM treatment and addition of recombinant NSF were performed as described (Apodaca et al., 1996). In some experiments 0.5 - 0.05 μM recombinant SNAP-23 was added to the transport buffer during the 90 min reaction at 37˚ C. In other experiments affinity purified rabbit anti-SNAP-23 or affinity purified anti-human IgA antibodies were added (following the SLO binding step) in the warm-up step at 37˚ C, during the cytosol wash-out at 4˚ C and in the transport buffer during the 90 min reaction at 37˚ C.

BIBLIOGRAPHY

BIBLIOGRAPHY

Achiriloaie, M., B. Barylko, and J.P. Albanesi. 1999. Essential role of the dynamin pleckstrin homology domain in receptor-mediated endocytosis. *Mol. Cell Biol.* 19:1410-1415.

Adam, T., M. Giry, P. Boquet, and P. Sansonetti. 1996. Rho-dependent membrane folding causes *Shigella* entry into epithelial cells. *EMBO J.* 15:3315-3321.

Adamson, P., H.F. Paterson, and A. Hall. 1992. Intracellular localization of the p21^{rho} proteins. *J. Cell Biol.* 119:617-627.

Altschuler, Y., S.-H. Liu, L. Katz, K. Tang, S. Hardy, F. Brodsky, G. Apodaca, and K. Mostov. 1999. ADP-ribosylation Factor 6 and Endocytosis at the Apical Surface of Madin-Darby Canine Kidney Cells. *J. Cell Biol.* 147:7-12.

Annaert, W.G., B. Becker, U. Kistner, M. Reth, and R. Jahn. 1997. Export of cellubrevin from the endoplasmic reticulum is controlled by BAP31. *J. Cell Biol.* 139:1397-1410.

Apodaca, G. 2001. Endocytic Traffic in Polarized Epithelial Cells: Role of the Actin and Microtubule Cytoskeletons. *Traffic*. 2:149-159.

Apodaca, G., M. Bomsel, J. Arden, P.P. Breitfeld, K. Tang, and K.E. Mostov. 1991. The polymeric immunoglobulin receptor: a model protein to study transcytosis. *J. Clin. Invest.* 87:1877-1882.

Apodaca, G., M.H. Cardone, S.W. Whiteheart, B.R. DasGupta, and K.E. Mostov. 1996. Reconstitution of transcytosis in SLO-permeabilized MDCK cells: existence of an NSF dependent fusion mechanism with the apical surface of MDCK cells. *EMBO J.* 15:1471-1481.

Apodaca, G., L.A. Katz, and K.E. Mostov. 1994. Receptor-mediated transcytosis of IgA in MDCK cells is via apical recycling endosomes. *J. Cell Biol.* 125:67-86.

Araki, S., Y. Tamori, M. Kawanishi, H. Shinoda, J. Masugi, H. Mori, T. Niki, H. Okazawa, t. Kubota, and M. Kasuga. 1997. Inhibition of the binding of SNAP-23 to syntaxin 4 by munc18c. *Biochem. Biophys. Res. Comm.* 234:257-262.

Aroeti, B., P.A. Kosen, I.D. Kuntz, F.E. Cohen, and K.E. Mostov. 1993. Mutational and secondary structural analysis of the basolateral sorting signal of the polymeric immunoglobulin receptor. *J. Cell Biol.* 123:1149-1160.

Aroeti, B., and K.E. Mostov. 1994. Polarized sorting of the polymeric immunoglobulin receptor in the exocytotic and endocytotic pathways is controlled by the same amino acids. *EMBO J.* 13:2297-2304.

Bacallao, R., C. Antony, C. Dotti, E. Karsenti, E.H.K. Stelzer, and K. Simons. 1989. The subcellular organization of Madin-Darby canine kidney cells during the formation of a polarized epithelium. *J. Cell Biol.* 109:2817-2832.

Baker, J.P., and M.A. Titus. 1998. Myosins: matching functions with motors. *Curr. Opin. Cell Biol*. 10:80-86.

Banerjee, A., T.F.J. Martin, and B.R. DasGupta. 1993. Nerve growth factor induces sensitivity to botulinum neurotoxin type A in norepinephrine-secreting PC12 cells. *Neuroscience Letts.* 164:93-96.

Barroso, M., and E. Sztul. 1994. Basolateral to apical transcytosis in polarized cells is indirect and involves BFA and trimeric G protein sensitive passage through the apical endosome. *J. Cell Biol.* 124:83-100.

Barth, A.I., A.L. Pollack, Y. Altschuler, K.E. Mostov, and W.J. Nelson. 1997. NH2-terminal deletion of beta-catenin results in stable colocalization of mutant beta-catenin with adenomatous polyposis coli protein and altered MDCK cell adhesion. *J. Cell Biol.* 136:693-706.

Beckers, C.J.M., M.R. Block, B.S. Glick, J.E. Rothman, and W.E. Balch. 1989. Vesicular transport between the endoplasmic reticulum and the Golgi stack requires the NEM-sensitive fusion protein. *Nature*. 339:397-400.

Benli, M., F. Doring, D.G. Robinson, X. Yang, and D. Gallwitz. 1996. Two GTPase isoforms, Ypt31p and Ypt32p, are essential for Golgi function in yeast. *EMBO J.* 15:6460-6475.

Bennett, M.K., J.E. Garcia-Arrarás, L.A. Elferink, K. Peterson, A.M. Fleming, C.D. Hazuka, and R.H. Scheller. 1993. The syntaxin family of vesicular transport receptors. *Cell*. 74:863-873.

Bennett, M.K., and R.H. Scheller. 1993. The molecular machinery for secretion is conserved from yeast to neurons. *Proc. Natl. Acad. Sci. USA*. 90:2559-2563.

Bertrand, E., P. Chartrand, M. Scaefer, S.M. Chenoy, R.H. Singer, and R.M. Long. 1998. Localization of ASH1 mRNA particles in living yeast. *Mol. Cell.* 2:437-445.

Blanchoin, L., K.J. Amann, H.N. Higgs, J.-B. Marchand, D.A. Kaiser, and T.D. Pollard. 2000. Direct observation of dendritic actin filament networks nucleated by Arp2/3 complex and WASP/Scar proteins. *Nature*. 404:1007-1011.

Block, M.R., B.S. Glick, C.A. Wilcox, F.T. Wieland, and J.E. Rothman. 1988. Purification of an N-ethylmaleimide-sensitive protein catalyzing vesicular transport. *Proc. Natl. Acad. Sci. USA*. 85:7852-7856.

Bomsel, M., R. Parton, S.A. Kuznetsov, T.A. Schroer, and J. Gruenberg. 1990. Microtubule- and motor-dependent fusion in vitro between apical and basolateral endocytic vesicles from MDCK cells. *Cell*. 62:719-731.

Bomsel, M., K. Prydz, R.G. Parton, J. Gruenberg, and K. Simons. 1989. Endocytosis in filter-grown Madin-Darby canine kidney cells. *J. Cell Biol.* 109:3243-3258.

Borisy, G.G., and T.M. Svitkina. 2000. Actin machinery: pushing the envelope. *Curr. Opin. Cell Biol.* 12:104-112.

Brandli, A.W., E.D. Adamson, and K. Simons. 1991. Transcytosis of epidermal growth factor. The

epidermal growth factor receptor mediates uptake but not transcytosis. *J. Biol. Chem.* 266:8560-8566.

Breitfeld, P., J.E. Casanova, J.M. Harris, N.E. Simister, and K.E. Mostov. 1989a. Expression and analysis of the polymeric immunoglobulin receptor. *Meth. Cell Biol.* 32:329-337.

Breitfeld, P.P., J.E. Casanova, W.C. McKinnon, and K.E. Mostov. 1990a. Deletions in the cytoplasmic domain of the polymeric immunoglobulin receptor differentially affect endocytotic rate and postendocytotic traffic. *J. Biol. Chem.* 265:13750-13757.

Breitfeld, P.P., J.M. Harris, and K.M. Mostov. 1989b. Postendocytotic sorting of the ligand for the polymeric immunoglobulin receptor in Madin-Darby canine kidney cells. *J. Cell Biol*. 109:475-486.

Breitfeld, P.P., W.C. McKinnon, and K.E. Mostov. 1990b. Effect of nocodazole on vesicular traffic to the apical and basolateral surfaces of polarized MDCK cells. *J. Cell Biol.* 111:2365-2373.

Brown, A.M., A.J. O'Sullivan, and B.D. Gomperts. 1998. Induction of exocytosis from permeabilized mast cells by the guanosine triphosphatases Rac and Cdc42. *Mol. Biol. Cell*. 9:1053-1063.

Brown, D., and J.L. Stow. 1996. Protein trafficking and polarity in kidney epithelium: from cell biology to physiology. *Physiological Reviews*. 76:245-297.

Brown, P.S., E. Wang, B. Aroeti, S.J. Chapin, K.E. Mostov, and K.W. Dunn. 2000. Definition of distinct compartments in polarized Madin-Darby Canine Kidney (MDCK) cells for membrane-volume sorting, polarized sorting and apical recycling. *Traffic*. 1:124-140.

Brown, W.J., and M.G. Farquhar. 1989. Immunoperoxidase methods for the localization of antigens in cultured cells and tissue sections by electron microscopy. *In* Methods in Cell Biology. Vol. 31. Academic Press, Palo Alto, CA. 553-569.

Bucci, C., R.G. Parton, I.H. Mather, H. Stunnenberg, K. Simons, B. Hoflack, and M. Zerial. 1992. The small GTPase Rab5 functions as a regulatory factor in the early endocytic pathway. *Cell*. 70:715-728.

Bucci, C., A. Wandinger-Ness, A. Lutcke, M. Chiariello, C.B. Bruni, and M. Zerial. 1994. Rab5a is a common component of the apical and basolateral endocytic machinery in polarized epithelial cells. *Proc. Natl. Acad. Sci. USA*. 91:5061-5065.

Buss, F., S. D.Arden, M. Lindsay, J.P. Luzio, and J. Kendrick-Jones. 2001. Myosin VI isoform localized to clathrin-coated vesicles with a role in clathrin-mediated endocytosis. *EMBO J*. 20:3676-3684.

Calakos, N., M.K. Bennett, K.E. Peterson, and R.H. Scheller. 1994. Protein-protein interactions contributing to the specificity of intracellular vesicular trafficking. *Science*. 263:1146-1149.

Cameron, L.A., P.A. Giardini, F.S. Soo, and J.A. Theriot. 2000. Secrets of actin-based motility revealed by a bacterial pathogen. *Nat. Rev. Mol. Cell Biol.* 1:110-119.

Cardone, M.H., B.L. Smith, W. Song, D. Mochley-Rosen, and K.E. Mostov. 1994. Phorbol myristate

acetate-mediated stimulation of transcytosis and apical recycling in MDCK cells. *J. Cell Biol.* 124:717-727.

Caron, E. 2002. Regulation of Wiskott-Aldrich syndrome protein and related molecules. *Curr. Opin Cell Biol.* 14:82-87.

Casanova, J.E., G. Apodaca, and K.E. Mostov. 1991. An autonomous signal for basolateral sorting in the cytoplasmic domain of the polymeric immunoglobulin receptor. *Cell*. 66:65-75.

Casanova, J.E., X. Wang, R. Kumar, S.G. Bhartur, J. Navarre, J.E. Woodrum, Y.A. Altschuler, G.S. Ray, and J.R. Godenring. 1999. Association of Rab25 and Rab11a with the apical recycling system of polarized Madin-Darby canine kidney cells. *Mol. Biol. Cell*. 10:47-61.

Chen, L.-M., S. Hobbie, and J.E. Galán. 1996. Requirement of CDC42 for *Salmonella*-induced cytoskeletal and nuclear responses. *Science*. 274:2115-2118.

Chen, W., Y. Feng, D. Chen, and A. Wandinger-Ness. 1998. Rab11 is required for trans-Golgi network-to-plasma membrane transport and a preferential target for GDP dissociation inhibitor. *Mol. Biol. Cell*. 9:3241-3257.

Chen, Y.A., S.J. Scales, S.M. Patel, Y.-C. Doung, and R.H. Scheller. 1999. SNARE complex formation is triggered by Ca^{+} and drives membrane fusion. *Cell*. 97:165-174.

Chen, Y.A., S.J. Scales, and R.H. Scheller. 2001. Sequential SNARE Assembly Underlies Priming and Triggering of Exocytosis. *Neuron*. 30:161-170.

Chimini, G., and P. Chavrier. 2000. Function of Rho family proteins in actin dynamics during phagocytosis and engulfment. *Nature Cell Biol.* 2:E191-E196.

Chistoforidis, S., H.M. McBride, R.D. Burgoyne, and M. Zerial. 1999. The Rab5 effector EEA1 is a core component of endosome docking. *Nature*. 397:621-625.

Clary, D.O., I.C. Griff, and J.E. Rothman. 1990. SNAPs, a family of NSF attachment protein involved in intracellular membrane fusion in animals and yeast. *Cell*. 61:709-721.

Condeelis, J. 2001. How is actin polymerization nucleated *in vivo*? *Trends Cell Biol.* 11:288-293.

Cooper, J.A., and D.A. Schafer. 2000. Control of actin assembly and disassembly at filament ends. *Curr. Opin. Cell Biol.* 12.

Cremona, O., G. Di Paolo, M.R. Wenk, A. Luthi, W.T. Kim, K. Takei, L. Daniell, Y. Nemoto, S.B. Shears, and R.A. Flavell. 1999. Essential role of phosphoinositide metabolism in synaptic vesicle recycling. *Cell*. 99:179-188.

Cussac, D., P. Leblanc, A. L'Heritier, J. Bertoglio, P. Lang, C. Kordon, A. Enjalbert, and D. Saltarelli. 1996. Rho proteins are localized with different membrane compartments involved in vesicular trafficking in anterior pituitary cells. *Mol. Cell. Endocrinol.* 119:195-206.

DasGupta, B.R. 1990. Structure and biological activity of botulinum neurotoxin. *J. Physiologie (Paris)*. 84:220-228.

DasGupta, B.R., and S. Rasmussen. 1983. Purification and amino acid composition of type E

botulinum neurotoxin. *Toxicon*. 21:535-545.

De Camilli, P., S.D. Emr, P.S. McPherson, and P. Novick. 1996. Phosphoinositides as regulators in membrane traffic. *Science*. 271:1533-1539.

DePina, A.S., and G.M. Langford. 1999. Vesicle Transport: The Role of Actin Filaments and Myosin Motors. *Microscopy Research and Technique*. 47:93-106.

Dharmawardhane, S. 1997. Localization of p21-activated kinase 1 (PAK1) to pinocytic vesicles and cortical actin structures in stimulated cells. *J. Cell Biol.* 138:1265-1278.

Downward, J., J.D. Graves, P.H. Warne, S. Rayter, and D.A. Cantrell. 1990. Stimulation of p21ras upon T-cell activation. *Nature*. 346:719-723.

Dramsi, S., and P. Cossart. 1998. Intracellular Pathogens and the Actin Cytoskeleton. *Annu. Rev. Cell Dev. Biol.* 14:137-166.

Drubin, D.G., and W.J. Nelson. 1996. Origins of cell polarity. *Cell*. 84:335-344.

Dunn, K.W., T.E. McGraw, and F.R. Maxfield. 1989. Iterative fractionation of recycling receptors from lysosomally destined ligands in an early sorting endosome. *J. Cell Biol.* 109:3303-3314.

Durrbach, A., D. Louvard, and E. Coudrier. 1996. Actin filaments facilitate two steps of endocytosis. *J. Cell Sci.* 109:457-465.

Durrbach, A., G. Raposo, D. Tenza, D. Louvard, and E. Coudrier. 2000. Truncated Brush Border Myosin I Affects Membrane Traffic in Polarized Epithelial Cells. *Traffic*. 1:411-424.

Echard, A., F. Jollivet, O. Martinez, J.J. Lacapere, A. Rousselet, I. Janoueix-Lerosey, and B. Goud. 1998. Interaction of a Golgi-associated kinesin-like protein with Rab6. *Science*. 279:580-585.

Ellis, S., and H. Mellor. 2000. Regulation of endocytic traffic by Rho family GTPases. *Trends in Cell Biol.* 10:85-88.

Engqvist-Goldstein, A.E.Y., M.M. Kessles, V.S. Chopra, M.R. Hayden, and D.G. Drubin. 1999. An Actin-binding Protein of the Sla2/Huntingtin Interacting Protein 1 Family Is a Novel Component of Clathrin-coated Pits and Vesicles. *J. Cell Biol.* 147:1503-1518.

Fasshauer, D., W. Antonin, M. Margittai, S. Pabst, and R. Jahn. 1999. Mixed and Non-cognate SNARE Complexes. *J. Biol. Chem.* 274:15440-15446.

Fasshauer, D., R.B. Sutton, A.T. Brunger, and R. Jahn. 1998. Conserved structural features of the synaptic fusion complex: SNARE proteins reclassified as Q- and R-SNAREs. *Proc. Natl. Acad. Sci. USA*. 95:15781-15786.

Fath, K., and D.R. Burgess. 1993. Golgi-derived vesicles from developing epithelial cells bind actin filaments and possess myosin-I as a cytoplasmically-oriented peripheral membrane protein. *J. Cell Biol.* 120:117-127.

Feig, L.A. 1999. Tools of the trade: use of dominant-inhibitory mutants of Ras-family GTPases. *Nature Cell Biol.* 1:E25-E27.

Fölsch, H., H. Ohno, J.S. Bonifacino, and I. Mellman. 1999. A novel clathrin adaptor complex

mediates basolateral targeting in polarized epithelial cells. *Cell*. 99:189-198.

Frischknecht, F., and M. Way. 2001. Surfing pathogens and the lessons learned for actin polymerization. *Trends Cell Biol.* 11:30-38.

Fujimoto, L.M., R. Roth, J.E. Heuser, and S.L. Schmid. 2000. Actin assembly plays a variable, but not obligatory role in receptor-mediated endocytosis in mammalian cells. *Traffic*. 1:161-171.

Fukuda, R., J.A. McNew, T. Weber, F. Pariati, T. Engel, W. Nickel, J.E. Rothman, and T.H. Sollner. 2000. Functional architecture of an intracellular membrane t-SNARE. *Nature*. 407:198-202.

Fuller, S.D., and K. Simons. 1986. Transferrin receptor polarity and recycling accuracy in “tight” and “leaky” strains of Madin-Darby canine kidney cells. *J. Cell Biol.* 103:1767-1779.

Futter, C.E., A. Gibson, E.H. Allchin, S. Maxwell, L.J. Ruddock, G. Odorizzi, D. Domingo, I.S. Trowbridge, and C.R. Hopkins. 1998. In polarized MDCK cells basolateral vesicles arise from clathrin-gamma-adaptin-coated domains on endosomal tubules. *J. Cell Biol.* 141:611-623.

Gad, H., N. Ringstad, P. Low, O. Kjaeruff, J. Gustafsson, M. Wenk, G. Di Paolo, Y. Nemoto, J. Crun, and M.H. Ellisman. 2000. Fission and uncoating of synaptic clathrin-coated vesicles are perturbed by disruption of interactions with the SH3 domain of endophilin. *Neuron*. 27:301-312.

Gaisano, H.Y., M. Ghai, P.N. Malkus, L. Sheu, A. Bouquillon, M.K. Bennett, and W.S. Trimble. 1996. Distinct cellular locations of the syntaxin family of proteins in rat pancreatic acinar cells. *Molec. Biol. Cell*. 7:2019-2027.

Gaisano, H.Y., L. Sheu, P.P.C. Wong, A. Klip, and W.S. Trimble. 1997. SNAP-23 is located in the basolateral plasma membrane of rat pancreatic acinar cells. *FEBS Letters*. 414:293-302.

Galli, T., T. Chilcote, O. Mundigl, T. Binz, H. Niemann, and P. DeCamilli. 1994. Tetanus toxin-mediated cleavage of cellubrevin impairs exocytosis of transferrin receptor-containing vesicles in CHO cells. *J. Cell Biol.* 125:1015-1024.

Geli, M.I., and H. Riezman. 1996. Role of type I myosins in receptor-mediated endocytosis in yeast. *Science*. 272:533-535.

Gibson, A., C.E. Futter, S. Maxwell, E.H. Allchin, M. Shipman, J.P. Kraehenbuhl, D. Domingo, G. Odorizzi, I.S. Trowbridge, and C.R. Hopkins. 1998. Sorting mechanisms regulating membrane protein traffic in the apical transcytotic pathway of polarized MDCK cells. *J. Cell Biol.* 143:81-94.

Gingras, D., F. Gauthier, S. Lamy, R.R. Desrosiers, and R. Beliveau. 1998. Localization of RhoA GTPase to Endothelial Caveolae-Enriched Membrane Domains. *Biochem. Biophys. Res. Comm.* 247:888-893.

Glick, B.S., and J.E. Rothman. 1987. Possible role for fatty acyl-coenzyme A in intracellular protein transport. *Nature*. 326:309-312.

Goldenring, J.R., C.J. Soroka, K.R. Shen, L.H. Tang, W. Rodriguez, H.D. Vaughan, S.A. Stoch, and

I.M. Modlin. 1994. Enrichment of rab11, a small GTP-binding protein, in gastric parietal cells. *Am. J. Physiol.* 267:G187-G194.

Gorvel, J., P. Chavrier, M. Zerial, and J. Gruenberg. 1991a. rab5 controls early endosome fusion in vitro. *Cell*. 64:915-925.

Gorvel, J.-P., P. Chavrier, M. Zerial, and J. Gruenberg. 1991b. Rab5 controls early endosome fusion *in vitro*. *Cell*. 64:915-925.

Gottlieb, T.A., I.E. Ivanov, M. Adesnik, and D.D. Sabatini. 1993. Actin microfilaments play a critical role in endocytosis at the apical but not the basolateral surface of polarized epithelial cells. *J. Cell Biol.* 120:695-710.

Gouin, E., H. Gantelet, C. Egile, I. Lasa, H. Ohayon, V. Villiers, P. Gounon, P.J. Sansonetti, and P. Cossart. 1999. A comparative study of actin-based motilities of the pathogenic bacteria *Listeria monocytogenes, Shigella flexneri* and *Rickettsia conorii*. *J. Cell Sci.* 112:1697-1708.

Green, E.G., E. Ramm, N.M. Riley, D.J. Spiro, J.R. Goldenring, and M. Wessling-Resnick. 1997. Rab11 is associated with transferrin-containing recycling compartments in K562 cells. *Biochem. Biophys. Res. Commun.* 239:612-616.

Griffiths, G.R., R. Back, and M. Marsh. 1989. A quantitative analysis of the endocytic pathway in baby hamster kidney cells. *J. Cell Biol.* 109:2703-2720.

Grindstaff, K.K., R.L. Bacallao, and W.J. Nelson. 1998a. Apionuclear organization of microtubules does not specify protein delivery from the trans-Golgi network to different membrane domains in polarized epithelial cells. *Mol. Biol. Cell*. 9:685-699.

Grindstaff, K.K., C. Yeaman, N. Anandasabapathy, S.C. Hsu, E. Rodriquez-Boulan, R.H. Scheller, and W.J. Nelson. 1998b. Sec6/8 complex is recruited to cell-cell contacts and specifies transport vesicle delivery to the basal-lateral membrane in epithelial cells. *Cell*. 93:731-740.

Gruenberg, J., G. Griffiths, and K. Howell. 1989. Characterization of the early endosome and putative endocytic carrier vesicles in vivo and with an assay of vesicle fusion in vitro. *J. Cell Biol.* 108:1301-1316.

Gutiérrez, L.M., J.M. Cànaves, A.V. Ferrer-Montiel, J.A. Reig, M. Montal, and S. Viniegra. 1995. A peptide that mimics the carboxy-terminal domain of SNAP-25 blocks Ca^{2+}- dependent exocytosis in chromaffin cells. *FEBS Letters*. 372:39-43.

Hall, A. 1998. Rho GTPases and the actin cyotskeleton. *Science*. 279:509-514.

Hammer III, J.A., and X.S. Wu. 2002. Rabs grab motor: defining the connections between Rab GTPases and motor proteins. *Curr. Opin. Cell Biol.* 14:69-75.

Hansen, S.H., and J.E. Casanova. 1994. Gsα stimulates transcytosis and apical secretion in MDCK cells through cAMP and protein kinase A. *J. Cell Biol.* 126:677-688.

Hansen, S.H., A. Olsson, and J.E. Casanova. 1995. Wortmannin, an inhibitor of phosphoinositide 3-kinase, inhibits transcytosis in polarized epithelial cells. *J. Biol. Chem.* 270:28425-28432.

Hayashi, T., H. McMahon, S. Yamasaki, T. Binz, Y. Hata, T.C. Sudhof, and H. Niemann. 1994. Synaptic vesicle membrane fusion complex: action of clostridial neurotoxins on assembly. *EMBO J.* 13:5051-5061.

Hemery, L., A.-M. Durand-Schneider, G. Feldmann, J.-P. Vaerman, and M. Maurice. 1996. The transcytotic pathway of an apical plasma membrane protein (B10) in hepatocytes is similar to that of IgA and occurs via a tubular pericentriolar compartment. *J. Cell Sci.* 109:1215-1227.

Hill, E., M. Clarke, and F.A. Barr. 2000. The Rab6-binding kinesin, Rab6-KIFL, is required for cytokinesis. *EMBO J*. 19:5711-5719.

Hughson, E.J., and C. Hopkins. 1990. Endocytic pathways in polarized caco-2 cells: identification of an endosomal compartment accessible from both apical and basolateral surfaces. *J. Cell Biol.* 110:337-348.

Hunziker, W., P. Mâle, and I. Mellman. 1990. Differential microtubule requirements for transcytosis in MDCK cells. *EMBO J.* 9:3515-3525.

Hunziker, W., and P.J. Peters. 1998. Rab17 localizes to recycling endosomes and regulates receptor-mediated transcytosis in epithelial cells. *J. Biol. Chem.* 273:15734-15741.

Ihrke, G., V.M. Martin, M.R. Shanks, M. Schrader, T.A. Schroer, and A.L. Hubbard. 1998. Apical plasma membrane proteins and endolyn-78 travel through a subapical compartment in polarized WIF-B hepatocytes. *J. Cell Biol.* 141:115-133.

Ikonen, E., J.B. de Almeid, K.F. Fath, D.R. Burgess, K. Ashman, K. Simons, and J.L. Stow. 1997. Myosin II is associated with Golgi membranes: identification of p200 as nonmuscle myosin II on Golgi-derived vesicles. *J. Cell Sci.* 110:2155-2164.

Ikonen, E., M. Tagaya, O. Ullrich, C. Montecucco, and K. Simons. 1995. Different requirements for NSF, SNAP, and Rab proteins in apical and basolateral transport in MDCK cells. *Cell*. 81:571-580.

Jackman, M.R., W. Shurety, J.A. Ellis, and J.P. Luzio. 1994. Inhibition of apical but not basolateral endocytosis of ricin and folate in Caco-2 cells by cytochalasin D. *J. Cell. Sci.* 107:2547-2556.

Jahn, R., and H. Niemann. 1994. Molecular mechanisms of clostridial neurotoxins. *Annals of the New York Academy of Sciences*. 733:245-255.

Jahn, R., and T.C. Sudhof. 1999. Membrane Fusion and Exocytosis. *Annu. Rev. Biochem.* 68:863-911.

Jarousse, N., and R.B. Kelly. 2001. Endocytotic mechanisms in synapses. *Curr. Opin. Cell Biol.* 13:461-469.

Jou, T.-S., S.-M. Leung, L.M. Fung, W.G. Ruiz, W.J. Nelson, and G. Apodaca. 2000. Selective alterations in biosynthetic and endocytic protein traffic in Madin-Darby canine kidney epithelial cells expressing mutants of the small GTPase Rac1. *Mol. Biol. Cell*. 11:287-304.

Jou, T.-S., and W.J. Nelson. 1998. Effects of regulated expression of mutant RhoA and Rac1 small

GTPases on the development of epithelial (MDCK) cell polarity. *J. Cell Biol.* 142:85-100.

Jou, T.-S., E.E. Schneeberger, and W.J. Nelson. 1998. Structural and functional regulation of tight junctions by RhoA and Rac1 small GTPases. *J. Cell Biol.* 142:101-115.

Kelly, R.B. 1990. Microtubules, membrane traffic, and cell organization. *Cell*. 61:5-7.

Kirchhausen, T. 2000. Three ways to make a vesicle. *Nature Rev. Mol. Cell Biol.* 1:187-198.

Knight, A., E. Hughson, C. Hopkins, and D. Cutler. 1995. Membrane protein trafficking through the common apical endosome compartment of polarized Cac0-2 cells. *Mol. Biol. Cell.* 6:597-610.

Kozma, R., S. Ahmed, A. Best, and L. Lim. 1995. The Ras-related protein Cdc42Hs and bradykinin promote formation of peripheral actin microspikes and filopodia in Swiss 3T3 fibroblasts. *Mol. Cell. Biol.* 15:1942-1952.

Kroschewski, R., A. Hall, and I. Mellman. 1999. Cdc42 controls secretory and endocytic transport to the basolateral plasma membrane of MDCK cells. *Nature Cell Biol.* 1:8-13.

Kübler, E., and H. Riezmann. 1993. Actin and fimbrin are required for the internalization step of endocytosis in yeast. *EMBO J.* 12:2855-2862.

Lamaze, C., T.-H. Chuang, L.J. Terlecky, G.M. Bokoch, and S.L. Schmid. 1996. Regulation of receptor-mediated endocytosis by Rho and Rac. *Nature*. 382:177-179.

Lamaze, C., L.M. Fujimoto, H.L. Yin, and S.L. Schmid. 1997. The actin cytoskeleton is required for receptor-mediated endocytosis in mammalian cells. *J. Biol. Chem.* 272:20332-20335.

Lantz, V.A., and K.G. Miller. 1998. A class VI unconventional myosin is associated with a homologue of a microtubule-binding protein, cytoplasmic linker protein-170, in neurons and at the posterior pole of *Drosophila* embryos. *J. Cell Biol.* 140:897-910.

Lasa, I., P. Dehoux, and P. Cossart. 1998. Actin polymerization and bacterial movement. *Biochim. Biophys. Acta*. 1402:217-228.

Lee, A., D.W. Frank, M.S. Marks, and M.A. Lemmon. 1999. Dominant-negative inhibition of receptor-mediated endocytosis of a dynamin-1 mutant with a defective pleckstrin homology domain. *Curr. Biol.* 9:261-264.

Leung, S.-M., R. Rojas, C. Maples, C. Flynn, W.G. Ruiz, T.-S. Jou, and G. Apodaca. 1999. Modulation of endocytic traffic in polarized Madin-Darby canine kidney cells by the small GTPase RhoA. *Mol. Biol. Cell*. 10:4369-4384.

Li, G., D'Souza-Schorey, M.A. Barbieri, J.A. Cooper, and P.D. Stahl. 1997. Uncoupling of membrane ruffling and pinocytosis during ras signal transduction. *J. Biol. Chem.* 272:10337-10340.

Lindstedt, A.D., and H.P. Hauri. 1993. Giantin, a novel conserved Golgi membrane protein containing a cytoplasmic domain of at least 350 kDa. *Mol. Biol. Cell*. 1993:679-693.

Liscovitch, M., and L.C. Cantley. 1995. Signal transduction and membrane traffic: the PITP/phosphoinositide connection. *Cell*. 81:659-662.

Liskovitch, M. 1996. Phospholipase D: role in signal transduction and membrane traffic. *J. Lipid Mediators Cell Signal.* 14:215-221.

Liu, X., B. Ondeck, and D.S. Williams. 1998. Mutant myosin VIIa causes defective melanosome distribution in the RPE of shaker-1 mice. *Nature Genet.* 19:117-118.

Liu, X., I.P. Udovichenko, S.D.M. Brown, K.P. Steel, and D.S. Williams. 1999. Myosin VIIa participates in opsin transport through the photoreceptor cillium. *J. Neurosci.* 19:6267-6274.

Loisel, T.P., R. Boujemaa, D. Pantaloni, and M.F. Carlier. 1999. Reconstitution of actin-based motility of *Listeria* and *Shigella* using pure proteins. *Nature*. 401:613-616.

Lomneth, R., T.F.J. Martin, and B.R. DasGupta. 1991. Botulinum neurotoxin light chain inhibits norepinephrine secretion in PC12 cells at an intracellular membranous or cytoskeletal site. *J. Neurochem.* 57:1413-1421.

Low, S.-H., S.J. Chapin, T. Weimbs, L.G. Kömüves, M.K. Bennett, and K.E. Mostov. 1996. Differential localization of syntaxin isoforms in polarized Madin-Darby canine kidney cells. *Molec. Biol. Cell*. 7:2007-2018.

Low, S.H., P.A. Roche, H.A. Anderson, S.C.D. van Ijzendoorn, M. Zhang, K.E. Mostov, and W. Thomas. 1998. Targeting of SNAP-23 and SNAP-25 in Polarized Epithelial Cells. *J. Biol. Chem.* 273:3422-3430.

Lupashin, V.V., and M.G. Waters. 1997. t-SNARE activation through transient interaction with a rab-like guanosine triphosphatase. *Science*. 276:1255-1258.

Ma, L., L.C. Cantley, P.A. Janmey, and M.W. Kirschner. 1998. Corequirement of specific phosphoinositides and small GTP-binding protein Cdc42 in inducing actin assembly in *Xenopus* egg extracts. *J. Cell Biol.* 140:1125-1136.

Macaulay, S.L., S. Rea, K.H. Gough, C.W. Ward, and D.E. James. 1997. Botulinum E Toxin Light Chain Does Not Cleave SNAP-23 and Only Partially Impairs Insulin Stimulation of GLUT4 Translocation in 3T3-L1 Cells. *Biochem. Biophys. Res. Comm.* 237:388-393.

Machesky, L.M. 1999. Rocket-based motility: a universal mechanism? *Nat. Cell Biol.* 1:E29-E31.

Machesky, L.M., and K.L. Gould. 1999. The Arp2/3 complex: a multifunctional actin organizer. *Curr. Opin. Cell Biol.* 11:117-121.

Machesky, L.M., R.D. Mullins, H.N. Higgs, D.A. Kaiser, L. Blanchoin, R.C. May, M.E. Hall, and T.D. Pollard. 1999. WASP-related protein Scar activates dendritic nucleation of actin filaments by Arp2/3 complex. *Proc. Natl. Acad. Sci. USA.* 96:3739-3744.

Mackay, D.J.G., and A. Hall. 1998. Rho GTPases. *J. Biol. Chem.* 273:20685-20688.

Mammoto, A., T. Ohtsuka, I. Hotta, T. Sasaki, and Y. Takai. 1999. Rab11BP/Rabphillin-11, a downstream target of rab11 small G protein implicated in vesicle recycling. *J. Biol. Chem.* 274:25517-25524.

Maples, C.J., W.G. Ruiz, and G. Apodaca. 1997. Both microtubules and actin filaments are required

for efficient postendocytic traffic of the polymeric immunoglobulin receptor in polarized Madin-Darby canine kidney cells. *J. Biol. Chem.* 272:6741-6751.

Mariot, P., A.J. O'Sullivan, A.M. Brown, and P.E.R. Tatham. 1996. Rho guanine nucleotide dissociation inhibitor protein (RhoGDI) inhibits exocytosis in mast cells. *EMBO J.* 15:6476-6482.

Marsh, M., G. Griffiths, G.E. Dean, I. Mellman, and A. Helenius. 1986. Three-dimensional structures of endosomes in BHK-21 cells. *Proc. Natl. Acad. Sci. USA*. 83:2899-2903.

Martinez, O., and B. Goud. 1998. Rab Proteins. *Biochim. Biophys. Acta*. 1404:101-112.

Martyst, J., T. Shevell, and T. McGraw. 1996. Studies of transferrin recycling reconstituted in Streptolysin O permiabilized Chinese hamster ovary cells. *J. Biol. Chem.* 270:25976-25984.

Matter, K., K. Bucher, and H.-P. Hauri. 1990. Microtubule perturbation retards both the direct and the indirect apical pathway but does not affect sorting of plasma membrane proteins in intestinal epithelial cells (Caco-2). *EMBO J.* 9:3163-3170.

Mayer, A., W. Wickner, and A. Haas. 1996. Sec18p (NSF)-driven release of Sec17p (α-SNAP) can precede docking and fusion of yeast vacuoles. *Cell*. 85:83-94.

Mays, R.W., K.A. Beck, and W.J. Nelson. 1994. Organization and function of the cytoskeleton in polarized epithelial cells: a component of the protein sorting machinery. *Current Opinion in Cell Biology*. 6:16-24.

McBride, H.M., V. Rybin, C. Murphy, A. Giner, R. Teasdale, and M. Zerial. 1999. Oligomeric complexes link Rab5 effectors with NSF and drive membrane fusion via interactions between EEA1 and syntaxin 13. *Cell*. 98:377-386.

McGoldrick, C.A., C. Gruver, and G.S. May. 1995. *myoA* of *Aspergillus nidulans* encodes an essential myosin I required for secreation and polarized growth. *J. Cell Biol.* 128:577-587.

McGraw, T.E., K.W. Dunn, and F.R. Maxfield. 1993. Isolation of a temperature-sensitive variant Chinese hamster ovary cell line with a morpholotgically altered endocytic recycling compartment. *J. Cell Physiol.* 155:579-594.

McLauchlan, H., J. Newell, N. Morrice, A. Osborne, M. West, and E. Smythe. 1998. A novel role for Rab5-GDI in ligand sequestration into clathrin-coated pits. *Curr. Biol.* 8:34-45.

McMahon, H.T., Y.A. Ushkaryov, L. Edelmann, E. Link, T. Binz, H. Niemann, R. Jahn, and T.C. Sudhof. 1993. Cellubrevin is a ubiquitous tetanus-toxin substrate homologous to a putative synaptic vesicle fusion protein. *Nature*. 364:346-349.

McNew, J.A., F. Parlati, R. Fukuda, R.J. Johnston, K. Paz, F. Paumet, T.H. Sollner, and J.E. Rothman. 2000. Compartmental specificity of cellular membrane fusion encoded in SNARE proteins. *Nature*. 407:153-159.

Mermall, V., P.L. Post, and M.S. Mooseker. 1998. Unconventional Myosins in Cell Movement, Membrane Traffic, and Signal Transduciton. *Science*. 279:527-533.

Merrifield, C.J., S.E. Moss, C. Callestrem, B.A. Imhof, G. Glese, I. Wunderlich, and W. Almers. 1999. Endocytic vesicles move at the tips of actin tails in cultured mast cells. *Nat. Cell Biol.* 1:72-74.

Miki, H., K. Miura, and T. Takenawa. 1996. N-WASP, a novel actin-depolymerizing protein, regulates the cortical cytoskeletal rearrangement in a PIP_2-dependent manner downstream of tyrosine kinases. *EMBO J.* 15:5326-5335.

Miller, S.G., and H.-P.H. Moore. 1991. Reconstitution of constitutive secretion using semi-intact cells: regulation by GTP but not calcium. *J. Cell Biol.* 112:39-54.

Mimori-Kiyosue, Y., N. Shiina, and S. Tsukita. 2000. Adenomatous Polyposis Coli (APC) Protein Moves along Microtubules and Concentrates at Their Growing Ends in Epithelial Cells. *J. Cell Biol.* 148:505-517.

Molloy, S.S., L. Thomas, J.K. VanSlyke, P.E. Stenberg, and G. Thomas. 1994. Intracellular trafficking and activation of furin proprotein convertase: localization to the TGN and recycling from the cell surface. *EMBO J.* 13:18-33.

Mostov, K., M.B.A. ter Beest, and S.J. Chapin. 1999. Catch the μ1B train to the basolateral surface. *Cell.* 99:121-122.

Mostov, K.E., and M.H. Cardone. 1995. Regulation of protein traffic in polarized epithelial cells. *BioEssays*. 17:129-138.

Mott, H.R., J.W. Carpenter, and S.L. Campbell. 1997. Structural and functional analysis of a mutant Ras protein that is insensitive to nitric oxide activation. *Biochemistry*. 36:3640-3644.

Mukherjee, S., R.N. Ghosh, and F.R. Maxfield. 1997. Endocytosis. *Physiol. Rev.* 77:759-803.

Mullins, R.D. 2000. How WASP-family proteins and the Arp2/3 complex convert intracellular signals into cytoskeletal structures. *Curr. Opin. Cell Biol.* 12:91-96.

Mullins, R.D., J.A. Heuser, and T.D. Pollard. 1998. The interaction of Arp2/3 complex with actin: Nucleation, high affinity pointed end capping, and formation of branching networks of filaments. *Proc. Natl. Acad. Sci. USA.* 95:6181-6186.

Murphy, C., R. Saffrich, M. Grummt, H. Gournier, V. Rybin, M. Rubino, P. Auvinen, A. Lütcke, R.G. Parton, and M. Zerial. 1996. Endosome dynamics regulated by a Rho protein. *Nature*. 384:427-432.

Musch, A., D. Cohen, and E. Rodriguez-Boulan. 1997. Myosin II is Involved in the Production of Constitutive Transport Vesicles from the TGN. *J. Cell Biol.* 138:291-306.

Nabi, I.R., A. Le Bivic, D. Fambrough, and E. Rodriguez-Boulan. 1991. An endogenous MDCK lysosomal membrane glycoprotein is targeted basolaterally before delivery to lysosomes. *J. Cell Biol.* 115:1573-1584.

Neiman, A.M. 1998. Prospore membrane formation defines a developmentally regulated branch of the secretory pathway in yeast. *J. Cell Biol.* 140:29-37.

Newmyer, S.L., and S.L. Schmid. 2001. Dominant-interfering Hsc70 mutants disrupt mutiple stages of clathrin-coated vesicle cycle *in vivo*. *J. Cell Biol.* 152:607-620.

Nichols, B.J., and J. Lippincott-Schwartz. 2001. Endocytosis without clathrin coats. *Trends Cell Biol.* 11:406-412.

Nichols, B.J., C. Ungermann, H.R. Pelham, W.T. Wickner, and A. Haas. 1997. Homotypic vacuolar fusion mediated by t- and v-SNAREs. *Nature*. 387:199-202.

Nickel, W., T. Weber, J.A. McNew, F. Parlati, T.H. Sollner, and J.E. Rothman. 1999. Content mixing and membrane integrity during membrane fusion driven by pairing of isolated v-SNAREs and t-SNAREs. *Proc. Natl. Acad. Sci. USA*. 96:12571-12576.

Nielsen, E., S. F., J.M. Backer, A.A. Hyman, and M. Zerial. 1999. Rab5 regulates motility of early endosomes on microtubules. *Nature Cell Biol.* 1:376-382.

Norman, J.C., L.S. Price, A.J. Ridley, A. Hall, and A. Koffer. 1994. Actin filament organization in activated mast cells is regulated by heterotrimeric and small GTP-binding proteins. *J. Cell Biol.* 126:1005-1015.

Norman, J.C., L.S. Price, A.J. Ridley, and A. Koffer. 1996. The small GTP-binding proteins, Rac and Rho, regulate cytoskeletal organization and exocytosis in mast cells by parallel pathways. *Molec. Biol. Cell*. 7:1429-1442.

Novick, P., C. Field, and R. Schekman. 1980. Identification of 23 complementation groups required for post-translational events in the yeast secretory pathway. *Cell*. 21:205-215.

Nuoffer, C., H.W. Davidson, J. Matteson, J. Meinkoth, and W.E. Balch. 1994. A GDP-bound form of rab1 inhibits protein export from the endoplasmic reticulum and transport between Golgi compartments. *J. Cell Biol.* 125:225-237.

O'Sullivan, A.J., A.M. Brown, H.N. Freeman, and B.D. Gomperts. 1996. Purification and identification of FOAD-II, a cytosolic protein that regulates secretion in streptolysin-O permeabilized mast cells, as a rac/rhoGDI complex. *Mol. Biol. Cell*. 7:397-408.

Odorizzi, G., A. Pearse, D. Domingo, I.S. Trowbridge, and C.R. Hopkins. 1996. Apical and basolateral endosomes of MDCK cells are interconnected and contain a polarized sorting mechanism. *J. Cell Biol.* 135:139-152.

Olson, M.F. 1996. Guanine nucleotide exchange factors for the Rho GTPases: a role in human disease? *J. Mol. Med.* 74:563-571.

Parlati, F., J.A. McNew, R. Fukuda, R. Miller, T.H. Sollner, and J.E. Rothman. 2000. Topological restriction of SNARE-dependent membrane fusion. *Nature*. 407:194-198.

Parton, R.G., K. Prydz, M. Bomsel, K. Simons, and G. Griffiths. 1989. Meeting of the apical and basolateral endocytic pathways of the Madin-Darby canine kidney cell in late endosomes. *J. Cell Biology*. 109:3259-3272.

Pelham, H.R. 1999. SNAREs and the secretory pathway-lessons from yeast. *Exp. Cell Res.* 247:1-

8.

Peng, X.-R., X. Yao, D.-C. Chow, J.G. Forte, and M.K. Bennett. 1997. Association of syntaxin 3 and vesicle-associated membrane protein (VAMP) with H^+/K^+-ATPase-containing tubulovesicles in gastric parietal cells. *Molec. Biol. Cell*. 8:399-407.

Peterson, M.R., C.G. Burd, and S.D. Emr. 1999. Vac1p coordiantes Rab and phosphotidylinositol 3-kinase signalling in Vps45p-dependent vesicle docking/fusion at the endosome. *Curr. Biol.* 9:159-162.

Pevsner, J., S.-C. Hsu, and R.H. Scheller. 1994. n-Sec1: a neural-specific syntaxin-binding protein. *Proc. Natl. Acad. Sci. U.S.A.* 91:1445-1449.

Pevsner, J., and R.H. Scheller. 1994. Mechanisms of vesicle docking and fusion: insights from the nervous system. *Current Opin. Cell Biol.* 6:555-560.

Pimplikar, S.W., E. Ikonen, and K. Simons. 1994. Basolateral protein transport in streptolysin O-permeabilized MDCK cells. *J. Cell Biol.* 125(5):1025-1035.

Podbilewicz, B., and I. Mellman. 1990. ATP and cytosol requirements for transferrin recycling in intact and disrupted MDCK cells. *EMBO J.* 9:3477-3487.

Price, L.S., J.C. Norman, A.J. Ridley, and A. Koffer. 1995. The small GTPases Rac and Rho as regulators of secretion in mast cells. *Current Biol.* 5:68-73.

Protopopov, V., B. Govindan, P. Novic, and J.E. Gerst. 1993. Homologs of the Synaptobrevin/ VAMP Family of Synaptic Vesicle Proteins Function on the Late Secretory Pathway in S. cervisae. *Cell.* 74:855-861.

Pruyne, D.W., D.H. Schott, and A. Bretscher. 1998. Tropomyosin-containing actin cables direct the myo2p-dependent polarized delivery of secretory vesicles in budding yeast. *J. Cell Biol.* 143:1931-1945.

Qiu, R.-G., J. Chen, D. Kirn, F. McCormick, and M. Symons. 1995a. An essential role for Rac in Ras transformation. *Nature*. 374:457-459.

Qiu, R.-G., J. Chen, F. McCormick, and M. Symons. 1995b. A role for Rho in Ras transformation. *Proc. Nat. Acad. Sci. USA.* 92:11781-11785.

Qualmann, B., M.M. Kessels, and R.B. Kelly. 2000. Molecular Links between Endocytosis and the Actin Cytoskeleton. *J. Cell Biol.* 150:F111-F116.

Ramesh, N., I.M. Anton, N. Martinez-Quiles, and R.S. Geha. 1999. Waltzing with WASP. *Trends Cell Biol.* 9:15-19.

Raposo, G., M.-N. Cordonnier, D. Tenza, B. Menichi, A. Durrbach, D. Louvard, and E. Coudrier. 1999. Association of myosin I alpha with endosomes and lysosomes in mammalian cells. *Mol. Biol. Cell*. 10:1477-1494.

Ravichandran, V., A. Chawla, and P.A. Roche. 1996. Identification of a novel syntaxin- and synaptobrevin/VAMP-binding protein, SNAP-23, expressed in non-neuronal tissues. *J. Biol.*

Chem. 271:13300-13303.

Reinhard, J., A.A. Scheel, D. Diekmann, A. Hall, C. Ruppert, and M. Bahler. 1995. A novel type of myosin implicated in signalling by rho family GTPases. *EMBO J.* 14:697-704.

Ren, M., G. Xu, J. Zeng, C. De Lemos-Chiarandini, M. Adesnik, and D.D. Sabatini. 1998. Hydrolysis of GTP on Rab11 is required for direct delivery of transferrin from the pericentriolar recycling compartment to the cell surface but not from sorting endosomes. *Proc. Natl. Acad. Sci. USA*. 95:6187-6192.

Richardson, G.P., A. Forge, C.J. Kros, J. Fleming, S.D.M. Brown, and K.P. Steel. 1997. Myosin VIIA is required for aminoglycoside accumulation in cochlear hair cells. *J. Neurosci*. 17.

Ridley, A.J. 2001. Rho Proteins: Linking Signaling with Membrane Trafficking. *Traffic*. 2:303-310.

Ridley, A.J., and A. Hall. 1992a. The small GTP-binding protein Rho regulates the assembly of focal adhesions and actin stress fibers in reponse to growth factors. *Cell*. 70:389-399.

Ridley, A.J., and A. Hall. 1992b. The small GTP-binding protein rho regulates the assembly of focal adhesions and actin stress fibers in response to growth factors. *Cell*. 70:389-399.

Ridley, A.J., H.F. Paterson, C.L. Johnston, D. Diekmann, and A. Hall. 1992a. The small GTP-binding protein rac regulates growth factor-induced membrane ruffling. *Cell*. 70:401-410.

Ridley, A.J., H.F. Paterson, C.L. Johnston, D. Diekmann, and A. Hall. 1992b. The small GTP-binding protein rac regulates growth factor-induced membrane ruffling. *Cell*. 70:401-410.

Riederer, M.A., T. Soldati, A.D. Shapiro, J. Lin, and S. Pfeffer. 1994. Lysosome biogenesis requires Rab9 function and receptor recycling from endosomes to the *trans* Golgi network. *J. Cell Biol.* 125:573-582.

Rodman, J.S., and A. Wandinger-Ness. 2000. Rab GTPase coordinate endocytosis. *J. Cell Sci.* 113:183-192.

Rohatgi, R., L. Ma, H. Miki, M. Lopez, T. Kirchhausen, T. Takenawa, and M.W. Kirschner. 1999. The Interaction between N-WASP and the Arp2/3 Complex Links Cdc42-Dependent Signals to Actin Assembly. *Cell*. 97:221-231.

Rojas, R., W.G. Ruiz, S.-M. Leung, T.-S. Jou, and G. Apodaca. 2001. Cdc42-dependent Modulation of Tight Junctions and Membrane Protein Traffic in Polarized Madin-Darby Canine Kidney Cells. *Mol. Biol. Cell*. 12:2257-2274.

Rosenblatt, J., B.J. Agnew, H. Abe, J.R. Bamburg, and T.J. Mitchison. 1997. *Xenopus* Actin Depolymerizing Factor/Cofilin (XAC) is Responsible for the Turnover of Actin Filaments in *Listeria monocytogenes* Tails. *J. Cell Biol.* 136:1323-1332.

Rossi, G., A. Salminen, L.M. Rice, A.T. Brunger, and P. Brennwald. 1997. Analysis of a yeast SNARE complex reveals remarkable similarity to the neuronal SNARE complex and a novel function for the C terminus of the SNAP-25 homolog, Sec9. *J. Biol. Chem.* 272:16610-16617.

Rothman, J.E., and T.H. Söllner. 1997. Throttles and dampers: controlling the engine of membrane fusion. *Science*. 276:1212-1213.

Rozelle, A.L., L.M. Machesky, M. Yamamoto, M.H.E. Driessens, R.H. Insall, M.G. Roth, K. Luby-Phelps, G. Marriott, A. Hall, and H.L. Yin. 2000. Phosphatidylinositol 4,5-bisphosphate induces actin-based movement of raft-enriched vesicles through WASP-Arp2/3. *Curr. Biol.* 10.

Ruppert, C., J. Godel, R.T. Muller, R. Kroschewski, J. Reinhard, and M. Bahler. 1995. Localization of the rat myosin I molecules myr1 and my2 and *in vivo* targeting of their tail domains. *J. Cell Sci.* 108:3775-3786.

Rybin, V., O. Ullrich, M. Rubino, K. Alexandrov, I. Simon, M.C. Seabra, R. Goody, and M. Zerial. 1996. GTPase activity of Rab5 acts as a timer for endocytic membrane fusion. *Nature (Lond.)*. 383:266-269.

Sathyamoorthy, V., and B.R. DasGupta. 1985. Separation, purification, partial characterization and comparison of the heavy and light chains of botulinum neurotoxin types A,B and E. *J. Biol. Chem.* 260:10461-10466.

Scales, S.J., Y.A. Chen, B.Y. Yoo, S.M. Patel, Y.-C. Doung, and R.H. Scheller. 2000. SNAREs Contribute to the Specificity of Membrane Fusion. *Neuron*. 26:457-464.

Schiavo, G., A. Santucci, B.R. DasGupta, P.P. Mehta, J. Jontes, G. Benfenati, M.C. Wilsoln, and C. Montecucco. 1993. Botulinum neurotoxins serotypes A and E cleave SNAP-25 at distinct COOH-terminal peptide bonds. *FEBS Lett.* 335:99-103.

Schliwa, M. 1999. Myosin steps backwards. *Nature*. 401:431-432.

Schlossman, D.M., S.L. Schmid, W.A. Braell, and J.E. Rothman. 1984. An enzyme that removes clathrin coats: purification of an uncoating ATPase. *J. Cell Biol.* 99:723-733.

Schmalzing, G., H.-P. Richter, A. Hansen, W. Schwarz, I. Just, and K. Aktories. 1995. Involvement of the GTP binding protein Rho in constitutive endocytosis in Xenopus laevis oocytes. *J. Cell Biol.* 130:1319-1332.

Schmid, S.L. 1997. Clathrin-coated vesicle formation and protein sorting: an integrated process. *Annu. Rev. Biochem.* 66:511-548.

Schmidt, J.J., and K.A. Bostian. 1995. Proteolysis of synthetic peptides by type A botulinum neurotoxin. *J. Protein Chem.* 14:703-708.

Schoenenberger, C.-A., and K.S. Matlin. 1991. Cell polarity and epithelial oncogenesis. *Trends in Cell Biology*. 1:87-92.

Schoenenberger, C.-A., A. Zuk, D. Kendall, and K.S. Matlin. 1991. Multilayering and loss of apical polarity in MDCK cells transformed with viral K-ras. *J. Cell Biol.* 112:873-889.

Seaman, M.N.J., P.J. Sowerby, and M.S. Robinson. 1996. Cytosolic and membrane-associated proteins involved in the recruitment of AP-1 adaptors onto the *trans*-Golgi network. *J. Biol. Chem.* 271:25446-25451.

Senda, T., Y. Horiguchi, M. Umemoto, N. Sugimoto, and M. Matsuda. 1997. *Bordetella bronchideptica* Dermonecrotizing Toxin, Which Activates a Small GTP-Binding Protein Rho, Induces Membrane Organelle Proliferation and Caveolae Formation. *Exp. Cell Res.* 230:163-168.

Sheff, D.R., E.A. Daro, M. Hull, and I. Mellman. 1999. The receptor recycling pathway contains two distinct populations of early endosomes with different sorting functions. *J. Cell Biol.* 145:123-139.

Shone, C.C., C.P. Quinn, R. Wait, B. Hallis, S.G. Fooks, and P. Hambleton. 1993. Proteolytic cleavage of synthetic fragments of vesicle-associated membrane protein, isoform-2, by botulinum type B neurotoxin. *Eur. J. Biochem.* 217:965-971.

Shurety, W., N.L. Stewart, and J.L. Stow. 1998. Fluid-phase markers in the basolateral endocytic pathway accumulate in response to the actin assembly-promoting drug jasplakinolide. *Mol. Biol. Cell*. 9:957-975.

Simon, J.P., I.E. Ivanov, J. Ren, B. Shopsin, D. Hersh, P. Tempst, H. Erdjument-Bromage, M. Lui, C. De Lemos-Charandini, M. Rosenfeld, D. Gravotta, T. Morimoto, M. Adesnik, and D.D. Sabatini. 1995. Regulation of post-Golgi vesicle production in an in vitro system. *Cold Spring Harb. Symp. Quant. Biol.* 60:179-195.

Simon, J.P., T.H. Shen, I.E. Ivanov, D. Gravotta, T. Morimoto, M. Adesnik, and D.D. Sabatini. 1998. Coatomer, but not P200/myosin II, is required for the in vitro formation of trans-Golgi network-derived vesicles containing the envelope glycoprotein of vesicular stomatitis virus. *Proc. Nat. Acad. Sci. USA*. 95:1073-1078.

Simons, K., and S.D. Fuller. 1985. Cell surface polarity in epithelia. *Annu. Rev. Cell Biol.* 1:243-288.

Simonsen, A., R. Lippe, S. Christoforidis, J.M. Gaullier, A. Brech, J. Callaghan, B.H. Toh, C. Murphy, M. Zerial, and H. Stenmark. 1998. EEA1 links PI(3)K function to Rab5 regulation of endosome fusion. *Nature*. 394:494-498.

Simpson, L.L., and B.R. DasGupta. 1983. Botulinum neurotoxin type B: Studies on mechanism of action and on structure-activity relationships. *J. Pharmacol. Exp. Ther.* 234:135-140.

Sollner, T., S.W. Whiteheart, M. Brunner, H. Erdjument-Bromage, S. Geromanos, P. Tempst, and J.E. Rothman. 1993. SNAP receptors implicated in vesicle targeting and fusion. *Nature*. 362:318-324.

Song, J.C., B.J. Hrnjez, O.C. Farokhzad, and J.B. Matthews. 1999. PKC-ε regulates basolateral endocytosis in human T84 intestinal epithelia: role of F-actin and MARCKS. *Am. J. Physiol.* 277 (Cell Physiol. 46):C1239-C1249.

Song, W., G. Apodaca, and K. Mostov. 1994. Transcytosis of the polymeric immunoglobulin receptor is regulated in multiple intracellular compartments. *J. Biol. Chem.* 269:29474-29480.

Spaargaren, M., and J.L. Bos. 1999. Rab5 Induces Rac-independent Lamellipodia Formation and Cell Migration. *Mol. Cell Biol.* 10:3239-3250.

Stahlhut, M., and B. van Deurs. 2000. Identification of Filamin as a Novel Ligand for Caveolin-1: Evidence for the Organization of Caveolin-1-associated Membrane Domains by the Actin Cytoskeleton. *Mol. Biol. Cell*. 11:325-337.

Stamnes, M.A., and J.E. Rothman. 1993. The binding of AP-1 clathrin adaptor particles to Golgi membranes requires ADP-ribosylation factor, a small GTP-binding protein. *Cell*. 73:999-1005.

Steegmaier, M., K.C. Lee, R. Prekeris, and R.H. Scheller. 2000. SNARE Protein Trafficking in Polarized MDCK Cells. *Traffic*. 1:553-560.

Steele-Mortimer, O., L.A. Knodler, and B.B. Finlay. 2000. Poisons, Ruffles and Rockets: Bacterial Pathogens and the Host Cell Cytoskeleton. *Traffic*. 1:107-118.

Stenmark, H., R. Aasland, B.-H. Toh, and A. D'Arrigo. 1996. Endosomal localization of the autoantigen EEA1 is mediated by a zinc-binding FYVE finger. *J. Biol. Chem.* 271:24048-24054.

Stow, J.L., K.R. Fath, and D.R. Burgess. 1998. Budding Roles for myosin II on the Golgi. *Trends Cell Biol.* 8:138-141.

Sudhof, T. 1995. The synaptic vesicle cycle: a cascade of protein-protein interactions. *Nature*. 375:645-653.

Sutton, R.B., D. Fasshauer, R. Jahn, and A.T. Brunger. 1998. Crystal structure of a SNARE complex involved in synaptic exocytosis at 2.4 A resolution. *Nature*. 395:347-353.

Suzuki, T., H. Miki, T. Takenawa, and C. Sasakawa. 1998. Neural Wiskott-Aldrich syndrome protein is implicated in the actin-based motility of *Shigella flexneri*. *EMBO J.* 17:2767-2776.

Takai, Y., T. Sasaki, and T. Matozaki. 2001. Small GTP-Binding Proteins. *Physiological Reviews*. 81:153-208.

Takaishi, K., T. Sasaki, H. Kotani, H. Nishioka, and Y. Takai. 1997. Regulation of cell-cell adhesion by Rac and Rho small G proteins in MDCK cells. *J. Cell Biol.* 139:1047-1059.

Tall, G.G., H. Hama, D.B. DeWald, and B.F. Horazdovsky. 1999. The phosphatidylinositol 3-phosphate binding protein Vac1p interacts with a Rab GTPase and a Sec1p homologue to facilitate vesicle-mediated vacuolar protein sorting. *Mol. Cell Biol.* 10:1873-1889.

Taunton, J., B.A. Rowning, M.L. Coughlin, M. Wu, R.T. Moon, T.J. Mitchison, and C.A. Larabell. 2000. Actin-dependent Propulsion of Endosomes and Lysosomes by Recruitment of N-WASP. *J. Cell Biol.* 148:519-530.

Theriot, J.A. 2000. The Polymerization Motor. *Traffic*. 1:19-28.

Tsien, R., and T. Pozzan. 1989. Measurement of cytosolic free Ca^{2+} with Quin2. *In* Methods in Enzymology. Biomembranes. Part S. Transport: membrane isolation and characterization. Vol. 172. S. Fleischer and B. Fleischer, editors. Academic Press, San Diego, CA. 230-262.

Tuxworth, R.I., and M.A. Titus. 2000. Unconventional Myosins: Anchors in the Membrane Traffic

Relay. *Traffic*. 1:11-18.

Ullrich, O., S. Reinsch, S. Urbe, M. Zerial, and R.G. Parton. 1996. Rab11 regulates recycling through the pericentriolar recycling endosome. *J. Cell Biol.* 135:913-924.

Ungermann, C., B.J. Nichols, H.R.B. Pelham, and W. Wickner. 1998a. A vacuolar v-t-SNARE complex, the predominant form in vivo and on isolated vacuoles, is disassembled and activated for docking and fusion. *J. Cell Biol.* 140:61-69.

Ungermann, C., K. Sato, and W. Wickner. 1998b. Defining the functions of *trans*-SNARE pairs. *Nature*. 396:543-548.

Urban, J., K. Parczyk, A. Leutz, M. Kayne, and C. Kondor-Koch. 1987. Constitutive apical secretion of an 80-kD sulfated glycoprotein complex in the polarized epithelial Madin-Darby canine kidney cell line. *J. Cell Biol.* 105:2735-2743.

Urbé, S., L.A. Huber, M. Zerial, S.A. Tooze, and R.G. Parton. 1993. Rab11, a small GTPase associated with both constitutive and regulated secretory pathways in PC12 cells. *F.E.B.S. Letters*. 334:175-182.

Vallis, Y., P. Wigge, B. Marks, P.R. Evans, and H.T. McMahon. 1999. Importance of the pleckstrin homology domain of dynamin in clathrin-mediated endocytosis. *Curr. Biol.* 9:257-260.

Van Aelst, L., and C. D'Souza-Schorey. 1997. Rho GTPases and signaling networks. *Genes Develop.* 11:2295-2322.

van IJzendoorn, S.C.D., and D. Hoekstra. 1998. (Glyco)sphingolipids are sorted in sub-apical compartments in HepG2 cells: a role for non-Golgi-related intracellular sites in the polarized distribution of (glyco)sphingolipids. *J. Cell Biol.* 142:683-696.

van IJzendoorn, S.C.D., and D. Hoekstra. 1999. The subapical compartment: a novel sorting center? *T. Cell Biol.* 9:144-149.

van IJzendoorn, S.C.D., M.M.P. Zegers, J.W. Kok, and D. Hoekstra. 1997. Segregation of glucosylceramide and sphingomyelin occurs in the apical to basolateral transcytotic route in HepG2 cells. *J. Cell Biol.* 137:347-357.

Vaughan, K.T., S.H. Tynan, N.E. Faulkner, C.J. Echeverri, and V. R.B. 1999. Colocalization of cytoplasmic dynein with dynactin and CLIP-170 at microtubule distal ends. *J. Cell Sci.* 112:1437-1447.

Vojtek, A.B., and J.A. Cooper. 1995. Rho family members: activators of MAP kinase cascades. *Cell*. 82:527-529.

Vojtek, A.B., and C.J. Der. 1998. Increasing complexity of the ras signaling pathway. *J. Biol. Chem.* 273:19925-19928.

Walch-Solimena, C., J. Blasi, L. Edelmann, E.R. Chapman, G.F. von Mollard, and R. Jahn. 1995. The t-SNAREs syntaxin 1 and SNAP-25 are present on organelles that participate in synaptic vesicle recycling. *J. Cell Biol.* 128:637-645.

Wang, G., J.W. Witkin, G. Hao, V.A. Bankaitis, P.E. Scherer, and G. Baldini. 1997. Syndet is a novel SNAP-25 related protein expressed in many tissues. *J. Cell Sci.* 110:505-513.

Watarai, M., Y. Kamata, S. Kozaki, and C. Sasakawa. 1997. Rho, a small GTP-binding protein, is essential for *Shigella* invasion of epithelial cells. *J. Exp. Med.* 185:281-292.

Weber, T., B.V. Zemelman, J.A. McNew, B. Westermann, M. Gmachl, F. Parlati, T.H. Sollner, and J.E. Rothman. 1998. SNAREpins: Minimal Machinery for Membrane Fusion. *Cell*. 92:759-772.

Welch, M.D., A.H. DePace, S. Verma, A. Iwamatsu, and T.J. Mitchison. 1997. The Human Arp2/3 Complex Is Composed of Evolutionarily Conserved Subunits and Is Localized to Cellular Regions of Dynmaic Actin Filament Assembly. *J. Cell Biol.* 138:375-384.

Welch, M.D., J. Rosenblatt, J. Skoble, D.A. Portnoy, and T.J. Mitchison. 1998. Interaction of human Arp2/3 complex and *Listeria monocytogenes* ActA protein in actin filament nucleation. *Science*. 281:105-108.

Wells, A.L., A.W. Lin, L.-Q. Chen, D. Shafer, S.M. Cain, T. Hasson, B.O. Carragher, R.A. Milligan, and H.L. Sweeney. 1999. Myosin VI is an actin-based motor that moves backwards. *Nature*. 401:505-508.

West, M.A., A.R. Prescott, E.-L. Eskelinen, A.J. Ridley, and C. Watts. 2000. Rac is required for constitutive macropinocytosis by dendritic cells but does not control its downregulation. *Curr. Biol.* 10:839-848.

Whiteheart, S.W., and E.W. Kubalek. 1995. SNAPs and NSF: general members of the fusion apparatus. *Trends in Cell Biology*. 5:64-68.

Wilson, D.W., S.W. Whiteheart, L. Orci, and J.E. Rothman. 1991. Intracellular membrane fusion. *TIBS*. 16:334-337.

Wilson, K.L. 1995. NSF-independent fusion mechanisms. *Cell*. 81:475-477.

Wong, P.P.C., N. Daneman, A. Volchuk, N. Lassam, M.C. Wilson, A. Klip, and W.S. Trimble. 1997. Tissue distribution of SNAP-23 and its subcellular localization in 3T3-L1 Cells. *Biochem. Biophys. Res. Comm.* 230:64-68.

Wu, X., B. Bowers, K. Rao, Q. Wei, and J.A. Hammer III. 1998. Visualization of Melanosome Dynamics within Wild-Type and Dilute Melanocytes Suggests a Paradigm for Myosin V Function In Vivo. *J. Cell Biol.* 143:1899-1918.

Wu, X., G. Jung, and J.A. Hammer III. 2000. Functions of unconventional myosins. *Curr. Opin. Cell Biol.* 12:42-51.

Yamashita, R.A., and G.S. May. 1998. Constitutive activation of endocytosis by mutation of myoA, the myosin I gene of *Aspergillus nidulans*. *J. Biol. Chem.* 273:14644-14648.

Yang, B., L. Gonzalez Jr., R. Prekeris, M. Steegmaier, R.J. Advani, and R.H. Scheller. 1999. SNARE Interactions Are Not Selective. *J. Biol. Chem.* 274:5649-5653.

Zacchi, P., H. Stenmark, R.G. Parton, D. Orioli, F. Lim, A. Giner, I. Mellman, M. Zerial, and C. Murphy. 1998. Rab17 regulates membrane trafficking through apical recycling endosomes in polarized epithelial cells. *J. Cell Biol.* 140:1039-1053.

Zerial, M., and H. McBride. 2001. Rab Proteins as Membrane Organizers. *Nature Rev. Mol. Cell Biol.* 2:107-119.